Numerical characterization study of pressure drop and heat transfer phenomena in woven wire matrix of a Stirling engine regenerator

SOL CAROLINA COSTA PEREIRA

Thesis Advisor

Ph.D. Jon Ander Esnaola

Ph.D. Mustafa Tutar

Submitted in Partial Fulfilment of the Requirements for the

Degree of Doctor in Philosophy

Department of Mechanical and Industrial Production

May 2014

À meus velhinhos,
Edmundo e Mª. Natividade

"Pedras no caminho? Guardo todas, um dia vou construir um castelo..."
Fernando Pessoa

"Genius is 1% inspiration, and 99% perspiration."
Thomas Edison

ACKNOWLEDGEMENTS / AGRADECIMIENTOS:

ACKNOWLEDGEMENTS

This PhD study has been supported by the CS Centro Stirling S.Coop., SAIOTEK and DFG (Diputación Foral de Guipuzcoa) programs of Basque government. For this reason, my first words are to thank Dr. Javier Aranceta for the opportunity to do this work and the support given during all this time.

I would like to thanks my advisors, Dr. Jon Ander Esnaola and Dr. Mustafa Tutar for their support, guidance, suggestions, friendship and patience throughout this research work. I really appreciate your time and dedication. I would also like to thank Haritz Barrutia for all his support and assistance.

I am deeply thankful to my colleague and friend Igor Barreno for his encouragement, unconditional support, friendship and companionship during the countless dedicated weekends and holidays.

I also want to thank all the friends and people who have given me help and encouragement in specific moments. Thank you!

Last but definitely not least, I would like to express my deepest gratitude to my family, especially to my father, he has encouraged me to study all my life, and to my mother, she is the most hardworking person I know and the best example in my life.

AGRADECIMIENTOS

Esta investigación ha sido financiada por el CS Centro Stirling S.Coop y por los programas SAIOTEK (Gobierno Vasco) y la Diputación Foral del Gipuzkoa. Por esta razón, mis primeras palabras de agradecimiento son para el Dr. Javier Aranceta, por brindarme la oportunidad de terminar el doctorado y trabajar como investigador en el Centro Stirling.

Me gustaría agradecer a mi director y codirector de tesis, el Dr. Jon Ander Esnaola y el Dr. Mustafa Tutar por su apoyo, orientación, sugerencias, amistad y paciencia durante este trabajo de investigación. Realmente aprecio su tiempo y la dedicación. También me gustaría dar las gracias a Haritz Barrutia por su soporte y ayuda a lo largo del proyecto. Sinceramente, me alegro de haber formado parte de este equipo.

Estoy profundamente agradecida a mi compañero de trabajo y amigo Igor Barreno, por su incondicional apoyo, ayuda, amistad y compañía en los incontables fines de semana y vacaciones dedicadas. Sin él este trabajo hubiese sido muy duro.

También quiero agradecer a todos los amigos y personas que en momentos puntuales me han dado ánimo. ¡Gracias!

Por último, pero no menos importante, quiero expresar mi profundo agradecimiento a mi familia, especialmente a mi padre y a mi madre, por un lado, él me ha inculcado el estudiar siempre, y por otro, mi madre es la persona más trabajadora y luchadora que conozco, es el mejor ejemplo que he podido tener.

.

ABSTRACT:

ABSTRACT

Stirling engines are an attractive alternative for micro-cogeneration mainly motivated for it is able to use any heat source and achieve high efficiency. A crucial component in these engines is the regenerator, which has a strong impact on the engine performance and its cost. One of the most widely used types of regenerator is made of stacked woven wire matrix and a cost effective alternative of this type is the wound woven wire matrix. For this last configuration, there is not known experimental studies.

Different numerical methods can be applied to the analysis of the flow through the Stirling engine regenerator. One growing approach is to model the regenerator as porous medium in order to simulate and design the full Stirling engine. In general, the friction resistance coefficients and heat transfer coefficient are experimentally obtained to describe the flow and thermal non-equilibrium through a porous medium.

The aim of this work is to propose a finite volume method (FVM) based numerical methodology to characterize the fluid flow and heat transfer through woven wire regenerator matrix. Accordingly, a stepwise approach proposing a gradual increase in model complexity, starting from a small detailed 3-D regenerator matrix domain under unidirectional flow conditions to a final modelling of oscillating regeneration cycles through a full size regenerator porous media.

The first steps involve the validation of the numerical pressure drop and heat transfer characterization, through a small detailed 3-D stacked woven wire regenerator matrix with the use of well-known experimental correlations obtained under oscillating flow conditions. Considering that the numerical results agree well with the empirical correlations, the approach is further extended to wound woven wire matrices to numerically derive the friction factor and the Nusselt correlation equations at local instantaneous Reynolds number. It is believed that the developed correlation equations can be applied with confidence as a cost effective solution to characterize the stacked and wound woven wire matrix of Stirling engine regenerators in the range of Reynolds number studied.

Later, the characterization is extended to first validate the equivalent porous media model of a representative detailed 3-D matrix based on local instantaneous friction factor and Nusselt number correlations equations numerically obtained in formers steps. The agreement of the results for the equivalent porous media suggest that the numerical modelling methodology proposed can be applied with confidence to characterize the pressure drop and heat transfer through a woven wire regenerator matrix. Finally, the full size regenerator matrix is modelled as a porous media under oscillating regeneration cycles based on local instantaneous friction factor and Nusselt number correlation equations. It is believed that the numerical modelling and the approaches proposed in this work can be successfully applied to model the regenerator as a porous media in the multi-dimensional (multi-D) simulations of Stirling engines as a cost effective tool for further optimization and design of Stirling regenerators.

LAPURPENA:

LAPURPENA

Stirling motoreak mikrokogenerazioaren arloan alternatiba interesgarriak dira, besteak beste lor dezaketen efizientzia altuengatik eta bero iturri ezberdinak erabiltzeko daukaten gaitasunengatik. Motore hauen osagai garrantzitsuetako bat regeneradorea da, motoreen efizientzian eta kostean eragin zuzena izanik. Gehien erabiltzen den regeneradoreetako bat "*stacked woven wire"* deritzena da. Hala ere industrializazioa helburu, "*wound woven wire"* deritzen konfigurazioak eskaintzen duen fabrikazio koste lehiakorrak, azken modelo hau alternatiba interesgarri bilakatzen du. Gaur egungo literaturan, "*wound woven wire regenerator matrix*" deritzen konfigurazioaren inguruko ikerketak urriak dira.

Stirling motoreen regeneradoreetatik pasatzen den fluxua analizatzeko, zenbakizko metodo desberdinak aplika daitezke. Hurbilketa bat regeneradorea medio porotsu bat bezala modelatzea da, Stirling motore osoa diseinatu eta simulatu ahal izateko. Normalean, marruskadura eta bero transferentziaren koefizienteak esperimentalki lortzen dira, emaria eta bero transferentzia medio porotsuan zehar deskribatzeko.

Tesi honen helburua "*stacked woven wire regenerator matrix*" eta "*wound woven wire regenerator matrix*" deritzen konfigurazioetan zehar bero transferentzia eta emaria karakterizatzea da, horretarako, zenbakizko modeloetan oinarritutako bolumen finituzko metodoa ("*finite volume method*") erabiliz. Era berean, modeloaren konplexutasun maila igotzen doan metodo bat proposatzen da. Norantza bakarreko emariaren baldintzapean dagoen "*woven wire*" regeneradore matrizearen zehaztasun handiko frakzio txiki baten 3-D batetik abiatuta, regenerazio ziklo oszilakorrenpean dagoen regeneradorearen medio porotsu ekibalente bat modelizatzera heltzen da.

Lehenengo etapan, "stacked woven wire regenerator matrix" konfiguraziodun zehaztasun altuko frakzio txiki baten zenbakizko presio galera eta bero transferentzia karakterizatzen dira, fluxu oszilakorpean lortutako eta ezagunak diren korrelazio esperimentalen baldintzapean lortzen diren emaitzekin balioztatuz. Zenbakizko emaitzak korrelazio enpirikoekin bat datozela egiaztatu ondoren, ikuspuntua "wound woven wire matrix" deritzen konfiguraziora zabaltzen da, aldiuneko Reynolds zenbakiarekiko marruzkadura faktorearen eta Nusselt zenbakiaren deribatutako korrelazioak lortuz. Aztertutako Reynolds zenbakien tartean, soluzio errentagarri bezala stirling motore baten "*stacked woven wire matrix*" eta "*wound woven wire matrix*" regeneradoreak karakterizatzeko korrelazio ekuazioak konfiantzaz aplika daitezkeela aditzera ematen da.

Bigarren etapan, zenbakizko karakterizazio prozesu baten bidez aurreko etapan aztertu den 3-D matrize zehatza, medio porotsu modelo baliokide bat bezala balioztatzen da. Medio porotsu baliokidearekin lortu diren emaitzek, "*woven wire*" regeneradorearen matrize batean bero transferentzia eta presio galera karakterizatzeko proposatutako zenbakizko modelatze metodoa konfiantzaz aplika daitekeela erakusten dute.

Azken etapan, regeneradore osoa medio porotsu bat bezala modelatzen da regenerazio ziklo oszilakorpean eta aldiuneko marruskadura faktorearen eta Nusselt zenbakiaren korrelazio ekuazioetan oinarrituz. Stirling motoreen simulazio multidimentsionaletan (multi-D) regeneradoreak optimizatu eta diseinatzeko, ikerketan honetan proposatutako zenbakizko modelizazioa eta planteamendua arrakastaz aplika daitezke kostu efektibodun tresna bezala, regeneradorea medio porotsu bezala modelizatuz.

RESUMEN:

RESUMEN

Los motores Stirling son una alternativa atractiva para la micro-cogeneración principalmente motivado por su capacidad de utilizar cualquier fuente de calor y su alta eficiencia teórica. En los motores Stirling el regenerador es el componente crucial, debido al gran impacto que tiene sobre el rendimiento global y en algunos casos en su coste. Uno de los tipos de regeneradores más usado es el de malla apilada ("*stacked woven wire*") y una alternativa menos costosa a esta configuración son los regeneradores de malla enrollada ("*wound woven wire*"). Sin embargo, para esta última configuración de regeneradores de mallas de alambres no se conocen estudios experimentales o de caracterización en la literatura.

Para el análisis y estudio de los regeneradores Stirling se pueden aplicador distintos métodos numéricos. En los últimos años uno de los enfoques más utilizado es modelar el regenerador como un medio poroso y de esta manera poder simular y diseñar el motor Stirling completo. En general, los coeficientes de fricción y transferencia de calor necesarios para modelar un medio poroso (sin equilibrio térmico) se obtienen experimentalmente.

El objetivo de este trabajo es proponer una metodología numérica basada en el método volúmenes finitos (FVM) para caracterizar la transferencia de calor y el flujo a través de los regeneradores de malla de alambre. Para lograr este objetivo, se aumenta progresivamente la complejidad del modelo, comenzando por el modelado 3-D detallado de un volumen pequeño de matriz de malla de alambre bajo condiciones de flujo unidireccional e isotermo hasta llegar a modelar la longitud completa del regenerador bajo ciclos regenerativos de flujo oscilante.

En la primera etapa se realiza la caracterización numérica de la caída de presión y la transferencia de calor a través del modelo 3-D detallado de regeneradores de malla de alambre apilada ("*stacked woven wire*"), validando estos resultados con correlaciones conocidas obtenidas experimentalmente bajo condiciones de flujo oscilante. Considerando que los resultados numéricos concuerdan bien con las correlaciones empíricas, el enfoque se extiende a la caracterización de regeneradores de malla de alambre enrollados ("*wound woven wire*") derivando numéricamente correlaciones para el factor de fricción y el número de Nusselt en función del número de Reynolds instantáneo. Teniendo en cuenta la validación realizada, se considera que las correlaciones derivadas pueden ser usadas en el rango estudiado para el diseño de regeneradores de malla de alambre ("*woven wire*") en motores Stirling.

En la segunda etapa, la caracterización numérica se utiliza para modelar un medio poroso equivalente a la matriz 3-D detallada de la malla de alambre. El modelo de medio poroso se basa en el factor de fricción y el número de Nusselt obtenidos para número de Reynolds instantáneos. La concordancia de resultados entre los modelos, medio poroso equivalente y modelo 3-D detallado, sugieren que la metodología de modelado numérico propuesta puede ser utilizada con confianza para caracterizar la transferencia de calor y caída de presión a través de regeneradores de matriz de malla de alambre ("*woven wire*").

Finalmente, la longitud completa de un regenerador se modela como un medio poroso bajo ciclos de regeneración oscilantes; el modelo de medio poroso utiliza las correlaciones numéricamente obtenidas para el factor de fricción y el número de Nusselt para número de Reynolds instantáneos. Se cree que la modelización numérica y el enfoque propuestos pueden ser aplicados con éxito para modelar el regenerador como un medio poroso en las simulaciones multi-dimensionales (multi-D) de los motores Stirling, además se considera una herramienta rentable para el diseño y optimización de regeneradores Stirling de matriz de malla de alambre ("*woven wire*").

LIST OF CONTENTS:

LIST OF CONTENTS

CHAPTER VII:

CHAPTER VIII:

ANNEX:

NOMENCLATURE:

NOTATION – Latin/Greek Symbols

A_{fs}	Interfacial area density of porous media	[m^2]
A_{xr}	Regenerator matrix transversal área	[m^2]
A_{wr}	Regenerator matrix wetted área	[m^2]
A_0	Dimensionless fluid displacement	
a_1, a_2, a_3	Friction factor correlation equation constants	
$C_{1\varepsilon}, C_{2\varepsilon}, C_{3\varepsilon}$	Turbulent model constants	
C_2	Inertial resistance factor	
C_f	Friction factor	
C_E	Ergun coefficient	
c_{pg}	Heat capacity of the working gas at constant pressure	[J/kg K]
c_{pr}	Heat capacity of the regenerator material matrix	[J/kg K]
c_{vg}	Heat capacity of the working gas at constant volume	[J/kg K]
D	Hydraulic diameter of the pipe	[m]
d_h	Regenerator matrix hydraulic diameter	[m]
d_w	Regenerator matrix wire diameter	[m]
E, E_f, E_s	Total specific energy, fluid and solid	[J/kg]
f	Fanning friction factor	
f_D	Darcy friction factor $\left(f_D = 4f\right)$	
f_e	Engine frequency	[1/s]
F_M	Figure of merit	
$\vec{g}$	Gravitational body force	[m/s^2]
G_k, G_b	Generation of turbulent kinetic energy	[W/m^3]
h	Heat transfer coefficient	[W/m^2 K]
h_e	Sensible enthalpy	[J/kg]
h_{fs}	Heat transfer coefficient for the fluid/solid interface	[W/m^2 K]
j	Colburn modulus, $\left(Nu / \mathrm{Re}\,\mathrm{Pr}^{1/3}\right)$	
k	Turbulent kinetic energy	[J/kg]

k, k_f, k_s	Thermal conductivity of the fluid and solid	[W/m K]
k_{eff}	Effective thermal conductivity of the matrix	[W/m K]
k_g	Thermal conductivity of the working gas	[W/m K]
k_r	Thermal conductivity of the regenerator material matrix	[W/m K]
l	Light of the wire mesh	[m]
L	Lenght of the pipe	[m]
L_r	Regenerator matrix length	[m]
$\dot{m}$	Mass flow or mean flow rate	[kg/s]
m_r	Mass of the regenerator matrix	[kg]
$n_{i,r}$	Number of trajectories	
N_{FL}	Flush Ratio	
N_k	Effective thermal conductivity ratio	
NPH	Number of pressure heads pressure drop	
NTU	Number of transfer units	
Nu	Nusselt number	
Nu_d	Nusselt number defined by Miyabe	
Nu_e	Effective Nusselt number defined by Gedeon and Wood	
Δp	Mean pressure drop over a cycle	[Pa]
∇p	Pressure gradient	[Pa/m]
p	Working gas pressures and static pressure	[Pa]
Pe	Peclet number	
Pr	Prandtl number	
Q	Solid matrix to gas heat transfer	[W]
Q_{CL}	Conduction losses	[W]
Q_{in}	Heat supply at constant temperature	[W]
Q_{out}	Heat rejection at constant temperature	[W]
Q_R	Regenerator heat	[W]
Q_{RH}	Reheat losses	[W]
Q_{SW}	Temperature Swing losses	[W]
Q_t	Regenerator thermal losses	[W]
R	Ideal Gas law constant	[J/kg K]

Re	Reynolds number	
Re_d	Reynolds number defined by Miyabe for Nusselt number	
Re_l	Reynolds number defined by Miyabe for the friction factor	
Re_ω	Kinetic Reynolds number	
$S_{h,i,k,\varepsilon}$	Source terms	[W/m^3]
t	Time	[s]
T, T_f, T_s	Temperature of the fluid and solid	[K]
T_c	Compression constant temperature	[K]
T_e	Expansion constant temperature	[K]
T_g	Temperature of the working gas	[K]
T_r	Temperature of the regenerator matrix	[K]
T_{SWr}	Regenerator matrix temperature swing during one cycle	[K]
u_i	Fluid flow velocity	[m/s]
u, v, w	Cartesian component of fluid flow velocity vector	[m/s]
$\overline{u}_i$	Mean velocity components	[m/s]
u_i'	Fluctuating velocity components	[m/s]
$u_{\max}$	Maximum fluid flow velocity through regenerator matrix	[m/s]
u_0	Amplitude of the oscillating inlet flow velocity	[m/s]
Va	Valensi number	
V_{dr}	Regenerator matrix dead volume	[m^3]
V_r	Regenerator matrix volume	[m^3]
v_f	Darcy velocity vector	[m/s]
W_p	Regenerator pumping losses	[W]
x	Longitudinal coordinate along the regenerator length	[m]
$x_{\max}$	Maximum fluid displacement	[m]

NOMENCLATURE Greek Symbols

α_r	Thermal diffusivity of the regenerator material matrix	[m^2/s]
α	Intrinsic permeability of the porous matrix	[m^2]
β	Forchheimer coefficient	[1/m]
γ_g	Adiabatic coefficient of the working gas	
γ	Porosity of the porous media	
η	Carnot efficiency	
ε	Regenerator thermal efficiency	
ε	Turbulent kinetic energy dissipation	[W/kg]
ϕ	Shape factor of the regenerator matrix	[1/m]
φ	Spacific heat transfer area	[1/m]
μ	Dynamic viscosity of the working gas	[kg/m s]
μ_t	Turbulent viscosity	[kg/m s]
ρ, ρ_f, ρ_s	Density of the fluid and solid	[kg/m^3]
ρ_g	Density of the working gas	[kg/m^3]
ρ_r	Density of the regenerator material matrix	[kg/m^3]
$\sigma_k, \sigma_\varepsilon$	Turbulent Prandtl numbers	
τ_c	Blow time or cycle time flow	[s]
τ_h	Hot blow time	[s]
τ_s	Non-dimentional time step	
ω	Engine angular frequency,	[rad/s]
Π_v	Regenerator matrix volumetric porosity	
Π_w	Woven wire screen porosity	

LIST OF ILLUSTRATIONS:

LIST OF ILLUSTRATIONS

LIST OF TABLES:

LIST OF TABLES

CHAPTER I:

Introduction

I. INTRODUCTION

Energy is essential to modern life and one of the main concerns and problems of our time. This concern is mainly motivated by the growing consumption of energy (close to 60% over the next 30 years); as it is shown in Figure 1.1 the use of fossil fuels as the main energy source (supply almost 80% of the world's energy) and their strong impact on climate change (carbon emissions). The latter is the main motivation for the promotion of renewable energy sources (solar, wind, geothermal, etc.) and the development of new technologies for increasing the energy efficiency.

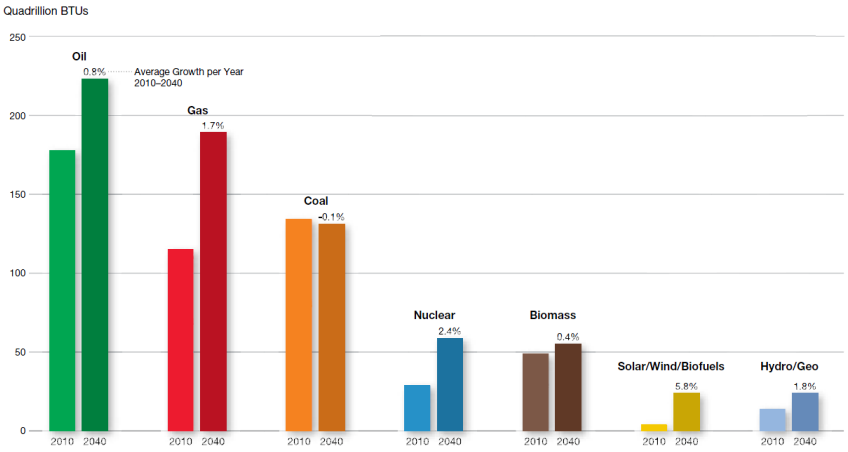

Figure 1. 1: World Energy Mix Consumption (The Outlook for Energy: A View to 2040)

Under this scenario the global community is demanding an energy model change. Many countries negotiated and adopted protocols and challenges, as the Kyoto Protocol and the Horizon 2020, to reduce net emissions of certain greenhouse gases (primarily CO_2). These challenges also involve greater advances in technology to increase the commercial viability and associated economical developing of renewable energy sources. Energy generation technology has to become cleaner, safer and more affordable. It is clear that research and development has to play a major role in this respect.

Energy is primarily used in the following sectors: electricity generation, industrial, transportation and residential/ commercial. The energy generation will continue being the largest global energy consumer in the next 30 years as it is shown in Figure 1.2. This means that the growing electricity demand will remain the biggest driver of energy needs, with electricity generation accounting for 40% of the global energy use by 2040 (ExxonMobil, 2013).

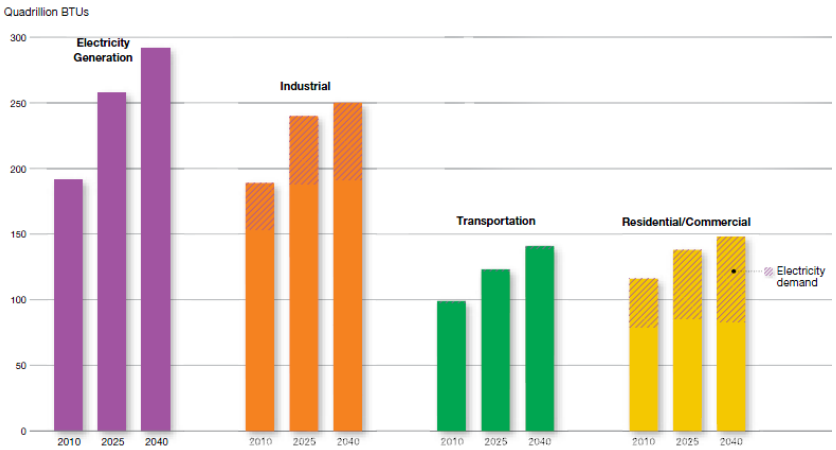

Figure 1. 2: Energy demand by Sector (ExxonMobil, 2013)

On the other hand, the standard centralised electricity generation, has been demonstrated to be quite inefficient if compared with de-centralised or distributed energy generation, as the Figure 1.3 exposes. Cogeneration systems represent an attractive option in particular for the residential sector (Knight, 2005) (Parente, y otros, 2012) (Onovwiona, 2006) which belongs to the main energy consumer sectors.

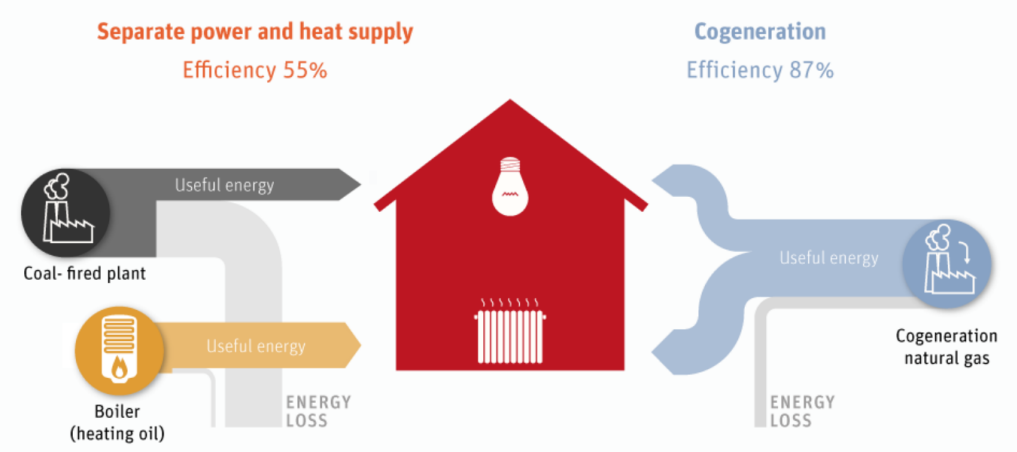

Figure 1. 3: CHP vs. Power Production (Ene)

Cogeneration in small scale or micro-CHP (Combined Heat and Power) is an interesting alternative for the residential sector, where heat and power are required. The micro-CHP systems are based on different technologies, among which are internal combustion engines, micro-turbines, fuel cells and Stirling engines. Figure 1.4 shows a comparison among these technologies pointed out the Stirling engine as one of the technologies with higher ratio of heat / electric power (Knight, 2005) (Onovwiona, 2006) (Morgado, et al., 2010) and with lower emissions offering flexibility from the point of view of energy sources. The cogeneration represents a mature technology even in micro-CHP applications, however the cogeneration based on the Stirling engine is not widely used but thanks to the advantages that characterize this technology, there is an increasing interest for its use in residential and small scale applications (micro-CHP).

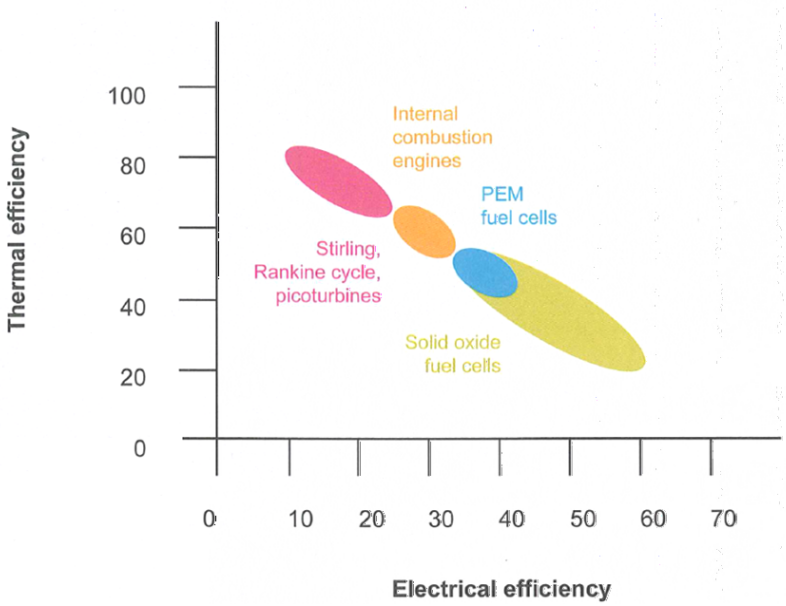

Figure 1. 4: Micro-CHP technologies (Morgado, et al., 2010)

I.1. Stirling Engine

A schematic Stirling engine is shown in Figure 1.5, the heat engine works in a regenerative closed thermal cycle with the expansion and compression of the working gas between two temperature ends through the regenerator converting the heat energy to mechanical work. Stirling Engine, even if it was created as early as two centuries ago, is receiving special attention again since Philips abandoned his big program in the 40´s (Hargreaves, 1991). Attributes of the Stirling engine that make it interesting are its theoretical high efficiency, fuel flexibility, low emissions, low noise/vibration levels and good performance at partial load (Prieto, et al., 1990) (Onovwiona, 2006). New materials and new concepts are gaining the interest of the scientific community again and many attempts with different energy sources (biomass, solar, gas, biofuel, etc.) are being done. Even NASA has a special program studying Stirling as one of the few technologies that could generate energy in the deep space for many years using radioactivity as a heat source (Ibrahim, et al., 2001) (Tew, et al., 2007).

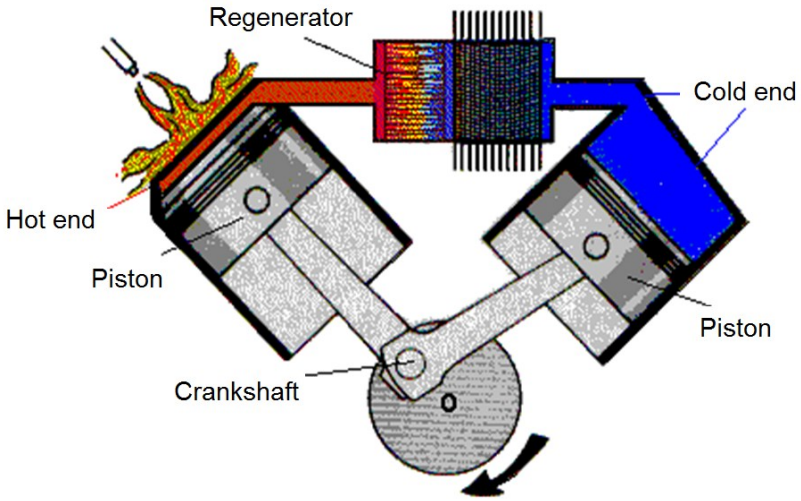

Figure 1. 5: Stirling engine (Ecotec, 2009)

The theoretical high efficiency of the Stirling engine depends of two primary requirements: maximum heat transfer efficiency and minimum power losses. These requirements in the heat exchangers, which are the main components of the Stirling engine, imply a contradiction. The Stirling regenerator is one of the three types of heat exchangers that constitute the Stirling machines. This component is sometimes referred to as the "heart", "key" or "crucial" component, because it is the component which presents the strongest impact on the engine performance (Wilson, y otros, 2004) and its cost. As an example, Ibrahim and Tew (Ibrahim, y otros, 2012) indicated that for small Stirling engine's regenerator, its thermal inefficiency contributes up to 1.5% of the engine's thermal inefficiency while pressure drop losses contribute to about 11% engine inefficiency. Therefore, in the Stirling engine the trade-off between pressure drop and heat transfer through the regenerator is especially critical.

According to Stirling Technology Company (STC) (Ibrahim, et al., 2001), which has been developing long-lasting and maintenance-free free-piston Stirling coolers and engines since 1985:

"If improved regenerator performance and/or cost is indeed achieved, it could aid in the commercialization of Stirling engines that are currently underway."

The most widely use kind of Stirling regenerators are the stacked woven wire matrices and the random fibers matrices, which tend to be the most expensive single component of the Stirling engines (Organ, 1997). There is a vast amount of literature that deals with the characterization of these kinds of Stirling regenerators, stacked woven wire and random fibers. However, there is no literature that deals with the characterization of wound woven wire regenerator matrix

which represents a suitable option in micro-CHP. The fundamental advantage of this type of regenerator is the cost and the main disadvantage is that no characterization studies of this type of regenerators are known.

In summary, an important lack with respect to the state of the art of Stirling regenerator, which applies mainly to new and forthcoming designs, is a cost effective methodology to characterize the main phenomena occurring during the regenerative cycles through the regenerator matrix. This thesis covers the numerical characterization of the woven wire regenerator matrix for the pressure drop and heat transfer phenomena.

I.2. Thesis Objectives

This thesis aims to establish a clear and cost effective numerically methodology to characterize the pressure drop and heat transfer phenomena through wound woven wire regenerator matrices as it is shown in Figure 1.6. This objective requires the use of a CFD commercial code and the following activities:

1. Development of a numerical procedure to characterize the pressure drop and heat transfer through a detailed stacked woven wire regenerator matrices.

2. Validation of the developed numerical procedure for stacked woven wire matrices with well-known experimental data.

3. Extension of validated numerical procedure to derive a friction factor and Nusselt numbers correlations through a wound woven wire regenerator matrices.

4. Implementation of the numerically obtained friction factor and Nusselt number correlations in an equivalent porous media model to enable full scale regenerator under oscillating regeneration cycles.

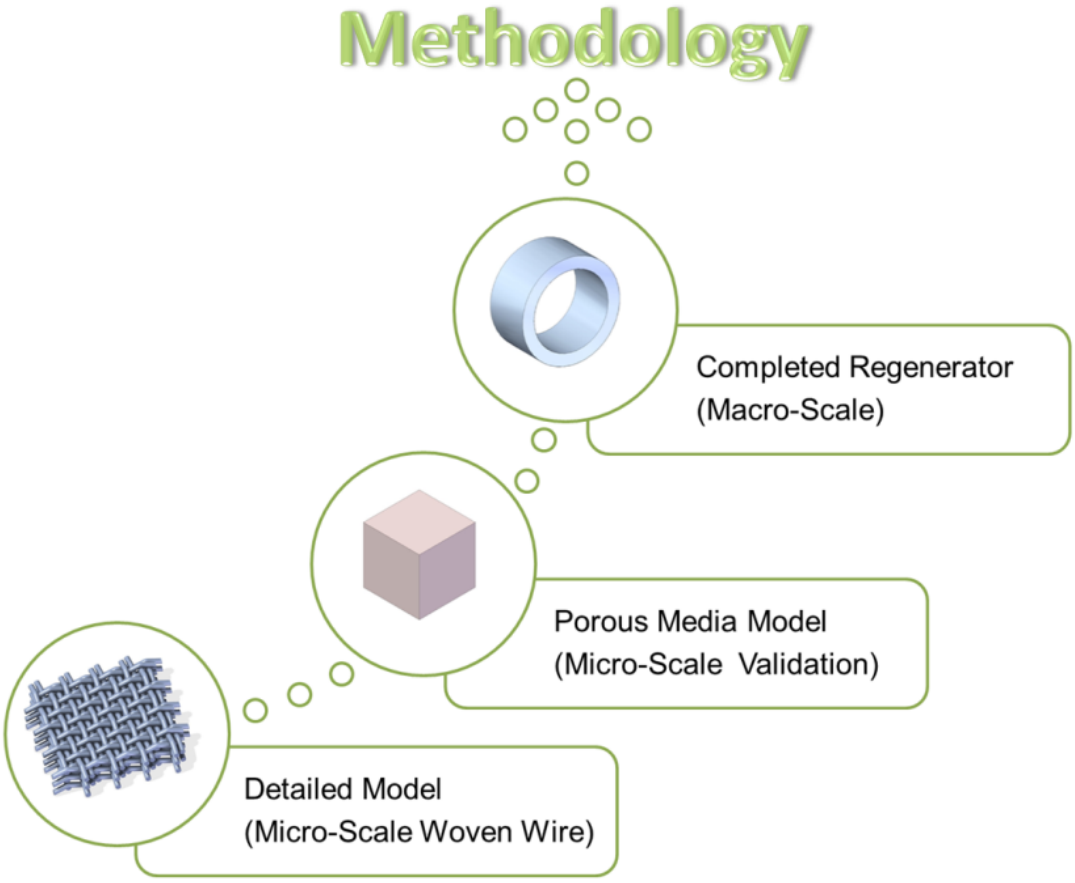

Figure 1. 6: Thesis Methodology

I.3. Thesis Structure

The structure of the thesis reproduces the stepwise approach of this works described above and the thesis is divided into the following seven chapters:

Chapter I Introduction: The chapter briefly describes the social and scientific scenario that motivates the present research work as well as the objectives of this research and the structure of thesis.

Chapter II Literature review: This chapter presents a brief history and explanation of the Stirling engines and the critical importance of the regenerator. It also presents a concise summary of the main parameters of the regenerator and their influence in the performance. The chapter briefly describes published analytical, experimental and numerical studies of the Stirling regenerators.

Chapter III Model development: This chapter summarises the governing equations of computational fluid dynamics (CFD) modelling for the flow and heat transfer characterization of the Stirling regenerators. In this chapter is also described the regenerator characterization procedure and the developed numerical methodology.

Chapter IV Pressure drop characterization: This chapter describes the first step in the approach followed for the numerical characterization of the Stirling regenerator. Stacked woven wire matrix configuration numerical results are compared to published experimental results for validation purpose. In the final section of the chapter, a friction factor correlation for wound woven wire matrix configuration is derived base on the 3D numerical results.

Chapter V Heat transfer characterization: This chapter explains the second step in the approach followed for the numerical characterization of the Stirling regenerator. More complex numerical model is presented including heat transfer effects and compared with experimental data. At the end of the chapter, a Nusselt number correlation at local instantaneous Reynolds number is derived base on the 3D numerical results.

Chapter VI Equivalent porous media model: This chapter presents a CFD numerical methodology to obtain the inputs required (viscous/inertia resistance and heat transfer coefficient) for modelling the regenerator as a porous media based on pressure drop and heat transfer numerical results of previous chapters. Finally, the full size regenerator matrix is modelled as a porous media under oscillating regeneration cycles based on local instantaneous friction factor and Nusselt number correlations.

Chapter VII Conclusions and recommendations for future work: Conclusions from investigations carried out in this work are exposed and recommendations for the future work are proposed.

CHAPTER II:

Literature Review

II. LITERATURE REVIEW

II.1. Stirling Engine

II.1.1. Brief History

The Stirling engine was invented by Robert Stirling in 1816 as a development of hot air engines. This engine is based on a closed reversible thermodynamic cycle. Originally, its main virtues were simplicity, reliability and safety in use. The Stirling engine main components are shown in Figure 2. 1: (A) the expansion chamber, maintained at a temperature typically above 500 °C by an external heat input, (B) the compression chamber, cooled by an external source, (C) the piston which separates the expansion and compression chambers, and finally, (D) the regenerator or economizer, which connects the expansion and compression chambers.

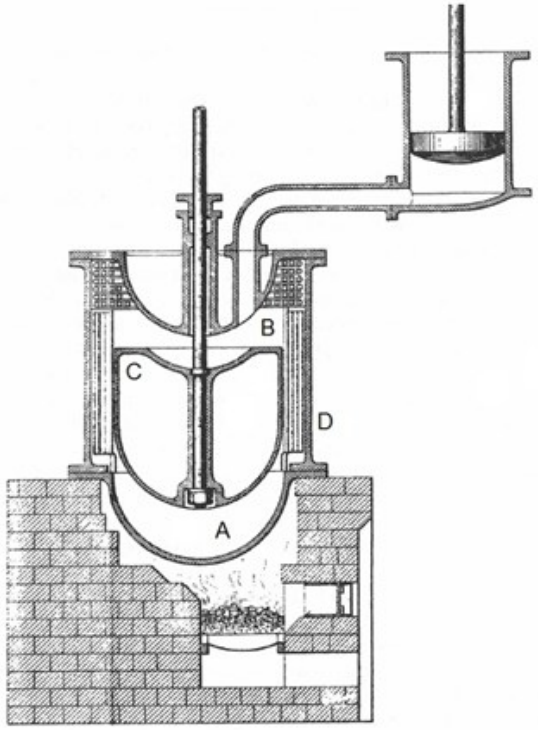

Figure 2. 1: Motor Stirling de 1928 (Hargreaves, 1991)

The theoretical efficiency of a Stirling engine with ideal regeneration is equal to the Carnot efficiency, which is the maximum achievable efficiency for machines running between the same heat sources. Thus, the main contribution of this invention was the "economiser", now known as a regenerator; it allows the Stirling cycle to reach high thermal efficiency because it acts as a temporary storage of heat between the hot and cold spaces. Actual Stirling engines do have comparatively high efficiency, typically between 20% and 60% of the theoretically maximum Carnot efficiency (Knowles, 1997).

At the time of the industrial revolution, the Stirling engine seemed to be the answer to the problems of steam machines. The steam machines were robust and reliable machines but they were also inefficient (large amounts of coal) and dangerous. Compared with the steam machines, the Stirling engine was reliable, reasonably efficient and, most importantly, safe. However, Stirling engines failed despite its safe and efficient operation, mainly because of problems associated with the corrosion of metals at high temperatures. By the First World War, the Stirling engine production had virtually ceased worldwide. Internal combustion engines became better and cheaper due to its development in that period, together with the invention of the electric motor.

The Stirling engine is possibly back today because in the late 1930´s Phillips became interested in its potential as a battery charger in markets without access to electricity grids. Philips conducted extensive research on the Stirling engine (Hargreaves, 1991) in collaboration with different companies, developing more than 312 patents in 6 European countries. Within five years the Phillips team designed a Stirling engine better in terms of efficiency, speed and power density to any other previously designed (Walker, 1973). However, its expansion failed due to the limitations in the identification and development of the market sector.

In the other hand, in early 1834, Stirling engines were recognized as a good alternative for cooling applications. However, it was not until the late 1940´s, when again Phillips Company dedicated effort to the development of a commercial Stirling cooling machine. Since at that time, the Stirling cycle was probed to be more suitable for the cryogenic range rather than the higher temperature range. The design of Phillips is still in the market with the company Stirling Cryogenics. Other companies as Sun Power and Global cooling are on the market with small Stirling cryogenics devices, too.

Today, mainly motivated by the growing concern about environment, there are companies developing Stirling engine for niche markets using alternative fuels. The main applications are cogeneration units and power generation. The Stirling engines have come a long way from Phillips research until today, there are advances in materials, manufacturing processes, and analysis methods, and on the other hand, there is a clear necessity for alternative fuels. Hence, a renewed interest arises about the Stirling engine and there is still a long way to go.

II.1.2 Ideal Stirling Cycle

The Stirling machine operates on a closed regenerative thermodynamic cycle, with cyclic compression and expansion of the working fluid at different temperature levels, converting heat energy to work energy or vice versa. The ideal Stirling cycle shown in Figure 2. 2a, it can be explained considering a cylinder containing two opposed pistons, with a regenerator between the pistons (Figure 2. 2b).

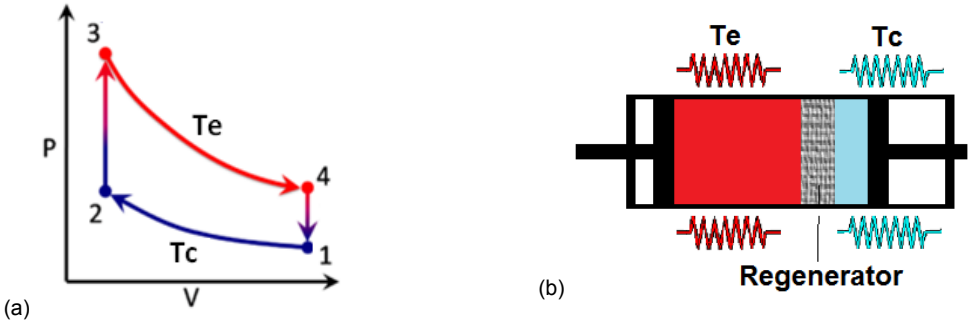

Figure 2. 2: (a) Ideal Stirling Engine Cycle (Omaña, 2007) and (b) Schematic Stirling Engine

The four processes of the cycle are the following:

Process 1→2: Isothermal compression of the working gas. Compression occurs at constant temperature (T_c) and heat is transferred reversibly from the low temperature reservoir.

Process 2→3: Isochoric heating. In this process heat is transferred reversibly at constant volume to the working fluid from the regenerative matrix.

Process 3→4: Isothermal expansion of the working gas. Expansion occurs at constant temperature (T_e) and heat is transferred reversibly from the high temperature reservoir.

Process 4→1: Isochoric cooling. In this process heat is transferred reversibly at constant volume from the working fluid to regenerative matrix.

In the ideal cycle all the heat transferred during process 4→1 is storaged into the regenerator matrix and the heat is transferred back to the working gas during process 2→3. The regenerator acts as a thermodynamic *"sponge"* and, in the ideal case, with an infinite rate of heat transfer

between the working fluid and the matrix. Therefore, there is a large temperature gradient $(T_e - T_c)$ across the transverse faces of the regenerator. In the cycle, the heat transferred between the engine and its surroundings are the heat supply (Q_{in}) and the heat rejection (Q_{out}) at constant temperature. This satisfies the second law of thermodynamics for maximum thermal efficiency, so the efficiency of the Stirling cycle is the same as the Carnot cycle $(\eta = 1 - T_c/T_e)$. The main advantages of the Stirling cycle over the Carnot cycle lies on the replacement of two isentropic processes by two isochoric processes, which increases the area of the P-V diagram obtaining more work from the cycle.

In a non-ideal regenerator (Figure 2. 3), during isochoric cooling, the regenerator absorbs the heat decreasing the working gas temperature until $T_1^{'}$ and during the isochoric heating the regenerator releases the heat, increasing working gas temperature until $T_3^{'}$. Therefore, the practical Stirling engine not only needs the heater and the cooler due to the limitations of heat transfer through the walls, but also because of the thermal inefficiency of the regenerator. From the above, it follows that the efficiency of Stirling cycle depends to a large extent on the efficiency of the regenerator.

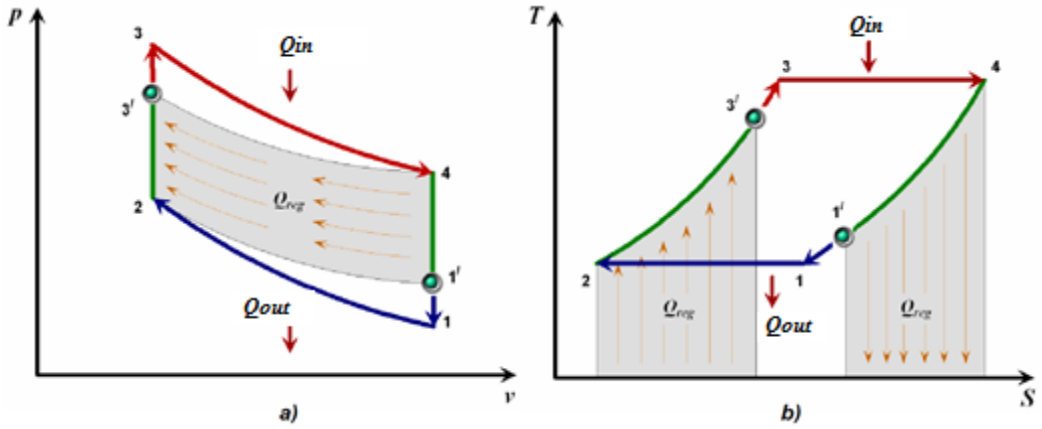

Figure 2. 3: Ideal Stirling engine cycles: a) P-V diagram and b) Ideal T-S diagram (Omaña, 2007)

II.1.3 Problems in the Stirling Engine

From its invention until now the fascinating Stirling engine has faced many problems in its development, and as Urielli (Urieli, 1977) indicated: the problems can be divided into practical and theoretical problems. From a practical point of view, the operating parameters (high pressure and temperatures) result in heat transfer and sealing problems, working in the metallurgical limits of materials. From the theoretical point of view, it was found that simple ideal cycle analysis is not appropriate for real engines as ideal cycle analysis does not consider the effects of working fluid friction, heat transfer and the non-linear variations of the properties of the working gas, among others. One of the most important contributing factors to the non-ideal performance of Stirling cycle machines is the working gas pressure drop due to flow friction. The pressure drop in the regenerator accounts for 70 to 90% of the total pressure drop through the heat transfer components (Chen, 1983).

Moreover, the energy conversion process in a Stirling engine is inherently irreversible due to the non-ideal nature of the power system (viscous friction, heat transfer, etc.). Prieto (Prieto, 2003) has provided a list of the main parameters influencing the indicated power of a Stirling engine:

- Temperature sources (expansion and compression)
- Average pressure of the working gas
- Geometric characteristics of the engine: piston displacement, piston gap, mechanisms, etc.

- Geometric characteristics of the heat exchangers: dead volume, heat transfer area.
- Physical properties of the working gas.
- Geometric characteristics of the regenerator: dead volume, cross sectional area, hydraulic radius and volumetric porosity.
- Properties of the regenerator material: thermal diffusivity, volumetric heat capacity.
- Operating frequency.

In fact, as indicated by Timoumi (Timoumi, et al., 2008) these engines have extremely complex phenomena related to: working gas compressibility, fluid mechanics, thermodynamics, and heat transfer.

Sankey diagram shown in Figure 2. 4 illustrates the relative proportion of heat flow which occurs in a Stirling engine. For a typical distribution of a Stirling engine heat exchanged periodically with the regenerator (Q_R) is about 4 to 5 times greater than the heat input to the engine (Q_{in}) (Thombare, et al, 2006). Therefore, the regenerator plays a major role in the operation of a Stirling engine with two main functions, “heat storage” and “thermal barrier” between both heat sources. The “heat storage” function is defined by the heat capacity of the matrix and the “thermal barrier” function is represented by its axial thermal conductivity and the gradient of temperatures. Thus, an ideal regenerator should provide high thermal capacity, low thermal conductivity in the fluid flow direction, and high thermal conductivity perpendicular to the fluid flow. In summary, an ideal regenerator must be a perfect insulator and a perfect conductor, with no internal volume but infinite flow area and surface area. These opposite requirements are difficult to fulfil making the design of the regenerator very challenging.

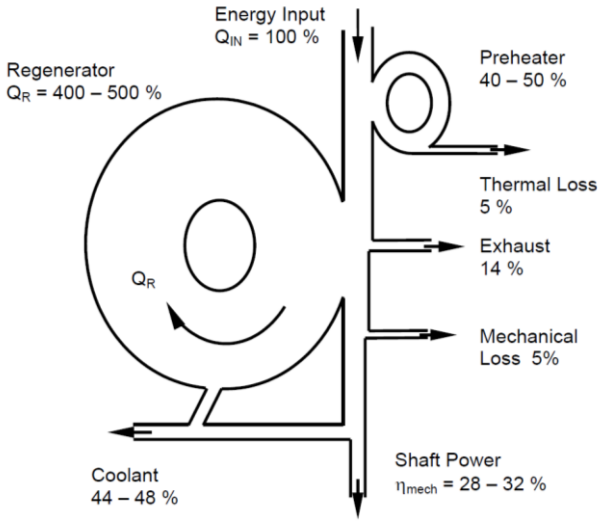

Figure 2. 4: Sankey Diagram of Typical Stirling Engine (Hieke, 2005)

II.2. Stirling Regenerator

Organ (Organ, 1997) said that the regenerator is probably the most vital component of a Stirling cycle machine, as well as the most difficult to understand. Consequently, their influence on the performance of the machines has been studied intensively. Both, efficiency and a high power output, are important because they affect the cost of power produced by an engine.

The optimization of the regenerator deals with the maximization of the heat transfer capacity and the minimization of the pumping losses, which are conflicting requirements. Therefore, it is important to reach a compromise between both, heat transfer and friction losses, which are two interdependent phenomena. Furthermore, in general, heat transfer and flow friction data are largely empirical.

The regenerator design is practically based on fundamental guidelines and few “rules of thumb”. Currently, despite the amount of literature, the situation has not changed much because as far as the writer is aware, there is still a need to study and characterize this component for Stirling applications.

II.2.1 Regenerator Parameters

Ideal regeneration performance is reached when the working gas enters and leaves the regenerator matrix at one of the two constant temperatures, T_e or T_c. The ideal regeneration could be possible if the engine operations are infinitely slowly or if the heat capacity of the fluid or the matrix is zero or infinite, respectively. On the other hand, in the ideal cycle there is no working fluid friction so there is no pressure drop across the matrix. Further, the void volume of the matrix is considered zero.

The working conditions of real Stirling regenerators are far from the ideal case. The temperatures of the working fluid through the regenerator matrix vary with cycling periodicity as it is shown in the Figure 2. 5. This phenomenon occurs as a consequence of the non-isothermal compression and expansion processes and the limited rate of heat transfer (coefficients of heat transfer and heat transfer area) within the matrix. In the regenerator matrix the flow conditions at the ends also vary along the cycle (pressure, density, velocity, temperature).

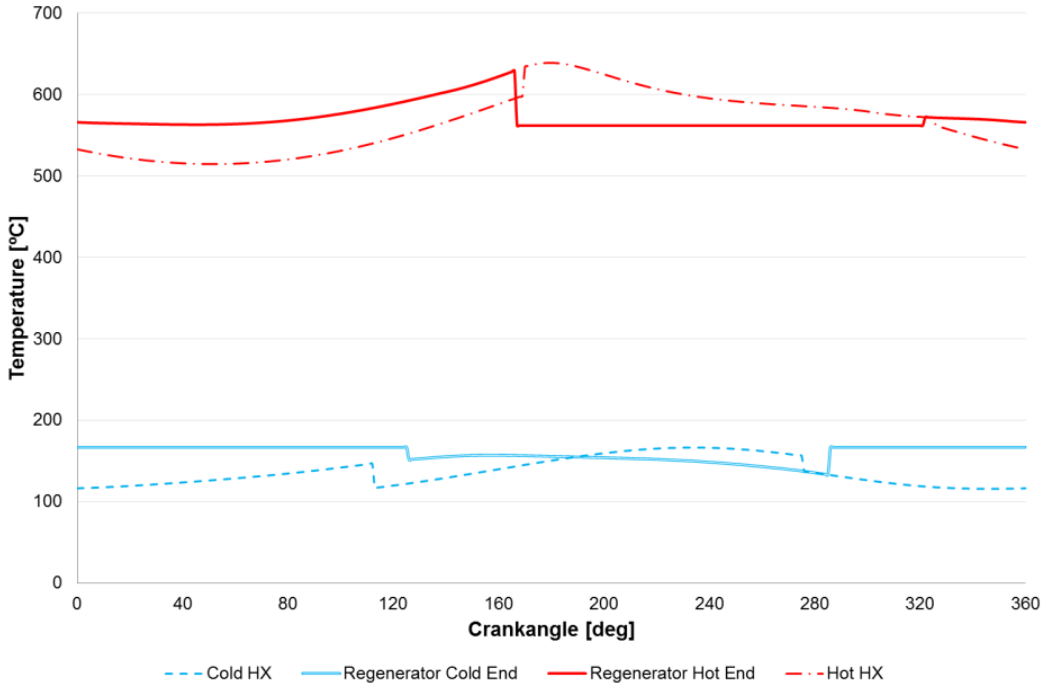

Figure 2. 5: Cyclic Temperature Variation in the Whispergen Stirling Engine

Further calculations are presented for the Whispergen Stirling Engine assuming it is operating strictly on the Schmidt cycle. Figure 2. 6 shows the cyclic mass flow diagram during a cycle, the diagram contains three curves, superimposed. One curve represents the mass flow rate along the expansion space, the other one along the compression space and the last one along the regenerator matrix. In the diagram the positive mass flow indicates that the flow is going from expansion to compression, and its importance is the net flow through the regenerator. In the Figure 2. 6 from time interval A to B is known as the “*hot-blow*”, which indicates a net flow through the regenerator towards the expansion space; from B to C the working fluid flows out of the regenerator in both directions; from C to D is known as the “*cold-blow*”, this indicates a net flow through the regenerator towards the compression space and from D to A the working fluid flows into the regenerator from both directions.

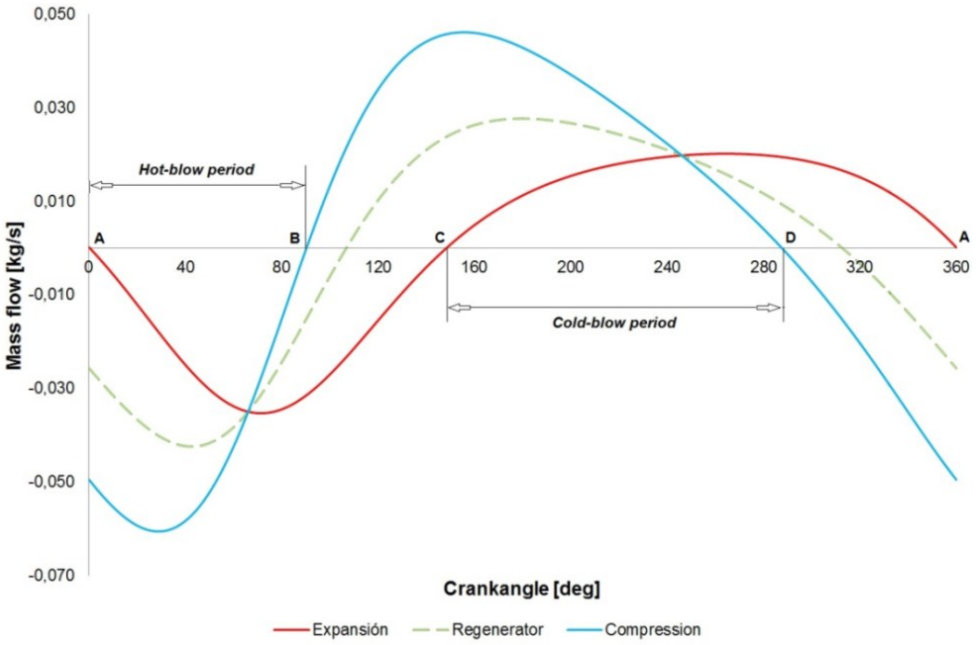

Figure 2. 6: Mass Flow diagram for Whispergen Stirling Engine

Figure 2. 7 shows the working fluid particle trajectories inside the micro-CHP Stirling engine Whispergen (EHE, 2011). In the figure are represented the five main volumes of the engine: compression, cooler, regenerator, heater and expansion. The dead volume of the engine are considered into the cooler and heater. The first curve (blue colour) represents the trajectory of particles touching compression piston and the last curve (red colour) represents the trajectory of particles touching expansion piston.

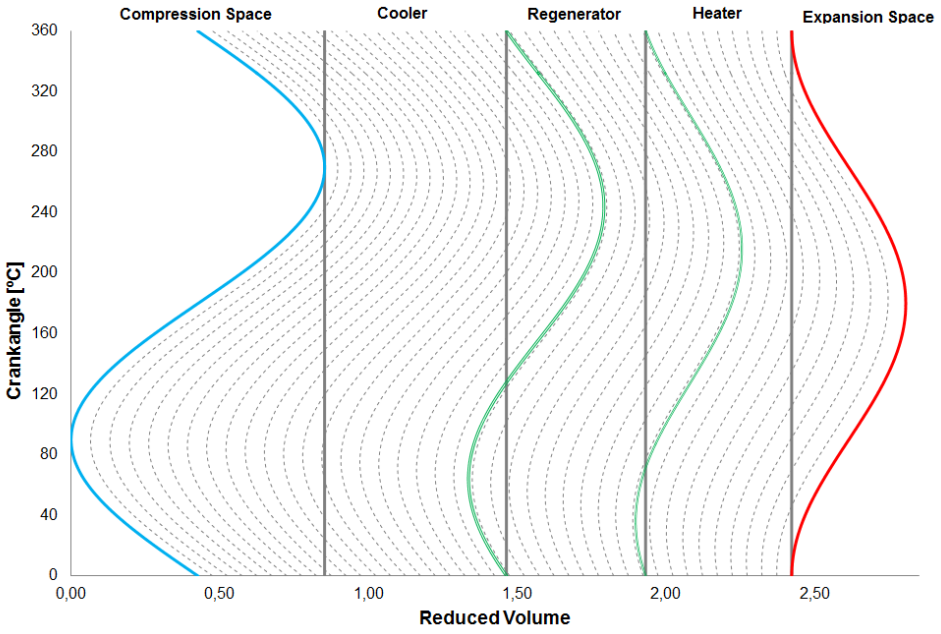

Figure 2. 7: Fluid Particle Displacement for Whispergen Stirling Engine

In the Figure 2. 7 is important observed that in the regenerator space exist particles than never leave or cross the regenerator matrix, this leads to the definition of Flush ratio. The Flush ratio, N_{FL}, is schematically explained in Figure 2. 8. In the first case, $N_{FL} < 1$, indicates that there are particles that never leave the regenerator. In the second case, $N_{FL} = 1$, all particles leave or enter into the regenerator. And in the last case, $N_{FL} > 1$, there are particles passing completely through the regenerator, passing from the heater to the cooler and vice versa.

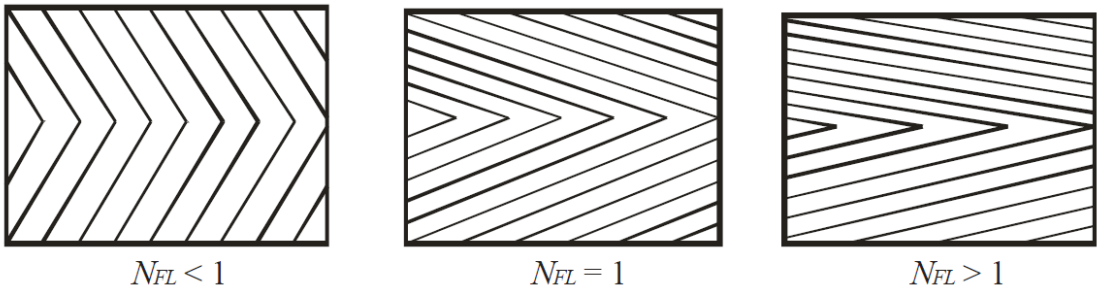

Figure 2. 8: Trajectory Map (Organ, 1997)

Organ (Organ, 1997) defined the Flush ratio on the consideration that the fluid particles trajectory map is based on equal subdivisions of total working fluid mass, the mass fraction which interacts directly with the regenerator matrix may be deduced by counting the number of trajectories, n_i, which cross any of the regenerator end faces and subtracting from the total, n. Regenerator mass content varies over the cycle with the pressure variations, for this the maximum contained mass is considered to estimate the flush ratio, n_r. Finally the flush ratio is defined as follows:

$$N_{FL} = \frac{n_i}{n_r} - 1 \qquad [2.1]$$

Considering the working fluid particle trajectory map shown for the Whispergen Stirling Engine (Figure 2. 7), the flush ratio is approximated 0.9. This means that a small fraction of mass never leaves the regenerator matrix. Organ (Organ, 1997) affirmed that in a Stirling engine flushing phenomena predominates and it cannot simply be ignored.

Apart from the flushing ratio, there are some difficulties to design a Stirling engine regenerator, such as the very high temperature gradients inside a very small regenerator volume. As the key thermodynamic component of Stirling engines is the regenerator, there is an important compromise for the regenerator's geometrical parameters to reach to an optimum heat transfer and pressure drop performance. The main characteristics of the regenerator of a Stirling engine are:

- Thermal energy storage: expressed by the product $\rho_r c_{pr}$, i.e. the volumetric heat capacity of the material of the regenerator where ρ_r is the density of the regenerator material and c_{pr} is the heat capacity of the regenerator material matrix.
- Maximum heat transfer capacity: characterized by heat transfer coefficient at the interface matrix material - working fluid, and determined by the thermal diffusivity of the material of the regenerator, α_r.
- Low frictional pressures losses: identified by the coefficient of friction at the interface matrix material - working fluid from the regenerator.
- Minimum longitudinal heat conduction losses: described by the degree of contact, or "connectivity" of the regenerator material in the longitudinal direction of the flow.
- Minimum dead volume to reduce the pressure variation in the engine. The regenerator has an unavoidable dead volume due to the porosity of the matrix, which decreases the indicated power of the engine. The relationship between the volume and the remaining dead volume of other areas affects the engine performance.

The Stirling regenerator designer has to satisfy a number of conflicting requirements. The desirable characteristics for a Stirling regenerator are:

- Maximum heat capacity which requires a large solid matrix.
- Minimum flow losses which requires a highly porous small matrix.

- Minimum dead space which requires a small and dense matrix.
- Maximum heat transfer which requires a large and finely divided matrix.
- Minimum contamination which requires a matrix with no obstruction.

As a conclusion of the preceding sections, the regenerator is essentially characterized by the geometric and physical properties of the materials from which it is built, as well as the physical properties of the working gas. Furthermore, these properties must be analysed together with the characteristic variables of the operating range of the engine.

II.2.1.1 Geometrical Parameters

Depending on the type of regenerator, there are specific geometric characteristics concerned. However, six parameters can be defined as macroscopic characteristic common to all known types of regenerator matrixes:

- Hydraulic diameter, d_h
- Volumetric porosity, Π_v.
- Transversal area, A_{xr}
- Wetted area, A_{wr}
- Length, L_r
- Dead volume, V_{dr}

The dead volume can be obtained based on Eq. [2.2]. Thus, the hydraulic diameter can be obtained based on Eq. [2.3].

$$V_{dr} = A_{xr} L_r \quad [2.2]$$

$$d_h = \frac{2V_{dr}}{A_{wr}} \quad [2.3]$$

II.2.1.2 Physical Parameters

The physical properties of both, material matrix and working gas, also influence the regenerator performance. The physical properties are:

- Thermal conductivity of the regenerator material matrix, k_r.
- Volumetric specific heat, $\rho_r c_{pr}$.
- Dynamic viscosity of the working gas, μ.
- Specific heat capacity at constant pressure of the working gas, c_{pg}.
- Adiabatic coefficient of the working gas, γ_g.
- Density of the working gas, ρ_g.
- Thermal conductivity of the working gas, k_g.

II.2.1.3 Working Variables

Once the geometry, material and the working gas are defined, the regenerator can work in different ways according to the following operating conditions to which it is subjected:

- Mass flow, $\dot{m}$.
- Engine angular frequency, ω.
- Expansion and compression space temperatures, T_e y T_c.
- Gas pressure, p.

Simon and Seume (Simon, 1986) examined eleven different Stirling engines and presented the working conditions in terms of dimensionless parameters (Reynolds number, kinetic Reynolds number and Aspect Ratio). The authors used the classification proposed by Dybbs in a steady flow for porous media according to a Reynolds number based on the average pore diameter.

- $Re < 1$ Darcy flow regime
- $1 < Re < 10$ Boundary layers begin to develop on the pore wall
- $10 < Re < 175$ Laminar flow
- $175 < Re < 250$ Separated laminar flow, vortex shedding
- $250 < Re < 300$ Separated flow with random wakes
- $Re > 300$ Turbulent flow

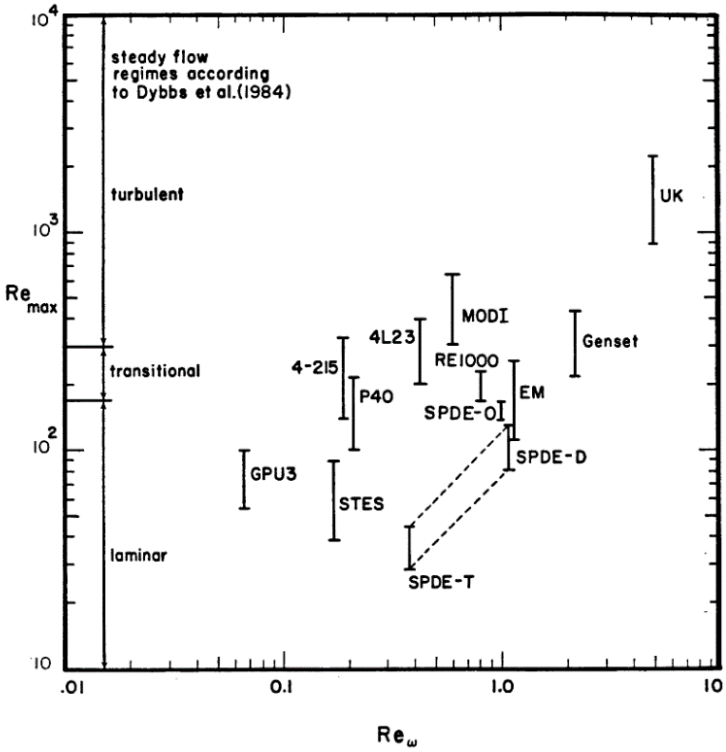

Figure 2. 9: Reynolds maximum vs. Kinetic Reynolds number in regenerators (Simon, 1986)

Figure 2. 9 shows that according to the previous classification the flow would be turbulent or transitional for 8 out of 12 Stirling regenerators. On the other hand, the maximum Reynolds number in a Stirling regenerator is lower than 1000 and the kinetic Reynolds number is lower than 10. Simon and Seume (Simon, 1986) also indicated that Mach number in the regenerators are lower than 0.01 therefore, choking of the regenerators is not expected.

Luo (Luo, 2004) classified the regenerator oscillating flow based on the kinetic Reynolds number into three zones: the viscosity controlling zone ($Re_\omega < 32$), the transition zone ($32 < Re_\omega < 3200$), and the inertia controlling zone ($Re_\omega > 3200$). The author pointed out that for the viscosity controlling zone, the pressure drop factor of the oscillating flow is very close to that of steady, laminar flow, while for the inertia controlling zone, the "superficial" pressure drop factor can be much larger than that of a steady, laminar flow. Moreover, he provides some reasons why the "superficial" pressure drop was 2 to 6 times larger for the cases having higher operating frequency and low-temperature.

II.2.2 Performance Characterization

The thermal regeneration process is the alternating heat transfer between an oscillating fluid and a surface around it. The working gas present a resistance to movement, therefore the heat transfer process cannot be analysed isolated, this mean that increasing the heat transfer capacity also increases the pressure losses. The pressure losses directly affect the engine indicated power. These two phenomena, the pressure drop and the heat transfer, are the most important phenomena observed in Stirling regenerators and both are influenced by different parameters. The characterization of these two phenomena in a Stirling regenerator is fundamental to evaluate and design the Stirling engine, and it is a starting point for the study and development of the regenerators.

II.2.2.1 Figure of Merit

Comparison of different heat transfer surfaces shows great potential for improving the regenerators, with respect to the ratio between the pressure drop and heat transfer. Figure of Merit represents the “heat transfer performance per unit of flow resistance”, this means that there is a relation between the main two phenomena in a Stirling regenerator. The conventional Figure of Merit can be obtained based on Eq. [2.4] (Ibrahim, et al., 2012):

$$F_M \infty \frac{1}{W_p Q_t A_{xr}^2} \qquad [2.4]$$

Where W_p is the regenerator pumping loss and Q_t is the regenerator thermal loss. As it can be observed in Eq. [2.4], a high Figure of Merit will correspond to a low pumping loss, a low thermal loss or even both. The Figure of Merit benefits the engine efficient depending on the relative size and importance of the two losses in the Stirling engine.

Ibrahim and Tew (Ibrahim, et al., 2012) adopted the Figure of Merit proposed by Gedeon as Eq.[2.5].

$$F_M = \frac{1}{\left(\frac{\mathrm{Re}\,\mathrm{Pr}}{4Nu} + \frac{N_k}{\mathrm{Re}\,\mathrm{Pr}}\right)} \qquad [2.5]$$

Where Re is the Reynolds number, Pr is the Prandtl number, Nu is the Nusselt number and N_k is the effective thermal conductivity ratio. Figure 2. 10 shows a comparison of the Figure of Merit of various matrices by used the definition of Eq. [2.5].

In the definition of Eq. [2.5], the two terms in the denominator measure the effects of heat transfer and thermal dispersion, respectively. Another ratio between the heat transfer and the pressure drop is used by Radebaugh (Radebaugh, 1985), the ratio between the Colburn modulus, j, and the friction factor, f. In this case the higher ratio represents the better regenerator geometry (see Figure 2. 11).

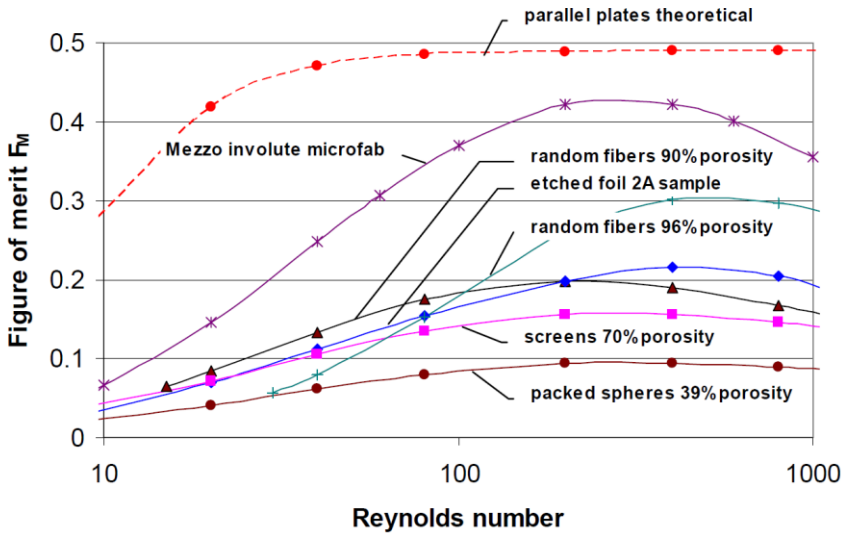

Figure 2. 10: Figure of Merit test results in function of Reynolds number for various matrices (Tew, et al., 2007)

Rühlich and Quack (Rühlich, et al., 1999) obtained the graph shown in Figure 2. 12, which basically contains the same information as Figure 2. 11, indicating that there is little dependence on the Reynolds number (longitudinal conduction is not included in the analytical studies).

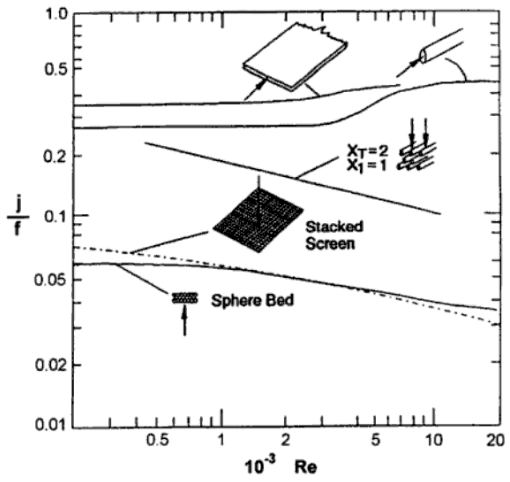

Figure 2. 11: Ratio j/f vs. Re (Radebaugh, 1985)

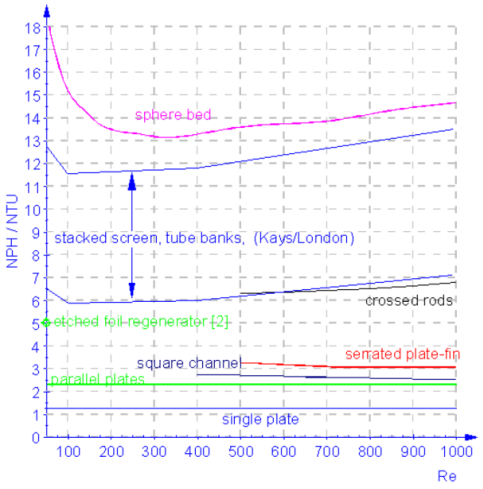

Figure 2. 12: NPH/NTU vs. Re for Pr = 0.7 (Rühlich, et al., 1999)

Rühlich and Quack (Rühlich, et al., 2002) published results of systematic investigations on the ideal inner regenerator geometry concerning the heat transfer to pressure drop ratio. In their work instead of the definition of the Figure of Merit, the ratio NPH/NTU (NPH is the number of pressure heads and the NTU is the number of transfer units) is proposed:

$$\frac{NPH}{NTU} = \frac{f\,\mathrm{Re}}{4Nu}\mathrm{Pr} \qquad [2.6]$$

Theoretically, flat plates are superior because they offer the highest ratio of heat transfer to pressure drop loss. However, solid flat plate regenerators are unstable: they do not allow cross flow between layers, and without cross flow, uneven flow patterns develop and persist. Moreover, solid flat plates conduct heat well in the direction of fluid flow, tending to destroy their regenerative effectiveness.

II.2.2.2. Regenerator efficiency

In the literature there are different definitions of the regenerator thermal efficiency (Miyabe, et al., 1982) (Bartolini, et al., 1984) (Naso, et al., 2001). The simplest regenerator thermal efficiency is evaluated in terms of the temperature profile of the 'hot' and 'cold' working gas with respect to the regenerator matrix.

II.2.3 Stirling Regenerators Losses

Many researchers (Martini, 1983) (Timoumi, et al., 2008) studied the effects of losses and the irreversibility during operation of the engine. In a Stirling engine the losses can be classified in power and heat losses, the regenerator losses are presented below. The major thermal losses in the regenerator are due to the imperfect heat transfer between the working gas and the regenerator matrix and due to the longitudinal or axial heat conduction. In order to improve the efficiency of Stirling engines it is necessary to reduce the regenerator losses due to its impact in the engine efficiency. The typical regenerator temperature profile is shown in Figure 2. 13, based on this temperature the thermal efficiency for heating and cooling process is defined as follows:

$$\varepsilon^{+} = \frac{T_{g-Lr_{\min}} - T_{g-0_{\min}}}{T_{r-Lr} - T_{g-0_{\min}}} \quad [2.7]$$

$$\varepsilon^{-} = \frac{T_{g-Lr_{\max}} - T_{g-0_{\max}}}{T_{g-Lr_{\max}} - T_{r-0}} \quad [2.8]$$

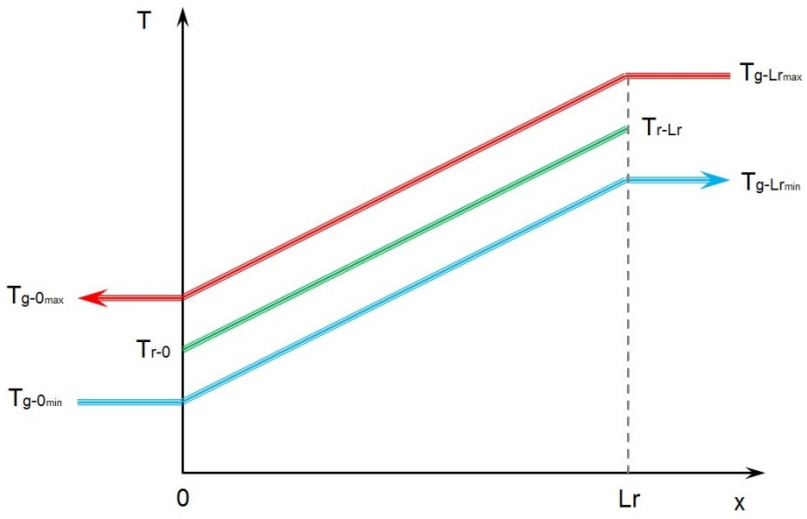

Figure 2. 13: Regenerator Temperature Profile

where ε^{+} is the thermal efficiency during heating process, ε^{-} is the thermal efficiency during cooling process and temperatures are defined in Figure 2. 3 as follows: $T_{g-Lr_{\min}}$ and $T_{g-Lr_{\max}}$ are the minimum and maximum temperature of the working gas at the hot end of the regenerator, $T_{g-0_{\min}}$ and $T_{g-0_{\max}}$ are the minimum and maximum temperature of the working gas at the cold end of the regenerator, T_{r-Lr} is the regenerator matrix temperature at the hot end, T_{r-0} is the regenerator matrix temperature at the cold end.

II.2.3.1 Power Losses (Flow Friction Losses)

Power loss in the regenerator, also called windage loss (Martini, 1983), is due to the flow of the working gas through the different engine spaces. Generally, the fluid friction inside the engine can be computed using different empirical correlations for fluid flow through the regenerator and heat exchangers. In the experimental studies of the flow resistance in a Stirling engine there are two characteristics considered as important: the first one is the oscillatory nature of the flow and the second one is the density variation throughout the cycle.

The rate of energy dissipation caused by irrecoverable pressure drops, which is the power required to overcome friction in the regenerator, is estimated from:

$$W_p = \frac{\dot{m}\Delta p}{\rho_g} \quad [2.9]$$

Where $\dot{m}$ is the mean flow rate and Δp is the mean pressure drop over a cycle. This loss becomes very important at high speeds.

II.2.3.2 Heat Losses

The heat losses in a Stirling engine are defined as the heat which must be added to the heat input to reach the constant expansion temperature. Heat losses can be divided in: reheat loss, conduction through regenerator matrix, temperature swing loss and internal swing loss.

- Reheat Loss

The inefficiency of the regenerator is one of the main causes of heat losses in a Stirling engine. The reheat loss is the heat not supplied by the regenerator which must be supplied as extra heat input, in other words it is the heat necessary to increase the temperature of the working gas from T_3' to T_3. Martini (Martini, 1983) defined the reheat loss using Eq. [2.10].

$$Q_{RH} = \frac{\tau_h}{\tau_c}\dot{m}c_{vg}\left(T_e - T_c\right)\frac{2}{NTU+2} \quad [2.10]$$

Where τ_h/τ_c is the fraction of time flowing into the hot space (approximated 1/3 of the total cycle time as is shown in Figure 2. 6) and c_{vg} is the heat capacity of the working gas at constant volume. In the regenerator the number of heat transfer units, NTU are defined as follows:

$$NTU = \frac{hA_{wr}}{c_{pg}\dot{m}} \quad [2.11]$$

- Conduction through Regenerator Matrix

There is a loss associated to the temperature gradient between the hot and cold space. In a Stirling regenerator the temperature difference could reach 600K in a length close to 30mm, therefore the gradient is 20.000K/m. The analytical estimation of this loss could be difficulty due to the complex geometry of the matrix; estimating the effective conductivity through the matrix and the effective area is not evident. Eq. [2.12] is an approximation of this loss.

$$Q_{CL} = k_{eff}A_{eff}\frac{(T_e - T_c)}{L_r} \quad [2.12]$$

Where k_{eff} is the effective thermal conductivity of the matrix, A_{eff} is the effective area.

Organ and Maeckel (Organ, et al., 1996) defined the "connectivity" of the thermal flow path and identified a simple experimental technique to specify this loss. The observations of these authors showed that the compaction pressure of the stacked woven wire screens considerably affect the connectivity or the conduction loss through regenerator matrices.

- Temperature Swing Loss

There is a heat loss associated to the temperature oscillation of the regenerator matrix due to the finite heat capacity of the regenerator; this temperature swing loss is an additional heat that must be added to the working gas. Martini (Martini, 1983) estimated the temperature drop in the regenerator matrix using Eq. [2.13]:

$$T_{SWr} = \frac{\tau_h}{\tau_c} \frac{\dot{m} c_{vg} (T_e - T_c)}{\omega m_r c_{pr}} \quad [2.13]$$

Where the m_r is the mass of the regenerator matrix.

From the previous equation Martini defined the temperature swing loss as Eq. [2.14]:

$$Q_{SW} = \frac{\tau_h}{\tau_c} \dot{m} c_{vg} \frac{T_{SWr}}{2} \quad [2.14]$$

- Internal Temperature Swing Loss

Some types of regenerator matrices could have such low thermal conductivity that all the mass of the matrix would not undergo the same temperature swing. The interior would undergo less swing and the outside would undergo additional swing would result in an additional heat loss. Moreover, the surface temperature of each element of the matrix of the regenerator does not vary instantaneously due to the thermal inertia of the material.

II.2.4 Regenerator Types

The regenerator geometry in particular is a key optimization variable. Regenerators are usually made of stacked, woven wire screens, randomly stacked metal fibres, folded sheet metal, metal sponge, sintered metals, foils, composite, etc. (See Figure 2. 14). New materials and manufacturing processes for regenerators are researched and developed around the world to improve the performance of regenerators in Stirling engine applications (Ibrahim, et al., 2012) (Knowles, 1997).

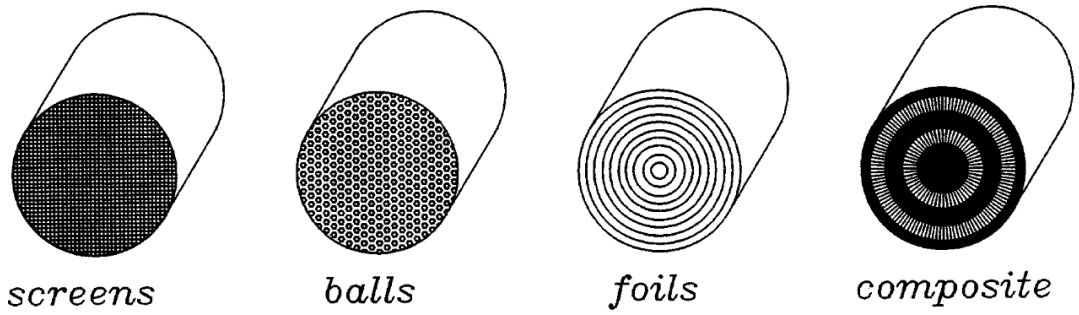

Figure 2. 14: Different kinds of Regenerator Matrices (Knowles, 1997)

Currently, the most widely used kind of regenerator matrices are stacked woven wire screen (Figure 2. 15) and random fibers (Figure 2. 16) (Ibrahim, et al., 2007). In both kind of matrices the flow is around wires and as the flow around cylinders tend to cause flow separation resulting

in high flow friction and considerable thermal dispersion, a thermal loss mechanism that causes an increase in apparent axial thermal conduction (Ibrahim, et al., 2012). In general, the regenerator matrix has been studied extensively considering it as a porous media in studies related to gas turbine and Stirling engine regenerators (Simon, 1986).

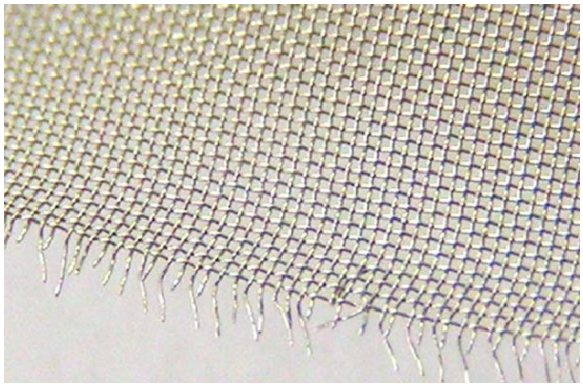

Figure 2. 15: Woven Wire Screen

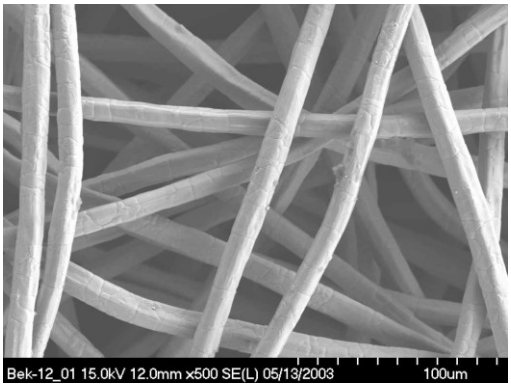

Figure 2. 16: Electron micrograph of a random fiber regenerator matrix. (Ibrahim, et al., 2007)

Below the main types of regenerators used in Stirling engines are presented.

II.2.4.1 Woven Wire Matrix

Undoubtedly, the most widely used type of Stirling regenerator is the stacked woven wire matrix, mainly made of stainless steel, although other metals have been studied (Tong, 1957), (Miyabe, et al., 1982), (Tanaka, et al., 1990), (Gedeon, et al., 1996), (Organ, 1994). Woven wire screen regenerators have relatively high flow friction and stacked woven wire matrices also require long assembly time which tends to increase their cost (Ibrahim, et al., 2007). Moreover, woven wire screens have some randomness associated with their stacking and thus may have local non-uniform flow. The ideal case of aligned screen is not a cost effective solution as high precision is required.

An alternative to the stacked woven wire matrix is the wound woven wire matrix. In this case, the assembly time is reduced drastically because the woven wire is just a winding process. Therefore, the cost is an advantage compared with random fibers regenerator matrices. The main disadvantage of this kind of woven wire matrix is the high axial conductivity, which increase the thermal losses through the matrix regenerator.

II.2.4.2 Random Fibers Matrix

Random fiber regenerators, due to the method of fabrication, the fibers are random primarily in a plane perpendicular to the main flow path (Ibrahim, et al., 2007) therefore also have high flow friction but are easy to fabricate and therefore are inexpensive. However, it is difficult to guarantee a homogeneous porosity in them due to microfusions that occur in the base material during sintering.

The main problems of the sintered random fiber regenerators are: surface contamination and fiber shedding. Any compromise of the surface (by oxidation for example) degrades the performance of the regenerator. The other major failure mode is that eventually some fibers will be loosened and migrate out of the regenerator. The release of fibers can be catastrophic if they find their way into one of the many tight clearances between the moving parts of the Stirling machine. Besides the reliability issues, random fiber regenerators are close to the ideal regenerator because of their performance in terms of heat transfer and flow resistance (Andersen, et al., 2002) (Ibrahim, et al., 2012).

II.2.4.3 Other Regenerator Matrices

The regenerator is the key component of the engine and although there are many related studies, there is still a clear necessity to find a geometry that is closer to the ideal regenerator. Some of the geometries, configurations and processes proposed are summarized below.

- Metal Foam Matrix(Figure 2. 17): Metal foams could potentially offer a solution for Stirling engine regenerators, due to their excellent fluid flow and thermal properties, coupled with cheap manufacturability. Unfortunately the results obtained in different investigations (Ibrahim, et al., 2001) (Bangert, 2010) were not as good as expected.
- Photo-etched screens and Micro-perforated Plates (Figure 2.18): The photo-etching and micro-perforated plate processes enable the production of highly uniform screens (minimal variations of wire cross section and separation around their average values) (O´Hern, 1993) (Kagawa, et al., 2002) (Matsuguchi, et al., 2009). Michell et al. (Mitchell, et al., 2007) indicated that the Figure of Merit for the etched stainless steel foil regenerator is higher than woven wire screens or random fiber of 70% porosity, or packed spheres of 39% porosity. The cost of a mesh sheet is currently four times that of a woven wire screen mesh.
- Lenticular and Honeycomb Arrays: Tew et al. (Tew, et al., 2007) worked in new concepts of regenerator matrices; the initial considered concept was a “lenticular” structure. Previously published computational analyses (Rühlich, et al., 2002) showed that the 2-D lenticular structure produced a very good Figure of Merit compared with those of the theoretical parallel-plate, random fiber, and a hexagonal array. Unfortunately, the authors found that this lenticular geometry could not be made at a reasonable cost by then-current technology.
- Segmented Involute Foils Concept: Tew et al. (Tew, et al., 2007) investigated many concepts of regenerator matrices and finally the selected design was the “segmented involute foils” concept shown in Figure 2. 19. In this design all disks were to be manufactured identically, but adjacent disks would be “flipped” so that the involute-foil segments of adjacent disks would cross at angles approximating 90°. This crossing of involute segments would help avoid channelling of flow. Ibrahim et al. (Ibrahim, et al., 2009) proved that the resulting figure of merit of segmented-involute-foil concept regenerators (proportional to the ratio of heat transfer to pressure drop) is superior to the currently used random fibers and woven wire screen regenerator matrices.
- Rolled Foil Regenerators: Yaron (Yaron, 1994) on Phillips Laboratories proposed a rolled foil regenerator (RFR) combining the best features of wire mesh screens and parallel flat plates. The results confirmed the superiority of the flow characteristics of the RFR compared with woven wire matrix regenerator. Green and Superczynski (Green, 2007) fabricated a regenerator as a ribbon with embossed ridges across the width of the ribbon and coiled in a jelly roll configuration (See Figure 2. 20). The authors claimed that a ribbon regenerator is able to optimize the heat capacity of the regenerator to maximize the performance of the Stirling machine.
- Composite Matrices: Knowles (Knowles, 1997) investigated the use of carbon fibers in Stirling regenerator design due to the high temperature capability, strength and thermal conductivity (Figure 2. 21). Other configurations with composite matrices have been used by Moran et al. (Moran, et al., 2004) for regenerating micro scale alternating multilayer composite metal (nickel) and a dielectric compound in a grid pattern with offset. This novel design (Figure 2. 22) minimizes losses axial heat conduction and pressure drops, while maximizing regenerative performance. The main advantage of composite regenerator matrices is minimized the thermal axial losses (heat conduction) between the hot end and cold end of the Stirling engine. In contrast, the main disadvantage is the high cost of manufacturing and the technology required.

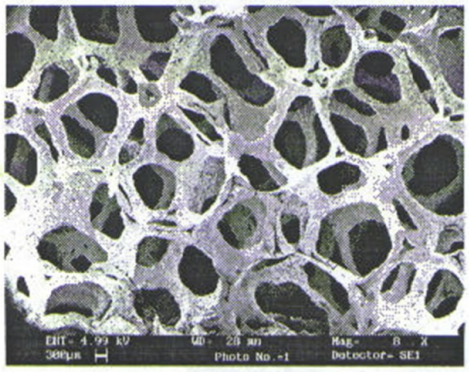

Figure 2. 17: Porvair Advanced Porous Material (Ibrahim, et al., 2001)

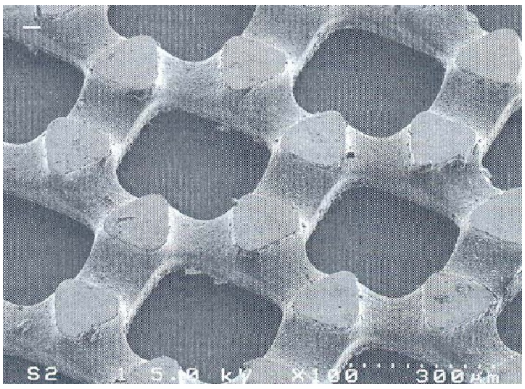

Figure 2. 18: Micrographic perforated plate (Kagawa, et al., 2005)

Figure 2. 19: Concept of Stacked Segmented Involute Foil and Regenerator disc (Tew, et al., 2007)

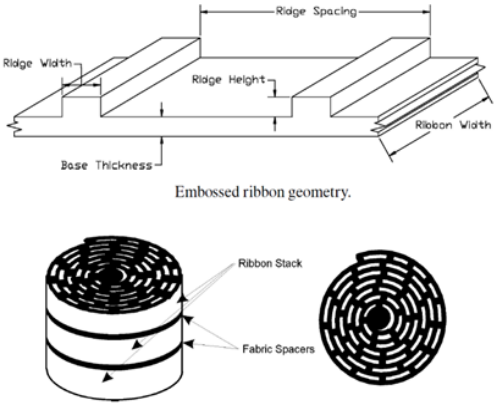

Figure 2. 20: Ribbon Regenerator assembly (Green, 2007)

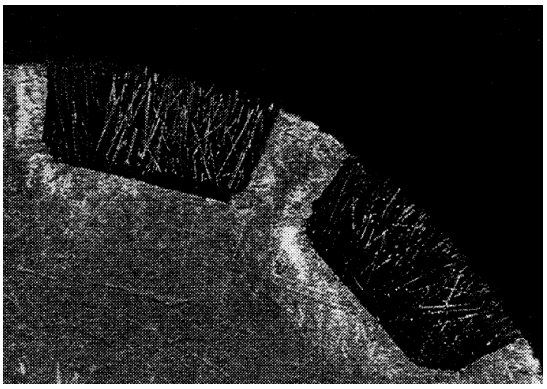

Figure 2. 21: Carbon Fiber Regenerator (Knowles, 1997)

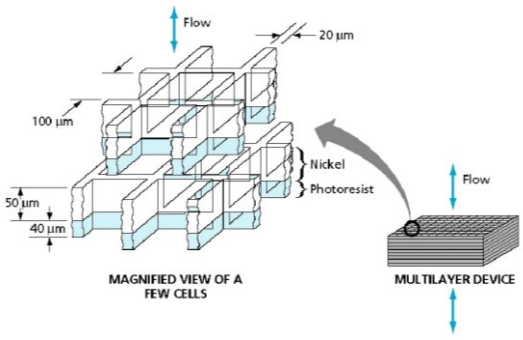

Figure 2. 22: Regenerator design composed of nickel and photoresist material (Moran, et al., 2004)

II.3. Stirling Regenerator Performance Studies

To predict the performance of Stirling engines different analytical and numerical models have been developed. Some models consider the entire system while other models concentrate on specific parts of the system where significant energy losses are expected, as in the regenerator. Due to the high relevance, many researches have worked in the study and optimization of the Stirling regenerator. As it has been already explained, the design of a Stirling regenerator must have a compromise between both fundamental phenomena, pressure drop and heat transfer, for an optimum engine performance.

Next section summarizes some of the most outstanding work in reference to the main phenomena to be analysed, pressure drop and heat transfer, mostly for wire regenerators.

II.3.1 Theoretical Approach

The pressure drop and heat transfer through the regenerator matrices are evaluated by its equation state and by the application of the mass, momentum and energy conservation equations. These equations would provide the flow characterization in three dimensions (3-D) and at each instant of time. However, significant simplifications of these equations are needed to be solved in one dimension (1-D), and this affects the agreement between predicted and actual machine performance.

II.3.1.1 Pressure Drop

Flow characteristics in a Stirling regenerator are very complex due to the geometry of the matrix, gas compressibility, entrance effects, turbulence effects, etc. The complete analytical solution of the equations cannot be addressed directly. However, there are two essential approaches to the problem of pressure drop through regenerators that assume different theoretical concepts of the flow mechanics. The first, flow-through or internal-flow, treats the system as a bundle of model tubes or pipes and the second, flow-around or external-flow, sums the resistances of submerged elements (wire). Porous medium may be considered inside this latter approach.

- Flow-through or Internal-Flow

The classical reference of Kays and London (Kays, et al., 1964) established a rational basis for the design of regenerators, correlated with the design of other forms of compact heat-exchanger using Hagen–Poiseuille's equation. The Hagen–Poiseuille´s equation is obtained assuming that the fluid is incompressible and Newtonian; the laminar flow through a pipe of a constant circular cross-section that is substantially longer than its diameter; and there is no acceleration of the fluid in the pipe. However, none of the work was directed specially to the applications of Stirling regenerators.

In case of laminar and turbulent flow in pipes the equation used is the Darcy-Weisbach (Eq. [2.15]), given as follows:

$$\Delta p = f_D \frac{L}{D} \frac{\rho_g v_f^2}{2} \qquad [2.15]$$

where Δp is the pressure drop, L is the length, D is the diameter, v_f is the Darcy velocity vector and f_D is Darcy friction factor.

In order to estimate the pressure drop the friction factor through the regenerator is requested. There are two common friction factors in use, the Darcy and the Fanning friction factor. The Darcy friction factor is also known as the Darcy–Weisbach friction factor or the Moody friction factor. The only difference between the two friction factors is that the value of the Darcy friction factor is 4 times higher than the Fanning friction factor.

The friction factor in internal flows, for the case of steady flow, is primarily dependent on Reynolds number. In the case of oscillatory flow, the friction factor could depend on both, Reynolds number and Valensi number. In general, the friction factor correlation is obtained based on empirical results.

- Flow-around or External-Flow

A regenerator matrix is a much more complex geometric structure than a pipe. Thus, it is not easy to obtain the 2-D momentum equations for it. Therefore another approach is to treat the pressure losses through the regenerator matrix as an external flow. In general, there are presently three techniques used to study external flows: (1) numerical (CFD) solutions, (2) experimentation, and (3) boundary-layer theory (White, 2009). Experimentation is the most common method of studying external flows. However, modern research is focused on detailed CFD simulations of separated flow to get further insight.

One of the most important characteristic quantities of the flow around is the drag coefficient. The resistance of a body as it moves through a fluid is well known of technical importance in hydrodynamics and aerodynamics. The combined effect of pressure and shear stress (skin friction) give rise to a resultant force on the body. This result may be resolved into two components: a component in the direction of the flow, called drag force, and a component normal to the direction of flow, called the lift force. This means that the friction factor showed in Eq. [2.15] will be the addition of these two effects: drag and skin friction (Thomas, 1999).

The treatment of the problem of flow through a porous structure is largely dependent on the scale considered, micro-scale (pore-scale) o macro-scale. In the macro-scale (large number of porous) a volume averaging (continuum) approach is used. The continuum approach of the porous media used in regenerator matrices requires the definition of the laws for conservation of mass, momentum and energy. In order to estimate the pressure drop, the macro-scale momentum balance equations is presented for the fluid flow through porous media.

Generally in porous media, the Darcy law is used to describe slow or creeping flows and the Forchheimer law is used for the description of high velocity flows. Both, the Darcy law and the Forchheimer law coefficients are obtained experimentally in order to describe the flow through a porous medium.

The Darcy law obtained from performing steady-state unidirectional flow experiments for a uniform sand column can be written as Eq. [2.16]:

$$\nabla p = -\frac{\mu}{\alpha} v_f \qquad [2.16]$$

where ∇p is the applied pressure gradient and α is the intrinsic permeability tensor of the porous matrix.

The Forchheimer law (1901) is based on Darcy's law including inertial effects (Eq.[2.17]). The inertial effects start to dominate the flow through porous media in the high velocity regime. The Forchheimer equation is given as follows:

$$\nabla p = -\frac{\mu}{\alpha} v_f - \beta \rho_g v_f^2 \qquad [2.17]$$

Here, the parameter β is called the Forchheimer coefficient. The Forchheimer coefficient is generally obtained from experimental results, as the permeability.

Ergun (1952) proposed an expression (Eq. [2.18]) for the Forchheimer coefficient based on the investigation of fluid flow through packed columns and fluidized beds:

$$\beta = \frac{C_E}{\sqrt{\alpha}} \qquad [2.18]$$

where C_E is called the Ergun coefficient and it accounts for inertial (kinetic) effects and α is the intrinsic permeability tensor of the porous matrix (Eq. [2.16]). From Equation [2.17] and Equation [2.18], the Ergun equation (Eq.[2.19]) is obtained:

$$\nabla p = -\frac{\mu}{\alpha} v_f - \frac{C_E}{\sqrt{\alpha}} \rho_g v_f^2 \qquad [2.19]$$

The Ergun coefficient is strongly dependent on the flow regime. For slow flows, the inertial effects are very small and can be neglected. This reduces the Forchheimer equation to the Darcy equation. As the flow velocity increases, inertial effects also increase and the flow adapts to the Forchheimer flow regime. These inertial effects are accounted by the Ergun coefficient and the kinetic energy of the fluid. However, a constant Ergun coefficient is valid as long as the fluid flow is laminar. Thus, in the high velocity flow regime, the Ergun coefficient needs to be adapted to reflect the experimental inertial effects.

Ergun (1952), after experimenting with different packing material and different flow rate, also determined the general form friction factor equation and this form is used for many friction factor correlations in Stirling regenerators (Miyabe, et al., 1982) (Tanaka, et al., 1990) (Thomas, 1999) (Gedeon, et al., 1996):

$$C_f = \frac{a_1}{\mathrm{Re}} + a_2 \qquad [2.20]$$

where a_1 is a correlation constant related with the form drag, a_2 is a correlation constant related with the skin friction and Re is the Reynolds number.

II.3.1.2 Heat Transfer

In the same manner as in the analysis of pressure drops, the thermal behaviour analysis of regenerator matrices has been studied from different points of view. The phenomenon of heat transfer is solved with the energy equations considering many simplifications or assumptions.

Walker (Walker, 1973) summarised some of the main simplifications used in regenerator analytical models in order to render the analysis of operation feasible:

a. Thermal conductivity: The thermal conductivity in the matrix must be simple and in different cases:

   - It is infinitely large: this means there is no temperature difference in the matrix. This assumption is far from the actual matrix.
   - It is infinitely large parallel to the flow and finite normal to the flow. This assumption is far from the actual matrix.
   - It is zero parallel to the flow and infinitely large normal to the flow.
   - It is zero parallel to the flow and finite normal to the flow.

The last two assumptions are the closest to actual regenerators, but the analysis for these assumptions is more complicated.

b. Specific Heat: The specific heats of the fluid and of the matrix material are constant.
c. The fluid inlet temperatures are constant over the flow section and with the time.
d. The heat transfer coefficient and fluid velocities are constant with time and space, even though they may be different.
e. The mass flow rate is constant during the blow period.

Ignoring the kinetic energy term, considering the fluid mass flow rate constant and uniform across the flow direction and the gas specific heat capacity is independent of temperature; the energy equation in 1-D for the wire regenerator matrix can be written as follows:

$$\left[\rho_g c_{vg} \frac{\partial T_g}{\partial t} + \rho_g u c_{pg} \frac{\partial T_g}{\partial x}\right] A_{xr} dx = h A_{wr} \left(T_r - T_g\right) \frac{dx}{L_r} \qquad [2.21]$$

where u is the velocity vector and x is the longitudinal coordinate along the regenerator length.

There are many analytical studies based on heavy mathematical transformations of equations similar to Eq. [2.21] and simplifications for the thermal performance of Stirling regenerators, mainly focussing on computing the thermal efficiency or recovery ratio.

The first analytical studies used on the Stirling regenerator were developed for the blast-furnace or regenerative gas turbine with operating condition that exclude the Stirling regenerator mainly for the large blow time (Organ, 1997). The classical reference, Hausen (1929), analysed the regenerator model assuming a 1-D steady flow, uniform and constant pressure, constant coefficient and a regenerator matrix formed by a flat plate parallel to the flow. Under these conditions obtained curves show the effect of the regenerator effectiveness of variation in two dimensionless parameters called the “reduced length” and the “reduced period”. Although the theory developed by Hausen was for furnace air preheaters, for years there was no better alternative. It was the reference used to analyse the thermal response of the regenerator in the work of many authors: Shultz (Schultz, 1951), Collins (Collins, et al., 1955), Schalkwijk (Schalkwijk, 1960), Edwards (Edwards, et al., 1971), Kolin (Kolin, 1991), among others.

Organ (Organ, 1994) (Organ, 1997) conducted an exhaustive and extensive review of the analytical approach of regenerators pointing out that all previous works were “unrevealing of the crucial flushing phenomenon in the regenerator”. He worked in finding a simple form of solution for the differential equations defining transient thermal performance of the Stirling engine regenerator.

Miyabe et al. (Miyabe, et al., 1982) performed other relevant work, where the authors made a theoretical analysis on the thermal behaviour of the regenerator matrix and on the thermal effectiveness of the regenerator. The authors proposed a regenerator design method validated with testing in an experimental Stirling engine.

For the case of internal flows, the convective heat transfer is basically dependent on the velocity profile. Therefore, for fully developed laminar flow, the same parameters that govern the fluid flow are applied for the heat transfer: Reynolds maximum and Valensi number in addition to Prandtl number (Ibrahim, et al., 2012). Also, the wall boundary condition (constant temperature or heat flux) will influence the heat transfer process.

For the case of porous media, there are two possible thermodynamic scenarios: local thermal equilibrium and local thermal non-equilibrium. For the first scenario, the system is not necessarily in thermal equilibrium globally. This means that at any given point the working gas and the regenerator matrix are at the same temperature. In such a case, only one energy equation is required for the description of the temperature at any given point. For the other scenario, it do not exist thermal equilibrium. Thus, at any given point the working gas and the regenerator matrix are at different temperatures.

- Porous Media Local thermal equilibrium

For low velocities, as working gas and the regenerator matrix are in contact for a sufficient period of time, the possibility for the system to exchange energy locally and to establish local thermal equilibrium always exists. In such a case, only one energy equation is sufficient for the description of temperature at any given location within the regenerator.

- Porous Media Local thermal non-equilibrium

For high velocity flow, the interaction between working gas and the regenerator matrix is fast. Thus, working gas and the regenerator matrix cannot exchange sufficient amount of energy to establish local thermal equilibrium. Therefore, at any given location exists at different temperatures. In such a case, one needs different energy equations for the description of the temperature of working gas and the regenerator matrix.

II.3.2 Experimental Studies and Empirical Correlations

As has been explained, both, heat transfer and pressure drop through regenerator matrices are essential considerations for the design of Stirling engines with higher efficiency. Therefore, experimental studies of regenerators have mostly been conducted to generate correlations for friction factor and the heat transfer coefficient. In those experimental studies of Stirling regenerators, two leading techniques can be identified: a single-blow and oscillating flow. Although the differences in the techniques are not covered here, it is important to keep this in mind because there are conflicting opinions about results obtained in both techniques.

In this section some relevant experimental works conducted for Stirling regenerator are present.

II.3.2.1 Pressure Drop

Kays and London (Kays, et al., 1964) present curves of Fanning friction factor (Figure 2. 23) for random stacked woven wire mesh matrices with various porosities (from 0.602 to 0.832). The data is based on steady flow experiments for both matrices. The authors did no present a direct correlation for friction factor or heat transfer.

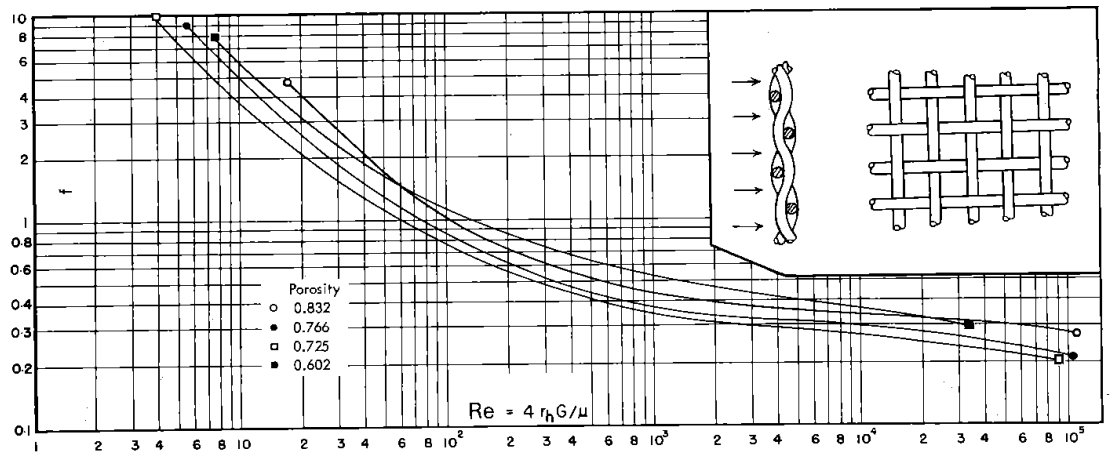

Figure 2. 23: Flow through an infinite randomly stacked woven-screen matrix: Flow friction (Kays, et al., 1964)

Miyabe et al. (Miyabe et al., 1982) (Hamaguchi, et al., 1984), derived generalized experimental correlations of flow friction factor and heat transfer coefficient for stacked wire screen with different wire diameters from 0.04 to 0.51 mm and volumetric porosities from 0.59 to 0.84. From the experiments carried out by a steady flow apparatus the following friction factor correlations were obtained:

$$C_f = \frac{33.6}{\mathrm{Re}_l} + 0.337 \qquad [2.22]$$

where Reynolds number is based on the mesh aperture and the friction factor include the number of meshes. They concluded that in steady flow experiments it is easier to choose the

aperture as hydraulic equivalent diameter because the experimental value variance is smaller than using wire diameter in the tested range of mesh.

Chen and Griffin (Chen, 1983) studied the pressure drop in Stirling engine applications demonstrating the significant effects of the regenerator pressure drop on engine performances. Moreover, they presented an improved friction factor correlation for steady unidirectional flow through wire-screen matrices based on data published by Kays and London (Kays, et al., 1964) and they conducted a theoretical analysis of the friction factor for oscillating laminar flow through circular tubes. Chen and Griffin (Chen, 1983) showed that no significant difference exists between the regenerator (woven wire screen matrix) pressure drop at slow oscillations flow compared with unidirectional flow. Therefore, the regenerator pressure drop may be predicted adequately from the correlation developed for steady unidirectional flow.

Tanaka et al. (Tanaka, et al., 1990) investigated the flow and heat transfer characteristics of stacked woven wire (wire diameter from 0.05 to 0.23 mm; volumetric porosities from 0.65 to 0.73) and random fiber regenerator materials in an oscillating flow. The prediction of the pressure drop was based on the hydraulic diameter as the representative length defined the friction factor and Reynolds number. The friction factor correlation proposed for woven wire was:

$$C_f = \frac{175}{\mathrm{Re}} + 1.60 \qquad [2.23]$$

where Reynolds number is based on maximum velocity through the regenerator matrix and on the hydraulic diameter of the regenerator matrix, d_h, defined as:

$$d_h = \frac{4\Pi_v d_w}{\phi(1-\Pi_v)} \qquad [2.24]$$

where Π_v is the matrix volumetric porosity, d_w is the wire diameter and ϕ is the shape factor defined as the ratio of the mesh surface area to the mesh volume. The results showed that the oscillating flow friction factor is about 30% greater than that obtained theoretically for a unidirectional flow.

Chen et al. (Chen, et al., 1996) used a single-blow test method to investigate the effects of oversizing the thermal performance of regenerators, performing heat transfer and pressure measurements on three test regenerators. The authors provided empirical correlations for the Nusselt number and friction factor versus the Reynolds number for each test regenerator.

Zhao y Cheng (Zhao, 1996) experimentally investigated the pressure drop characteristic in packed columns (woven screen) subjected to a periodically reversing flow of air. In their investigations they found that the oscillatory pressure drop factor increases with the kinetic Reynolds number defined in Eq. [2.25] (from 0.001 to 0.13) and with the dimensionless fluid displacement defined in Eq. [2.26]. Based on the experimental results, Zhao y Cheng (Zhao, 1996) obtained a correlation equation for the maximum (Eq. [2.27]) and the cycle-averaged (Eq. [2.28]) pressure drop in terms of these two similarity parameters. They indicate that the value of the cycle-averaged pressure drop of the oscillatory flow is four to six time higher than in steady flow at the same Reynolds number. However, at small kinetic Reynolds number, their results demonstrate that the pressure drop depends only on the geometry of the woven screen and it is independent of the kinetic Reynolds number and the dimensionless fluid displacement.

$$\mathrm{Re}_\omega = \frac{\rho_g \omega d_h^2}{\mu} \qquad [2.25]$$

$$A_0 = \frac{x_{\max}}{d_h} \qquad [2.26]$$

where x_{max} is the maximum fluid displacement.

$$C_{f\max} = \frac{1}{A_0}\left(\frac{403.2}{\mathrm{Re}_\omega} + 1789.1\right) \quad [2.27]$$

$$\bar{C}_f = \frac{1}{A_0}\left(\frac{247.3}{\mathrm{Re}_\omega} + 1003.6\right) \quad [2.28]$$

Gedeon and Wood (Gedeon, et al., 1996) conducted a relevant work in the characterization of stacked woven wire (wire diameter from 0.05 to 0.09 mm; volumetric porosities from 0.62 to 0.78) and random matrix regenerator under oscillating flow conditions measuring pumping dissipation and thermal energy transport. The experimental results of the authors yielded generic correlation for the friction factor, Nusselt number, enhanced axial conduction ratio and overall heat flux ratio. The friction factor correlation proposed by Gedeon and Wood (Gedeon, et al., 1996) for woven wire matrix is:

$$C_f = \frac{129}{\mathrm{Re}} + 2.91\mathrm{Re}^{-0.103} \quad [2.29]$$

Equation [2.29] presented three coefficients instead of the Ergun equation form of two coefficients (Eq. [2.20]). The authors started out modelling friction factors in the standard two-parameter Ergun form. However, they got a much better fit to data by introducing a relatively minor modification to the Ergun equation calling it the three-parameter modified-Ergun form. The idea is that the third parameter will be negative but small, allowing the correlation to better track observed reality at high Reynolds numbers. At low Reynolds numbers (creeping viscous flow) the first term of the equation will dominate, exactly as in the original Ergun equation (Gedeon, et al., 1996).

On the theoretical side Gedeon and Wood (Gedeon, et al., 1996) concluded that under the range of tested conditions, which were representative of most Stirling applications, no essential differences compared to steady flow were found for woven wire matrix. In other words, instantaneous local Reynolds number or Peclet number characterized the flow quite adequately. The authors affirmed that porous-material friction factors obtained under steady-flow conditions should be sufficient for oscillating-flow conditions in Stirling regenerators. However, they indicated that the exception to this might be for Valensi numbers above 20. The definition used by Gedeon and Wood (Gedeon, et al., 1996) of Valensi number is as follows:

$$Va = \frac{\rho_g \omega d_h^2}{4\mu} \quad [2.30]$$

where the hydraulic diameter is defined as 4 divided by the matrix surface area per unit void volume.

Sodré and Parise (Sodré, 1997) designed an experimental procedure to investigate the friction factor of the plain-square woven metal screen adopted in the Stirling engine regenerator. The tests involved a turbulent, fully developed flow of air at steady-state conditions, with the modified Reynolds number, based on the hydraulic radius of the packed bed. The authors used a corrected Ergun equation to correlate the experimental data, considering the wall effects and that the correlation is valid for annular and circular cross-section beds.

Park et al. described a simple-to-fabricate woven mesh, consisting of bonded laminates of 2-D plain-weave conductive screens (Park, et al., 2002). The authors developed a mathematical model of the thermal performance of such a mesh and described an apparatus to measure both the pressure drop and heat transfer coefficient. Measurements of pressure drop and overall

heat transfer rate are reported and used to develop correlation equations of mesh friction factor and Colburn j-factor. The staggered-stacked screen-laminates friction factor is much higher than the friction factor of the inline configuration. The friction factor correlation for the inline configuration is the following expression:

$$C_f = \frac{24.5}{\mathrm{Re}} + 0.39 \qquad [2.31]$$

Park et al. (Park, et al., 2002) compared the results against Tong and London's (Tong, 1957) correlation obtaining higher friction factor. They attributed that different to the use of bonding screens. For a staggered screen laminate (stacking, see Figure 2. 24) configuration the correlation proposed is:

$$C_f = \frac{55.3}{\mathrm{Re}} + 0.90 \qquad [2.32]$$

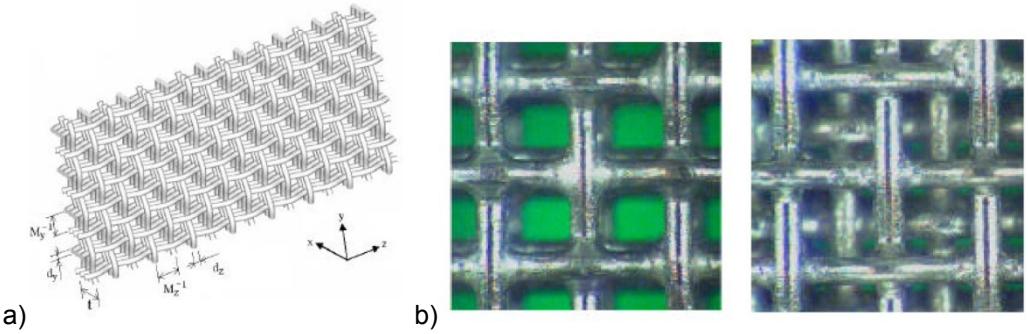

a) b)

Figure 2. 24: a) Screen laminate geometry and b) Inline and staggered stacked plain weave screen (Park, et al., 2002).

Park et al. (Park, et al., 2002) indicated that screen-laminate matrices can be modelled as a porous media. Since the fluid flow path length through the porous wall is short and flow rates are relatively high, local thermal equilibrium between the fluid and solid phases is probably not achieved; so a two-energy equation model is called for.

Ibrahim (Ibrahim, et al., 2004) performed a series of experiments to investigate the oscillatory flow and pressure drop through complex geometries (a rectangular duct with and without inserts). They found that the pressure drop of the oscillatory flow increases with increasing Reynolds number. In the cases studied where they used different inserts into the rectangular duct, the pressure drop has three sources: inertia, friction and local losses.

Luo (Luo, 2004) proposed a new perspective for understanding and evaluating the flow characteristics in oscillating-flow regenerators. In his study, the inertia effect is included, and the pressure drop is considered as a vector. The authors indicated that in addition, the unusual increase of the pressure drop in the oscillating-flow regenerator may result from early triggering or intensification of turbulence and entrance effects in the complex geometry structure.

Tian et al. (Tian, et al., 2004) experimentally investigated the overall pressure drop and heat transfer of stacked woven wire brazed copper matrix under steady-state forced air convection conditions for different topologies (Figure 2. 25). Results show that the friction factor of bonded wire screens is not simply a function of porosity as stochastic materials such as open-celled metal foams and packed beds, but also a function of orientation (open area ratio). For the range of Reynolds numbers considered, the friction factor based on the unit pore size depends mainly on the open area ratio.

Wu et al. (Wu, et al., 2005) measured the pressure drop of flow through woven wire metal (plain-square type) screens. The Reynolds number based on the equivalent spherical diameter of the metal screen ranged from 85 to 12000 and the range of porosity was from 0.83 to 0.92.

The authors noted that in order to obtain good agreement between the fitted empirical equation and measured data, a specific empirical equation should be developed for each type of woven metal screen. The authors, based on the measured pressure drops of four woven metal screens (plain square type) developed an empirical equation of the friction characteristic for plain-square-type metal screens. The empirical equation is

$$C_f = 250\frac{1-\Pi_v}{\mathrm{Re}} + 1.69\left(\frac{1-\Pi_v}{\mathrm{Re}}\right)^{0.071} \quad [2.33]$$

where they defined the friction coefficient and the Reynolds number based on the volumetric porosity of the matrix.

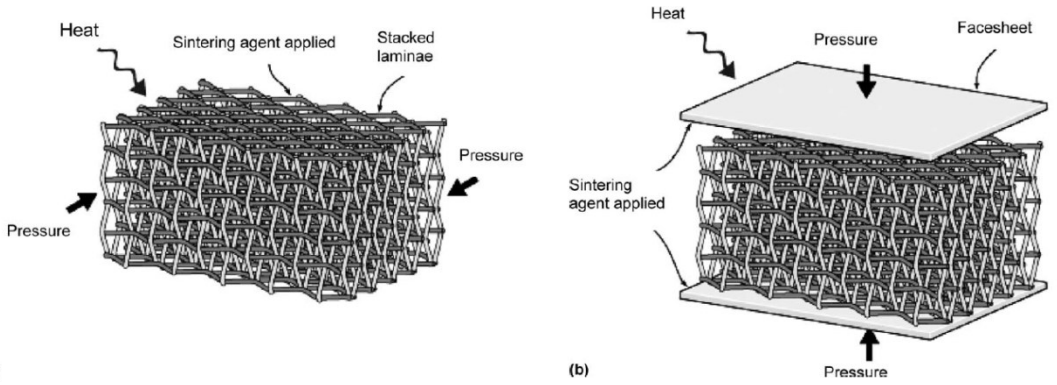

Figure 2. 25: Sandwich construction: a) joins the wire-mesh screen laminated at all points of contact; b) face sheets are added to the textile core (Tian, et al., 2004)

Ju and Shen (Ju, 2009) presented a review on previous experimental results and correlations of the friction factor for cryocooler regenerators. They covered oscillating flow and pulsating pressure conditions, for different mesh sizes of stacked woven wire screens, focusing on the effects of different operating frequencies ranging from 20 to 80 Hz. The authors presented a comparison of the friction factor data with those of other studies to clarify the reason for the difference. Ju and Shen (Ju, 2009) proposed an oscillating flow correlation of regenerators based on Reynolds number which can be applied in the range of 20 to 80Hz.

$$C_f = \frac{97.4}{\mathrm{Re}} + 1.67 \quad [2.34]$$

Thomas (Thomas, 1999) (Thomas, et al., 2000) compared different well known and often used correlations for the flow friction factor of Stirling engine regenerators (stacked woven wire and random fiber). For each correlation the authors summarized the experimental methods and the geometric constraints in terms of the range of wire diameter and porosity. Also, the author derived one general applicable set of equations for the Reynolds number and the friction factor in order to show all data in one plot as shown in Figure 2. 26.

Thomas (Thomas, 1999) (Thomas, et al., 2000) analysed Figure 2. 26, which clearly shows that Miyabe's (Miyabe, et al., 1982) correlation predicts the smaller friction factor or pressure drop together with Tong and London (Tong, 1957) and Gedeon and Wood (Gedeon, et al., 1996) predicts the highest friction factors. The correlation from Tanaka et al. (Tanaka, et al., 1990) for an oscillating flow is in the same range of magnitude as the data predicted by the other authors for steady flow conditions. Thus, Thomas and Pitman (Thomas, et al., 2000) concluded that the impact of the oscillating flow on the pressure drop of the regenerator is small.

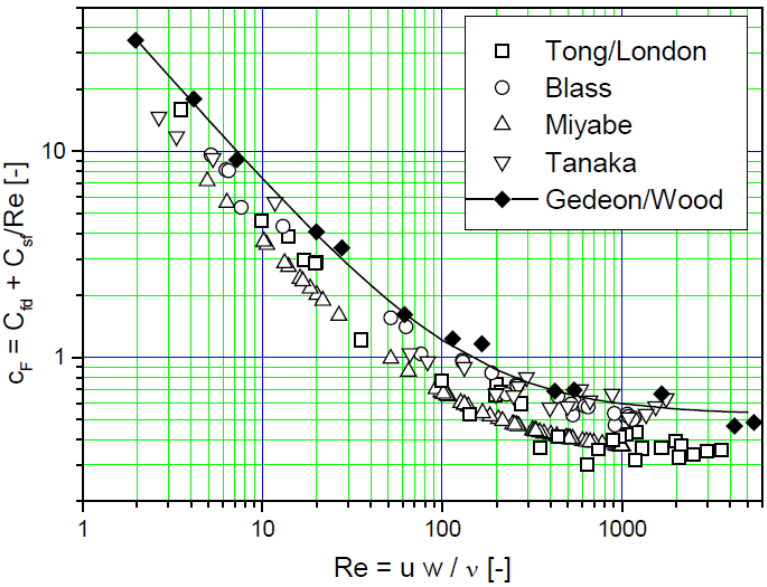

Figure 2. 26: Friction factor according to general applicable set of equations vs. Reynolds number for wire screens (Thomas, et al., 2000)

II.3.2.2 Heat Transfer

Tong and London (Tong, 1957) reported measurements of friction factor and mesh heat transfer coefficient for inline plain weave laminate and staggered cross-rod matrices (no interweaving). They used a calorimetric method to measure the local heat transfer coefficient of one heated filament inside the array. In their investigation both kind of screens were oriented at 45º with their neighbour in order to simulate a “random stacking” in contrast to a “regular stacking”.

Kays and London (Kays, et al., 1964) proposed curves of heat transfer characteristics (Figure 2. 27) for random stacked woven wire mesh matrices with various porosities (from 0.602 to 0.832) based on experimental results.

Miyabe et al. (Miyabe et al., 1982) derived a generalized experimental correlation of the Nusselt number for stacked wire screens based on experiments carried out by a steady flow apparatus:

$$Nu_d = 0.42\,\mathrm{Re}_d^{0.56} \qquad [2.35]$$

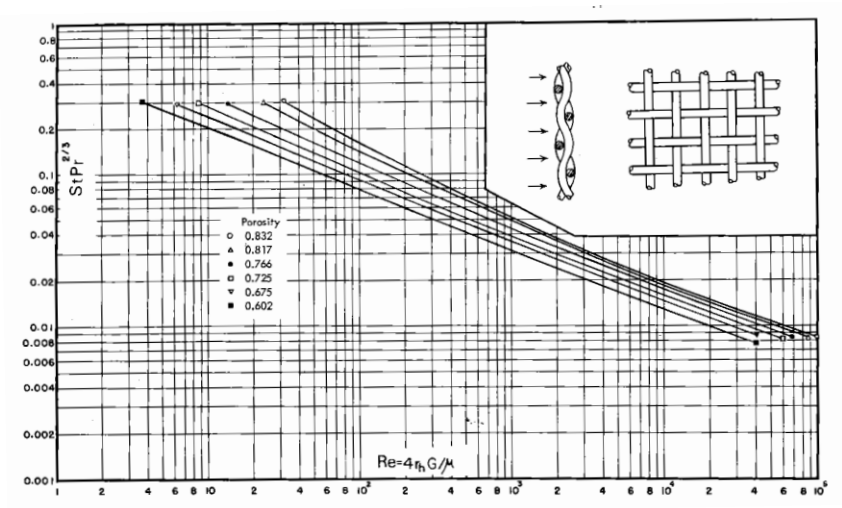

Figure 2. 27: Flow through an infinite randomly stacked woven-screen matrix: Heat transfer (Kays, et al., 1964)

The Nusselt number and Reynolds number are both based on wire diameter where:

$$Nu_d = \frac{d_w h}{k_g} \quad [2.36]$$

$$\mathrm{Re}_d = \frac{\rho_g u_{\max} d_w}{\mu} \quad [2.37]$$

where d_w is the wire diameter, h is the heat transfer coefficient, μ is the dynamic viscosity, ρ_g is the density of the working gas and u_{max} is the maximum fluid velocity.

Miyabe et al. (Miyabe, et al., 1982) reported heat transfer coefficient correlation for plain-weave screen laminates that are in close arrangement with those of Tong and London (Tong, 1957). Miyabe et al. (Miyabe, et al., 1982) observed that if there is a gap between the screens the friction factor and the Nusselt number will deviate from the actual value.

Tanaka et al. (Tanaka, et al., 1990) obtained the following empirical correlation for the Nusselt number through stacked woven wire matrices:

$$Nu = 0.33\,\mathrm{Re}^{0.67} \quad [2.38]$$

where the Nusselt and Reynolds numbers are average values referred to the hydraulic diameter, as in Eq. [2.24]. Unlike what was expected, the results of Tanaka et al. (Tanaka, et al., 1990) for the heat transfer coefficient in an oscillating flow were lower than that in an unidirectional flow obtained by Hamaguchi et al. (Hamaguchi, et al., 1984).

Gedeon and Wood (Gedeon, et al., 1996) presented a generic correlation for the Nusselt number in terms of Peclet number and volumetric porosity of the matrix, indicating that the correlations should be used together with the enhanced axial conduction correlation in an oscillating-flow regenerator model. The authors pointed out that porosity has a fundamental physical effect on Nusselt number and axial conductivity ratio that overwhelms any structural variations. The final correlating expression for woven wire matrix is:

$$Nu = \left(1 + 0.99 Pe^{0.66}\right)\Pi_v^{1.79} \quad [2.39]$$

where Pe is the Peclet number. Gedeon and Wood (Gedeon, et al., 1996) noticed the strong dependence of both, Nusselt number and axial conductivity ratio, on porosity; the Nusselt number increases with porosity while the axial conductivity ratio decreases.

Gedeon and Wood (Gedeon, et al., 1996) compared the results obtained by others under steady-flow conditions and their results under oscillating-flow conditions. Basically, the conclusion was that both, the heat-transfer and the friction factor, only depend on the local instantaneous Reynolds number. However, there is no known experimental apparatus that directly measures the heat transfer coefficient in realistic regenerator matrices, therefore the heat transfer coefficient is generally deduced from temperature in steady-flow conditions in both ends of regenerator matrix.

Gedeon and Wood (Gedeon, et al., 1996) suggested that in the experimental studies the omission or neglecting the axial thermal diffusion will introduce progressively larger errors into their data reduction methodology for Peclet (Reynolds) number below 10. For that reason Gedeon and Wood (Gedeon, et al., 1996) proposed an effective Nusselt number in accordance with the assumptions behind the Kays and London (Kays, et al., 1964) correlations: The

effective Nusselt number proposed captures the total oscillating-flow regenerator heat flux and for woven wire matrix it is written as:

$$Nu_e = \left(1 + 0.64 Pe^{0.72}\right) \Pi_v^{1.79} \quad [2.40]$$

Thomas (Thomas, et al., 2000) (Thomas, et al., 2000) compared different well known and often used correlations for the Nusselt number of Stirling engine regenerators (stacked woven wire and random fiber). The authors defined one general applicable set of equations for Reynolds, Nusselt number and the heat transfer area used to compare and evaluate the different correlations. Thomas (Thomas, et al., 2000) observed that with the exception of Tanaka's data (Tanaka, et al., 1990), the recalculation of the data of other authors reveals the impact of the porosity on the Nusselt number.

Tian et al. (Tian, et al., 2004) experimentally investigated the heat transfer of stacked woven wire brazed copper matrix under steady-state flow. They concluded that the overall heat transfer depends on porosity and surface area density, but only weakly on orientation. Consequently, for a fixed surface area density, an optimal porosity for maximum heat dissipation exists.

Tao et al. (Tao, et al., 2009) numerically investigated the fluid flow and heat transfer performances of mesh regenerators under different geometric mesh parameters and material properties based on an anisotropic porous media. The results indicate that the cooling power increases with the increases of specific heat capacity and density of the regenerator mesh material, and decreases with the increases of penetration depth and thermal conductivity ratio.

Forooghi et al. (Forooghi, et al., 2010) numerically investigated the steady and pulsatile flow heat transfer in a channel lined with two porous layers subject to constant wall heat flux under local thermal non-equilibrium conditions. The objective of their work was, first to assess the effects of local solid-to-fluid heat transfer (a criterion indicating on departure from local thermal equilibrium conditions), solid-to-fluid thermal conductivity ratio and porous layer thickness on convective heat transfer in steady condition inside a channel partially filled with porous media; secondly, to examine the impact of pulsatile flow on heat transfer in the same channel. They concluded that the overestimation of local thermal equilibrium assumption is not more than 5% in a typical problem.

II.3.3 Numerical (CFD) Studies

The phenomena occurring in Stirling regenerators are quite complex, due to the combination of the transient nature of the flow and heat transfer phenomena. On one hand the equations for determining the behaviour of the regenerator constitute a system of nonlinear partial differential equations unlikely to be resolved by direct methods. On the other hand, the experimental studies due to the internal structures of the regenerator matrix are limited and expensive, in terms of facilities and manpower, and it is proportional to the number of data and the number of configurations tested (Ibrahim, et al, 2001). Consequently, numerical analysis is necessary for regenerator design.

The use of computational fluid dynamics (CFD) models significantly extends the capabilities of analysis for the complex geometry of the regenerator beyond the analytical simplification and experimental limitations. It is also an inexpensive tool compared to experimentation.

Different methods can be applied for the numerical analysis of the gas flow through the regenerator. One method is to assume that the regenerator is filled with a porous medium. Another method consists in simulating a small portion of the matrix of the regenerator where the flow is simulated in detail.

O´Hern and Torezynski (O´Hern, 1993) presented combined experimental and numerical examinations of the steady laminar flow through highly-uniform fine-mesh photo-etched screens. The authors performed 3-D flow simulations for flow through the mesh screen. The

drag coefficient determined from the simulations over predicted the experimental values. The principal cause of this overprediction appears to be that the screen wires in the computational model have rectangular cross sections.

Yaron (Yaron, 1994) in Phillips Laboratories used CFD to evaluate 2-D flow characteristics of a rolled foil regenerator used in cryocoolers. The author obtained a pressure drop and convective heat transfer correlations for the rolled foil regenerator within various flow rates.

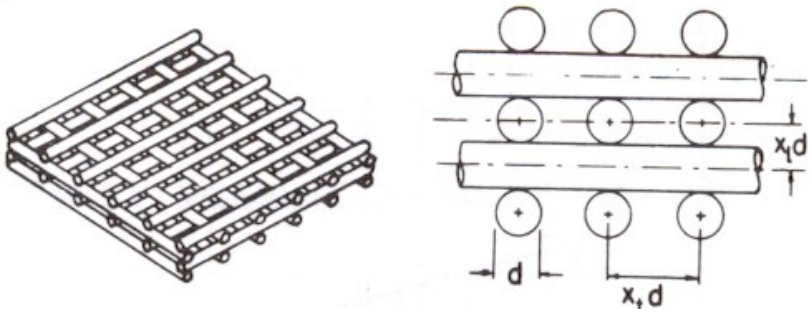

Figure 2. 28: A Cross Rods Matrix, Inline Stacking (Ibrahim, et al., 2001)

Ibrahim et al. (Ibrahim, et al., 2001) worked with different Stirling-engine development companies, STC and Sunpower, and on several government-funded Stirling-engine research projects in the study and identification of important issues faced concerning the regenerator. They conducted a fundamental research for improving the regenerator heat transfer while reducing pressure drop. At the beginning the authors chose random-fiber regenerators as the most promising for commercialization conducting analytical, experimental and numerical studies. They preliminary modelled the regenerator matrix over a range of steady Reynolds numbers representative of different instants during the periodic cycle starting with singles cylinder geometries (Figure 2. 28). The objective of this preliminary modelling was to compare the results of CFD modelling against correlations for pressure-drop and heat transfer in an identical geometry published by Kays and London.

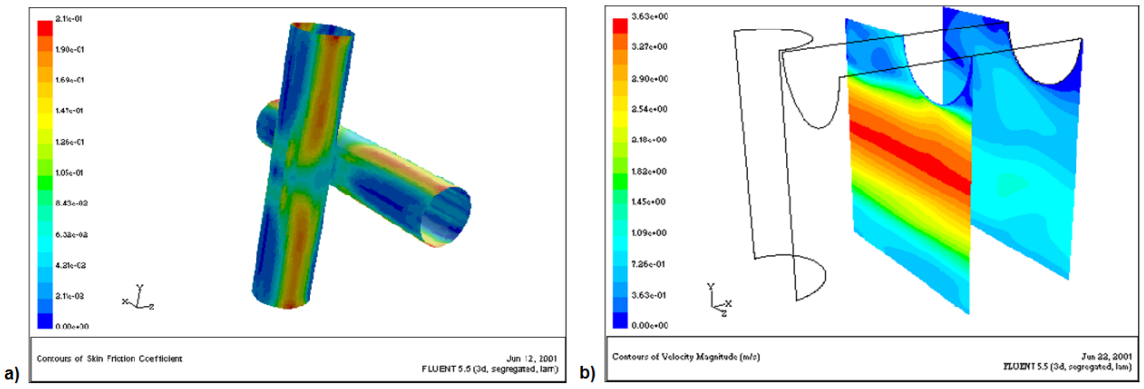

Figure 2. 29: CFD Results for: a) Skin Friction Factor and b) Velocity Contours (Ibrahim, et al., 2001)

Also, Ibrahim et al. (Ibrahim, et al., 2001) worked on CFD to develop a multi-dimensional computer model of a portion of the regenerator matrix. The modelling effort took place in the following areas: multi-cylinder regenerator, the designed test rig and the porous media via momentum resistance modelling. Regarding the multi-cylinder (Cross-Rods Matrix) modelling; the first simulation conducted was a 3-D model of 9 wires in cross flow arrangements (Figure 2. 28) for steady state flow. Figure 2. 29 shows typical results for the contours of the skin friction and the velocity contours (m/s) at a particular cross section in the computational domain. Later a 2-D simulation for a single cylinder with Re= 100 in transient conditions was conducted. For that case a finer grid was attempted and heat transfer was employed by keeping the fluid at 300 K and the cylinder wall at 310 K. Figure 2. 30 shows the velocity and temperature contours for this case at a certain given time.

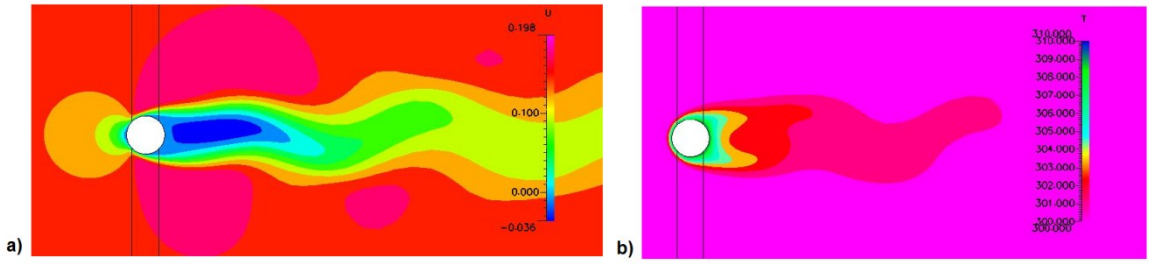

Figure 2. 30: Cylinder in Cross Flow, Re=100: a) Velocity Contours and b) Temperature Contours (Ibrahim, et al., 2001)

Rühlich and Quack (Rühlich, et al., 2002) investigated and compared regenerator matrices using CFD with various shapes and arrangements in order to improve regenerator performance (see Figure 2. 31). Their results revealed the influence of geometrical parameters on the ratio of pressure drop and heat transfer regenerator matrices and indicated that the best results would be expected in matrices where accelerations and decelerations are minimal.

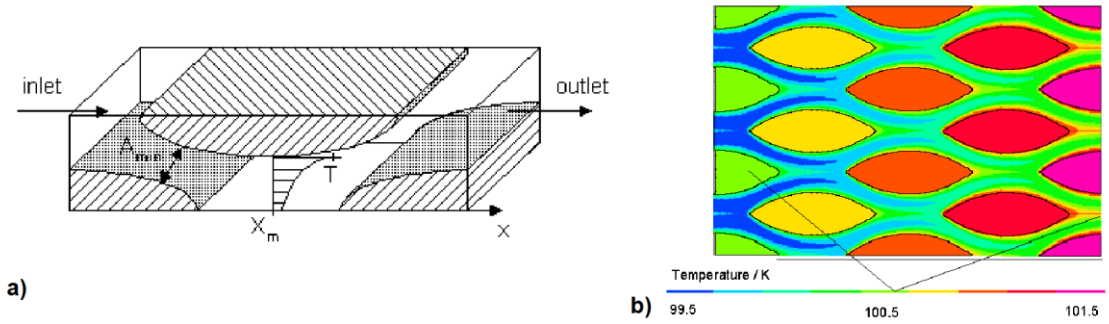

Figure 2. 31: a) Unit-cell and b) Temperature Field (Rühlich, et al., 2002)

Harvey (Harvey, 2003) performed a demonstration calculation using the CFD software Fluent (ANSYS, 2009), he modelled a solid representative, periodic cell of woven wire mesh. A steady flow through the mesh was then simulated. Figure 2. 32 shows some preliminary results of this type of simulation. These simulations were performed for steady flows only.

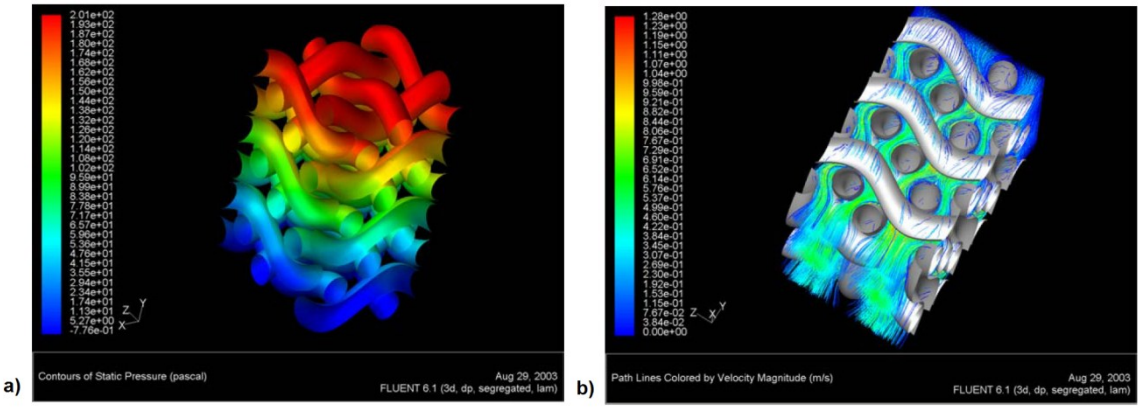

Figure 2. 32: Demonstration calculation for flow through wire mesh screens: a) Surface pressure and b) Pathlines (Harvey, 2003)

Yarbrough et al. (Yarbrough, et al., 2004) investigated the pressure drop under steady and oscillating flow conditions through a wire screen regenerator using Fluent. The authors compared three different computational models of matrices: 3-D model of plain weave wire screens, a 2-D staggered tube bank model (the oscillating flow was only used in this model) and a porous media regenerator model (Figure 2. 33). The 3-D model of plain weave wire screen was formed by one, two and three screens or layers without contact and with a rotating angle in order to avoid a direct flow path (Figure 2. 34a).

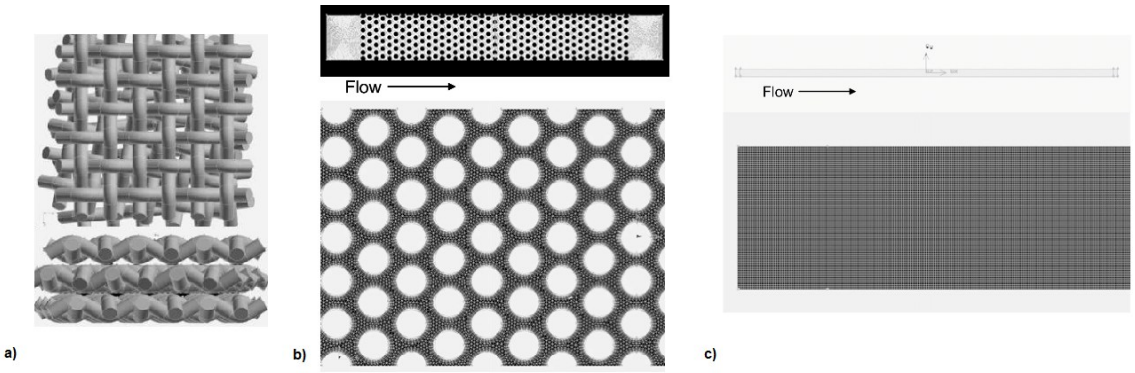

Figure 2. 33: Model Investigated: a) 3-D plain weave wire screens model; b) 2-D staggered tube bank model and c) porous media model (Yarbrough, et al., 2004)

Yarbrough et al. (Yarbrough, et al., 2004) compared their CFD results with steady unidirectional flow published data (Tong and London (Tong, 1957), Miyabe et al. (Miyabe, et al., 1982) and Tanaka et al. (Tanaka, et al., 1990)) as it is shown in Figure 2. 34b. They obtained higher friction factor than the experimental data for all the 3-D models of wire screen. They justified the differences based on the computational model limitations, testing conditions and experimental measurement points. The authors concluded that for wire screen, 3-D modelling is the most realistic method compared to actual regenerators but it is limited by computational size and requirements; therefore they pointed out that the porous media as the most promising model despite needing some empirical input such as permeability and resistance factors.

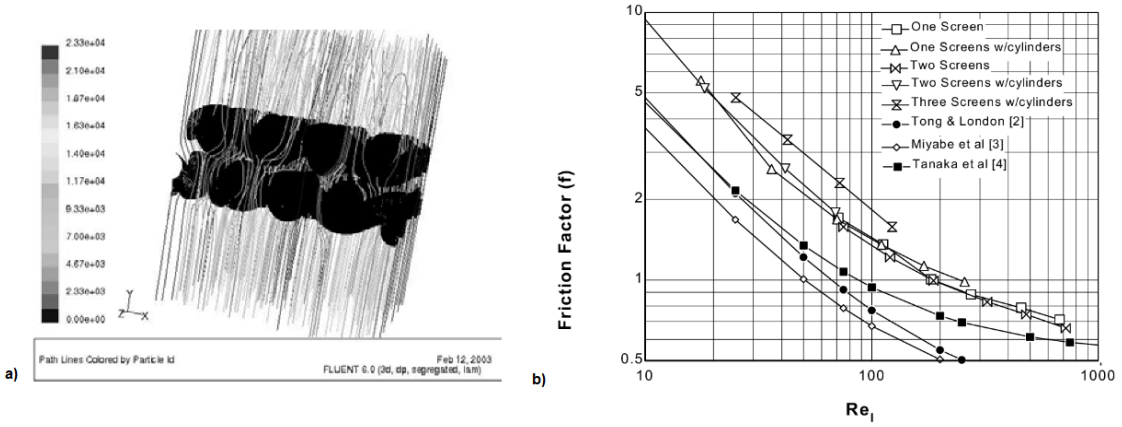

Figure 2. 34: a) Flow path lines for a 3-D two-screen model and b) Friction factor versus Reynolds number comparison for multi-screen models and published correlations (Yarbrough, et al., 2004)

Hieke et al. (Hieke, 2005) performed 3-D numerical simulations under steady state regimes on the flow inside small reference volumes of different geometries of the regenerator matrix. The author modelled three configurations of woven wire matrices: perfectly aligned stacked (Figure 2. 35c), wound (Figure 2. 35a) and inclined as it is shown in Figure 2. 35. The last two models included a plane foil stripe between the screens in order to avoid intermesh or mesh penetration, the authors proposed this in order to simplify the winding process.

The calculation procedure under steady-flow applied by Hieke et al. (Hieke, 2005) is illustrated graphically in Figure 2. 36a. The author established the periodic temperature manually by iteration, in other words, the fluid inlet temperature is varied in the course of the iteration process until the temperature difference between solid and fluid becomes constant over the length of the unit cell.

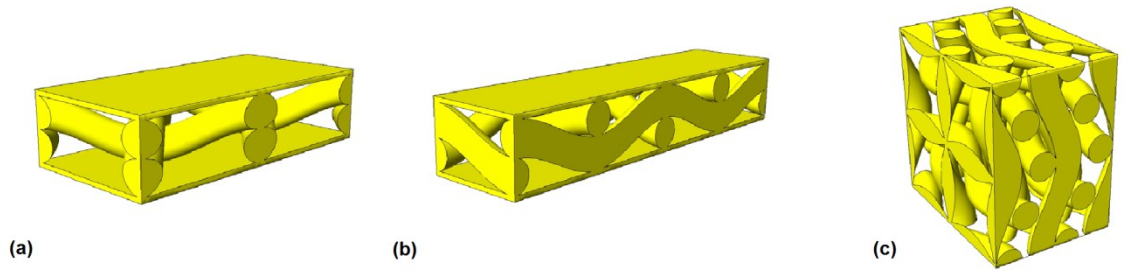

Figure 2. 35: Simulated Unit Cell Volumes (Hieke, 2005)

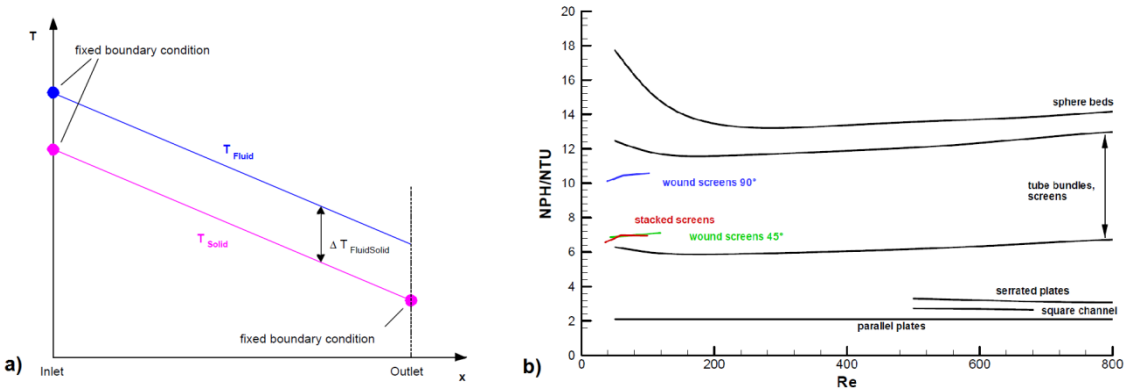

Figure 2. 36: a) Temperature Boundaries Conditions and b) Ratio between Pressure Drop and Heat Transfer (Hieke, 2005)

The results obtained by Hieke et al. (Hieke, 2005) show that the ratio between pressure drop and heat transfer is higher for the wound woven wire matrix and practically the same for the other two models (see Figure 2. 36b). The author indicated that the idealized model with perfectly stacked screens might lead to predicting better performance characteristic than those effectively achieved in real regenerators and that randomly stacked regenerators might only be simulated with considerable difficulties. Figure 2. 37 shows the streamlines obtained by Hieke et al. (Hieke, 2005).

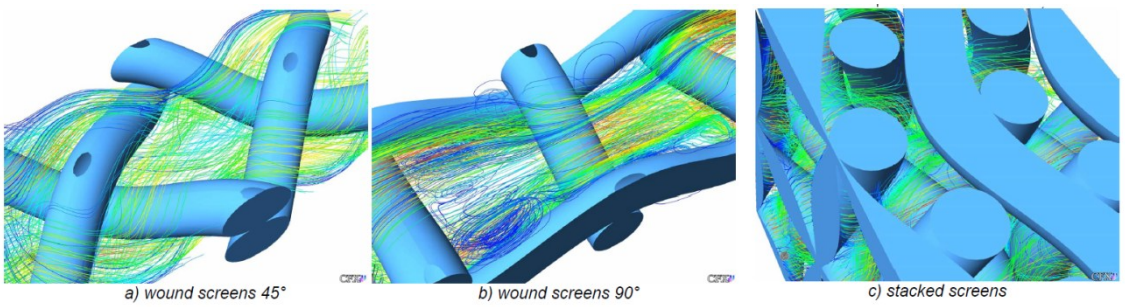

Figure 2. 37: Path lines in the models simulated (Hieke, 2005)

Dyson et al. (Dyson, et al., 2005) (Dyson, et al., 2005) (Dyson, et al., 2008) worked in a project to enhance the Stirling industry´s suite of design tools beyond the currently employed 1-D analysis to the level of a virtual 3-D full convertor including structural, mechanical, electromagnetics, and thermal dynamics (see Figure 2. 38). They demonstrated that 1-D analysis has an important place in Stirling engine design, but the designed process really needs multidimensional capability as well to: properly simulate inherently 3-D turbulence (including transition), provide empirical heat transfer and friction factor coefficients for complex geometries to aid in hardware, assist experimentalists in determining flow and heat transfer physics in regions where measurements are difficult or impossible, etc. The authors indicated that the regenerator is difficult to model and since the regenerator roughly has a heat transfer which is 3

to 40 times more effective than the heater, any inefficiency of the regenerator represents a significant drawback for the entire Stirling engine. Hence, any numerical losses or inaccuracy in this region will disproportionately influence the entire Stirling simulation. Also, the geometrical shape of the matrix elements in the regenerator is important. In their model a representative elementary volume is often used and requires some closure assumptions that can be partially derived from experiment and potentially from micro-scale (pore level) numerical simulations.

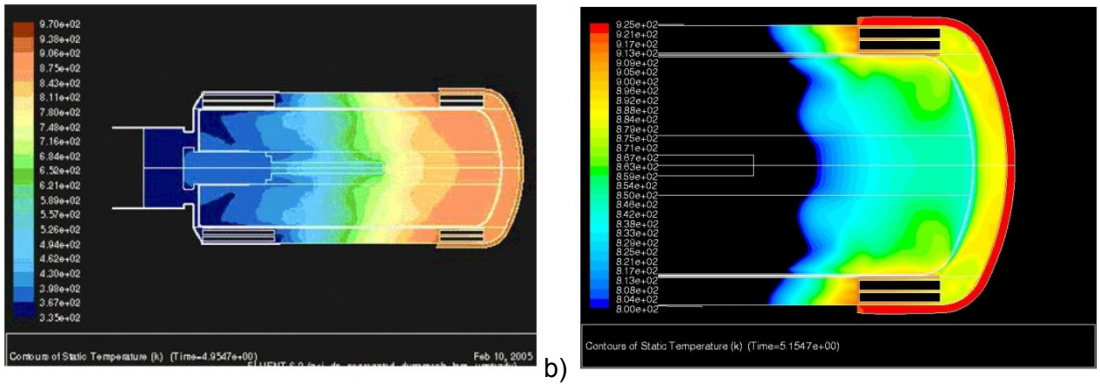

Figure 2. 38: a) Transient Simulation of Stirling Convertor-Colour by Temperature and b) Hot end regenerator temperature (Dyson, et al., 2005)

Tew et al. (Tew, et al., 2007) conducted many numerical simulations of different regenerator structures. The initial concept considered by the authors was a “lenticular” structure which is shown in a 2-D CFD result schematic in Figure 2. 39, this kind of matrices produced high Figure of Merit; comparisons of a lenticular Figure of Merit with those of the theoretical parallel-plate, random fiber, and a hexagonal array.

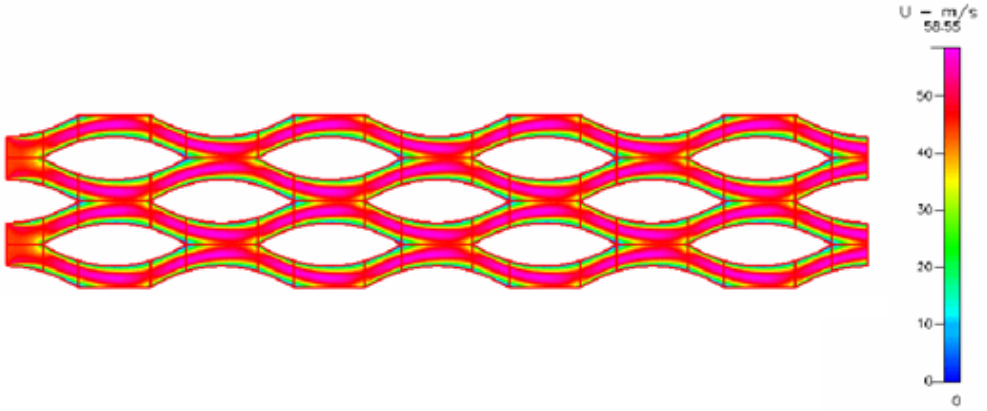

Figure 2. 39: Lenticular concept. A 2-D representation with CFD calculated velocity contours (Tew, et al., 2007)

Tew et al. (Tew, et al., 2007) used the Fluent CFD commercial code for 2-D and 3-D (steady and unsteady) fluid flow and heat transfer simulations of the segmented-involute-foil regenerator. The authors simplified or approximated the models in order to obtain a feasible computational model as shown in Figure 2. 40. The main simplification were: symmetries or angular periodicity, straight wall channels, a stack of just two types of alternating layers for steady-flow simulation, a stack of six layers for the transient oscillating model, etc.; it was expected that all these approximations capture most of the 3-D flow phenomena in the regenerator matrix.

The knowledge gained by Tew et al. (Tew, et al., 2007) enabled fundamental understanding of how fluid flow and heat transfer takes place inside the segmented-involute foil flow paths. It also helped to provide support for physical testing (large-scale and actual-size); comparison of the micro-scale CFD results with the test results and Sage 1-D code simulations, provided additional insight for making decisions about the involute-foil design details.

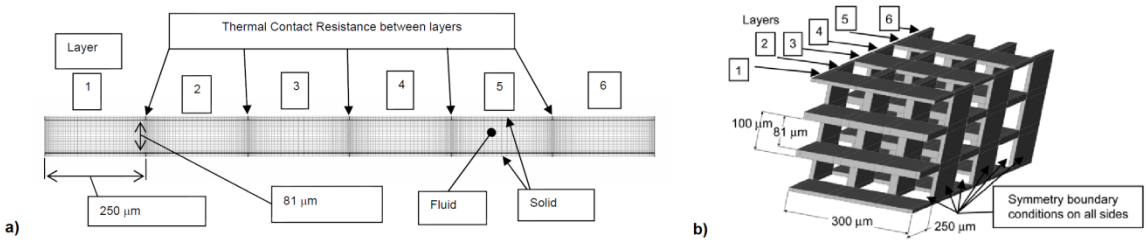

Figure 2. 40: a) 2-D Computational domain and b) 3-D straight-channel-layers computational domain (Tew, et al., 2007)

Ibrahim et al. (Ibrahim, et al., 2007) numerically simulated utilizing commercial CFD software (Fluent) under both steady-state and oscillatory-flow conditions the micro-fabricated involute-foil regenerator. The geometry consisted of a stack of disks with each disk containing involute-shaped micron-range channels, with channel flow direction perpendicular to the plane of the disk. The lateral orientation of the channels alternates from disk to disk in the flow direction. Simulations were done for both 2-D and 3-D computational domains. Steady-state simulations were performed for Reynolds numbers from 50 up to 2000 based on the channel hydraulic diameter and the mean flow velocity. Oscillatory flow simulations were conducted for maximum Reynolds number of 50 and a Valensi number of 0.229. The results of the CFD research were validated by comparing the CFD data with the literature and obtained experimental correlations.

Ibrahim et al (Ibrahim, et al., 2009) studied the effect of changing the oscillation frequency in a 2-D simplified model and they concluded that a change in frequency would alter both, the fluid flow and the heat transfer behaviour. Ibrahim et al (Ibrahim, et al., 2009) observed that the shapes of the friction factor and mean Nusselt number curves are similar for the 2-D and 3-D models as it is shown in Figure 2. 41. However, the effect of going from 2-D to 3-D resulted in shifts upward of both friction factor and mean Nusselt number curves, as might be expected because the 2-D simulations do not include the flow perturbations resulting from flow around the ends of the foil layers.

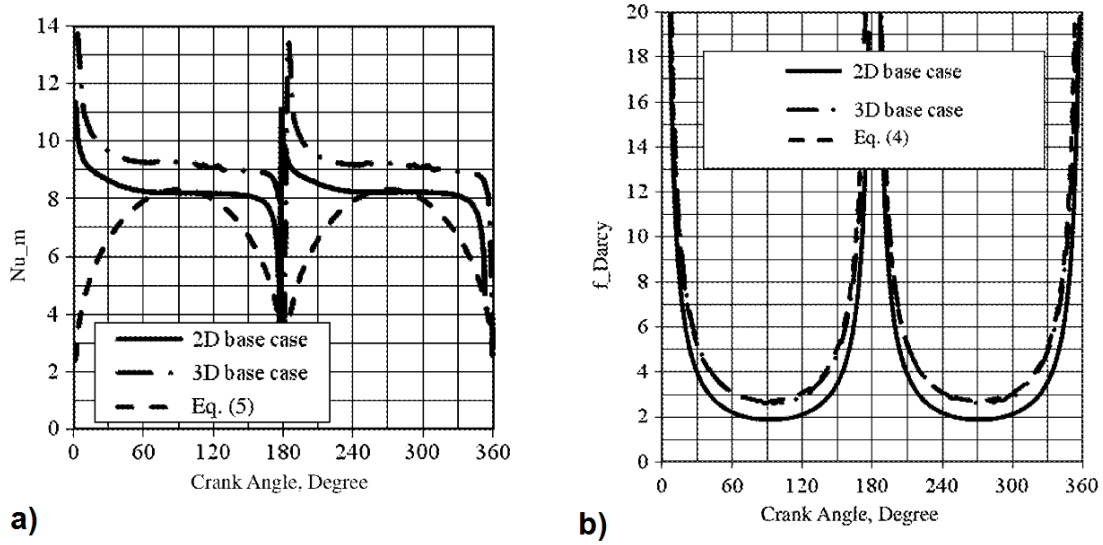

Figure 2. 41: Comparison between 2-D and 3-D oscillatory flow: a) mean Nusselt number and b) Friction factor (Ibrahim, et al., 2009)

Cha et al. (Cha, et al., 2007) performed CFD simulations for periodic flow, axisymmetric, 2-D test section of their test of pulse tube regenerators. They modelled the regenerator section as an isotropic porous medium with the assumption of local thermal equilibrium between the porous structure and the working fluid. The objective was to obtain the radial permeability and coefficients of inertia by trial and error. Cha et al. (Cha, et al., 2007) shown in their investigations that current CFD tools are in fact capable of simulating entire Pulse Tube

Regenerator devices, and can be useful tools for the final stages of design and optimization. These simulations provide detailed system and component-level information about the flow field and heat transfer processes that are beyond the current experimental measurement possibilities. However, such detailed design and optimization calculations are only reliable if the properties of all the components, in particular the regenerator, are known with reasonable accuracy. The existing regenerators are generally composed of micro porous solid structures, most of which are morphologically anisotropic. The hydrodynamic and thermal transport properties of the most widely-used regenerator filler materials are not well-understood. Among the poorly-understood and badly-needed properties are the permeability and inertia coefficient matrices, as well as the solid-fluid volumetric heat transfer coefficients under steady and periodic flow conditions.

Cha et al. (Cha, et al., 2008) investigated the pressure drop through Stirling regenerators. They established a systematic experimental and CFD-based procedure for the quantification of directional permeability and Forchheimer's coefficient for porous structures under steady-periodic flow conditions. In their investigation, the methodology applied for the quantification of the longitudinal and radial flow parameters for some widely used regenerator matrices (metallic mesh screens, sintered mesh screens, metal foam, stack of micro-machined nickel dicks, etc.) for pulse tube and Stirling cryocoolers. Cha et al. (Cha, et al., 2008) used Fluent CFD to model the entire test sections assuming an axisymmetric, 2-D flow mode and porous medium with local thermal equilibrium regenerator assumption. By systematic and iterative CFD simulations, the permeability and Forchheimer inertial coefficients were optimized to lead an agreement between simulations and measurements for the tested regenerator matrices. The obtained results showed that except for very low oscillation frequencies the cycle average friction factor under oscillatory flow conditions is different from the steady-flow friction factor. However, the directional permeability and Forchheimer inertial coefficients were found to be independent of the frequency of flow oscillations for the frequency range 5–60 Hz.

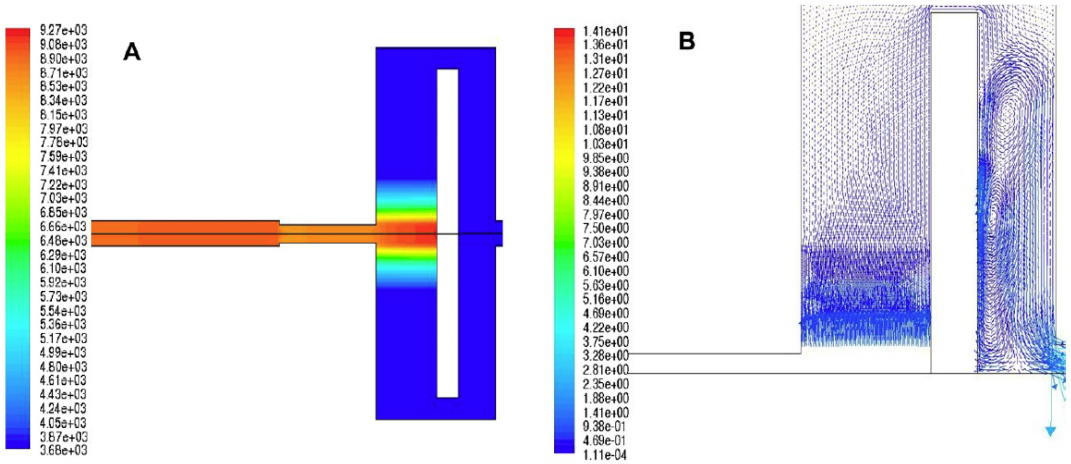

Figure 2. 42: Simulated regenerator pressure (A), in (Pa) and velocity vectors (B), in (m/s), in a snapshot for the 40 Hz frequency. (Cha, et al., 2008)

Mortazavy et al. (Mortazavy, et al., 2008) performed a 3-D numerical analysis to investigate the thermal/fluid characteristics of a special anisotropic stacked woven wire mesh structure (see Figure 2. 43a). They studied under oscillating flow conditions the effect of area to volume ratio, porosity, weight and material structural configuration of the mesh as well as flow parameters, such as the fluid flow rates, pressure drop characteristics and thermal performance of the regenerator. The conclusion of their study is that the thermal ratio of the regenerator will be increased due to higher reduced lengths and to higher angular velocities.

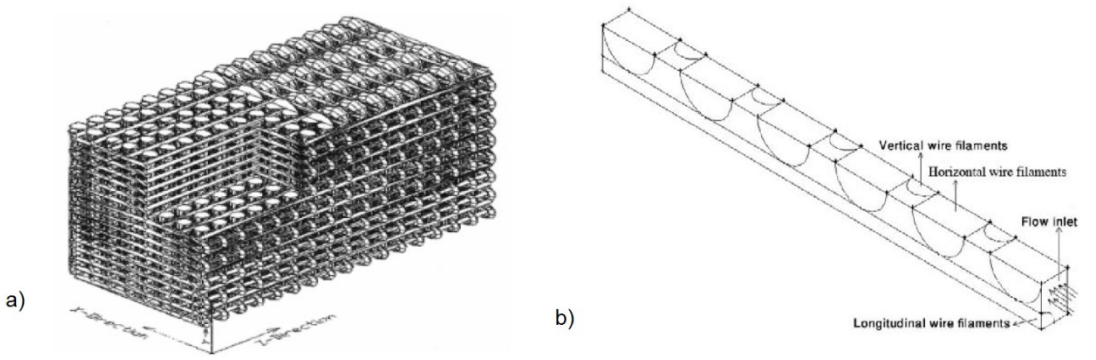

Figure 2. 43: a) 3D orthogonal "stacked" weave and b) Computational domain for a 3D stacked weave (Mortazavy, et al., 2008)

Kim (Kim, 2008) numerically studied the flow friction associated with laminar pulsating flows through porous media mainly for understanding the Stirling regenerators and pulse tube cryocoolers. The author simulated a 2-D flow in a system composed of a number of unit cells of generic porous structures using a CFD tool, with sinusoidal variations of flow with time. The author obtained the instantaneous as well as cycle-averaged permeability and Forchheimer coefficients based on the detailed numerical data. The result was that the cycle-averaged permeability coefficients were nearly the same as those for steady flow, but the cycle-averaged Forchheimer coefficients were about two times larger than those for steady flow in pulse tube.

Pathak and Ghiaasiaan (Pathak, 2011) investigated the pore-level thermal phenomena during pulsating and unidirectional sinusoidal flow through a generic 2-D porous medium by numerical analysis. The investigated porous media was modelled as periodic arrays of square cylinders with porosities of 0.75 and 0.84, with flow pulsation frequencies of 0 - 80 Hz for Reynolds numbers of 560 and 980. Based on the numerical data, the instantaneous as well as cycle-average thermal dispersion and heat transfer coefficients were derived. The authors indicated that, for a given Reynolds number at a particular porosity, as the frequency increases, the average convection heat transfer coefficient monotonically increases. As expected the higher flow rates (larger Reynolds numbers) result in greater heat transfer coefficients. Also, the higher porosity configurations resulted in heat transfer coefficients that were lower in magnitude than the lower porosity geometries, in both kinds of flows. Furthermore, the magnitude of the average convection heat transfer coefficients for unidirectional sinusoidal inlet flow is approximately 20% - 40% higher than the pulsating flow average convection heat transfer coefficients.

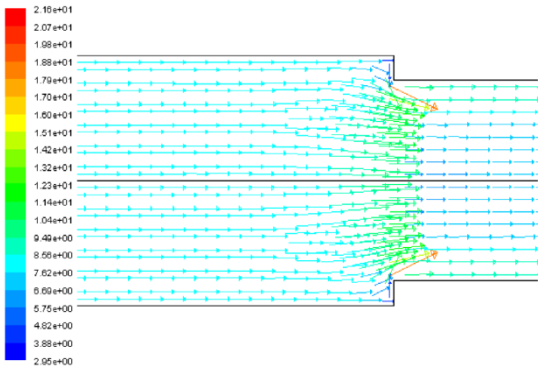

Figure 2. 44: Velocity vectors colour by magnitude (m/s) in the porous section (Landrum, et al., 2009)

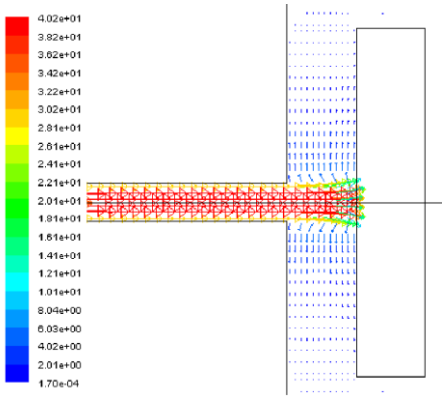

Figure 2. 45: Velocity vectors colour by magnitude (m/s) in the radial porous section (Conrad, et al., 2009)

Landrum et al. (Landrum, et al., 2009) experimentally investigated the effect of average pressure on the porous media through several regenerator fillers and modelled the test section and its vicinity as a porous structure using the Fluent CFD code. The porous media

hydrodynamic parameters were iteratively adjusted to match the model predictions to the experimental results. Using this methodology, the authors determined axial viscous and inertial resistances related to the Darcy permeability and Forchheimer inertial coefficient, respectively. The simulations used a 2-D axisymmetric mesh that modelled the laminar flow within the experimental test setup between static pressure transducers as is shown in Figure 2. 44.

Conrad et al. (Conrad, et al., 2009) determined the hydrodynamic parameters of stacked discs of 635 mesh stainless steel and 325 mesh phosphor-bronze using a 2-D CFD assisted methodology, whereby the hydrodynamic resistance parameters for these fillers are specified when they are modelled as anisotropic porous media (Figure 2. 45). The experimental results indicated that the Darcy and Forchheimer coefficients were generally insensitive to pressure and frequency.

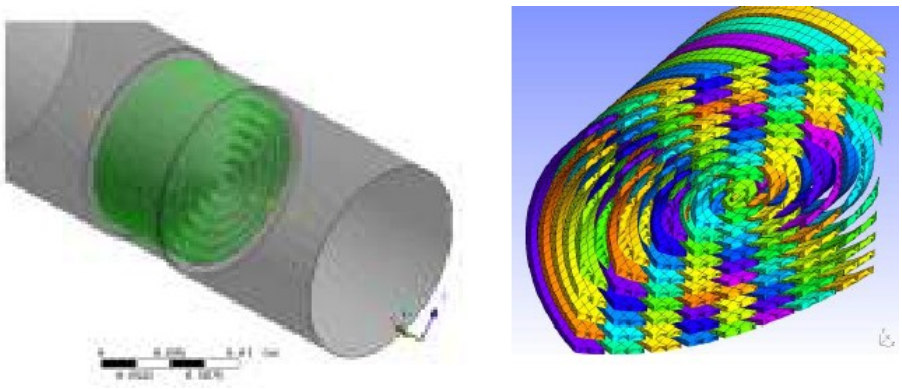

Figure 2. 46: Domain and Section of Regenerator (Avdeychik, et al., 2009)

Avdeychik et al. (Avdeychik, et al., 2009) presented a mathematical model which shows a complete fully developed and verified simulation environment capable of resolving real complex dynamics of alpha type Stirling engines. In the model the regenerator was simulated with several rows of nested concentric rings, (Figure 2. 46.). The authors concluded that the model can be used as an optimization instrument for the Stirling engine to advance its characteristic and properties.

Knefel and Wegenke (Knefel, 2009) simulated the pressure drop through woven wire meshes to optimize its filtration performance reducing the time and expense for developmental test weavings. They generated an accurate 3-D computer model of the woven wire mesh (Figure 2. 47) using a 3-D scanner. Comparison of results from simulations and classic laboratory experiments show a close correlation with minimal deviation.

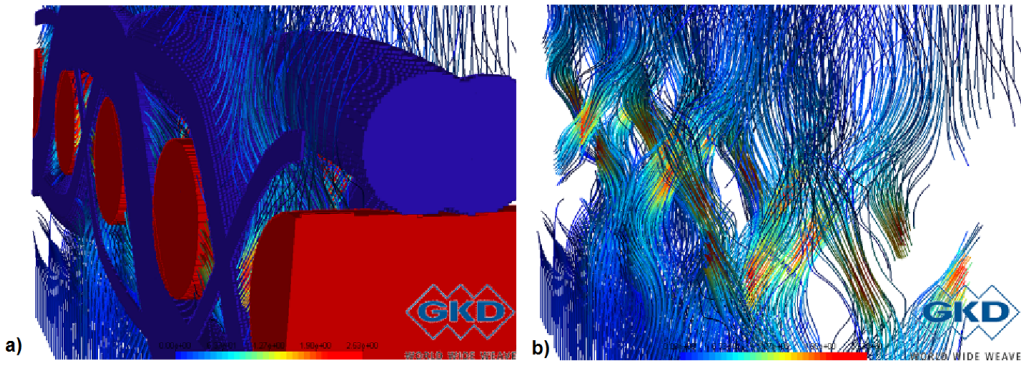

Figure 2. 47: Dutch twilled weave a) Air permeability flow path and b) Pathlines (Knefel, 2009)

Nair and Krishnakumar (Nair, 2009) use a 2-D Local Thermal Equilibrium porous media model to investigate the heat transfer in a wire screen mesh regenerator. The results are compared

with experimental single blow transient testing for laminar flow region ($Re < 1000$). Based on the empirically obtained inertia, viscous resistance factors and the stepped temperature input provided at the inlet section, the temperature response curve is obtained for regenerators of different porosities and materials. They found that there is close similarity between experimental and numerical results. However, they point out that the CFD model does not account for the conductive heat transfer that takes place in the pipe wall while the experimental results are influenced by this phenomenon.

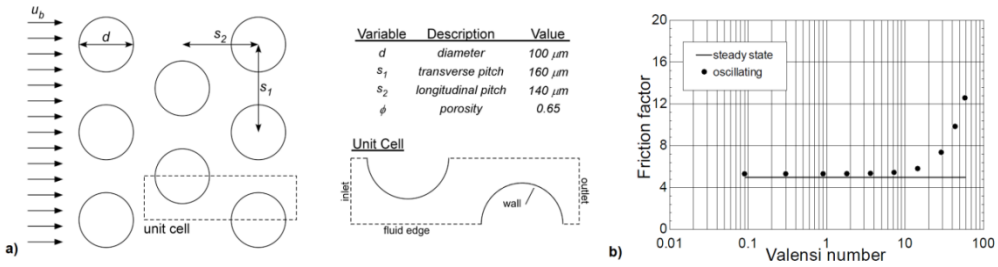

Figure 2. 48: a) 2-D model of Staggered cylinder array geometry and b) Friction factor as function of Valensi number for steady and oscillating flow (Cheadle, et al., 2010)

Cheadle et al. (Cheadle, et al., 2010), using CFD modelled a 2-D micro-scale unit-cell (consisting of a staggered array of cylinders, Figure 2. 48a) of a regenerator matrix to determine the conditions for which oscillating flow affects the friction factor. The results obtained by the authors clearly show a transition Valensi number beyond which oscillating flow significantly increases the friction factor, this Valensi number is approximately 10 as is shown in Figure 2. 48b. However, they indicated that most practical pulse tube regenerators will operate below this Valensi transition number and therefore suggested that the effect of flow oscillation on pressure drop can be neglected in macro-scale regenerator models. In a later work, Cheadle et al. (Cheadle, et al., 2011) developed a 2-D CFD model capable of deriving Nusselt number and friction factor correlations for steady and oscillating flow. The author pointed out that despite that the typical regenerator geometries are packed spheres or wire mesh screens, modelling these geometries would require 3-D models with prohibitively long solution times.

Bommisetty et al. (Bommisetty, et al., 2011) validated a model for a flow in a plain square mesh screen with a particular fractional free area of 0.25 using CFD approach (Figure 2. 49). The simulations were carried out for wide range of screen Reynolds numbers (0.1 to 105) covering both, laminar and turbulent flow regimes. Initial simulations were carried out for an incompressible fluid (water) and further extended to compressible fluid (air). Discharge coefficients obtained from the simulations were compared with experimental values. Effect of compressibility on discharge coefficients is described.

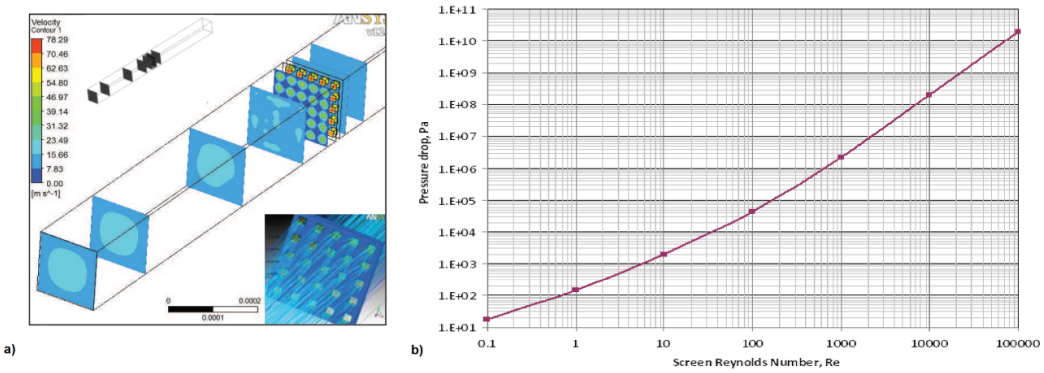

Figure 2. 49: a) Velocity contours at selected planes along the streamwise direction and b) Pressure drop across the channel for various screen Reynolds Numbers (Bommisetty, et al., 2011)

Pathak (Pathak, 2013) carried out a systematic experimental and CFD-based study for the quantification of the Darcy permeability and Forchheimer's coefficient for porous structures,

under steady and periodic flow conditions. The porous regenerator filler was made of spherical particles with an average diameter of 69 µm and a porosity of 38%.

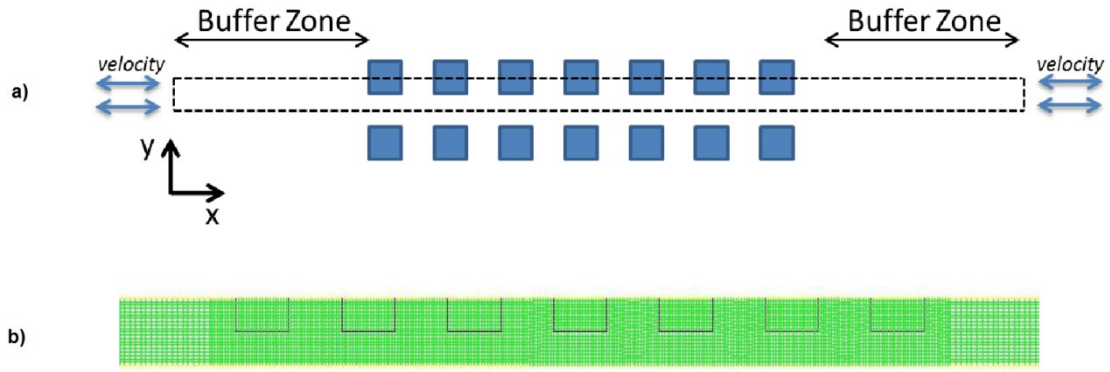

Figure 2. 50: a) Computational Domain and b) 2-D Mesh (Pathak, 2013)

By using systematic and iterative CFD simulations, the author optimized the hydrodynamic parameters leading to excellent agreements between simulations and experimental measurements. Pathak (Pathak, 2013) also conducted a pore-level numerical investigation of the hydrodynamics and thermal energy associated with steady and periodic flow in porous media covering frequencies of 0 - 60 Hz. The generic porous media simulated consists of 2-D regularly spaced square rods arranged in a linear pattern with rows parallel to the direction of the flow field. The domain is similar to those addressed by Kim (Kim, 2008) and Pathak and Ghiaasiaan (Pathak, 2011). Figure 2. 50 displays the physical configuration of the parallel square rods. The detailed numerical data was used for the calculation of the unit cell and cycle-average Darcy permeability, Forchheimer term, and Nusselt number, which appear in the standard volume-average momentum and thermal energy transport equations for flow in porous media. These terms, under periodic conditions, were sensitive to frequency and amplitude, and were significantly different from their counterparts that represented steady flow.

II.4. Literature Review Highlights

From the literature review performed, the following highlights are significant:

- The design and calculation of Stirling engine requires correlations for the friction factor and heat transfer coefficients of the main components, especially the regenerator. The correlations are limited in their range of applicability and no correlations exist for many geometries of interest, for example wound woven wire regenerators.
- Analytical or theoretical studies require many simplifications or assumptions which have repercussion in their precisions.
- Typically, the internal structures of the regenerator matrices are so small that the use of any measurement equipment would cause major disturbances in the flow. For this reason the measurements are only possible at the inlet and outlet of the regenerator limiting the empirical or experimental studies.
- The numerical based CFD studies are the only way to study the flow characteristics inside the regenerator matrix. The 3-D CFD modelling performs better understanding of the flow characteristics inside a regenerator matrix.
- There has been much debate in the literature about the effect of the oscillating flow on the friction factor and the associated adequacy of the steady-flow correlations that are typically used to predict the performance of Stirling regenerators.
- Porous media numerical models request the input of permeability and friction factor which are mostly empirically obtained.

CHAPTER III:

Model Development

III. MODEL DEVELOPMENT

Chapter III presents the fundamental governing equations of fluid dynamics required for computational fluid dynamics (CFD) modelling of flow and heat transfer in Stirling regenerators. The regenerator characterization and the corresponding numerical methodology implemented are also described.

The commercial CFD Fluent code (ANSYS,2009) is used to solve the governing flow equations using the finite volume method (FVM) based numerical discretization technique.

III.1. Governing Equations

The fluid phenomena can be mathematically represented by the Navier-Stokes equations, which are non-linear partial differential equations based on the universal laws of conservation of mass, momentum and energy. Therefore, the fundamental equations obtained from the conservations laws are: the continuity, momentum and energy equations. In the following sections these equations are briefly discussed.

III.1.1 Continuity Equation

The conservation of mass law applied to a fluid passing through an infinitesimal, fixed control volume is written in Cartesian tensor notation as:

$$\frac{\partial \rho}{\partial t} + \frac{\partial}{\partial x_i}\left(\rho u_i\right) = 0 \qquad [3.1]$$

In Equation [3.1] the source term is not included because in the regenerator case no mass is added to the control volume. In Equation [3.1] ρ is the density of the gas, t is the time and u is the velocity vector.

If the flow is steady and all properties are functions of position only, Eq. [3.1] reduces in Cartesian coordinate system to:

$$\frac{\partial}{\partial x}\left(\rho u\right) + \frac{\partial}{\partial y}\left(\rho v\right) + \frac{\partial}{\partial z}\left(\rho w\right) = 0 \qquad [3.2]$$

Since density and velocity are both variables, these are still nonlinear and rather formidable, but a number of special-case solutions can be found. A special case that affords great simplification is incompressible flow, where the density changes are negligible. Then, the density can be slipped out of the partial derivative in Eq. [3.1] and divided out. The result in Cartesian coordinate system is

$$\frac{\partial u}{\partial x} + \frac{\partial v}{\partial y} + \frac{\partial w}{\partial z} = 0 \qquad [3.3]$$

The most practical engineering flows are assuming incompressible and the Eq. [3.3] is used.

III.1.2 Momentum Equation

The conservation of momentum law applied to a fluid passing through an infinitesimal, fixed control volume yields the following equation of momentum:

$$\frac{\partial}{\partial t}(\rho u_i)+\frac{\partial}{\partial x_j}(\rho u_i u_j)=\rho\vec{g}-\frac{\partial p}{\partial x_i}+\frac{\partial \tau_{ji}}{\partial x_j} \quad [3.4]$$

Where p is the static pressure, τ is the total stress tensor, and $\rho\vec{g}$ is the gravitational body force and other external body forces are not included into the equation. The stress tensor is given by:

$$\tau=\mu\left[\left(\frac{\partial u_i}{\partial x_j}+\frac{\partial u_j}{\partial x_i}\right)-\frac{2}{3}\frac{\partial u_l}{\partial x_l}\delta_{ij}\right] \quad [3.5]$$

Where μ is the molecular viscosity and δ_{ij} is the Kronecker´s delta and second term on right hand side is effect of volume dilation.

III.1.3 Energy Equation

The energy equation in conservation form including the viscous dissipation can be written as below:

$$\frac{\partial(\rho E)}{\partial t}+\frac{\partial}{\partial x_i}(u_i(\rho E+p))=\frac{\partial}{\partial x_i}\left(k\frac{\partial T}{\partial x_i}+\tau_{ij}u_j\right)+S_h \quad [3.6]$$

Where S_h is the heat source term and E is the total specific energy:

$$E=h_e-\frac{p}{\rho}+\frac{v^2}{2} \quad [3.7]$$

In solid regions, energy transport equation takes the following general form:

$$\frac{\partial(\rho h_e)}{\partial t}+\frac{\partial}{\partial x_i}(u_i\rho h_e)=\frac{\partial}{\partial x_i}\left(k\frac{\partial T}{\partial x_i}\right) \quad [3.8]$$

Where ρ is the density, h_e is the sensible enthalpy ($\int_{T_{ref}}^{T} c_p dT$), k is the conductivity and T is the temperature. The second term on left-hand side of Eq. [3.8] represents convective heat transfer due to rotational or translational motion of solids where the velocity field is computed from the motion specified for the solid zone. The term on the right-hand side of Eq. [3.8] is the heat flux due to conduction.

III.2. Governing Equations for Turbulence Models

Turbulence is the three-dimensional unsteady random motion observed in fluids at moderate to high Reynolds numbers. As technical flows are typically based on fluids of low viscosity, almost all technical flows are turbulent.

While turbulence is, in principle, described by the Navier-Stokes equations, it is not feasible in most situations to resolve the wide range of scales in time and space by direct numerical simulation (DNS) as the central processing unit (CPU) requirements would by far exceed the available computing power for any foreseeable future. For this reason, averaging procedures have to be applied to the Navier-Stokes equations to filter out all, or at least, parts of the turbulent spectrum. The most widely applied averaging procedure is Reynolds Averaging (which, for all practical purposes is time-averaging) of the equations, resulting in the Reynolds-

Averaged Navier-Stokes (RANS) equations. By this process, all turbulent structures are eliminated from the flow and a smooth variation of the averaged velocity and pressure fields can be obtained. However, the averaging process introduces additional unknown terms into the transport equations (Reynolds Stresses and Fluxes) which need to be provided by suitable turbulence models (turbulence closure).

The quality of the simulation can depend crucially on the selected turbulence model and it is important to make the proper model choice as well as to provide a suitable numerical grid for the selected model.

III.2.1 Reynolds Averaged Navier-Stokes (RANS) Equations

RANS equations based turbulence models offer the most economic approach for computing complex turbulent industrial flows.

In Reynolds averaging, the solution variables in the instantaneous (exact) Navier-Stokes equations are decomposed into the mean (ensemble-averaged or time-averaged) and fluctuating components as it is shown in Figure 3. 1. For the velocity components:

$$u_i = \overline{u}_i + u_i' \qquad [3.9]$$

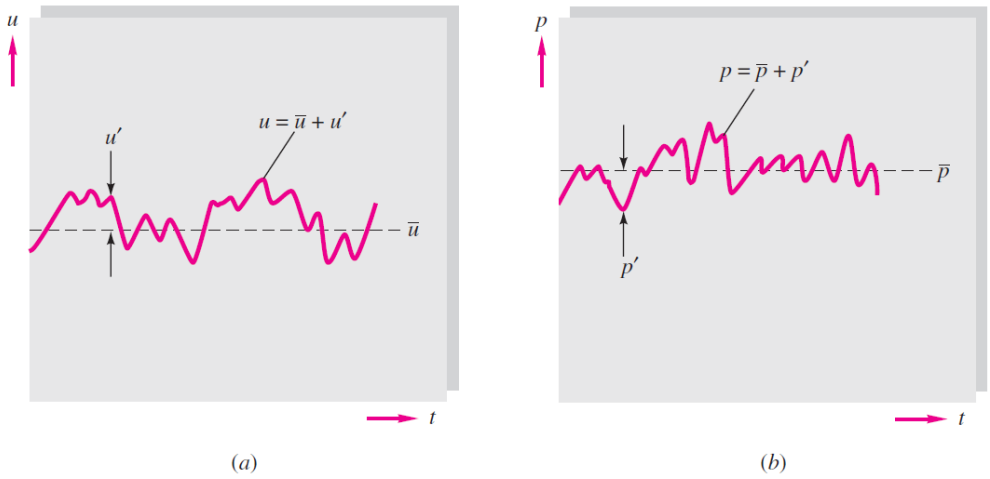

Figure 3. 1: Definition of mean and fluctuating turbulent variables: (a) velocity; (b) pressure. (White, 2009)

Where $\bar{u}_i$ and u_i' are the mean and fluctuating velocity components ($i = 1,2,3$). Likewise, for pressure and other scalar quantities.

Substituting expressions of this form for the flow variables into the instantaneous continuity and momentum equations and taking a time (or ensemble) average yields the ensemble-averaged momentum equations. They can be written in Cartesian tensor form as:

$$\frac{\partial \rho}{\partial t} + \frac{\partial}{\partial x_i}\left(\rho \overline{u}_i\right) = 0 \qquad [3.10]$$

The momentum equation is given as follows:

$$\frac{\partial}{\partial t}\left(\rho \overline{u}_i\right) + \frac{\partial}{\partial x_j}\left(\rho \overline{u}_i \overline{u}_j\right) = -\frac{\partial \overline{p}}{\partial x_i} + \frac{\partial}{\partial x_j}\left[\mu\left(\frac{\partial \overline{u}_i}{\partial x_j} + \frac{\partial \overline{u}_j}{\partial x_i} - \frac{2}{3}\delta_{ij}\frac{\partial \overline{u}_l}{\partial x_l}\right)\right] + \frac{\partial}{\partial x_j}\left(-\rho \overline{u_i' u'}_j\right) \qquad [3.11]$$

Equation [3.10] and Equation [3.11] are called Reynolds-averaged Navier-Stokes (RANS) equations. They have the same general form as the instantaneous Navier-Stokes equations, with the velocities and other solution variables now representing ensemble-averaged (or time-averaged) values. Additional terms now appear that represent the effects of turbulence. These Reynolds stresses, $-\rho\overline{u_i' u_j'}$, must be calculated in order to close Equation [3.11].

The Reynolds-averaged approach to turbulence modelling requires that the Reynolds stresses in Equation [3.11] are appropriately calculated. A common method employs the Boussinesq hypothesis to relate the Reynolds stresses to the mean velocity gradients:

$$-\rho\overline{u_i' u'}_j = \mu_t\left(\frac{\partial u_i}{\partial x_j}+\frac{\partial u_j}{\partial x_i}\right)+\frac{2}{3}\left(\rho k+\mu_t\frac{\partial u_k}{\partial x_k}\right)\delta_{ij} \qquad [3.12]$$

The advantage of this approach is the relatively low computational cost associated with the computation of the turbulent viscosity, μ_t. In the case of the $k-\varepsilon$ model, two additional transport equations (for the turbulence kinetic energy, k, and for the turbulence dissipation rate, ε) are solved, and μ_t is computed as a function of k and ε. The disadvantage of the Boussinesq hypothesis as presented is that it assumes μ_t is an isotropic scalar quantity, which is not strictly true. However the assumption of an isotropic turbulent viscosity typically works well for shear flows dominated by only one of the turbulent shear stresses.

Correspondingly, the time averaged energy equation is given as follows:

$$\frac{\partial(\rho E)}{\partial t}+\frac{\partial}{\partial x_i}\left[u_i\left(\rho E+\bar{p}\right)\right]=\frac{\partial}{\partial x_i}\left(k_{eff}\frac{\partial T}{\partial x_i}+u_{ji}\left(\tau_{ij}\right)_{ef}\right)+S_h \qquad [3.13]$$

Where E is the total specific energy, k_{eff} is the effective thermal conductivity including turbulence effects, T T is the time-averaged temperature, S_h is heat source term, and $\left(\tau_{ij}\right)_{ef}$ is the deviatoric stress tensor representing the viscous heating, including turbulence effects.

III.2.2 Standard $k-\varepsilon$ Turbulence Model

In eddy-viscosity-based $k-\varepsilon$ turbulence models, the velocity and length scales which characterize the turbulent field are obtained from two parameters: the turbulent kinetic energy k and dissipation ε. The velocity scale is taken to be $\sqrt{k}$ and the length scale is taken to be $\sqrt{k^3}/\varepsilon$. Therefore, the turbulent viscosity μ_t in Eq. [3.13] is computed by combining k and ε as:

$$\mu_t=\rho C_\mu\frac{k^2}{\varepsilon} \qquad [3.14]$$

The standard $k-\varepsilon$ turbulence model initially developed by Launder and Spalding, is a semi-empirical model based on model transport equations for the turbulent kinetic energy k and its dissipation rate ε. The model transport equations for k is derived from the exact equation, while the model transport equation for ε is obtained using physical reasoning and bears little resemblance to its mathematically exact counterpart. In the derivation of the $k-\varepsilon$ turbulence model, it is assumed that the flow is highly turbulent and the effects of the molecular viscosity are negligible. The turbulent kinetic energy k and its rate of dissipation rate ε are obtained from the following transport equations given by Launder and Spalding (ANSYS, 2009).

$$\frac{\partial}{\partial t}(\rho k)+\frac{\partial}{\partial x_i}(\rho k\bar{u}_i)=\frac{\partial}{\partial x_j}\left[\left(\mu+\frac{\mu_t}{\sigma_k}\right)\frac{\partial k}{\partial x_j}\right]+G_k+G_b-\rho\varepsilon-Y_M+S_k \qquad [3.15]$$

And

$$\frac{\partial}{\partial t}(\rho\varepsilon)+\frac{\partial}{\partial x_i}(\rho\varepsilon\overline{u}_i)=\frac{\partial}{\partial x_j}\left[\left(\mu+\frac{\mu_t}{\sigma_\varepsilon}\right)\frac{\partial\varepsilon}{\partial x_j}\right]+C_{1\varepsilon}\frac{\varepsilon}{k}(G_k+C_{3\varepsilon}G_b)-C_{2\varepsilon}\rho\frac{\varepsilon^2}{k}+S_\varepsilon \quad [3.16]$$

In these equations, G_k represents the generation of turbulence kinetic energy due to the mean velocity gradients, calculated as follows:

$$G_k=-\rho\overline{u_i'u'}_j\frac{\partial u_j}{\partial x_i} \quad [3.17]$$

G_b is the generation of turbulence kinetic energy due to buoyancy, in these case this term is zero. Y_M represents the contribution of the fluctuating dilatation in compressible turbulence to the overall dissipation rate for the case of incompressible flow this term is zero. $C_{1\varepsilon}$, $C_{2\varepsilon}$ and $C_{3\varepsilon}$ are constants determined from experiments for fundamental turbulent flows. σ_k and σ_ε are the turbulent Prandtl numbers for k and ε, respectively. S_k and S_ε are user-defined source terms.

The default values of the model constants in FLUENT have the following default values:

Table 3. 1: Standard *k-ε* Turbulence Model Constants

$C_{1\varepsilon}$	$C_{2\varepsilon}$	$C_{3\varepsilon}$	σ_k	σ_ε
1.44	1.92	0.09	1.0	1.3

III.2.3 RNG $k-\varepsilon$ turbulence model

Yakhot and Orszag (Yakhot, 1986) proposed another variant of the $k-\varepsilon$ turbulence model, the performance characteristics of which are improved relative to the standard model. The proposed model is based on renormalized group theory and is referred to as the RNG turbulence model. This model is similar in form to the standard turbulence model; however, the RNG turbulence model differs from the standard model by the inclusion of an additional sink term in the turbulence dissipation equation to account for non-equilibrium strain rates and employs different values for the various model coefficients. The form of the k equation remains same. The turbulence dissipation equation of the RNG $k-\varepsilon$ turbulence model includes the following sink term:

$$\frac{C_\mu\rho\eta^3(1-\eta/\eta_0)}{1+\beta\eta^3}\frac{\varepsilon^2}{k} \quad [3.18]$$

Where $\eta_0=4.38$ and $\beta=0.012$: The above sink term also employs parameter η, which is the ratio of the characteristic time scales of turbulence and mean flow field as follows:

$$\eta=\frac{Sk}{\varepsilon} \quad [3.19]$$

where

$$S=\sqrt{\frac{G_k}{\mu_t}} \quad [3.20]$$

The primary model coefficients of the RNG $k-\varepsilon$ turbulence model are C_{μ}, $C_{1\varepsilon}$, $C_{2\varepsilon}$, , σ_k, σ_{ε} and Von Karman constant κ.

Table 3. 2: RNG *k-ε* Turbulence Model Constants

C_{μ}	$C_{1\varepsilon}$	$C_{2\varepsilon}$	σ_k	σ_{ε}	κ
0.0845	1.42	1.68	0.7179	0.7179	0.4187

The RNG $k-\varepsilon$ model was first derived using a statistical technique called renormalization group theory. It is similar in form to the standard model, but includes the following refinements:

• The RNG model has an additional term in its ε equation that improves the accuracy for rapidly strained flows.

• The effect of swirl on turbulence is included in the RNG model, enhancing accuracy for swirling flows.

• The RNG theory provides an analytical formula for turbulent Prandtl numbers, while the standard $k-\varepsilon$ model uses user-specified, constant values.

• While the standard $k-\varepsilon$ model is a high-Reynolds number model, the RNG theory provides an analytically derived differential formula for effective viscosity that accounts for low-Reynolds number effects. Effective use of this feature does, however, depend on an appropriate treatment of the near-wall region.

These features make the RNG $k-\varepsilon$ model more accurate and reliable for a wider class of flows than the standard $k-\varepsilon$ model.

III.2.4 Near wall treatment in time averaged turbulence models

The form of turbulence model which has been presented under the eddy viscosity concept is valid only for fully turbulent flows. Close to the solid walls, and some other interfaces, there are inevitably regions where the local Re of turbulence is so small that viscous effects predominate over turbulent ones and flow is strongly anisotropic. Therefore, in the near wall regions, for instance the standard form of the $k-\varepsilon$ model is often not adequate to predict the effects of viscosity and to cope with the difficulties caused by considerably varying velocity gradients. Consideration therefore needs to be given as to how to make these models suitable for wall-bounded flows.

III.3. Governing Equations for Porous Media

III.3.1 Momentum Equations for Porous Media

The porous media models for single -and multiphase flows use the Superficial Velocity Porous Formulation as the default (ANSYS, 2009). The present CFD code calculates the superficial phase or mixture velocities based on the volumetric flow rate in a porous region. The porous media model is described in the following sections for single phase flow, however, it is important to note the following for multiphase flow:

• In the Eulerian multiphase model (ANSYS, 2009), the general porous media modelling approach, physical laws, and equations described below are applied to the corresponding phase for mass continuity, momentum, energy, and all the other scalar equations.

• The Superficial Velocity Porous Formulation generally gives good representations of the bulk pressure loss through a porous region. However, since the superficial velocity values within a porous region remain the same as those outside the porous region, it cannot predict the velocity increase in porous zones and thus limits the accuracy of the model.

Porous media are modelled by the addition of a momentum source term to the standard fluid flow equations. The source term is composed of two parts: a viscous loss term (Darcy, the first term on the right-hand side of Eq. [3.21], and an inertial loss term (the second term on the right-hand side of Eq. [3.21].

$$S_i = -\left(\sum_{j=1}^{3} D_{ij} \mu u_j + \sum_{j=1}^{3} C_{ij} \frac{1}{2} \rho |u| u_j \right) \quad [3.21]$$

Where S_i is the source term for the i (x , y or z) momentum equation, $|u|$ is the magnitude of the velocity and D and C are prescribed matrices. This momentum sink contributes to the pressure gradient in the porous cell, creating a pressure drop that is proportional to the fluid velocity (or velocity squared) in the cell. The equation [3.21] recovers the case of simple homogeneous porous media:

$$S_i = -\left(\frac{\mu}{\alpha} u_i + C_2 \frac{1}{2} \rho |u| u_i \right) \quad [3.22]$$

Where α is the permeability and C_2 is the inertial resistance factor, simply specify D and C as diagonal matrices with $1/\alpha$ and C_2, respectively, on the diagonals (and zero for the other elements).

III.3.1.1 Darcy´s Law in Porous Media

In laminar flows through porous media, the pressure drop is typically proportional to velocity and the constant C_2 can be considered to be zero. Ignoring convective acceleration and diffusion, the porous media model then reduces to Darcy's Law:

$$\nabla p = -\frac{\mu}{\alpha} \vec{v} \quad [3.23]$$

III.3.1.2 Inertial Losses in Porous Media

At high flow velocities, the constant C_2 in Eq. [3.24], provides a correction for inertial losses in the porous medium. This constant can be viewed as a loss coefficient per unit length along the flow direction, thereby allowing the pressure drop to be specified as a function of dynamic head.

III.3.2 Energy Equations for Porous Media

There are two approaches for the energy equation in the porous media, thermal equilibrium model and non-thermal equilibrium model. ANSYS FLUENT solves the standard energy transport equation Eq. [3.6] in porous media regions with modifications to the conduction flux and the transient terms only.

III.3.2.1 Equilibrium Thermal Model Equations

For simulations in which the porous medium and fluid flow are assumed to be in thermal equilibrium, the conduction flux in the porous medium uses an effective conductivity and the transient term includes the thermal inertia of the solid region on the medium:

$$\frac{\partial}{\partial t}\left(\gamma\rho_f E_f + (1-\gamma)\rho_s E_s\right) + \frac{\partial}{\partial x_i}\left(u_i\left(\rho_f E_f + p\right)\right) = \frac{\partial}{\partial x_i}\left[k_{eff}\frac{\partial T}{\partial x_i} + \tau_{ij}u_j - \left(\sum_i h_i J_i\right)\right] + S_f^h \quad [3.24]$$

Where E_f is the total fluid energy, E_s is the total solid medium energy, ρ_f is the fluid density, ρ_s is the solid medium density, γ is the porosity of the medium, k_{eff} is the effective thermal conductivity of the medium and S_f^h is the fluid enthalpy source term.

The effective thermal conductivity in the porous medium, k_{eff}, is computed by ANSYS FLUENT as the volume average of the fluid conductivity and the solid conductivity:

$$k_{eff} = \gamma k_f + (1-\gamma)k_s \quad [3.25]$$

Where k_f is the fluid phase thermal conductivity (including the turbulent contribution, k_t) and k_s is the solid medium thermal conductivity.

III.3.2.2 Non-Equilibrium Thermal Model Equations

For simulations in which the porous medium and fluid flow are not assumed to be in thermal equilibrium, a dual cell approach is used. In such an approach, a solid zone that is spatially coincident with the porous fluid zone is defined, and this solid zone only interacts with the fluid with regard to heat transfer. The conservation equations for energy are solved separately for the fluid and solid zones. The conservation equation solved for the fluid zone is

$$\frac{\partial}{\partial t}\left(\gamma\rho_f E_f\right) + \frac{\partial}{\partial x_i}\left(u_i\left(\rho_f E_f + p\right)\right) = \frac{\partial}{\partial x_i}\left[\gamma k_f\frac{\partial T_f}{\partial x_i} + \tau_{ij}u_j - \left(\sum_i h_i J_i\right)\right] + S_f^h + h_{fs}A_{fs}(T_f - T_s) \quad [3.26]$$

and the conservation equation solved for the solid zone is

$$\frac{\partial}{\partial t}\left((1-\gamma)\rho_s E_s\right) = \frac{\partial}{\partial x_i}\left((1-\gamma)k_s\frac{\partial T_s}{\partial x_i}\right) + S_s^h - h_{fs}A_{fs}(T_f - T_s) \quad [3.27]$$

Where E_f is the total fluid energy, E_s is the total solid medium energy, ρ_f is the fluid density, ρ_s is the solid medium density, γ is the porosity of the medium, k_f is the fluid phase thermal conductivity (including the turbulent contribution), k_s is the solid medium thermal conductivity, h_{fs} is the heat transfer coefficient for the fluid / solid interface, A_{fs} is the interfacial area density (the ratio of the area of the fluid / solid interface and the volume of the porous zone), T_f is the temperature of the fluid, T_s is the temperature of the solid medium, S_f^h is the fluid enthalpy source term and S_s^h is the solid enthalpy source term.

III.4. General Description and Computational Principles

One important issue in the progress to improvements in Stirling models is the geometric shape of the matrix in the regenerator as most regenerator models do not assume a precise geometric

shape for the elements of the regenerator (Dyson, y otros, 2005). Dyson et al. (Dyson, y otros, 2005) indicated that the shape of the regenerator has an important impact on the overall Stirling system design.

In general the macroscopic models used in the design and development of different regenerator matrices do not explicitly consider the complex microscopic interaction between the working fluid and the solid matrix. However, it would not be feasible from a microscopic computational point of view to model the whole regenerator due to the complexity of the regenerator matrix. On the other hand, a simplified 2-D model has the handicap of not considering the interactions between working fluid and solid matrix. Therefore, a small detailed 3-D matrix domain is generated as a representative of the whole Stirling regenerator for the numerical procedure. The micro scale model includes individual wires trying to catch any non-uniformity or 3-D flow inside the matrix.

III.4.1. Problem description

One of the most widely used types of regenerator is made of woven wire matrix. For these kind of regenerators there are plenty of possible configurations/variations: the geometry and combination of the wires, the type of weave, the type of matrix and the configuration inside the matrix (aligned, misaligned, random, porosity, etc.).

In general, the woven wire screen is formed by wires woven in two directions, and the range of diameters and combinations (including materials) are huge. Moreover, although it is not a commercial option, the shape of the wires could be customized, for example oval section instead of circular one.

There are commercially available many possible types of weave structures, for general purposes the most used ones are the square mesh and the plain dutch weave (see Figure 3. 2). However, in Stirling regenerator the majority of the studies are for square mesh. The matrix models simulated are based on square mesh using the same wire diameter (circular section) in both directions.

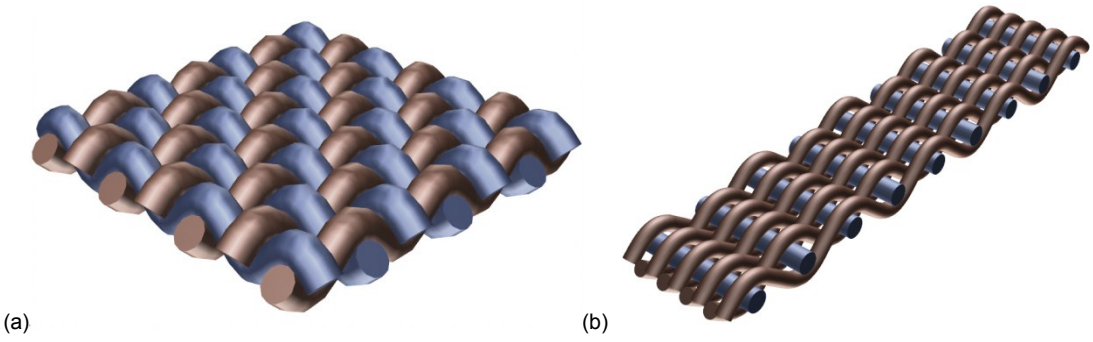

(a) (b)

Figure 3. 2: Types of Woven Wire Screen: (a) Square Mesh and (b) Plain Dutch Weave (GKD Gebr. Kufferath AG, 2010-2014)

The remaining configurations of the Stirling regenerator matrices based on square woven wire screen are still numerous. This study focuses on the most used one, stacked woven wire matrix, and on the wound woven wire matrix as a more cost effective option (see Figure 3. 3).

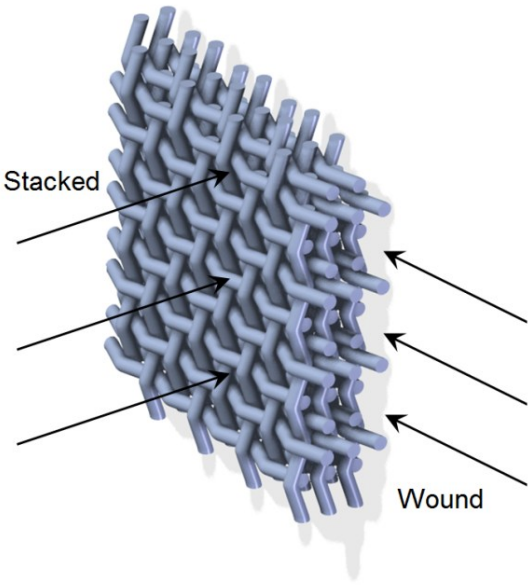

Figure 3. 3: Types of Configurations for Woven Wire Screen: Stacked and Wound

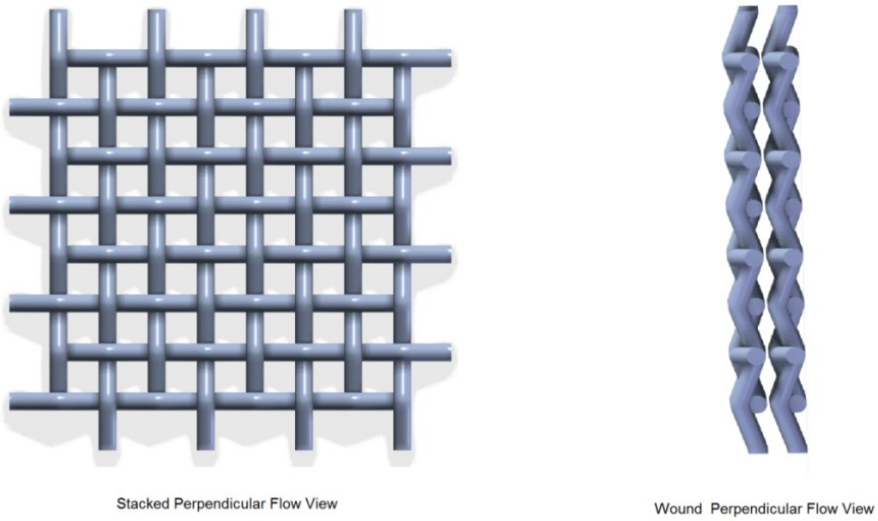

Figure 3. 4: Flow direction view for Stacked and Wound Woven Wire Screen:

The stacked woven wire regenerator matrix consists of a stack of woven wire screens or layers. It can be seen in Figure 3. 3 that the working gas flow direction is perpendicular to the array of screens, therefore in a perfect aligned structure the pore size is the opening of the screen as can be observed in Figure 3. 4. In this kind of configuration the volumetric porosity of the matrix depends on the pressure applied during the stacking manufacturing process.

The wound woven wire regenerator matrix consists of a wound strip of woven wire. As seen in Figure 3. 3, the working gas flow direction is parallel to the array. In this configuration the volumetric porosity of the matrix depends on the tension and pressure applied during the winding manufacturing process.

The configurations shown before are for the perfectly aligned or ideal cases for pressure drop, where the flow path performance could be approximated to a pipe (no obstacles). However, this configuration is difficult to be constructed in a manufacturing process considering the wire diameter, in general the matrix configuration is randomly misaligned as can be observed in Figure 3. 5 for a wound woven wire regenerator matrix.

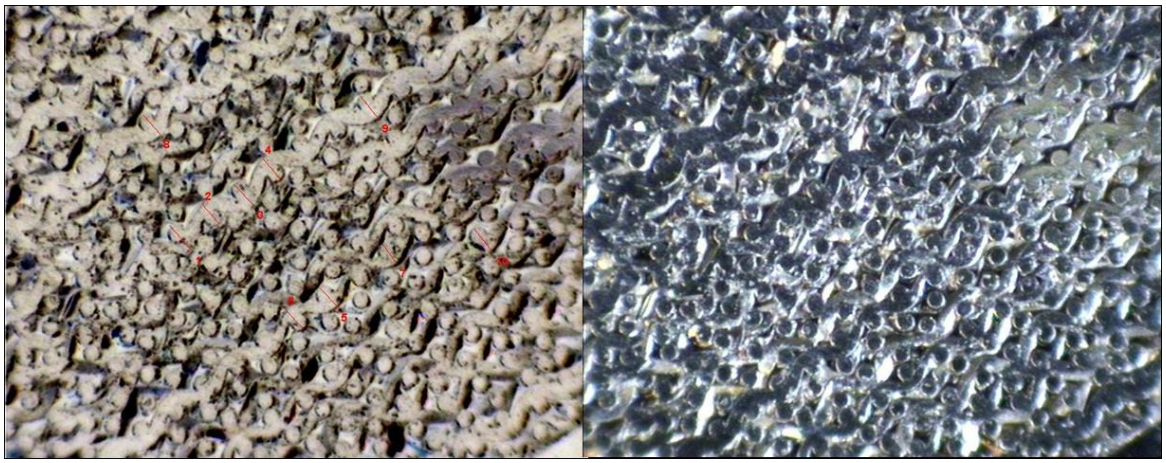

Figure 3. 5: Macroscopic picture of the wound woven wire (80 μm) screen matrix

Both configurations, perfectly aligned and random (misaligned), are studied for stacked and wound woven wire regenerator matrices.

III.4.1.1. Geometric Factors Woven Wire Regenerator Matrix

The geometric parameters of a woven wire screen are shown in Figure 3. 6. Using the wire diameter d_w, the opening or light l and the volumetric porosity of the matrix, Π_v the geometric factors of the matrix are defined as follows:

Hydraulic diameter d_h:

$$d_h = \frac{d_w \Pi_v}{(1-\Pi_v)} \qquad [3.28]$$

Porosity of the woven wire screen Π_w:

$$\Pi_w = 1 - \frac{\pi d_w}{4(d_w + l)} \qquad [3.29]$$

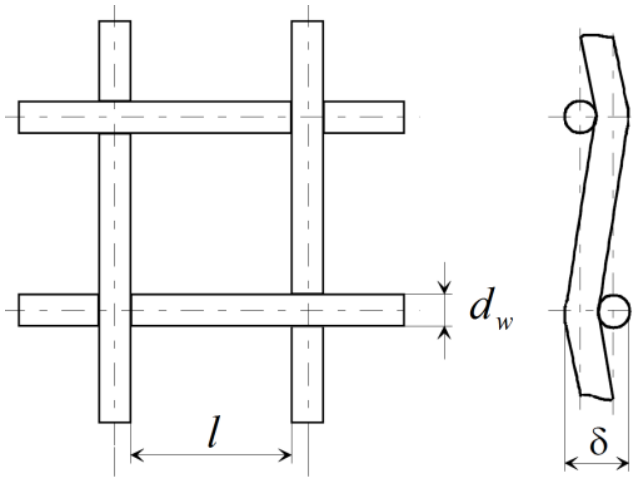

Figure 3. 6: Geometric parameters of woven wire screen

Volumetric Porosity of the regenerator matrix Π_v:

$$\Pi_v = \frac{V_{dr}}{V_r} \quad [3.30]$$

Maximum flow velocity through the regenerator matrix u_{max}:

$$u_{\max} = \frac{u}{\Pi_v} \quad [3.31]$$

Specific heat transfer area φ:

$$\varphi = \frac{4\left(1-\Pi_v\right)}{d_w} \quad [3.32]$$

The total volume of the regenerator matrix V_r, the dead volume V_{dr} and the heat transfer surface area A_{wr} are directly computed from the CAD program for each matrix studied. The representative length or hydraulic diameter for both configurations of the matrix, stacked and wound, are defined identically. Therefore, Reynolds number can be defined as:

$$Re = \frac{\rho_g u_{max} d_h}{\mu} \quad [3.33]$$

III.4.1.2. Woven Wire Matrix Configurations Studied

The configurations of the woven wire matrices characterized are summarized in Tables 3.3 and 3.4. In Table 3. 3 the geometrical parameters of the two modelled woven wire screen are presented, wire diameter 80 and 110μm, typical for micro-CHP Stirling engines (Whispertech (EHE, 2011)). The porosity given in Table 3. 3 corresponds to the volumetric porosity defined in Eq. [3.30] of a single woven wire screen.

Table 3. 3: Geometry Parameters of Woven Wire Screen

Nomenclature	Woven Wire Screen Geometry			
	Wire/inch	d_w [μm]	l [μm]	Π_w
80	113	80	144	0.72
110	100	110	144	0.66

The matrix nomenclature shown in Table 3.4 is described as follows: the first letter S or W denotes the basic configuration, stacked or wound; the following number is referred to as the wire diameter, 80 or 110μm, the following two numbers after the dash, represent the volumetric porosity in percentage; and finally, the configuration for stacked. As shown in Figure 3. 7, for the stacked configuration there are four variations: misaligned, cross misaligned (X), aligned (A) and misaligned no-contact (NC) between layers. Figure 3. 8 shows an example of the nomenclature used.

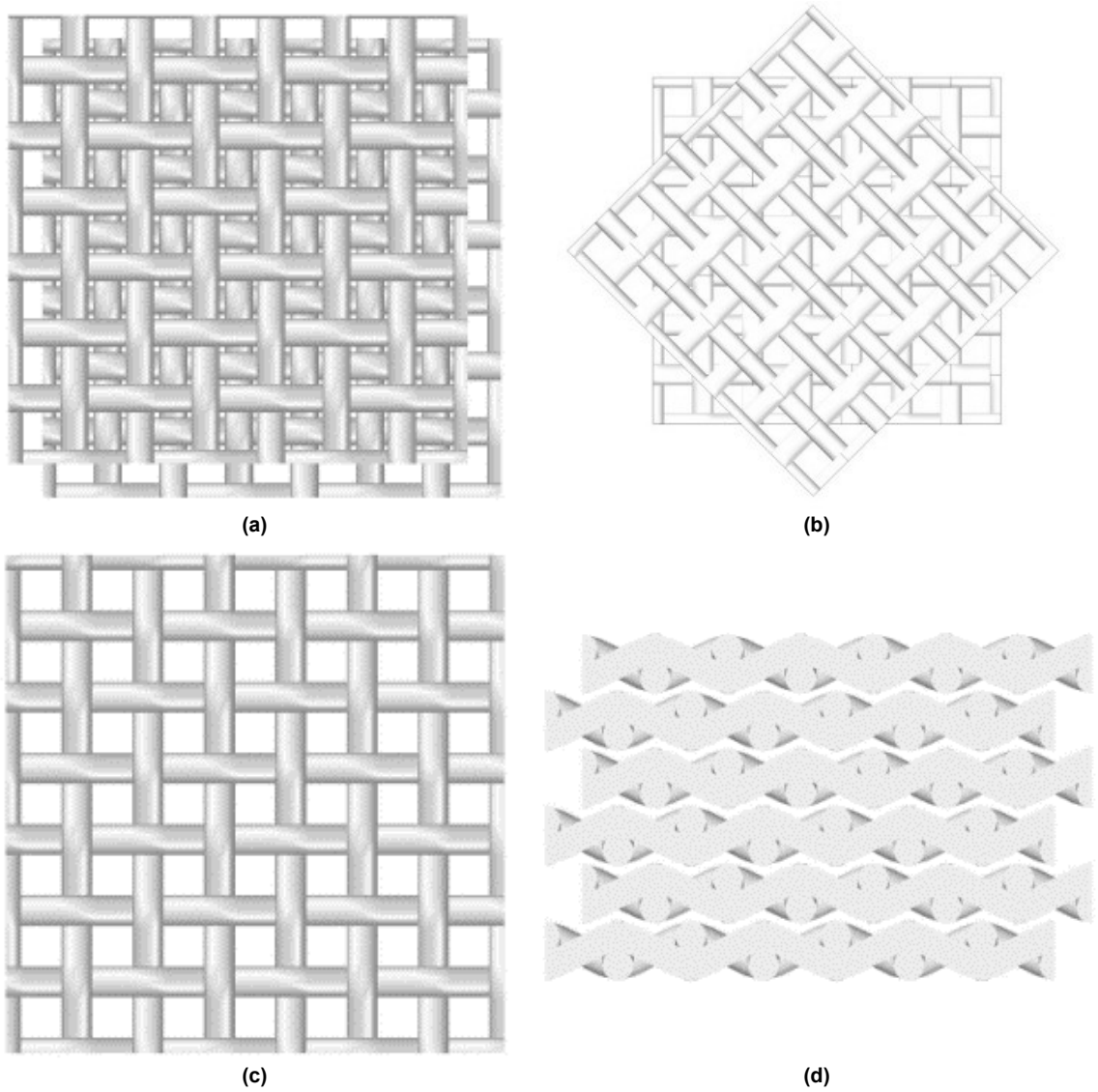

Figure 3. 7: Stacked Woven Wire Matrix variations: (a) random parallel misaligned; (b) cross misaligned (X); (c) aligned (A) and (d) misaligned no-contact (NC).

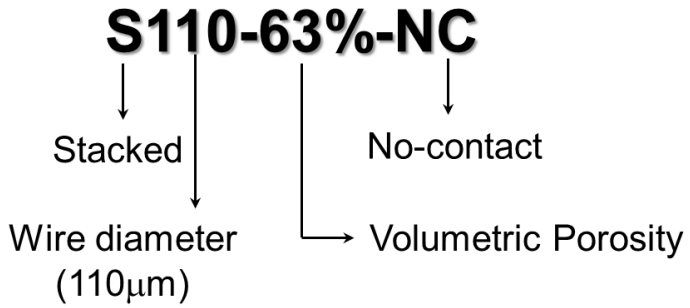

Figure 3. 8: Nomenclature Example

Regarding the misalignment configuration, the percentage of misalignment could affect the performance of the regenerator matrix. Based on this hypothesis, the preliminary models attempt to cover for the same volumetric porosity range of fix misalignment. However, the option of random misaligned is considered to be closer to the real configuration of a woven wire regenerator matrix. For this reason last configuration studied are random misaligned.

The geometrical parameters of the woven wire matrices modelled are also summarized in Table 3.4. The volumetric porosity, Π_v, is obtained based on Eq. [3.31] by measuring the dead volume and the total volume of the matrix in the geometry CAD model. The volumetric porosity shown in

Table 3.4 represents the average volumetric porosity of the configurations modelled, the volumetric porosity is calculated in the geometry of the matrix. The ΔPorosity provided in Table 3.4 is a measure of difference between the single woven wire screen porosity and the volumetric porosity of the matrix ($\Pi_w - \Pi_v$), and in a typical stacked regenerator matrix this difference should be positive.

Table 3. 4: The Geometry Parameters of Woven Wire Matrices

Matrix Nomenclature	Π_v	ΔPorosity	φ [1/mm]	d_h [μm]
S80-49%	0.490	- 23%	25.5	77
S80-57%	0.567	- 15%	21.7	105
S80-61% / -A	0.616	- 11%	19.2	128
S80-64%-A / W80-64%	0.638	- 8%	18.1	141
S80-66% / -X / W80-66%	0.666	- 6%	16.7	160
S80-68% / -X / W80-68%	0.685	- 4%	15.8	174
S110-39%	0.387	- 27%	22.3	69
S110-45%	0.452	- 21%	19.9	91
W110-47%	0.472	- 19%	19.2	98
W110-53%	0.533	- 13%	17.0	126
W110-59%	0.588	- 7%	15.0	157
S110-60% / -X / W110-60%	0.603	- 6%	14.4	167
S110-63% / -X / -A / -NC / W110-63%	0.632	- 3%	13.4	189
S110-71%-NC	0.718	+ 5%	10.3	280

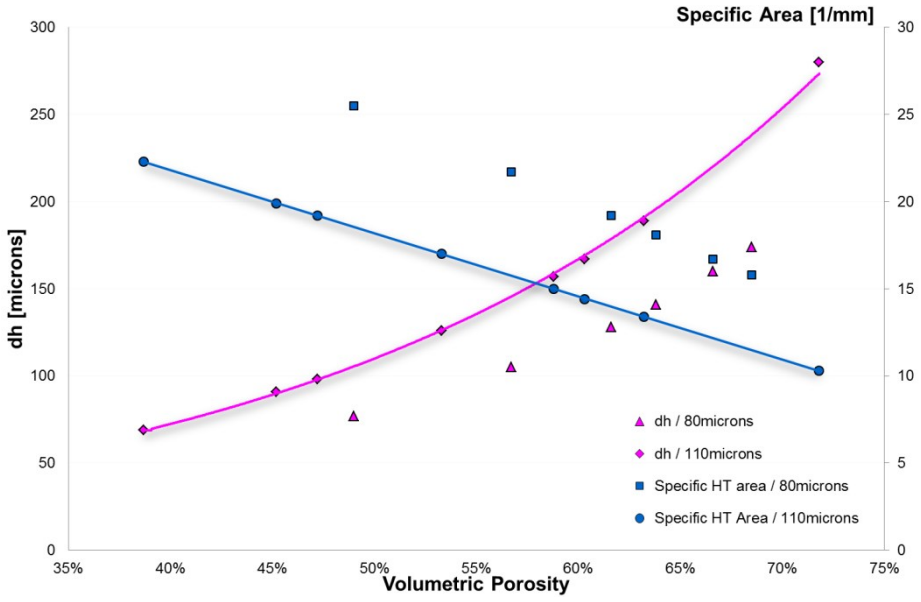

Figure 3. 9: Chart of Matrix Configurations: Hydraulic diameter and Specific Heat Transfer Area vs. Volumetric Porosity of the Matrix

Figure 3. 9 shows the hydraulic diameter and the specific heat transfer area as a function of the matrix volumetric porosity for the configurations studied. In the chart is plotted the trend-line corresponding to 110μm for both parameters. The linear proportionality of the hydraulic diameter with the volumetric porosity (Eq. [3.29]) and the exponential proportionality of the specific heat transfer area are clearly observed here.

III.4.2. Computational Principles

The commercial code ANSYS FLUENT (ANSYS, 2009) is used to solve the governing equations described above.

III.4.2.1 Solver

The solution algorithm chosen in the present CFD code (ANSYS, 2009) is the pressure-based solver where the velocity field is obtained from the momentum equations while the density field is determined from the equation of state. On the other hand, the pressure field is extracted by solving a pressure or pressure correction equation which is obtained by manipulating continuity and momentum equations. A control-volume-based discretization technique adopted here consists of:

- Division of the domain into discrete control volumes using a computational grid.
- Integration of the governing equations on the individual control volumes to construct algebraic equations for the discrete dependent variables ("unknowns") such as velocities, pressure, temperature, and conserved scalars.
- Linearization of the discretized equations and solution of the resultant linear equation system to yield updated values of the dependent variables.

This results in a system of linear equations with one equation for each cell in the domain. A point implicit (Gauss–Seidel) linear equation solver is used in conjunction with an algebraic multi-grid method to solve the resultant scalar system of equations for the dependent variable in each cell with a second-order upwind scheme for the discretization of the continuity and momentum equations for the laminar flow solutions. The Standard pressure interpolation scheme and Standard algorithm with skewness correction and neighbour correction as a pressure–velocity coupling scheme are used for all simulations. All fluid properties—including density, viscosity are assumed constant. The convergence criterion for all the velocity and pressure components and for the continuity is set to 10^{-6} to attain high numerical accuracy.

The pressure-based solver uses a solution algorithm where the governing equations are solved sequentially. Because the governing equations are non-linear and coupled, the solution loop must be carried out iteratively in order to obtain a converged numerical solution.

In the segregated algorithm, the individual governing equations for the solution variables are solved one after another. Each governing equation, while being solved, is "decoupled" or "segregated" from other equations, hence its name. The segregated algorithm is memory-efficient, since the discretized equations need only be stored in the memory one at a time. However, the solution convergence is relatively slow. With the segregated algorithm, each iteration consists of the steps outlined below (ANSYS, 2009):

1. The update fluid properties (e.g., density, viscosity, specific heat) including turbulent viscosity (diffusivity) based on the current solution.
2. Solve the momentum equations, one after another, using the recently updated values of pressure and face mass fluxes.
3. Solve the pressure correction equation using the recently obtained velocity field and the mass-flux.

4. Correct face mass fluxes, pressure, and the velocity field using the pressure correction obtained from Step 3.

5. Solve the equations for additional scalars, if any, such as turbulent quantities, energy, species, and radiation intensity using the current values of the solution variables.

6. Update the source terms arising from the interactions among different phases (e.g., source term for the carrier phase due to discrete particles).

7. Check for the convergence of the equations.

These steps are continued until the convergence criteria are met.

III.4.2.2 Numerical Methodology

In the present numerical study, the fluid is considered to be viscous, incompressible, Newtonian, and 3-D with assumption of laminar flow behaviour at very low Reynolds number range and of turbulent flow behaviour at high Reynolds number.

The present flow is mathematically governed by the flow equations presented in the previous sections, since there is no known analytical solution, or direct mathematical representation, these governing equations are discretized and solved using a finite volume method (FVM) based numerical flow solver (ANSYS, 2009). The non-linear conservation equations in the present FVM method are transformed into analogous algebraic equations for each control volume and these equations are solved by a segregated solution algorithm.

III.4.2.3 Laminar vs. Turbulent flow analysis

It is observed that, after a certain value of defined Reynolds number (approximated Reynolds number of 160), there may be emergence of local turbulence instabilities leading to convergence problem for laminar flow simulations. Hence it has to be resolved or modelled by a turbulence model to accurately predict the pressure drop values at high Reynolds numbers. This local transitional characteristic change in the flow of different regenerators has been also previously investigated and well documented.

Simon and Seume (Simon, 1986) studied the type of flow regime in the regenerator of different engines, the characteristic Reynolds numbers are low between 60 and 350, despite which the flow regime is not always laminar. Dybbs and Edwards (Dybbs, 1984) classified the steady flow regimes in porous media according to a Reynolds number based on the average pore diameter: $Re < 1$ Darcy flow regime; $1 < Re < 10$ boundary layers begin to develop on the pore wall, $10 < Re < 175$ laminar flow, $175 < Re < 250$ separated laminar flow, vortex shedding, $250 < Re < 300$ separated flow with random wakes and $Re > 300$ turbulent flow.

The complex and irregular geometry of the present porous media makes the 3-D flow resolution difficult and the associated pressure drop predictions may become inaccurate. Therefore, for $Re > 175$ for stacked woven wire matrix and for $Re > 350$ for wound woven wire matrix configuration with use of laminar model computations, there may be a requirement of using turbulence model to accurately represent the local turbulence and their effects on prediction of pressure drops. With this respect, turbulence is modelled here using Reynolds averaged Navier-Stokes (RANS) equations based RNG $k - \varepsilon$ turbulence model to account for the effects of smaller scales of motion to improve the capabilities of the standard $k - \varepsilon$ model for flows in which highly swirling patterns and separation prevail.

CHAPTER IV:

Pressure Drop Characterization

IV. PRESSURE DROP CHARACTERIZATION

This chapter describes the pressure drop characterization of the Stirling regenerator as a first step of the numerical characterization and optimization of such device under stationary inflow and isothermal flow computations with adiabatic wall boundary conditions. In this first step of the model development process, a three-dimensional (3-D) isothermal model with an initial flow field described is proposed for determining pressure drop characteristics, thus providing a straightforward insight in how to determine frictional losses at different geometric configurations in the typical range of Reynolds number for Stirling regenerators. Although, there is a large temperature gradient across the transverse faces of the regenerator, the temperature effects are not considered in the characterization of the pressure drop, since, the characteristic streamwise dimension of the matrix domain (around 1mm) is small compare with the regenerator length. Moreover, the friction factor is calculated at local instantaneous Reynolds number.

Firstly, the results obtained for stacked matrix configurations are directly compared with the well-known experimental data (Gedeon and Wood (Gedeon, et al., 1996)) which are also obtained under the isothermal flow conditions for a large range of Reynolds number. The approach is then extended to wound woven wire matrices to numerically drive a friction factor correlation equation, in order to easily evaluate the pressure drop through this kind of regenerator.

IV.1. Introduction

The regenerator is the crucial component of a Stirling cycle machine and most of the research works in this field focus on the characterization and optimization of the performance of this component in order to achieve high energy efficiency. Especially in co-generation applications of Stirling engines, pressure losses through the regenerator have a direct influence on the engine indicated power and, consequently, on the obtained electric power. Therefore, the characterization of this phenomena through experimental, theoretical and numerical studies is important in those applications to maximize the incoming outsource energy.

The programs or softwares employed for modelling the flow in the Stirling cycle machines calculate the pressure drop through the regenerator matrix based on friction factor. In general the friction factor is obtained from empirical correlations; because it is not feasible solve the complete set of Navier-Stokes equations for woven wire or random fibers configurations representing complex regenerator geometries. The majority of available empirical friction factor correlations are for stacked woven wire screens and random fibers regenerator matrices. There are no known empirical friction factor correlations for wound woven wire regenerator matrices and the cost associated to experimental derived correlations is elevated. For these reason a CFD numerical methodology is implemented in order to derive friction factor coefficient to evaluate the Stirling cycle performance.

IV.2. Computational Principles

The computational principles, the governing flow equations and the simulation models employed are described in Chapter III.

IV.2.1 Numerical Methodology

The numerical methodology adopted is previously explained in Chapter III. As a brief summary, the fluid is considered to be viscous, incompressible, Newtonian, and 3-D with assumption of laminar flow behaviour at very low Reynolds number range and of turbulent flow behaviour at high Reynolds number. As the Reynolds number, exceeds a certain value depending on the configuration of the wire matrix used, the local instabilities due to emergence of turbulence leads to numerical convergence problem and the simulations are required to be conducted in turbulent manner.

IV.2.2. Computational domain and boundary conditions

As Cheadle et al. (Cheadle, et al., 2010) mentioned the modelling of typical regenerator geometries would require detailed 3-D models with prohibitively long solutions times. For this reason, in order to capture the heat and momentum interactions at the microscopic level, a small representative portion of the regenerator is modelled. The generated 3-D geometry domain is composed of at least five layers overlapping woven wire screens. Figure 4. 1 illustrates the region of flow of interest (geometry set-up) in which the flow through woven wire matrix geometry is extensively analysed as a representation of a differential part of a Stirling regenerator arrangement. The inlet and outlet flow areas are set to a maximum of 1 mm^2. In some simulations the computational domain is further extended in the downstream direction (in the nominal direction of the outlet flow) in order to avoid reverse flow conditions at the outflow boundary.

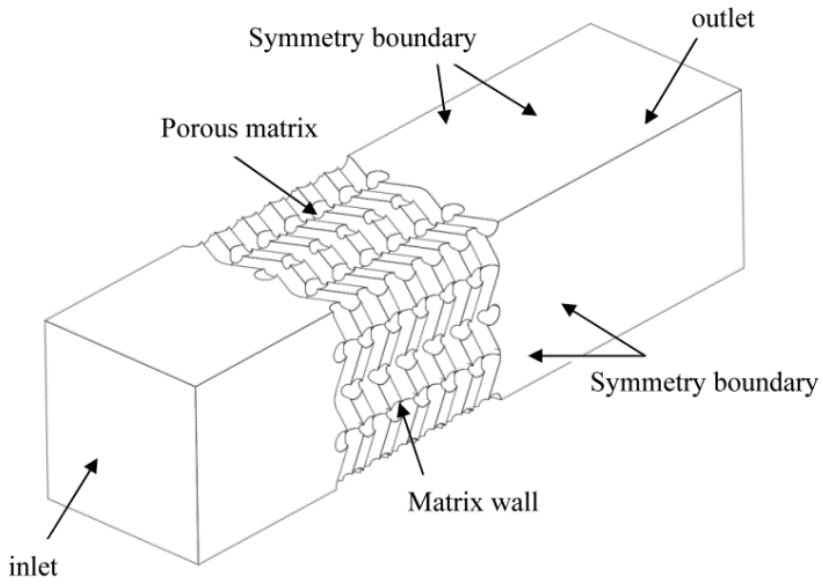

Figure 4. 1: Global Computational domain for Stacked Woven Wire Matrix

Two different configurations, perfectly aligned and misaligned (random), for each woven wire matrix, stacked wire and wound woven wire, are generated and studied. Furthermore, for same aligned and misaligned levels, different volumetric porosity ranges, Π_v, from 0.387 to 0.641 are also taken into consideration.

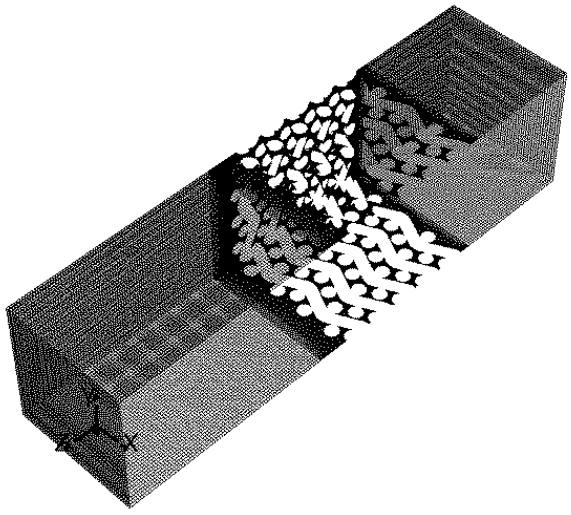

Figure 4. 2: 3-D view of the grid layout for the computational domain.

3-D view of the grid layout for the computational domain is represented in Figure 4. 2 and 2-D sections of two planes in the flow direction are also provided for two different configurations in Figure 4. 3. The computational domain is constructed of non-uniformly distributed different hybrid mesh systems with over 2.5 million tetrahedral and/or hexahedral volume cells for the final mesh system. The tetrahedral cells are used in the air volume inside the matrix with very fine mesh resolution in the close vicinity of the wire surfaces to resolve sharply varying velocity and pressure gradients there. As the accuracy of the present numerical results may depend on the mesh resolution in the computational domain, the effect of the mesh resolution on the present flow is initially tested for three different mesh systems containing non-uniformly distributed hybrid grid cells (from 1.5 million to 5 million volume cells). As seen in Figure 4. 4, although the discrepancy among pressure drop values obtained from different mesh configurations becomes larger as the flow velocity increases, there is no major difference among the computed values and the mesh system of over 2.5 million hybrid volume cells. Thus, it could be considered to be fine enough to study the effects of Reynolds number on the pressure drop characterization through subsequent flow simulations.

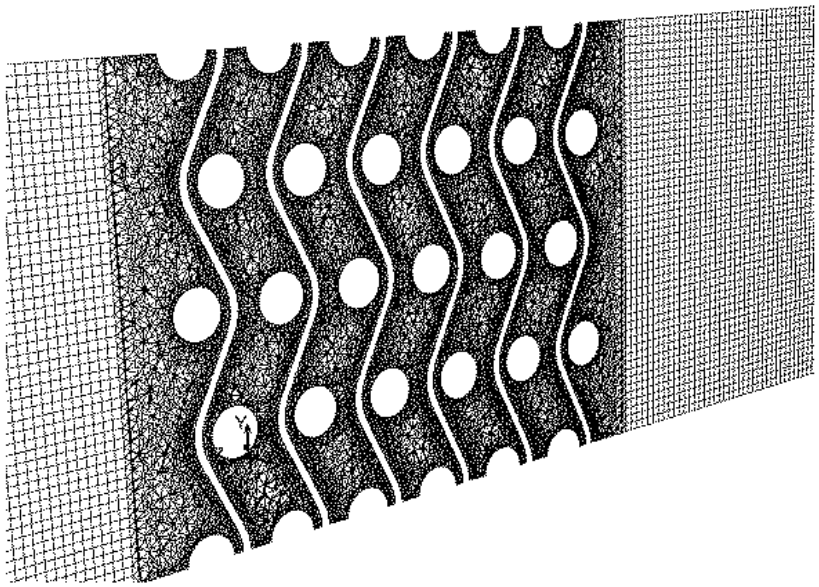

(a)

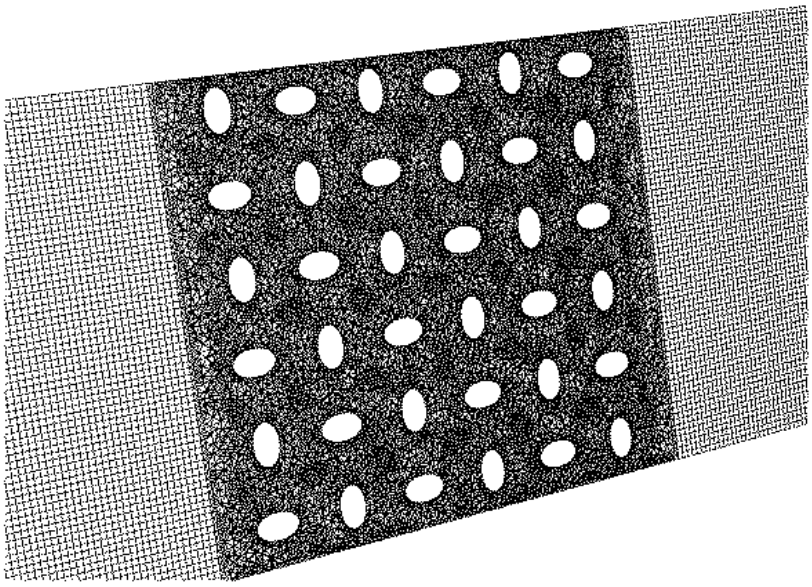

(b)

Figure 4. 3: 2-D plane view of woven wire flow matrices for two different configurations; (a) stacked woven mesh configuration; and (b) wound woven mesh configuration.

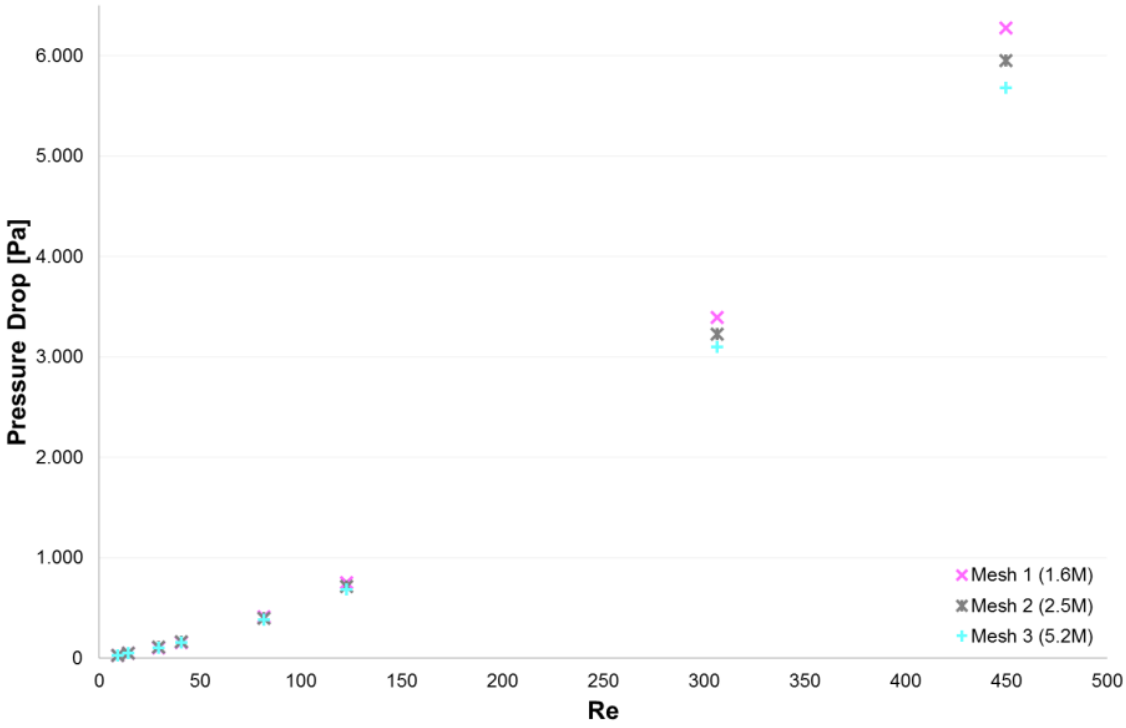

Figure 4. 4: Mesh sensibility for different number of volume cells: pressure drop vs. Re.

For all woven wire matrix configurations, all model simulations are carried out by considering the following boundary conditions:

1. Velocity inlet boundary conditions: Velocity inlet boundary conditions are used to define the fluid uniform velocity profile at the inlet.

2. Pressure outlet boundary conditions: Pressure outlet boundary conditions are used to define the static (gauge) pressure at the outlet boundary and to eliminate reverse flow problem.

3. Symmetry boundary conditions: Free-slip boundary conditions at the four side boundaries of the computational domain are imposed. The normal velocity components and the normal gradients of all velocity components are assumed to have a zero value.

4. Interior wall boundary conditions: No-slip wall boundary conditions together with the standard wall functions are used to define the interior wall boundaries between wires and flow for turbulent simulation cases.

IV.3. Results and Discussion

IV.3.1. Numerical Validation: friction factor correlation for stacked woven wire matrix

The numerical simulations are performed using the proposed numerical modelling approach for the stacked woven wire matrix and a friction factor correlation is derived from the results of the simulations to fit into the results of Tanaka et al. (Tanaka, et al., 1990) and Gedeon and Wood (Gedeon, et al., 1996) over a range of wire diameter, Reynolds number and volumetric porosity as summarized in Table 4. 1.

Table 4. 1: Tanaka et al. (Tanaka, et al., 1990) and Gedeon and Wood (Gedeon, et al., 1996) experimental range for stacked woven wire matrix and experimentally obtained empirical correlations for frictional pressure coefficient.

	Wire diameter [μm]	Matrix Volumetric Porosity	Re range
Tanaka et al. (Tanaka, et al., 1990)	50 - 230	0.645 – 0.754	10 - 2000
Gedeon and Wood (Gedeon, et al., 1996)	53 - 94	0.623 - .781	0.45 - 6100
Present Study	80 -110	0.387 – 0.641	1 - 400

Tanaka et al. (Tanaka, et al., 1990) and Gedeon and Wood (Gedeon, et al., 1996) obtain friction coefficient correlations based on experimental oscillating flow. For this reason, those correlations are considered for the validation of the numerical model presented for the study of stacked woven wire matrix regenerator.

Tanaka et al. (Tanaka, et al., 1990) investigated the flow and heat transfer characteristics of regenerator materials in an oscillating flow for conventional stacked woven wire matrix, sponge metal (felt) and sintered metal. The prediction of pressure drop loss was possible by use of the hydraulic diameter as the representative length defined by the friction factor and Reynolds number. Tanaka et al. (Tanaka, et al., 1990) observed that the wire diameter is not suitable as the representative length for various porosities and mesh shape. Tanaka et al. (Tanaka, et al., 1990) observed that the friction factor in oscillating flow is about 30 percent higher than the theoretical value of unidirectional flow.

Gedeon and Wood (Gedeon, et al., 1996) obtained correlations for friction factor, Nusselt number and other parameters for stacked and sintered woven wire matrices, and metal felt test regenerator samples. In previous investigations they concluded that there was no significant difference in heat-transfer or pressure drop characteristics produced by sintering compared to cold stacking (random orientation). Gedeon and Wood (Gedeon, et al., 1996) started the modelling friction factors with the standard two-parameter Ergun form (Eq. (2.20)), but this equation showed a better fit to data by introducing a relatively minor modification to the Ergun equation, that they called three-parameter modified-Ergun form:

$$C_f = \frac{a_1}{\mathrm{Re}} + a_2 \,\mathrm{Re}^{a_3} \qquad [4.1]$$

In this correlation, the first and second terms account for the viscous and inertia effects, respectively. The Reynolds number variation in the second term is usually weak (Sun, 2007). The parameter a_3 will be negative but allowing the correlations to better track at high Reynolds numbers, at low Reynolds numbers the a_1/Re will dominate, exactly as the original Ergun equation. In addition, Gedeon and Wood (Gedeon, et al., 1996) introduced the matrix porosity as a parameter in the Ergun equation; unfortunately that expression did not seem to fit the data very well. Even without explicit porosity dependence, porosity does affect the calculation of the hydraulic diameter d_h and maximum flow velocity u_{max} in terms of which friction factor was defined. The error of the combined correlation proposed by them to a generic woven wire matrix is 10%.

In both studies the maximum Reynolds number is calculated based on hydraulic diameter, d_h instead of wire diameter and the pressure drop is defined as follows:

$$\Delta p = C_f \frac{L_r}{d_h} \frac{\rho\left(u_{\max}\right)^2}{2} \qquad [4.2]$$

Although the purpose is to estimate the pressure drop in a wound woven wire matrix, since there are no experimental data available for this case, the first step is to validate the

computational model for a stacked woven wire matrix in comparison with the experimentally obtained empirical correlations proposed by cited researchers above. The validation is made using two wire diameters and two configurations of matrices in which, the first configuration is a stacked woven wire screens perfectly aligned and the second matrix configuration is with the maximum misalignment between them. In Table 4.1 the parametric study range for stacked woven wire matrices is summarized.

Tanaka et al. (Tanaka, et al., 1990) proposed the following empirical relationship (also given in Eq. [2.23]):

$$C_f = \frac{175}{\mathrm{Re}} + 1.60 \qquad [4.3]$$

Gedeon and Wood (Gedeon, et al., 1996) suggested the following three-parameter friction factor correlation (also given in Eq. [2.29]):

$$C_f = \frac{129}{\mathrm{Re}} + 2.91\,\mathrm{Re}^{-0.103} \qquad [4.4]$$

Based on the pressure drop simulation results for four stacked woven wire matrices (defined in Table 3.4), the friction factor is calculated for each Reynolds number value. By fitting these results to the three-parameter Ergun equation form (Eq. [4.1]), a friction factor correlation is obtained.

Figure 4. 5 shows the relationship between friction factor and Reynolds number for the experimental correlations due to Tanaka et al. (Tanaka, et al., 1990) and Gedeon and Wood (Gedeon, et al., 1996) (Eqs. [4.3] and [4.4]) and the friction factor obtained from the results for the first two random misaligned stacked woven wire matrices. It is observed that the friction factor obtained from the misaligned matrix shows a good correspondence with Gedeon and Wood (Gedeon, et al., 1996) correlations with less than 5 percent deviation for low Reynolds number range. When the present stacked wire model is further extended to analyse the pressure drop for a perfectly aligned configuration, 30 percent lower pressure drop values are observed compared to the misaligned case. Based on the results shown, the perfectly aligned ideal configuration can be considered to be the most appropriate solution from the efficiency point of view, even if it is hardly achievable by conventional manufacturing processes.

Having obtained the results from the three-parameter equation (Eq. [4.1]), the friction factor correlation for the misaligned configuration can be derived as in the following equation, where the Reynolds number is calculated based on the hydraulic diameter:

$$C_f = \frac{123}{\mathrm{Re}} + 3.20\,\mathrm{Re}^{-0.104} \qquad [4.5]$$

Based on three-parameter comparison with that of Gedeon and Wood (Gedeon, et al., 1996), it is observed that the main deviation of calculated $C_f$values from those of Gedeon and Wood (Gedeon, et al., 1996) is due to change in values of the principal parameters a_1 (reproduces 4,6% maximum deviation) and a_2 (reproduces of 9,1% maximum deviation). It can be noted here that $a_1$is responsible for the surface friction effect at low Reynolds number while a_2 is responsible for the friction resistance form due to increasing local turbulence effects at higher Reynolds number.

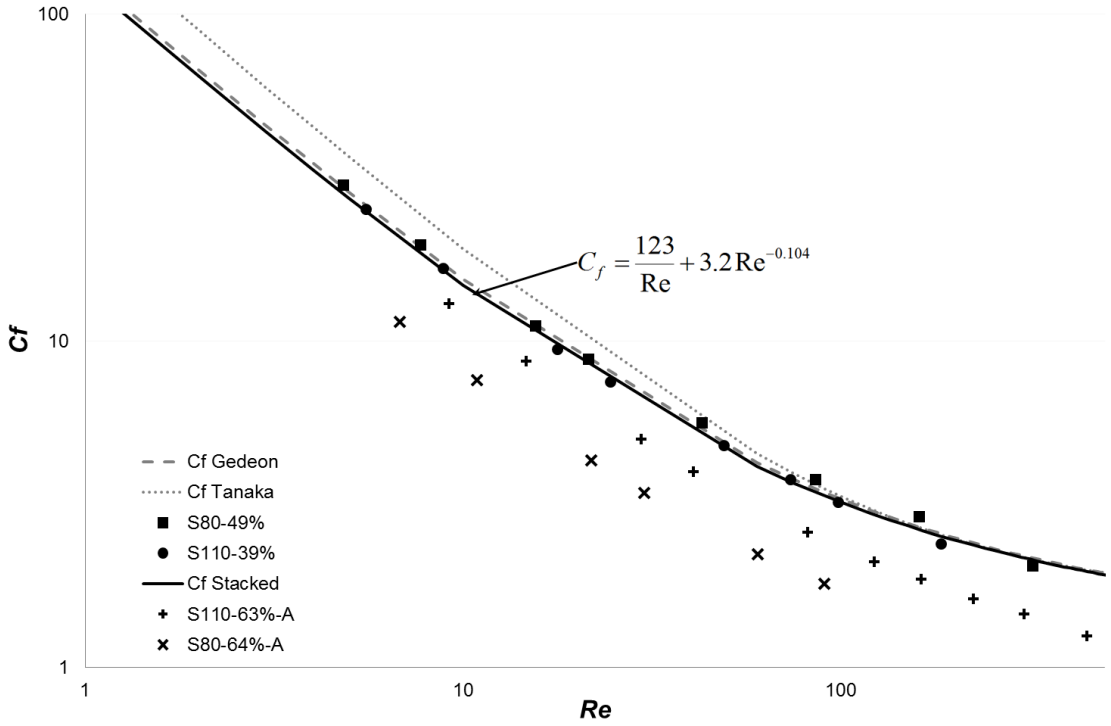

Figure 4. 5: Four Stacked woven wire matrices: friction factor vs. Reynolds number.

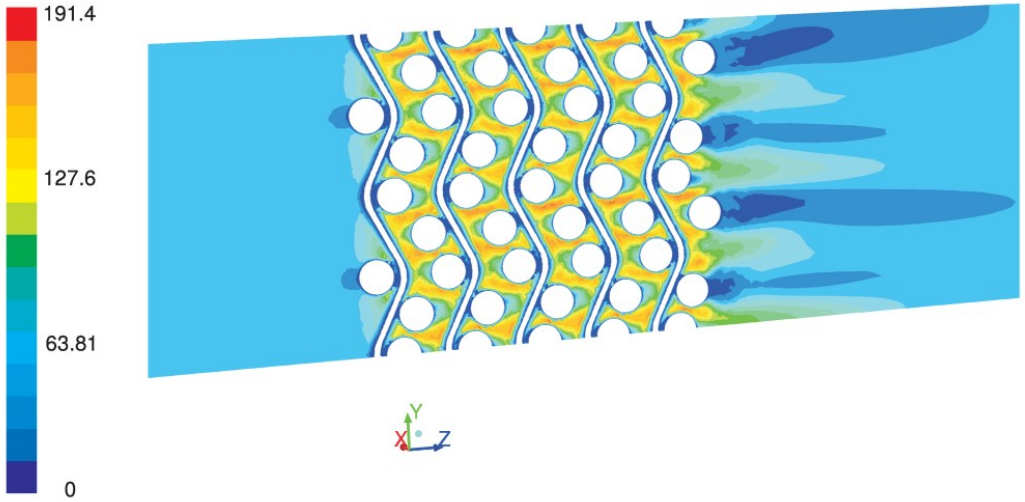

Figure 4. 6: Velocity magnitude (m/s) contours on the mid-span plane of the flow domain at Re = 238 for the stacked woven wire misaligned matrix.

The overall static pressure drop for the present flow problem is mainly governed by the form drag and the skin friction due to wall shear stress at the matrix walls. Thus, the local distribution of the skin friction on the matrix walls demonstrates its significant effects in the determination of the skin friction dependent pressure losses in the flow domain of the stacked woven misaligned matrix configuration (Figure 4. 7a and b). As seen in these figures, the walls of the woven wire matrices are the main sources of the skin friction coefficient and its magnitude increases as the Reynolds number increases. In addition, almost similar local skin friction distributions are obtained for each case. The velocity contours in the mid-span plane of the flow domain shown in Figure 4. 6 also signifies the importance of local increase of velocity magnitudes within the matrix domain as an indication of shear gradients leading to higher wall shear stress and hence friction pressure drops there in comparison with the rest of the flow domain.

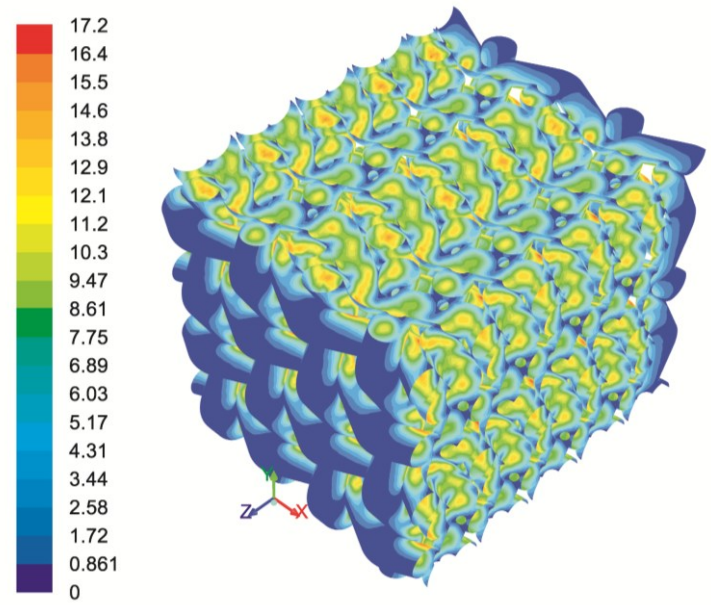

(a)

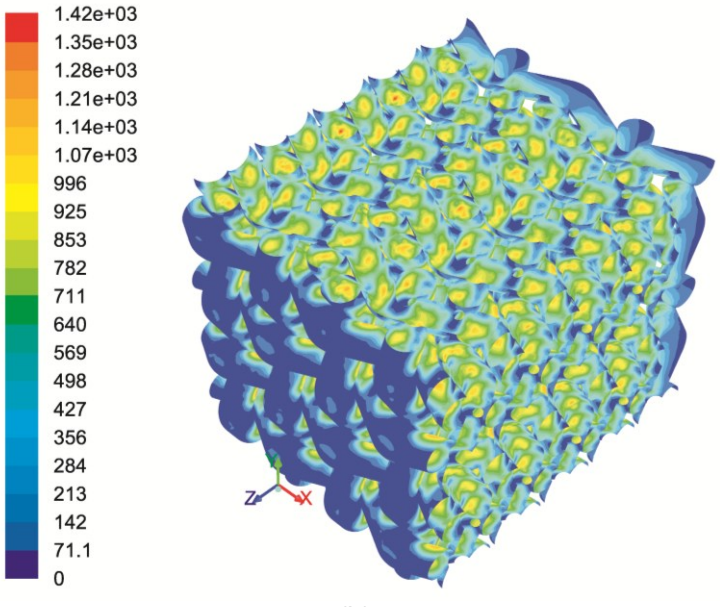

(b)

Figure 4. 7: Friction factor contours obtained for the wall surfaces of the matrices for the stacked woven wire misaligned matrix $(\Pi_v = 0.387)$ domain at different inflow velocities; (a) Re = 5; (b) Re = 170.

In Figure 4. 5 are shown the results for two random configurations of average volumetric porosity of 0.44 and two aligned configurations of average volumetric porosity of 0.64. The friction factor correlation proposed in Eq. [4.5] is based on the results of two stacked woven wire matrix random configurations with a low volumetric porosity. Figure 4. 8 shows the results for a large range of volumetric porosity, Π_v, from 0.387 to 0.685 for random configurations (matrices defined in Table 3.4).

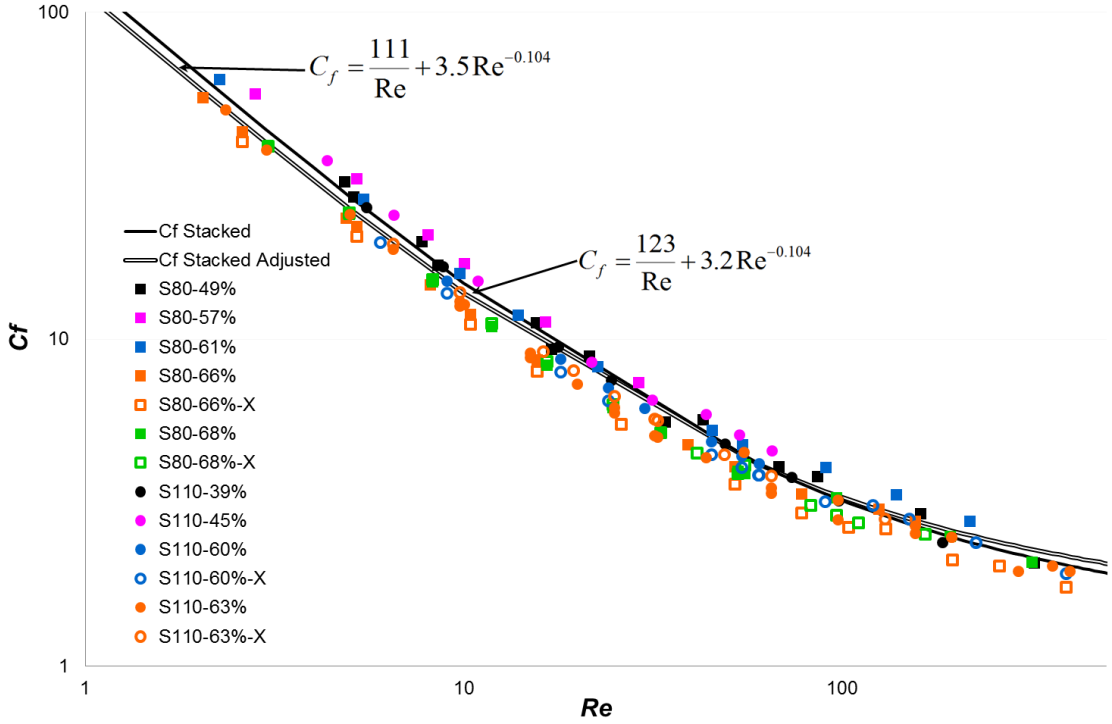

Figure 4. 8: Adjusted Stacked woven wire matrices: friction factor vs. Reynolds number.

The obtained numerical data (Figure 4. 8) ratify the results presented by the authors (Costa, et al., 2012) and suggest that no clear influence of the volumetric porosity over the friction factor through regenerator matrices it observed. However, the effect of the volumetric porosity is included in the hydraulic diameter defined by Eq. [3.28]. In spite of this, the friction factor correlation for stacked woven wire matrices proposed in Eq. [4.5] is adjusted to provide a better fit in all the range of volumetric porosity studied. The adjusted friction factor correlation for the random is given by:

$$C_f = \frac{111}{\mathrm{Re}} + 3.50\,\mathrm{Re}^{-0.104} \qquad [4.6]$$

The following plot (Figure 4. 9) compares the friction factor results for random configuration, aligned configuration and random no-contact configuration (defined in Table 3.4).

The above results (Figure 4. 9) give more evidence about the substantial influence of the geometric configuration of the matrix over the friction factor, independently of the volumetric porosity. The results for the aligned configuration provide the lower friction factor in the same range of volumetric porosity than the random configuration matrices. On the other hand, it is observed that the friction factor increases when there is no contact between screen layers and this could be significantly affected by the volumetric porosity. Consequently, the pressure drop is also function of the hydraulic diameter (Eq. [4.2]) and the hydraulic diameter is function of the volumetric porosity (Eq. [3.28]). For that reason, the interaction between the matrix geometrical parameters, configuration, wire diameter, hydraulic diameter and volumetric porosity require an in-depth study to isolate the influence of each one.

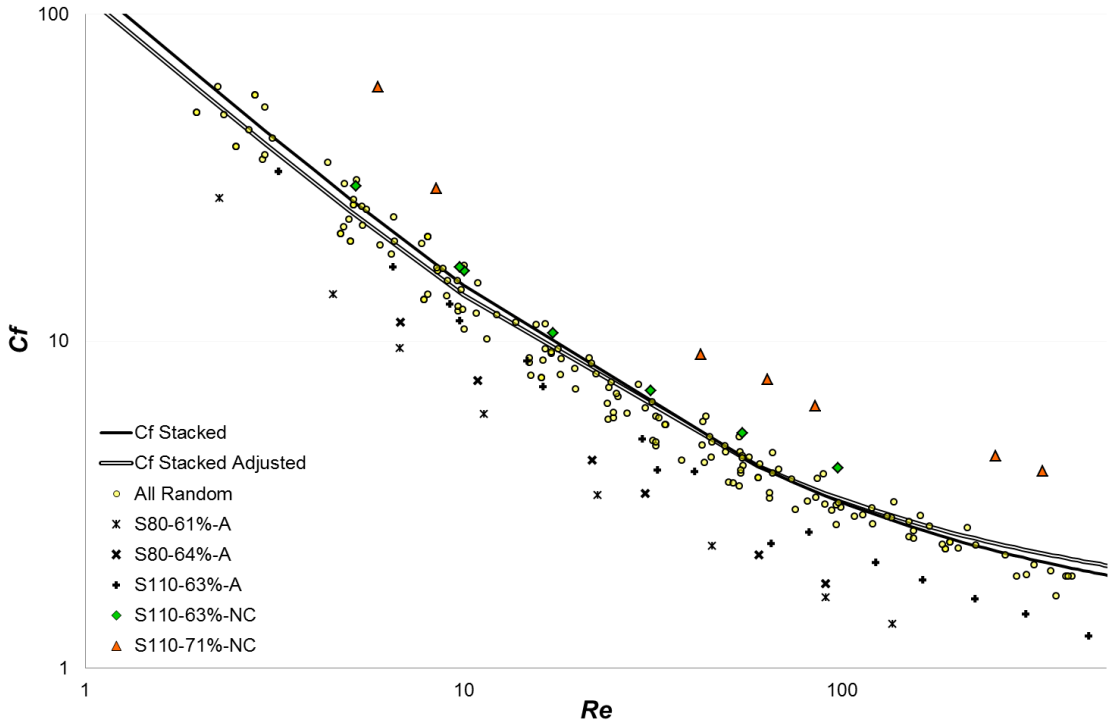

Figure 4. 9: Stacked woven wire matrices: friction factor vs. Reynolds number.

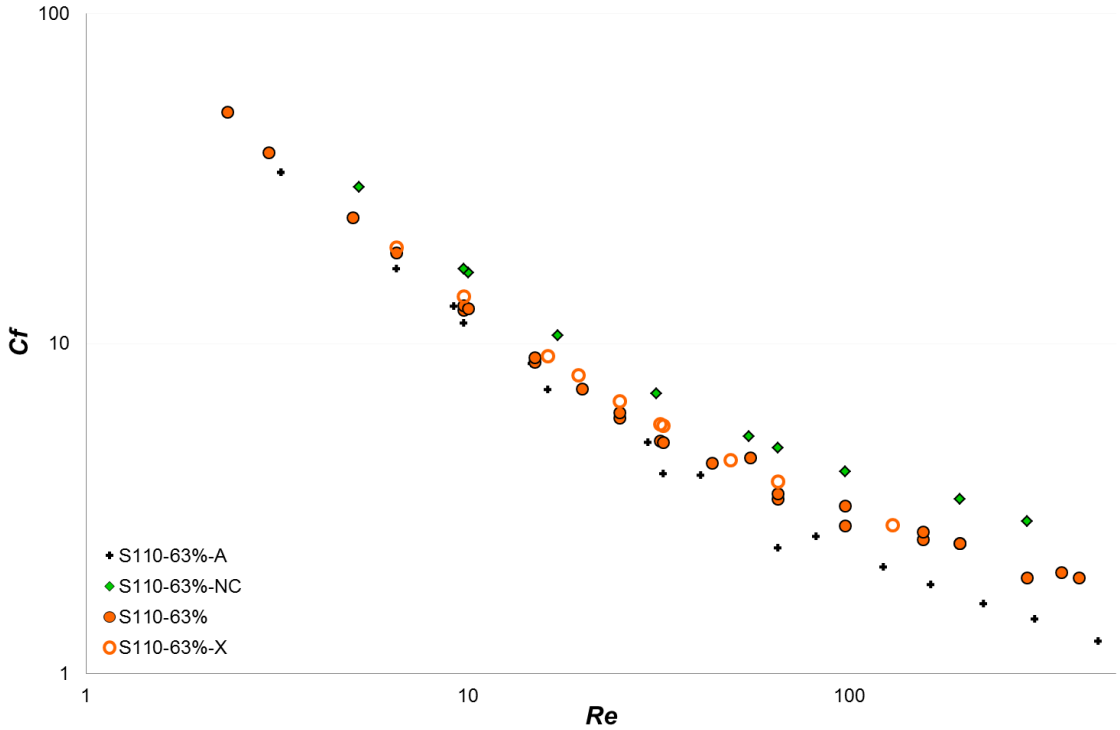

Figure 4. 10: S110-63% configuration matrices: friction factor vs. Reynolds number.

The results shown in Figure 4. 10 suggest that the influence of the geometrical configuration over the flow performance is more noticeable at high Reynolds numbers.

Figure 4. 11 shows the flow velocity vectors through the regenerator matrices within the mid-cutting plane. The inlet velocity and flow direction in all the configurations are the same and the solid matrix is not represented. It is observed that flow regions accompanied with high accelerations and decelerations prevail in all the configurations studied. Also, the low velocity and recirculating flow (wake) accompanied flow regions also prevail, but they are less noticeable in the aligned configuration. In the case of the aligned configuration (Figure 4. 11a), the cutting plane selected represents the flow plane with higher velocity. In the cutting plane shown not any longitudinal wire appears therefore the flow path and the velocity gradient is smaller, in the figure wake regions are observed in the areas between wires. Figure 4. 11 confirms the importance of the internal geometry of the matrix in the velocity gradient and flow characteristics, which determine the pressure drop through the regenerator matrix.

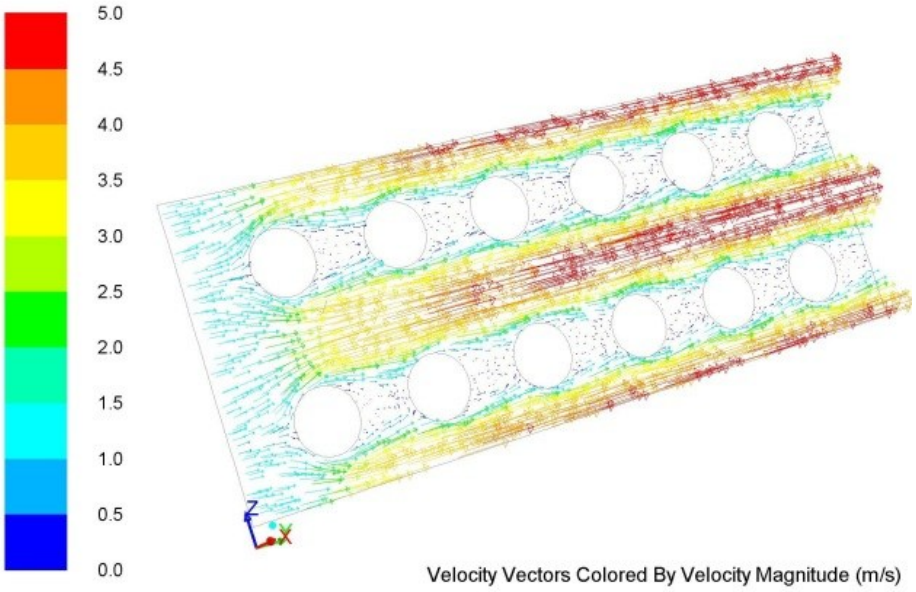

(a)

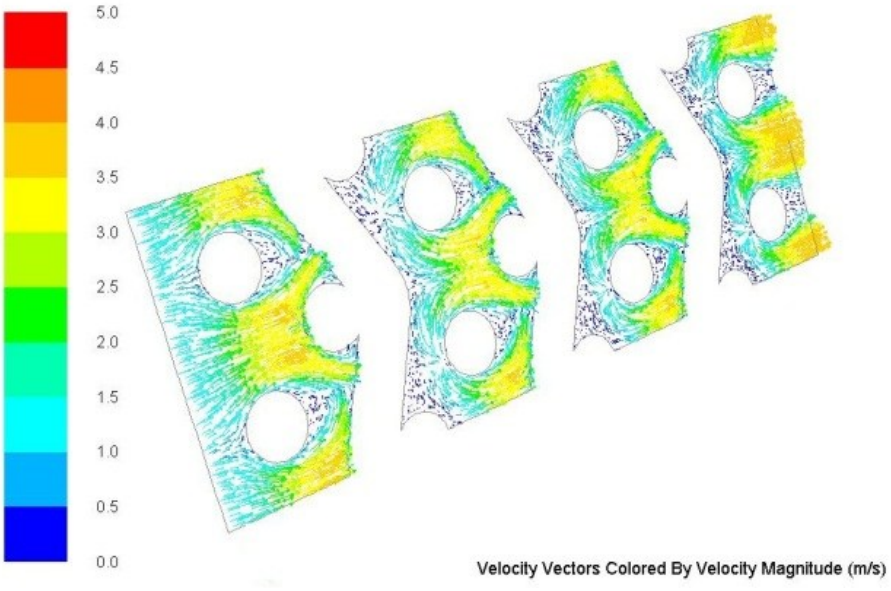

(b)

Figure 4. 11: Velocity magnitude (m/s) contours on the mid-span plane of the flow domain at Re = 50 for the S110-63% Stacked Woven Wire Matrices: (a) Aligned; (b) No-Contact; (c) Random and (d) Cross Random.

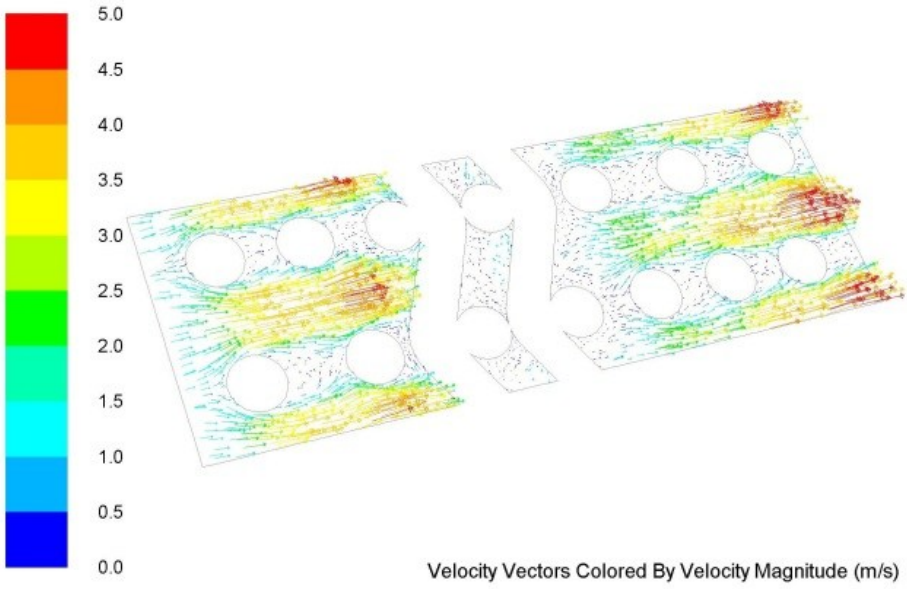

(c)

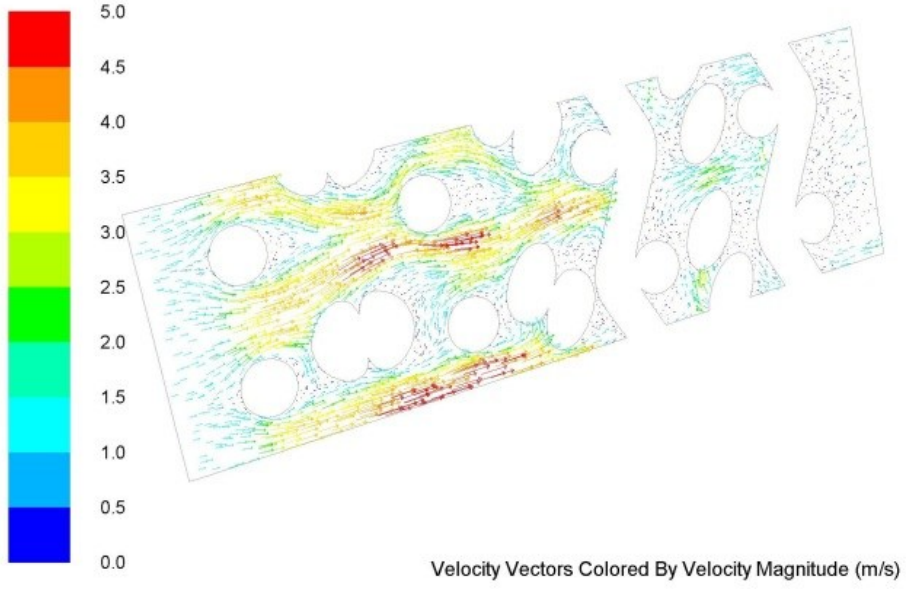

(d)

Figure 4.11 (Cont.): Velocity magnitude (m/s) contours on the mid-span plane of the flow domain at Re = 50 for the S110-63% Stacked Woven Wire Matrices: (a) Aligned; (b) No-Contact; (c) Random and (d) Cross Random.

The next figures present the pressure drop as a function of the length through the regenerator matrix for the four configurations shown in Figure 4. 11. It is observed that the pressure drop behaviour is linear, stepwise and uniform through the regenerator matrix. The lower pressure drop gradient is obtained through the aligned matrix configuration and the higher through the non-contact matrix configuration. For both misaligned configurations the pressure drop gradient obtained per layer is practically the same being slightly lower in the random configurations. This variation is expected through the regenerator matrix.

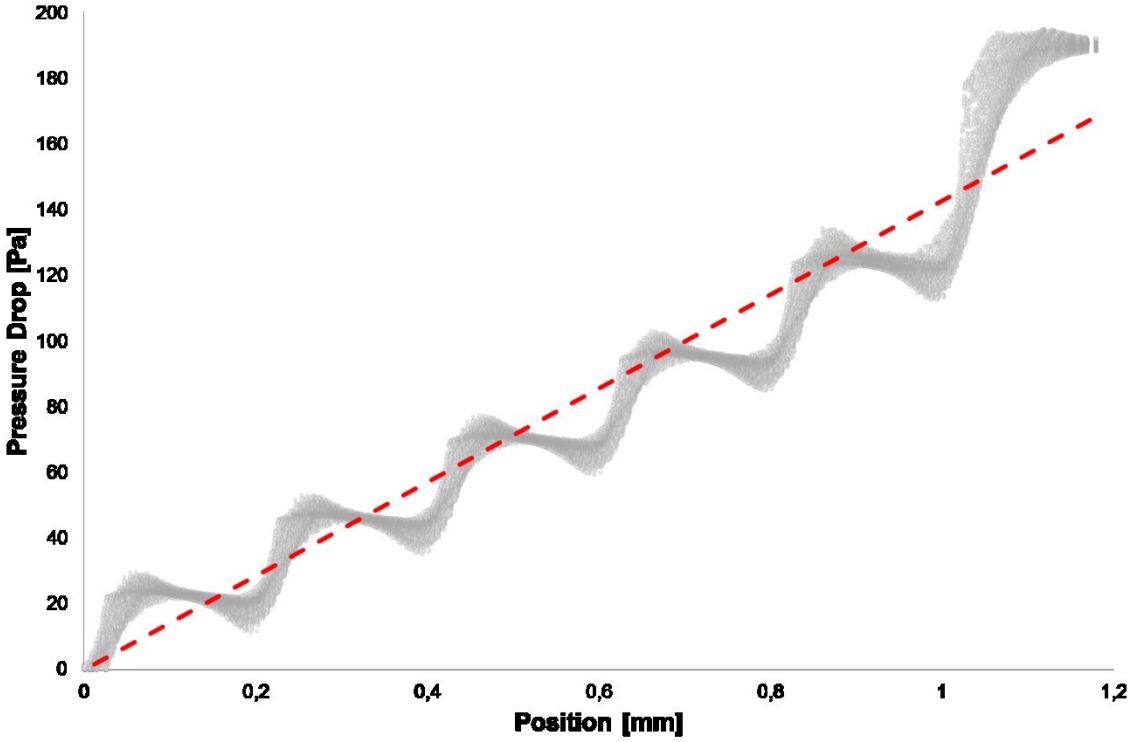

Figure 4. 12: Pressure Drop vs Position through Stacked woven wire matrix S110-63%-A for Re ≈ 50 (1m/s)

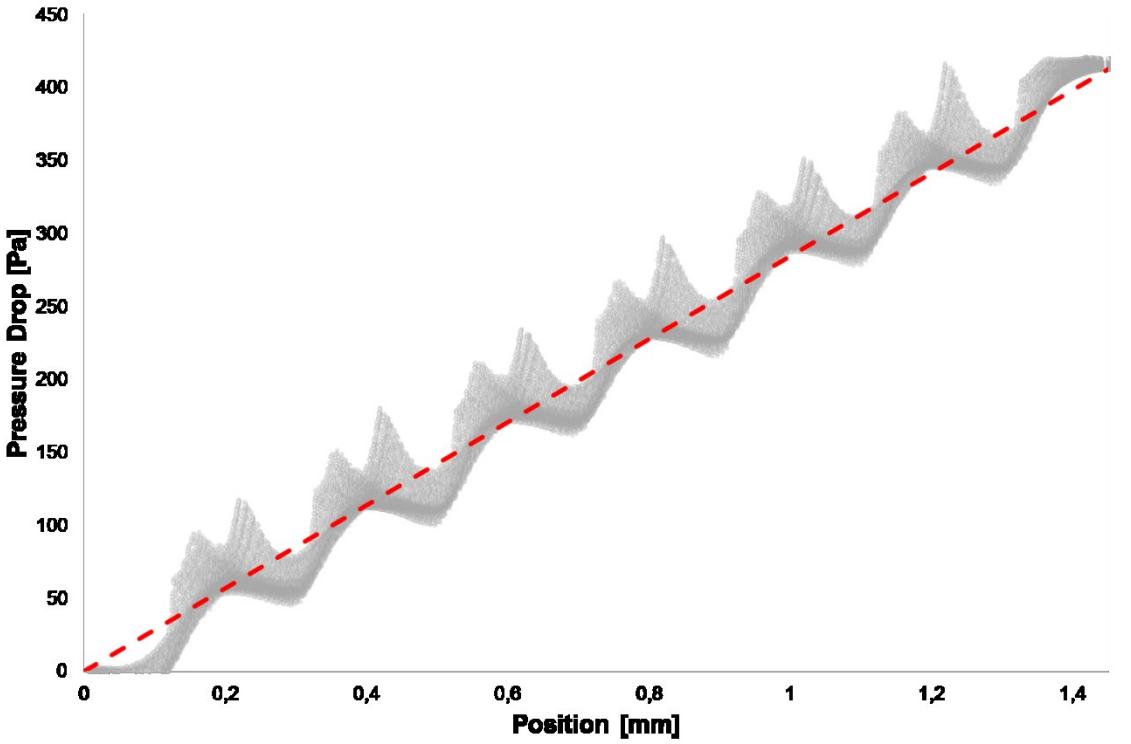

Figure 4. 13: Pressure Drop vs Position through Stacked woven wire matrix S110-63%-NC for Re ≈ 50 (1m/s)

The pressure drop gradient observed is in agreement with the accelerations and decelerations shown in Figure 4. 11, which directly affect the pressure drop through the matrix. In the figures it is shown that the regenerator matrix configuration with lower pressure drop through the matrix is the aligned configuration, therefore this is the more appropriated configuration to minimize power losses.

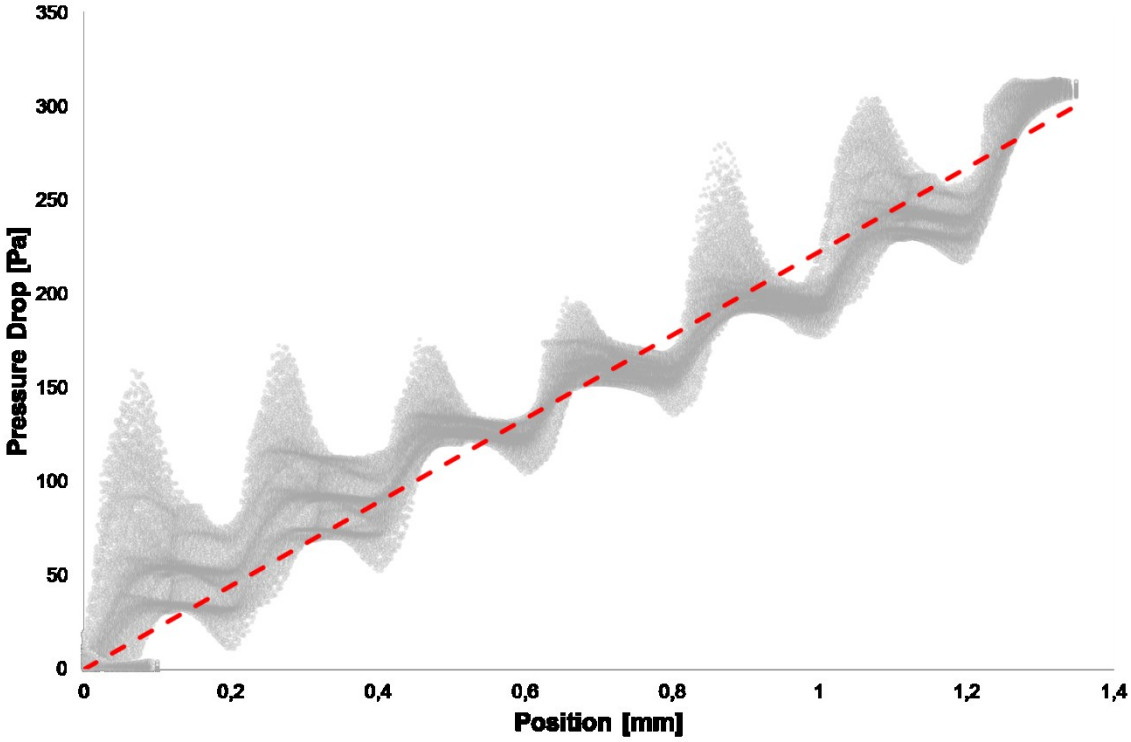

Figure 4. 14: Pressure Drop vs Position through Stacked woven wire matrix S110-63% for Re ≈ 50 (1m/s)

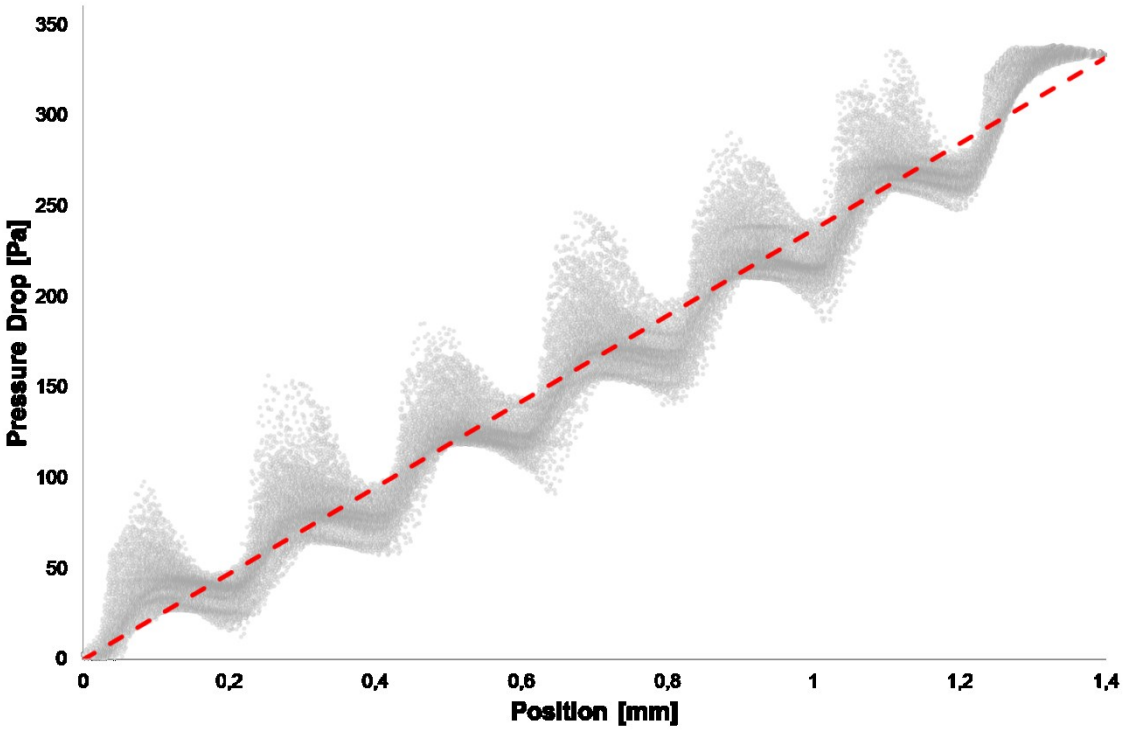

Figure 4. 15: Pressure Drop vs Position through Stacked woven wire matrix S110-63%-X for Re ≈ 50 (1m/s)

IV.3.2. The friction factor correlation for wound woven wire matrix

In the previous section, the numerical methodology is validated and used to derive the friction factor correlation for stacked woven wire matrices. In this section, the numerical methodology is extended to analyse the flow through a wound woven wire matrix configuration. Table 3.4

summarizes the geometrical parameters of the wound woven wire matrices configurations studied.

Figure 4. 16 shows the relationship between friction factor and Reynolds number based on the results for five wound woven wire matrix configurations as proposed by the Costa et al (Costa, et al., 2012). In this figure, the solid line represents the friction factor correlation derived from the results shown in the investigated Reynolds number range. It is found that the average friction factor coefficients obtained for wound woven wire matrix are significantly greater than those obtained from the stacked woven case at low Reynolds numbers (<100), but for high Reynolds numbers the different is less significant.

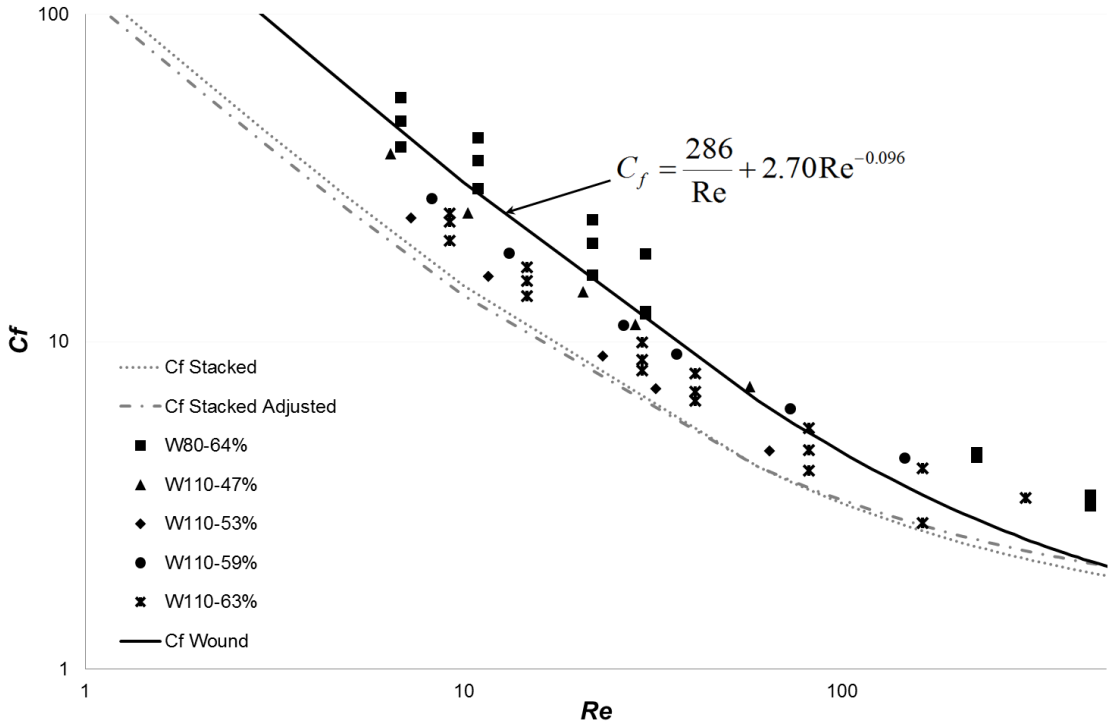

Figure 4. 16: Wound woven wire matrices: friction factor vs. Reynolds number.

Considering that the woven wire matrix winding process is not easily controllable in regard to the alignment of different layers, the approach of an average ratio of the different cases are considered appropriated. Based on the results obtained, the three-parameter equation (Eq. [4.1]) that better fits with the results for the wound woven wire matrix is shown in the next equation (Eq. [4.7]), where the Reynolds number is calculated based on the hydraulic diameter (Eq. [3.33]):

$$C_f = \frac{286}{\mathrm{Re}} + 2.70\,\mathrm{Re}^{-0.096} \qquad [4.7]$$

In the results shown in Figure 4. 16, it is remarkable that for the case corresponding to W80-64% there are three different friction factor results at the same Reynolds number. These results correspond to variations of the misalignment in the matrix configuration. The lowers and higher friction factors correspond to those obtained from the maximum and the minimum misalignment, respectively.

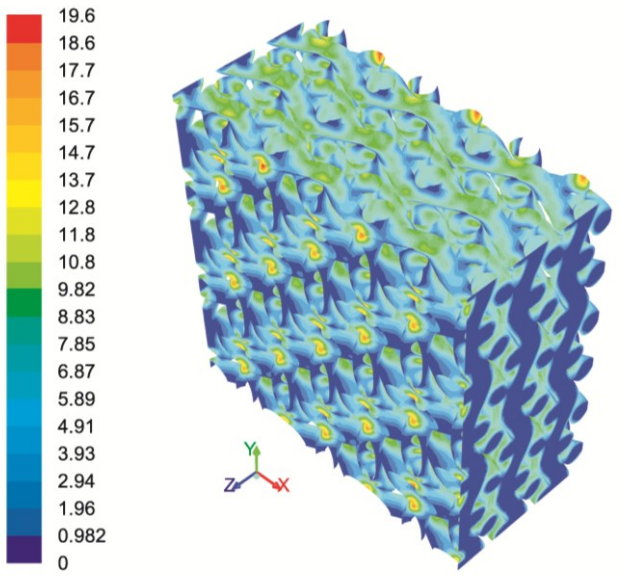

(a)

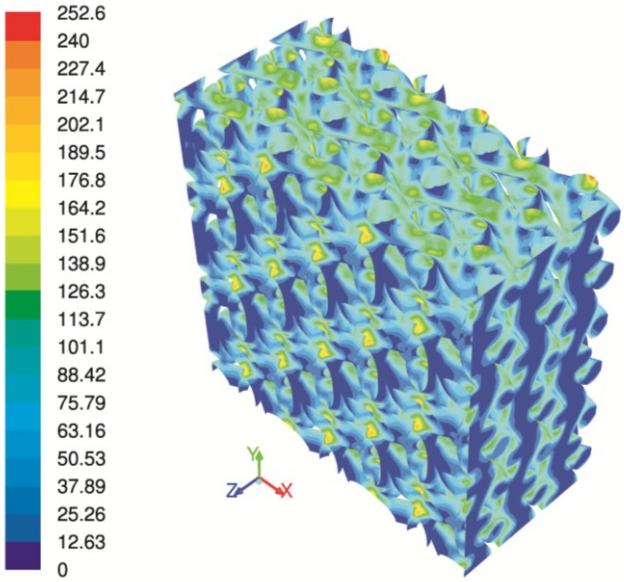

(b)

Figure 4. 17:Friction factor contours obtained for the wall surfaces of the matrices for the wound woven wire misaligned matrix domain at different inflow velocities; (a) Re = 8 and (b) Re = 250.

The skin friction coefficient contours (Figure 4. 17a and b) for the misaligned wound woven wire matrixes at different Reynolds numbers are also provided to make a qualitative comparison between the low and high Reynolds number effects on the distribution of the skin friction and hence the friction pressure losses for the matrix configuration. The similar trend of local skin friction coefficient for the matrix domain is obtained as that of stacked woven wire matrix i.e. the higher the Reynolds number, the lower the skin friction coefficient.

In Figure 4. 18 are presented the results for an increased number of wound woven wire matrices (detailed in the Table 3.4). For the case corresponding to W80-64% the results shown are the average of three misaligned configurations studied. The proposed friction factor correlations (Eq.[4.7]) can be here further adjusted to provide a better fit with all the results shown in Figure 4. 18. Based on the results shown in Figure 4. 18, the three-parameter equation that shows a good agreement with the numerical results obtained for the friction factor as function of the Reynolds number is Eq. [4.8]:

$$C_f = \frac{183}{\mathrm{Re}} + 4.26\,\mathrm{Re}^{-0.104} \qquad [4.8]$$

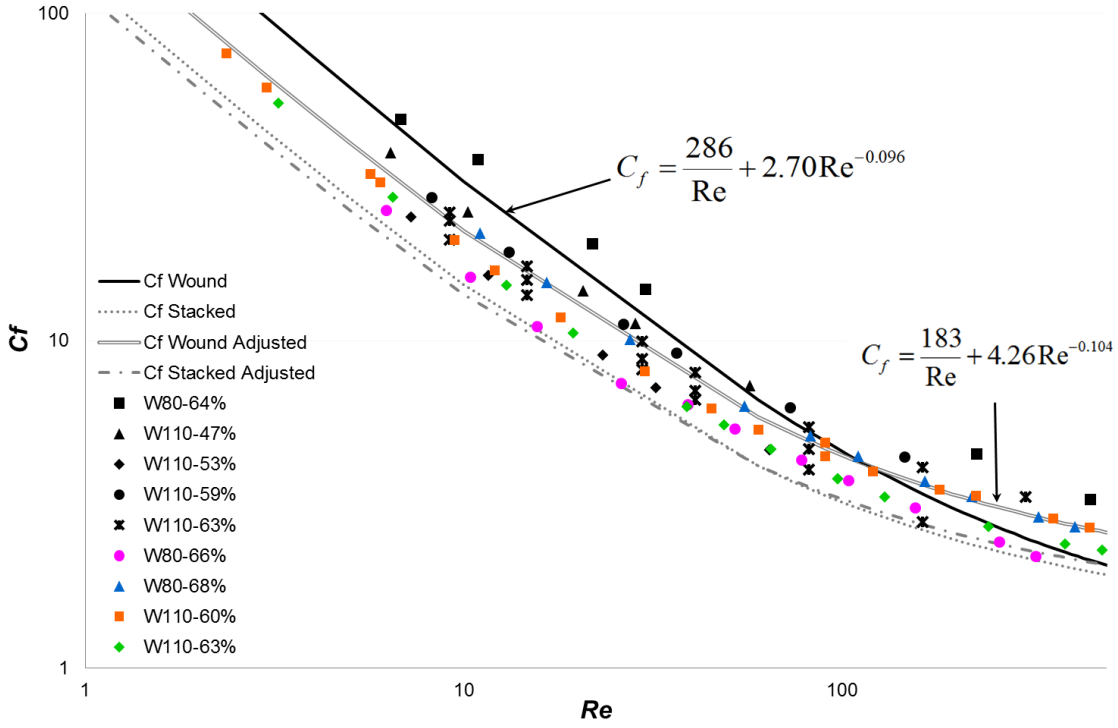

Figure 4. 18: Adjusted Wound woven wire matrices: friction factor vs. Reynolds number.

The general friction factor correlations Eq.[4.8] covers better the new configurations shown in Figure 4. 18 than Eq. [4.7]. The average agreement is within 15% in all the range studied. Based on three-parameter comparison, it is observed that there is an adjustment in the surface friction coefficient (skin) a_1, responsible for the performance at low Reynolds number and in the friction resistance form (drag) a_2, responsible for the performance at higher Reynolds number. The coefficient a_3 allows a better fit at high Reynolds number and the trend observed is similar to stacked woven wire configuration results.

Figure 4. 19 shows the numerical friction factor results for the stacked and wound woven wire matrices, and the lines represent the proposed friction factor correlations for both configurations. Figure 4. 19 demonstrates that the friction factors are higher in the wound woven wire matrix configuration in comparison with the stacked woven wire matrix configuration. Comparing the friction factor adjusted correlations Eq.[4.6] and Eq. [4.8], it is observed that the performance is maintained in the Reynolds number range studied.

Figure 4. 20 shows the pressure drop results obtained from the wound woven wire matrix with a volumetric porosity of 63%. It is observed that the pressure drop behaviour through the wound woven wire mesh matrix is stepped and uniform across the layers of the mesh as in the stacked woven wire matrix configuration.

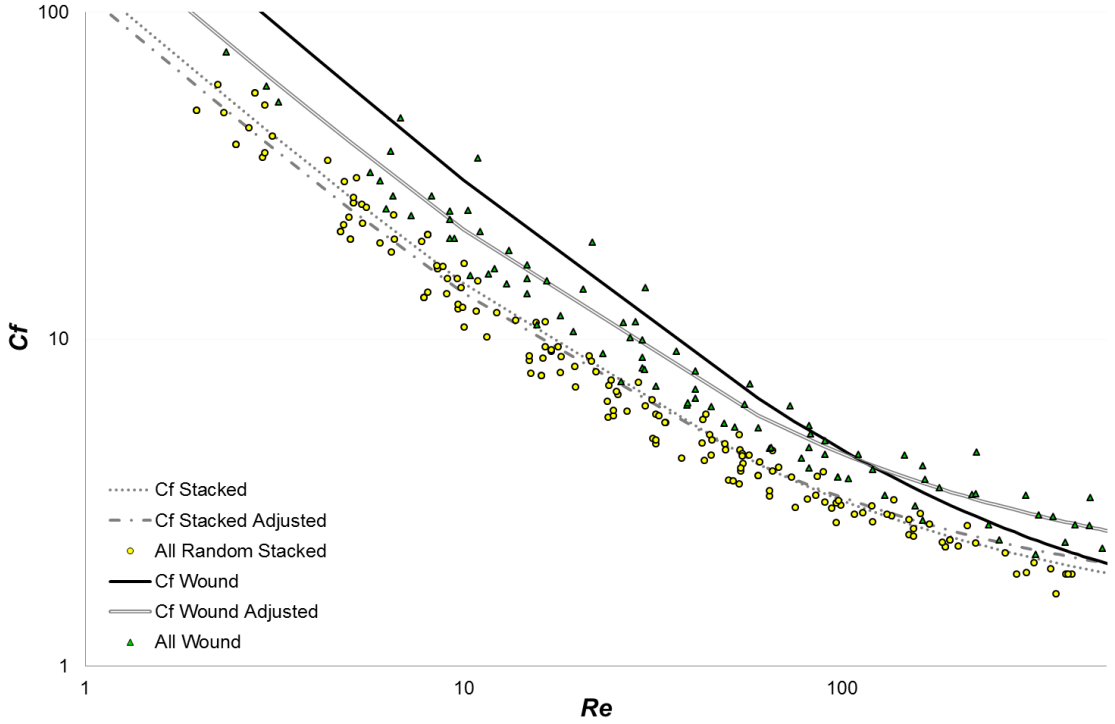

Figure 4. 19: Random Stacked and Wound woven wire matrices: friction factor vs. Reynolds number.

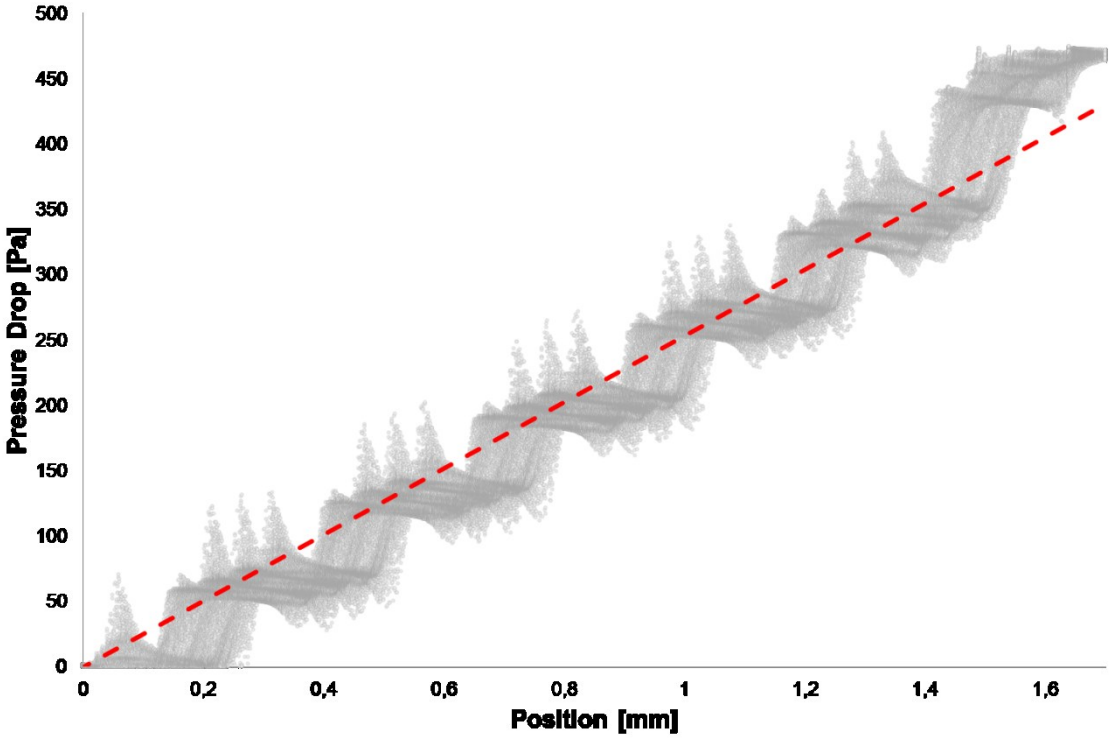

Figure 4. 20: Pressure Drop vs Position through Wound woven wire matrix W110-63% for Re ≈ 50 (1m/s)

Figure 4. 21 shows the tendency of pressure drop through the different regenerator matrix configurations studied for a volumetric porosity of 63%. The tendency is approximated to a straight line as a function of the length. It is clearly observed that the pressure drop gradient for the aligned configuration is the most preferable to minimize power losses in a Stirling engine.

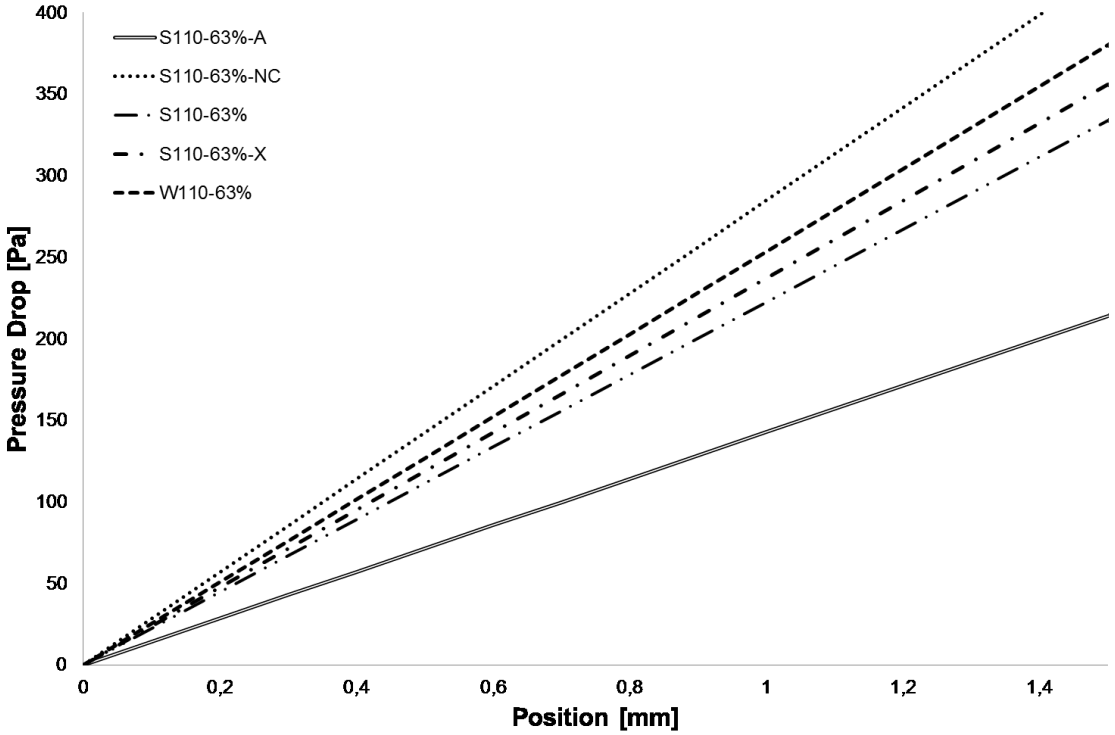

Figure 4. 21: Pressure Drop vs Position through Woven wire matrix 63% for Re ≈ 50 (1m/s) at 0.02s

IV.4. Conclusions

A general correlation equation (Eq. [4.8]) is numerically derived to characterize pressure drop through wound woven wire regenerator matrices under isothermal flow conditions with stationary inflow velocity imposed after an initial numerical validation against experimentally obtained correlation Eq. [4.6] for stacked woven wire.

The validation results show that the derived correlation equation-Eq. [4.8] can be successfully applied in the Reynolds number working range in Stirling regenerators ($Re < 400$), for diameter range from 80 to 110μm and a volumetric porosity range from 0,40 to 0,65 (detailed in Table 3.4). The numerical study extended to wound woven wire model case also demonstrates an easy and effective use of the derived correlation for determining the pressure drop friction factor for the wound woven wire woven model for a large Reynolds number range up to 400. It is believed that the correlations can be used with confidence as a cost effective tool to optimize pressure drop through this type of regenerator minimizing the experimental studies. However, it is expected that the developed correlation be experimentally validated in the future and adjusted with more numerical results.

The quantified comparative analysis between the stacked wire matrix system and the wound woven wire matrix system shows that even though the pressure drop for the wound woven matrices is higher than that of the stacked case, the numerical methodology can be used to optimize wound woven wire matrix configuration by reducing the pressure losses and the cost of this component in the engine. Thus, by reducing pressure losses, it is possible to maximize the indicated power and hence incoming outsource energy to generated electric power transformation ratio for cogeneration and micro-cogeneration applications.

CHAPTER V:

Heat Transfer Characterization

V. HEAT TRANSFER CHARACTERIZATION

This chapter describes the pressure drop and heat transfer characterization of the Stirling regenerator as a second step of the numerical characterization and optimization of such device under non-isothermal flow computations concerning the heat transfer effects of pressure drop phenomena. Considering that the pressure drop results obtained in Chapter IV agree well with the empirical correlations, the approach is extended to characterize the heat transfer together with the pressure drop. The model complexity is increased because the flow simulation is transient (time-dependent) and non-isothermal due to inclusion of heat transfer effects and additional governing flow equation – i.e. the energy equation (Eq.[3.6]) is required to be resolved together with the continuity and momentum equations. In accordance with the numerical modelling approach followed in the first step for determining pressure drop, the heat transfer results obtained for stacked matrix configurations are also directly compared with the well-known experimental data (Gedeon and Wood (Gedeon, et al., 1996)) in this second step for a large range of Reynolds number. Once validated, the present approach is further extended to wound woven wire matrices to derive a Nusselt correlation equation at local instantaneous Reynolds number, in order to facilitate the heat transfer mechanism through this kind of regenerators.

V.1. Introduction

Some Stirling cycle models are based on the heat transfer and pressure drop coefficients for the regenerator. For stacked woven wire screen regenerator matrices, these coefficients are necessarily based upon empirical data because it is not yet possible to solve the complete set of continuity and momentum equations for a random medium such as stacked screens of wire mesh. For the wound woven wire mesh regenerator there are not known empirical heat transfer coefficients. Thus, there is still a very high necessity of characterizing heat transfer in this type of regenerator.

Consequently, the objective is to numerically develop a heat transfer correlation for wound woven matrix regenerator. With this respect, numerical 3-D detailed models for a stacked woven wire matrix are first developed to obtain heat transfer correlations for different configurations and the results are compared with well-known experimentally obtained correlations in order to validate the proposed modelling approach over a specified range of Reynolds number. Later, the numerical study is extended to obtain heat transfer correlation equation for wound woven wire matrices.

V.2. Computational domain and boundary conditions

V.2.1. Numerical methodology

The numerical methodology adopted in the previous chapter for characterization of pressure drop across the Stirling regenerator matrix under isothermal flow condition is extended here to investigate the heat transfer phenomena by solving additional differential governing flow equation for the conservation of energy in de-coupled (segregated) manner. All the fluid properties are assumed constant due to the small range of temperature used in each case (including density, viscosity, specific heat, and conductivity).

The convergence criterion for all the velocity components and for the continuity is set to 10^{-6}, whereas it is set to 10^{-8} for the energy for all simulations. The non-dimensional time step, $\tau_s = u_{max}t/s$ is expressed as the product of the maximum velocity component at the inflow boundary and time elapsed divided by the volume cell size. The non-dimensional time step value is chosen as 0.01 following an initial sensitivity analysis performed for the variation of Nusselt number with respect to different non-dimensional time step size ranging from 0.001 to 0.01 for different Reynolds number of 64 and 355. This test shows that there is no significant influence of choice of non-dimensional time step size between 0.01 and 0.001 on the results of computed Nusselt number value for the investigated Reynolds number.

V.2.2. Computational domain and boundary conditions

The computational domain is illustrated in Figure 4.1 (geometry set-up) in which the woven wire matrix and the flow through woven wire matrix geometry is extensively analysed as a representation of a differential part of a Stirling regenerator arrangement. The inlet and outlet flow areas are set to approximately 0.5 mm^2 and woven wire matrix length is approximately 1.5 mm. The Reynolds number (Eq. [3.33]) based on hydraulic diameter (Eq. [3.28]) is varied from 4 to 400. In some simulations the computational domain is further extended in the downstream direction (in the nominal direction of the outlet flow) in order to avoid reverse flow conditions at the outflow boundary.

Miyabe et al. (Miyabe, et al., 1982) indicated that the empirical equation derived for Nusselt number is expressed in a generalized form, and it is recommended that the matrix be made so that all screens are closely stacked. If each screen is not stacked perfectly, or when any gap exists between the screens, the friction coefficient and Nusselt number will deviate from the actual value to some extent.

In Figure 5. 1 are shown the matrix surface mesh for a stacked and wound woven wire matrix and a two-dimension (2-D) section in the flow direction for fluid. In the heat transfer characterization, working fluid flow domain and solid wire matrix are both meshed.

The computational domain is constructed of non-uniformly distributed different hybrid mesh systems containing over 2.5 million tetrahedral and/or hexahedral volume cells for the final mesh system. The tetrahedral cells are used in the wire matrix and air volume inside the matrix with very fine mesh resolution in the close vicinity of the wire surfaces to resolve sharply varying velocity and pressure gradients there. The effect of the mesh resolution on the flow is previously assessed in Chapter IV (Figure 4.4) for three different mesh systems containing non-uniformly distributed hybrid grid cells in a quarter of the computational domain. It is demonstrated that there is no major difference among the computed values and the mesh system of over 2.5 million hybrid volume cells, the number of cell is multiplying by four. Thus, the final mesh system could be considered to be fine enough to study the effects of Reynolds number on the heat transfer characterization.

The boundary conditions for the numerical characterization of the heat transfer through the regenerator matrix are imposed with the same manner for those specified in Chapter IV except additional thermal boundary conditions here with constant working fluid temperature at the inlet and initial temperature in the solid matrix.

V.2.3. Heat transfer model

Although the following equations represent a very simplified form of the general energy conservation equation, they are useful to construct a basis for a comprehensive study of the regenerator applications. This may also facilitate a reasonable qualitative interpretation of the results.

Figure 5. 2 shows a volume of the regenerator matrix of hydraulic diameter d_h and length L_r, volumetric porosity Π_v, temperature of the solid matrix wall T_r, temperature of the working gas T_g and a differential control volume $A_x dx$. The solid matrix to gas heat transfer Q can be expressed in terms of average heat transfer h coefficient for the whole regenerator volume $A_x L_r$ as follows:

$$Q = hA_{wr}\left(T_r - T_g\right) \qquad [5.1]$$

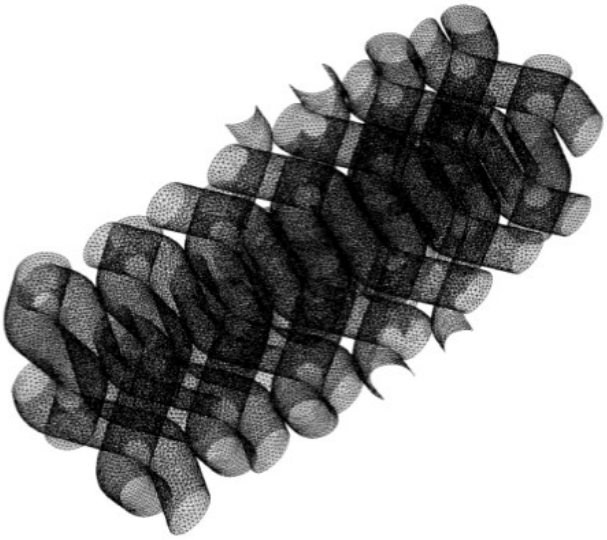

(a)

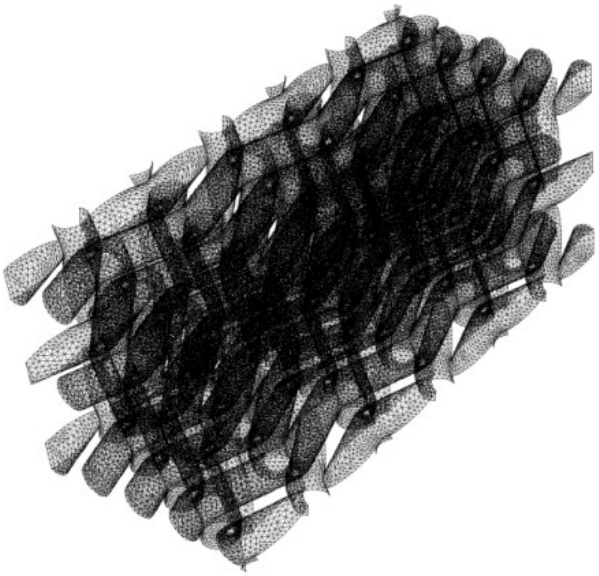

(b)

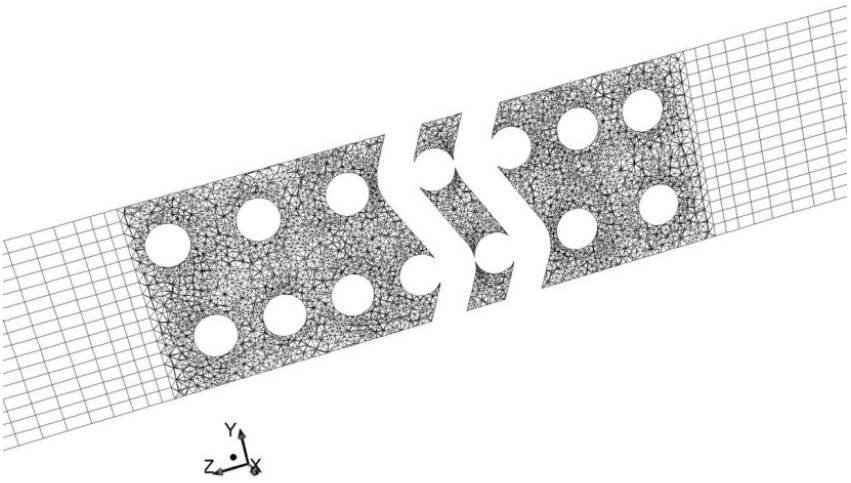

(c)

Figure 5. 1: a) 3-D view of the surface mesh for a stacked woven wire matrix; b) 3-D view of the surface mesh for a wound woven wire matrix and c) 2-D plane view of stacked woven wire flow mesh.

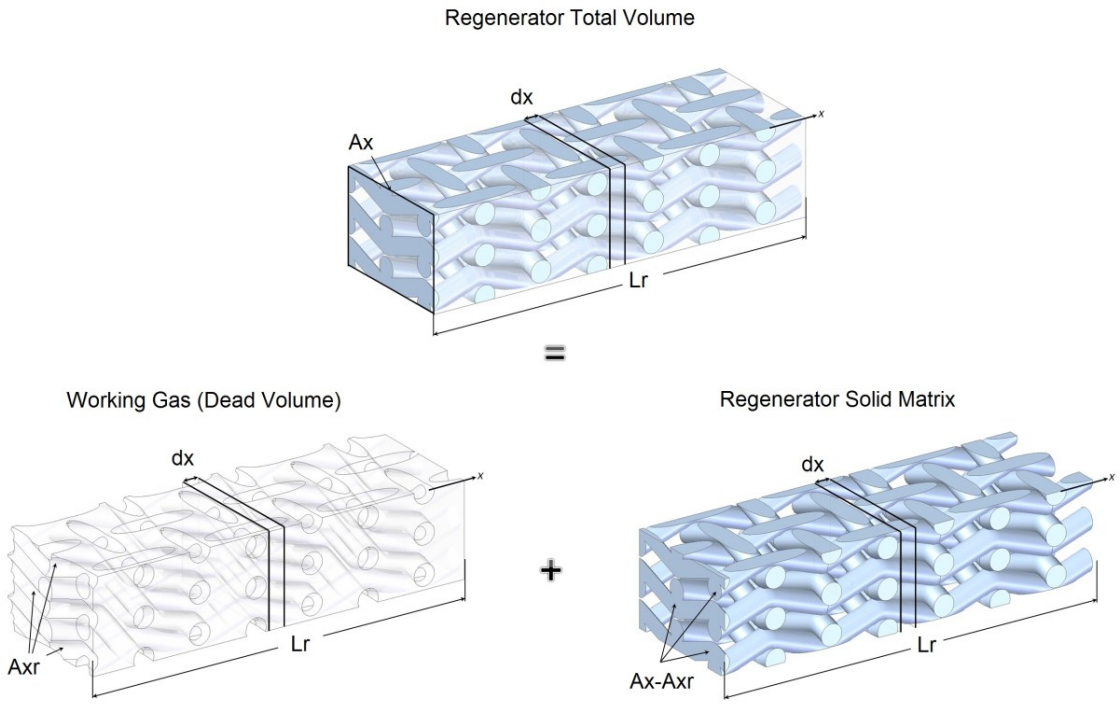

Figure 5. 2: Thermal Analysis of Regenerator Matrix

Starting from one-dimensional gas energy equation given by Eq. [3.6] and considering the following simplifications:

- Neglected kinetic energy effects $(u^2/2)$
- expressing $\rho_g E = (c_{vg}/R)p$ and, $\rho_g E + p = c_{pg} R T_g$
- Assuming the mass flow is uniform in the matrix,
- Specific gas capacities are independent on temperature,
- Matrix temperature is linear and
- Apparent conductivity is not a function of x.

By combining the last two assumptions the term becomes as $\frac{\partial q}{\partial x} = k_a \frac{\partial^2 T}{\partial x^2} \approx 0$. In the differential control volume $A_x dx$ the gas mass is the density ρ_g multiplied by the fraction of the control volume occupied by the gas, $\Pi_v A_x dx = A_{xr} dx$ and considering the solid matrix to gas heat transfer the gas energy equation is converted to:

$$\left[\rho_g c_{vg} \frac{\partial T_g}{\partial t} + \rho_g u c_{pg} \frac{\partial T_g}{\partial x}\right] A_{xr} dx = h A_{wr} \left(T_r - T_g\right) \frac{dx}{L_r} \qquad [5.2]$$

The gas energy Eq. [5.2] is expressed in terms of regenerator matrix hydraulic diameter as follows:

$$\rho_g c_{vg} \frac{\partial T_g}{\partial t} + \rho_g u c_{pg} \frac{\partial T_g}{\partial x} = \frac{4}{d_h} h \left(T_r - T_g\right) \qquad [5.3]$$

For the regenerator matrix, the solid energy equation of the control volume is given by Eq. [5.4]:

$$dm_r c_{pr} \frac{\partial T_r}{\partial t} = h A_{wr} \left(T_g - T_r\right) \frac{dx}{L_r} \qquad [5.4]$$

The elemental regenerator matrix mass, dm_r is obtained by multiplying the regenerator material density ρ_r by the fraction of the control volume occupied by solid material. In terms of the volumetric porosity, the fraction is $A_{xr}(1-\Pi_v)dx/\Pi_v$. Therefore, the regenerator solid energy equation is transformed into Eq. [5.5]:

$$\rho_r c_{pr} A_{xr} dx \frac{(1-\Pi_v)}{\Pi_v} \frac{\partial T_r}{\partial t} = h A_{wr} (T_g - T_r) \frac{dx}{L_r} \quad [5.5]$$

The solid energy Eq. [5.5] is expressed in terms of regenerator matrix hydraulic diameter as follows:

$$\rho_r c_{pr} \frac{\partial T_r}{\partial t} = \frac{4}{d_h} \frac{\Pi_v}{(1-\Pi_v)} h(T_g - T_r) \quad [5.6]$$

From a macroscopic engineering point of view, the heat transfer through the regenerator matrix could be easily solved by Eq. [5.7] to obtain the instantaneous heat transfer coefficient based on numerical modelling results between two planes as follows:

$$h = \frac{\dot{m} c_{pg} \Delta T_g}{A_{wr} \Delta T_m} \quad [5.7]$$

Where the $\dot{m}$ is the mass flow of the working gas, c_{pg} is the gas specific heat at constant pressure, ΔT_g is the difference in gas temperature between the entrance and exit plane in the model, A_{wr} is the regenerator wetted area and ΔT_m is the log-mean temperature difference between the regenerator matrix surface and working gas.

Eq. [5.7] implies that in the experimental analysis of the regenerator matrices the specific heat transfer area is necessary to calculate the heat transfer coefficient. In the majority of experimental studies (Tanaka, et al., 1990) (Gedeon, et al., 1992) the heat transfer area of woven wire screens is expressed as $\varphi = \pi V_t / s$ where s is the pitch of the mesh and V_t is the total volume of the regenerator (Thomas, et al., 2000). Miyabe et al. (Miyabe, et al., 1982) suggested reducing the gross heat transfer area, given by the total surface of the wires in the matrix, by the contact areas between each two wires. Thomas and Bolleber (Thomas, et al., 2000) proved that the reduction of the total surface area of the matrix by the contact areas between the wires is necessary in order to correlate experimental heat transfer data of Stirling engine regenerators. Moreover, the results presented by Kolodziej et al. (Kolodziej, et al., 2012) indicated that the number of wire sheet stacked in the test did not influence the heat transfer intensity because in their experiments the sheets were separated by thin gaps to avoid their contact.

The wetted regenerator area, A_{wr}, is measured in the detailed geometry where the solid matrix is only considered as the working fluid heat transfer area. For stacked woven wire matrices studied (See Table 3.4), the porosity difference between single screen and matrix volumetric porosity is similar to the difference in the samples used by Gedeon and Wood (Gedeon, et al., 1996) (see Table 5. 1).

V.3. Results and Discussion

V.3.1. Numerical Validation: Heat transfer correlation for stacked woven wire matrix

In this section, the numerical simulations are performed using the proposed FVM method based numerical modelling approach for the stacked woven wire matrix and a Nusselt number correlation equation is derived from the results. The derived correlation is validated against empirical results provided by Tanaka et al. (Tanaka, et al., 1990) and Gedeon and Wood (Gedeon, et al., 1996), over a range of wire diameter, Reynolds number and volumetric porosity as summarized in Table 5. 1.

Tanaka et al. (Tanaka, et al., 1990) investigated the flow and heat transfer characteristics of regenerator materials in an oscillating flow for conventional stacked woven wire matrix, sponge metal (felt) and sintered metal. Tanaka et al. (Tanaka, et al., 1990) obtained the heat transfer area by multiplying the specific area of the mesh by the regenerator total volume. Tanaka et al. (Tanaka, et al., 1990) suggested that the heat transfer coefficient in the oscillating flow may be higher than in unidirectional flow.

Gedeon and Wood (Gedeon, et al., 1996) presented correlating expressions in terms of Reynolds or Peclet number for friction factors, Nusselt numbers, enhanced axial conduction ratios and overall heat flux ratios in stacked woven wire matrices and metal felt test regenerator samples. One of the main conclusions of the Gedeon and Wood (Gedeon, et al., 1996) investigation was that under the range of conditions tested, which were intended to be representative of most Stirling applications, they found no essential differences compared to steady flow. In other words, instantaneous local Reynolds number or Peclet number appear to characterize the flow quite adequately.

As can be understood from the well documented literature above, there is not a clear consensus about the effect of the oscillating flow conditions in the Stirling regenerators. On one hand, Tanaka et al. (Tanaka, et al., 1990) suggested that it could enhance the heat transfer, on the other hand, Gedeon and Wood (Gedeon, et al., 1996) concluded that there are not significant different with steady conditions in the Stirling regenerator working range. In the previous chapter the numerical results show good agreement with the experimental results obtained under oscillating flow conditions, even though the numerical simulation is conducted under not oscillating flow conditions. Therefore, those experimental investigations are considered for the validation of the numerical model presented for the study of stacked woven wire matrix regenerator.

In both studies, Tanaka et al. (Tanaka, et al., 1990) and Gedeon and Wood (Gedeon, et al., 1996), the maximum Reynolds number is calculated from Eq. [3.33] based on hydraulic diameter, d_h instead of the wire diameter. The hydraulic diameter is defined by Tanaka et al. (Tanaka, et al., 1990) as:

$$d_h = \frac{4}{\phi}\frac{\Pi_v}{\left(1-\Pi_v\right)} \qquad [5.8]$$

Where Π_v is the volumetric porosity and ϕ is the shape factor defined as the ratio of the mesh surface area to the mesh volume.

The hydraulic diameter is defined by Gedeon and Wood (Gedeon, et al., 1996) as:

$$d_h = \frac{d_w \Pi_v}{\left(1-\Pi_v\right)} \qquad [5.9]$$

The difference between these two definitions (Eqs. [5.8] and [5.9]) of the hydraulic diameter is not significant. However, the definition of hydraulic diameter can be used here as proposed by Gedeon and Wood (Gedeon, et al., 1996). This definition is the same with the one defined in Chapter III by Eq. [3.28].

The specific heat transfer area in a woven wire mesh, φ, is generally defined by Eq. [3.32] and Reynolds number can be defined by Eq. [3.33]. The maximum flow velocity u_{max} is obtained by dividing the frontal maximum velocity by porosity by Eq. [3.31].

The Nusselt number, which is the dimensionless convective heat transfer coefficient, is defined as the ratio of the convective heat transfer to conductive heat transfer normal to the flow direction by:

$$Nu = \frac{hd_h}{k_g} \qquad [5.10]$$

Where d_h is the hydraulic diameter, $k_g$is the thermal conductivity of the working fluid, and h is the heat transfer coefficient. The heat transfer coefficient, h, is based on the instantaneous heat flux and instantaneous solid matrix to bulk mean fluid temperature difference. The heat transfer coefficient is calculated from the numerical result using Eq. [5.7].

Generally, the Nusselt number correlation is a function of Reynolds and Prandtl number (Peclet number). However, when dealing with the heat transfer in the regenerator of a Stirling machine, the Prandtl number is insignificant, since it can always be approximated as 0.7 for the gases used as working fluids in Stirling machines. Consequently, the impact of Re is given by the following general correlation (Thomas, et al., 2000):

$$Nu = c_1 + c_2 \mathrm{Re}^{c_3} \qquad [5.11]$$

In Eq. [5.11] the coefficients are constants and are determined by the experimental data. Thomas and Bolleber (Thomas, et al., 2000) observed that the Nusselt number is not only a function of Reynolds number. The majority of experimental data reveal the additional influence of the porosity on Nusselt number. Thus the effect of the porosity must be attributed to the specific heat transfer area. The impact of the property data on the working fluid, given by the Prandtl number, is also negligible.

Although the purpose is to estimate the heat transfer in a wound woven wire matrix, since there are no experimental data available for this case, the first step is to validate the computational model for a stacked woven wire matrix in comparison with the experimentally obtained empirical correlations proposed by cited researchers above. The validation is made using two different wire diameters and two configurations of matrices in which, the first configuration is a stacked woven wire screens paralleled misaligned and the second matrix configuration is oriented 45º with its neighbour so as to simulate a “random stacking”. Furthermore, the stacking volumetric porosity has two levels for the same woven wire mesh in order to cover any possible stacking process variation. In Table 3.4 the parametric study range for stacked woven wire matrices is summarized.

Tanaka et al. (Tanaka, et al., 1990) proposed the following empirical relationship (the same as Eq. [2.38]) for Nusselt number in a Re number range of $10 \le \mathrm{Re} \le 150$:

$$Nu = 0.33\mathrm{Re}^{0.67} \qquad [5.12]$$

Table 5. 1: Gedeon/Wood (Gedeon, et al., 1996) and Tanaka et al. (Tanaka, et al., 1990) tested regenerators

	Woven Wire Mesh Geometry				Stacked Regenerator Matrix		
	Wire/inch	d_w [μm]	l [μm]	**Porosity**	Π_v	φ [1/μm]	d_h [μm]
Gedeon and Wood (Gedeon, et al., 1996)	200	53.3	74	0.670	0.623 (-4.7%)	0.028	88
	100	55.9	198	0.827	0.781 (-4.6%)	0.016	199
	80	94.0	224	0.767	0.710 (-5.7%)	0.012	230
Tanaka et al. (Tanaka, et al., 1990)	50	230	278	0.644	0.645 (+0.1%)	0.006	418
	100	100	154	0.691	0.711 (+2.0%)	0.012	246
	150	60	109	0.722	0.754 (+3.2%)	0.016	184
	200	50	77	0.691	0.729 (+3.8%)	0.022	135

Gedeon and Wood (Gedeon, et al., 1996) based on combining data sets proposes the following master correlation (the same as Eq. [2.39]) for woven wire matrix in terms of Peclet number ($RePr$):

$$Nu = \left(1 + 0.99 Pe^{0.66}\right) \Pi_v^{1.79} \qquad [5.13]$$

Gedeon and Wood (Gedeon, et al., 1996) justified the constant "1" in the Nusselt number expression (Eq. [5.13]) because Nu tends to become a constant value for $Pe \approx 0$ as occurs in fully developed internal laminar flow. Gedeon and Wood (Gedeon, et al., 1996) claimed that a value of $Nu_0 \approx 1$ seems reasonable in the light of the published limiting value of 0.43 for flow normal to a single cylinder. Eq. [5.13] becomes Equation [5.14] for $Pr \approx 0.73$ and $\Pi_v \approx 0.69$ (Average volumetric porosity in the heat transfer study presented):

$$Nu = 0.51 + 0.40 \mathrm{Re}^{0.66} \qquad [5.14]$$

The relative accuracy of the results of Gedeon and Wood (Gedeon, et al., 1996) for heat transfer correlations is more dependent on Reynolds number. Thus the worst relative error is about 10% at peak Reynolds number on the order of 1000 and it is about 50% for peak Reynolds numbers below about 5.

Table 5. 1 summarizes the geometrical characteristics of the woven wire mesh and the samples tested for different authors. It is important to highlight that in the regenerator samples used by Gedeon and Wood (Gedeon, et al., 1996) for obtained empirical correlations, the volumetric porosity, Π_v, is approximated 5% lower than the single mesh porosity. However, in the samples used by Tanaka et al. (Tanaka, et al., 1990), the volumetric porosity, Π_v, is approximated 3% higher, this could means that there is not contact between different layers. The models simulated are similar to the Gedeon and Wood (Gedeon, et al., 1996) as is defined in Table 3.4.

Eight different configurations of stacked woven wire matrices are numerically studied here, four of them are parallel configurations (Fig. 3.7a) and the others are cross configurations (Fig. 3.7b). Based on heat transfer results the Nusselt number is calculated for a Reynolds number range from 4 to 400. By fitting these results to the three coefficient equation form (Eq. [5.11]), Nusselt number correlation equation is obtained.

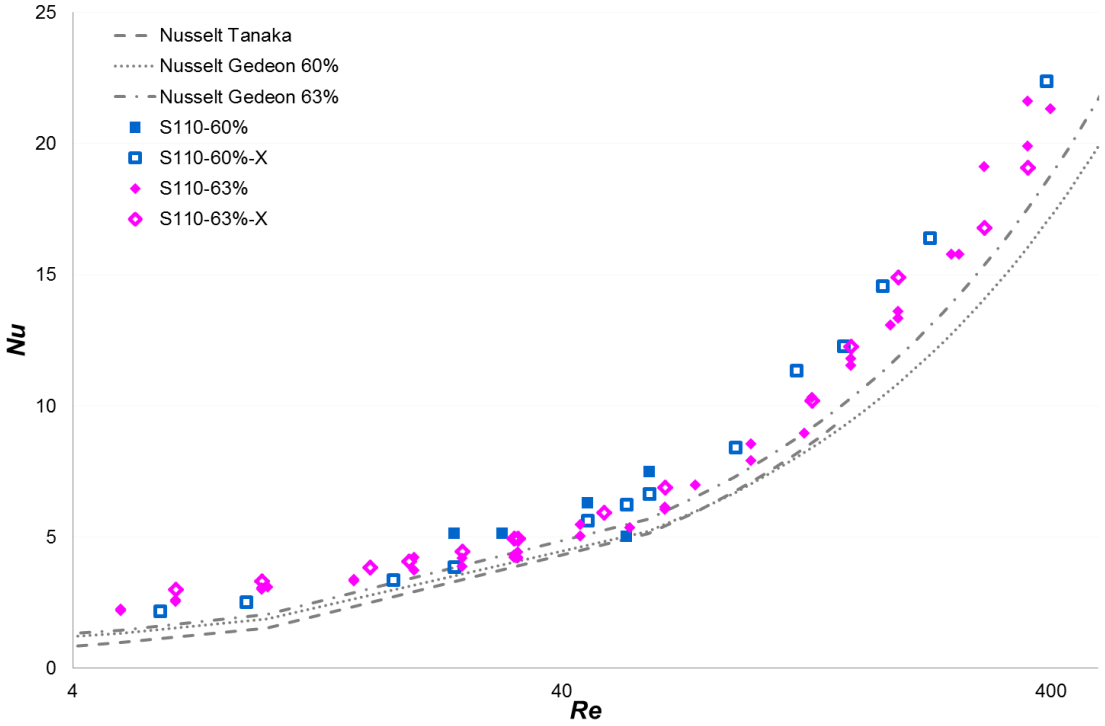

Figure 5. 3: Stacked woven wire matrices for 110μm wire diameter: Nusselt number versus Reynolds number

Figure 5. 3 shows the numerical results obtained for stacked woven wire matrices for the110 μm wire diameter, together with the Nusselt number evolution determined due to Tanaka et al. (Tanaka, et al., 1990) and Gedeon and Wood (Gedeon, et al., 1996) for two volumetric porosities, 0.60 and 0.63. On the other hand, Figure 5. 4 shows the results for the 80 μm wire diameter together with the Nusselt number evolution determined due to Tanaka et al. (Tanaka, et al., 1990) and Gedeon and Wood (Gedeon, et al., 1996) for two volumetric porosities, 0.66 and 0.68.

As seen in Figure 5. 3 and Figure 5. 4, neither the matrix volumetric porosity nor the configuration type (parallel and cross) has a noticeable influence on the Nusselt number obtained. Nevertheless, it is necessary to emphasize here that the variation in volumetric porosity is not significant and the same behaviour is also observed for the woven wire mesh geometry. Moreover, the effect of the volumetric porosity is included in the hydraulic diameter (Eq. [3.28]) and the Reynolds number is directly proportional to hydraulic diameter (Eq. [3.33]). On the other hand, the matrix heat transfer area (specific heat transfer area) decreases with an increase in the volumetric porosity. In the majority of the samples tested by Gedeon and Wood (Gedeon, et al., 1996) the volumetric porosity increases with the specific heat transfer area (Table 5. 1).

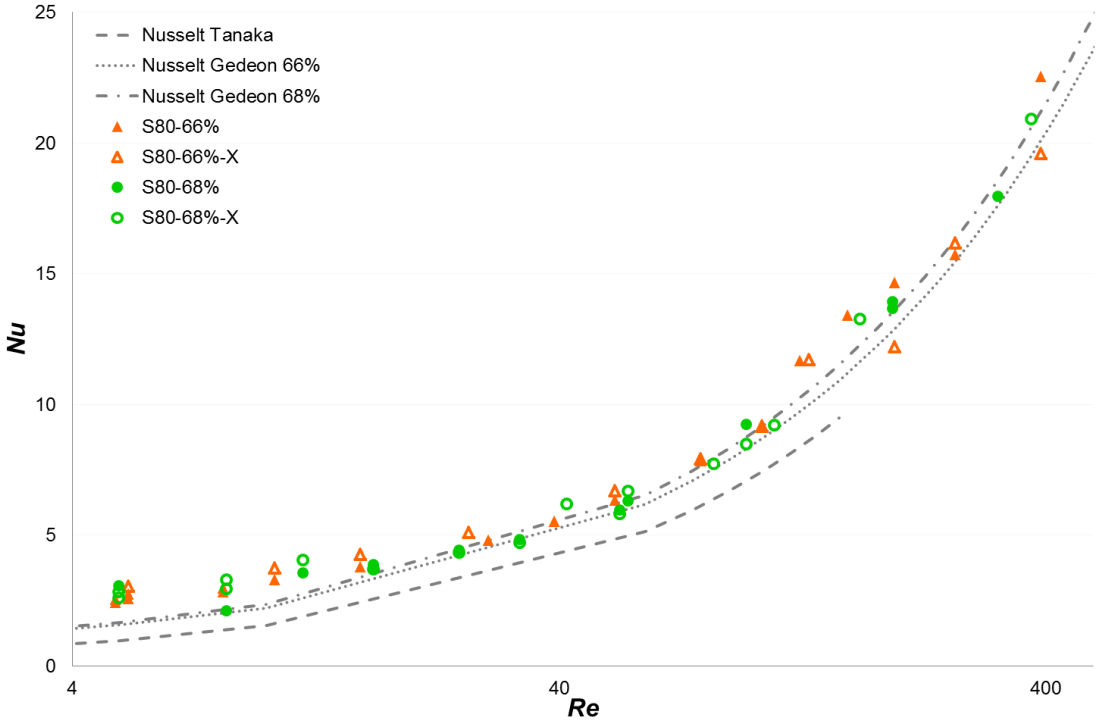

Figure 5. 4: Stacked woven wire matrices for 80μm wire diameter: Nusselt number versus Reynolds number

Eq. [5.15] shows the derived numerical correlation for the stacked woven wire matrix which fit the numerical results for the Nusselt number.

$$Nu = 1.14 + 0.39\,\mathrm{Re}^{0.66} \qquad [5.15]$$

Figure 5. 5 demonstrates that Nusselt number correlation proposed for the stacked woven wire matrices (Eq. [5.15]) shows a good agreement with the numerical results obtained for the Nusselt number as a function of Reynolds number. Moreover, for the Nusselt number, with the exception of the Reynolds number range below 40, the agreement is within 10% with Gedeon and Wood (Gedeon, et al., 1996) empirical correlations for volumetric porosity of 0.69. However, for $Re < 40$ the present numerical results deviate significantly from the empirical correlations suggested due to Gedeon and Wood (Gedeon, et al., 1996). One of the conclusions of Gedeon and Wood (Gedeon, et al., 1996) work is that the experimental correlation proposed is not appropriate for low Reynolds number range. On the other hand, the correspondence of the Eq. [5.15] with the correlation proposed by Tanaka et al. (Tanaka, et al., 1990) is unsatisfactory as can be observed in Figure 5. 5.

The effect of the volumetric porosity on the Nusselt number is not observed and this is probably due to the fact that the specific heat transfer area in the configuration studied (Table 3.4) does not represent a significant range of variation. Moreover, it is expected that the heat transfer behaviour be improved with the increase of specific heat transfer area. The effect of the volumetric porosity and specific heat transfer area on the regenerator heat transfer could be studied in future investigation.

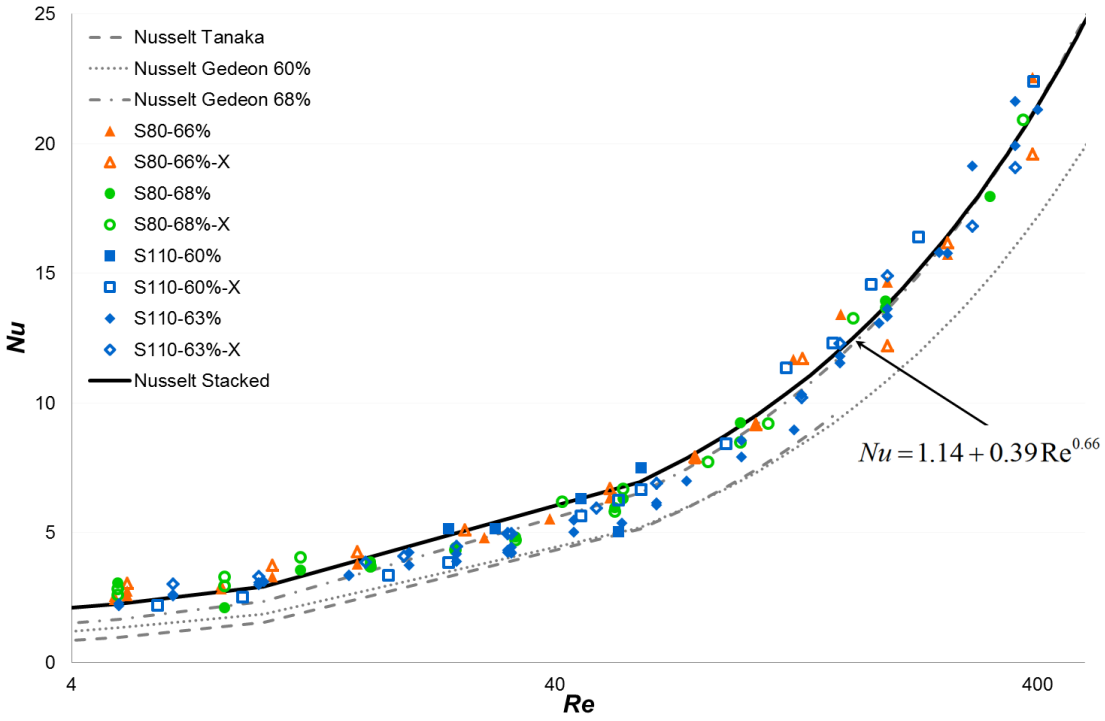

Figure 5. 5: Nusselt number correlation comparison for stacked woven wire matrices.

The qualitative results obtained for velocity and temperature field for the stacked woven wire matrices, are illustrated in Figure 5. 6 to Figure 5. 13 at Reynolds number of 50. The results are presented for two different wire diameters (80 and 110 μm) random configurations. No significant differences are observed at different wire diameters except slightly higher maximum local velocity distributions obtained from the higher wire diameter of 110 μm for the stacked woven wire matrices. The velocity contours in the wire matrix domain also signifies the importance of local increase of velocity magnitudes as an indication of shear gradients leading to the higher shear stress and hence friction pressure drops for each case. The higher local temperature values obtained in the flow entry region for each wire diameter case can be considered to be the main source of the heat energy to be transferred to the entire flow domain as the flow progresses. The velocity vectors shown in different 2-D cutting planes through the stacked woven wire matrices clearly identify the flow acceleration and deceleration i.e. velocity gradient regions and low velocity (wake) regions where the heat transfer mechanism is negatively affected. In regard to temperature contours, the 3-D temperature can be shown within fluid and solids.

In the next figures (from Figure 5. 6 to Figure 5. 13) it is clearly observed that there is not a thermal equilibrium between fluid and solid matrix. However, it is not easy to evaluate the trend of the temperature gradient between the working fluid and solid matrix. The mass average flow fluid and the area average solid matrix temperature distributions as a function of the length through the regenerator matrix are shown from Figure 5. 19 to Figure 5. 22. It could be observed that the temperature trend is not linear neither for the working fluid nor for solid matrix; instead in both cases the trend is closer to a logarithmic equation. The entrance and exit effects are not considered in this trend. It is also observed that there is a thermal contact between layers that produce a longitudinal thermal conduction loss through the regenerator matrix.

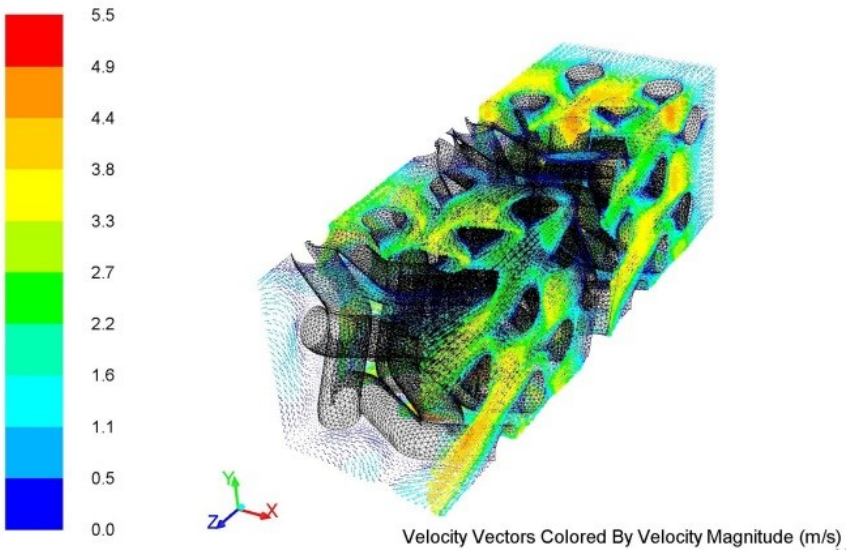

(a)

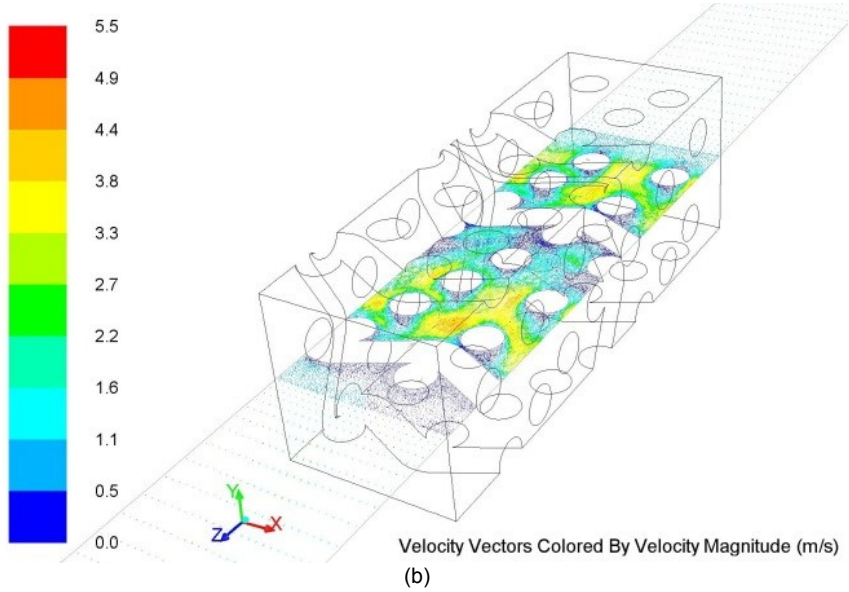

(b)

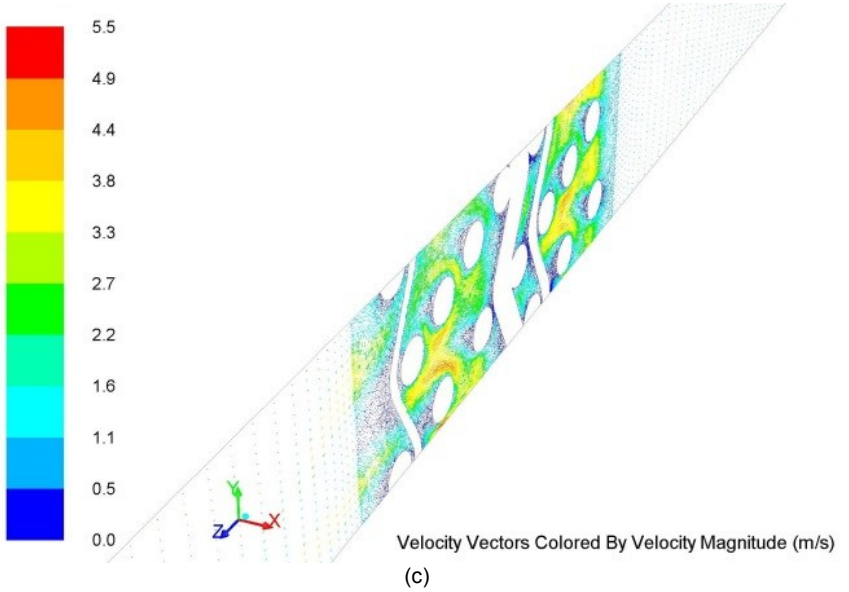

(c)

Figure 5. 6: Velocity vector through Stacked woven wire matrix S110-60% for Re ≈ 50 (0.9m/s) at 0.02s

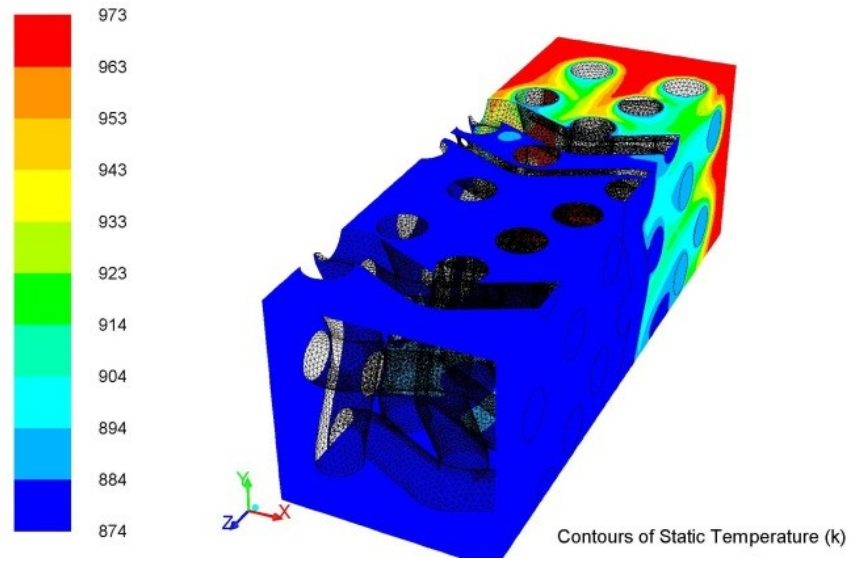

(a)

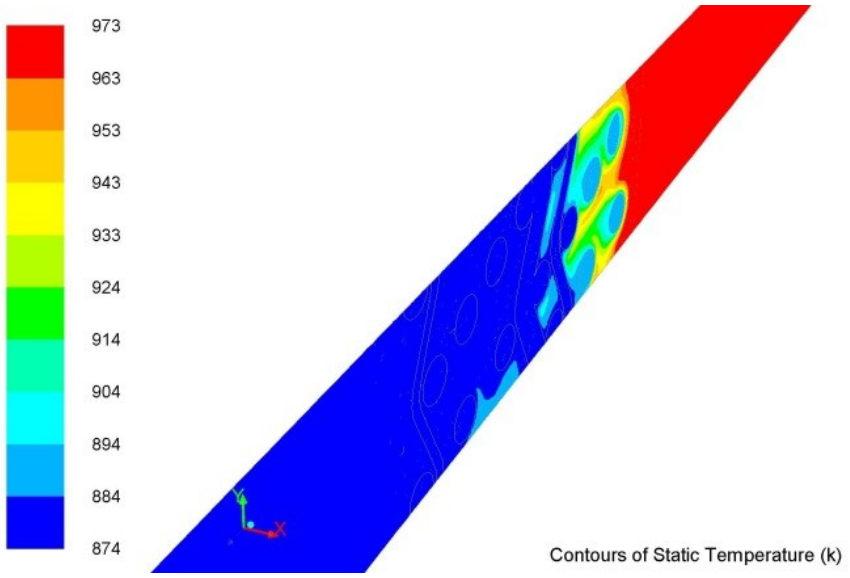

(b)

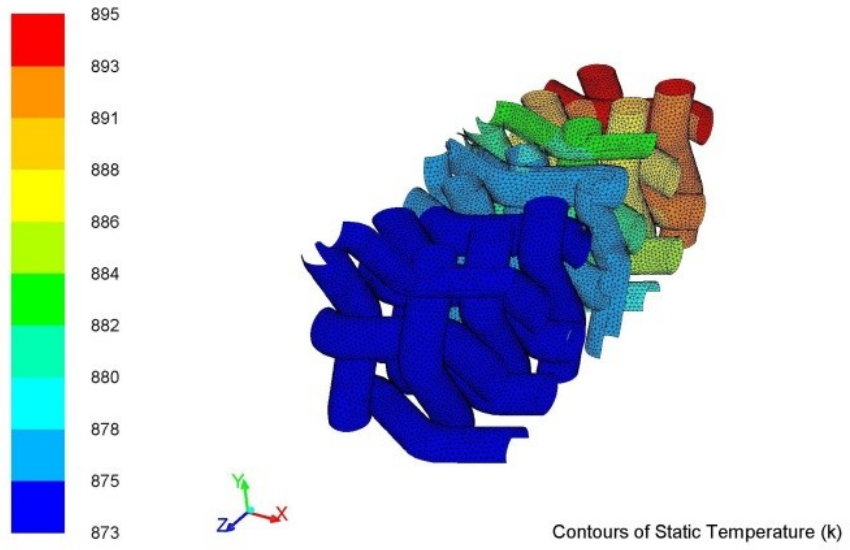

(c)

Figure 5. 7: Temperature contours through Stacked woven wire matrix S110-60% for Re ≈ 50 (0.9m/s) at 0.02s

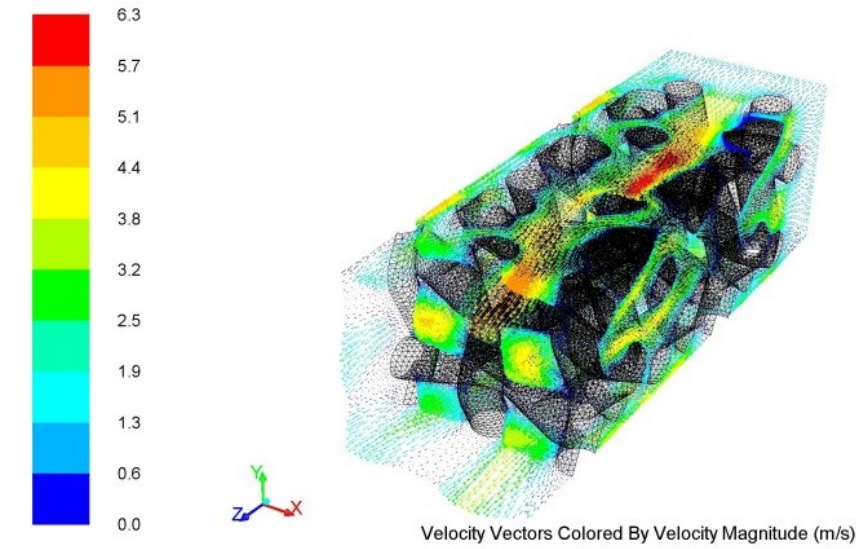

(a)

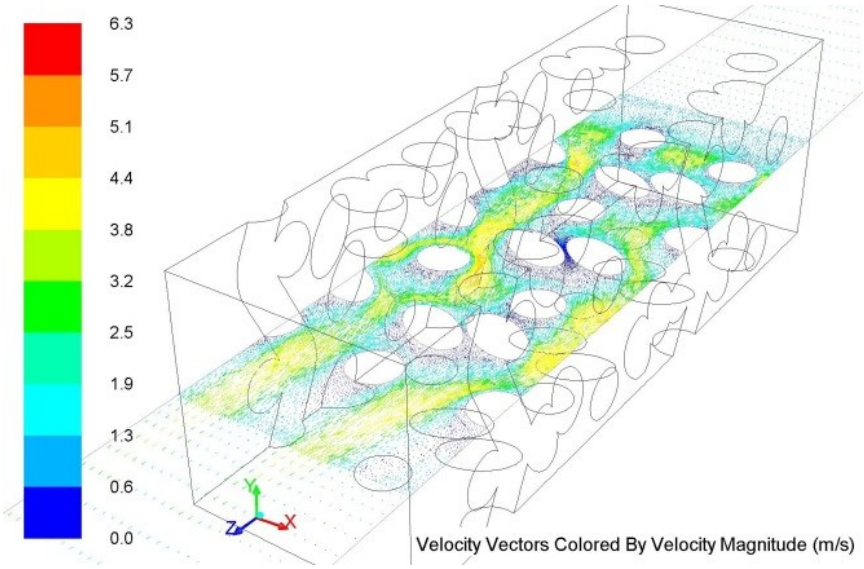

(b)

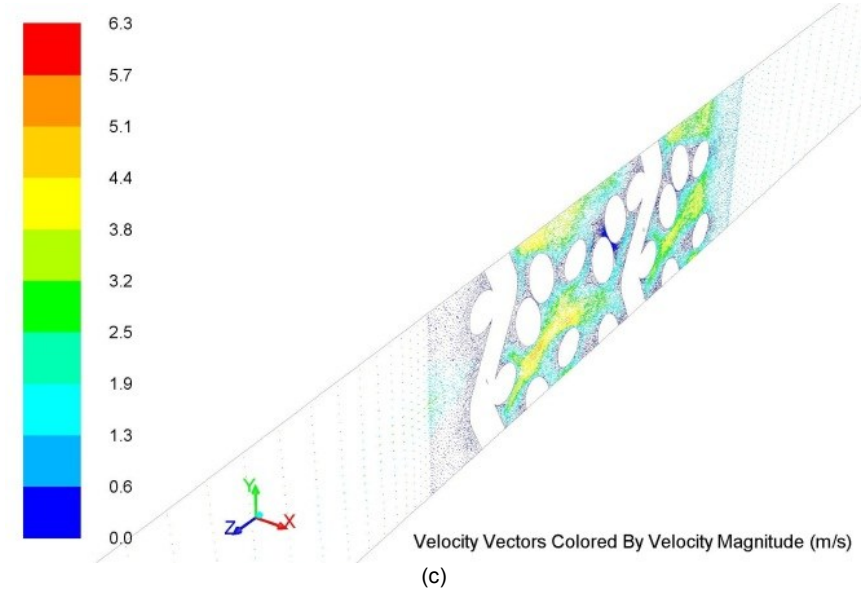

(c)

Figure 5. 8: Velocity vector through Stacked woven wire matrix S110-60%-X for Re ≈ 50 (0.9m/s) at 0.02s

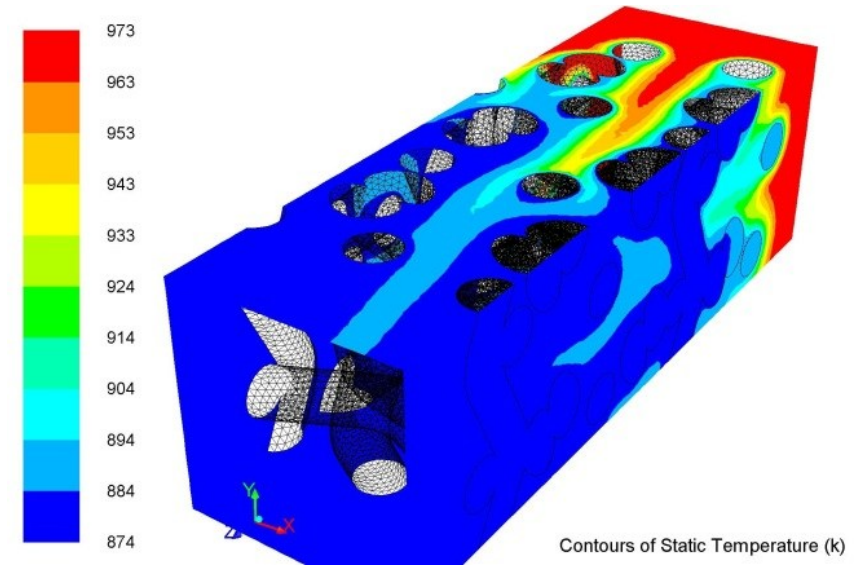

(a)

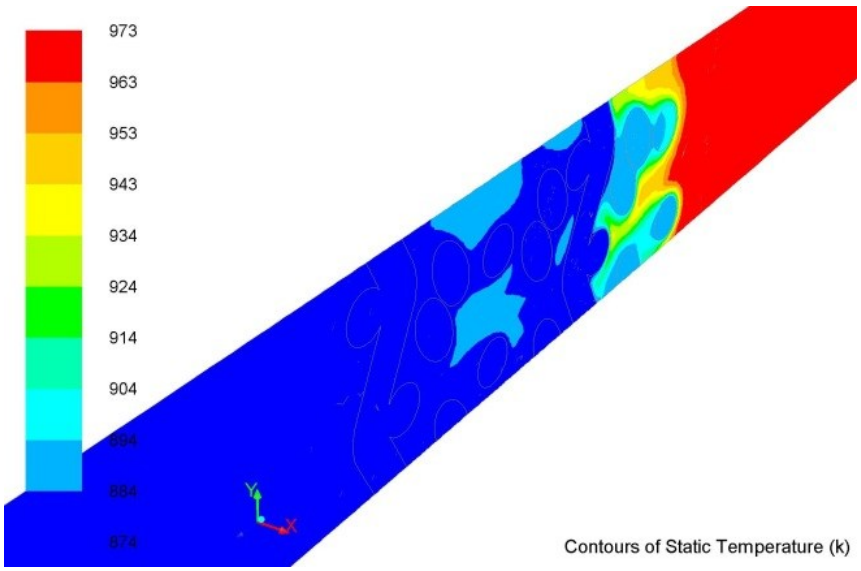

(b)

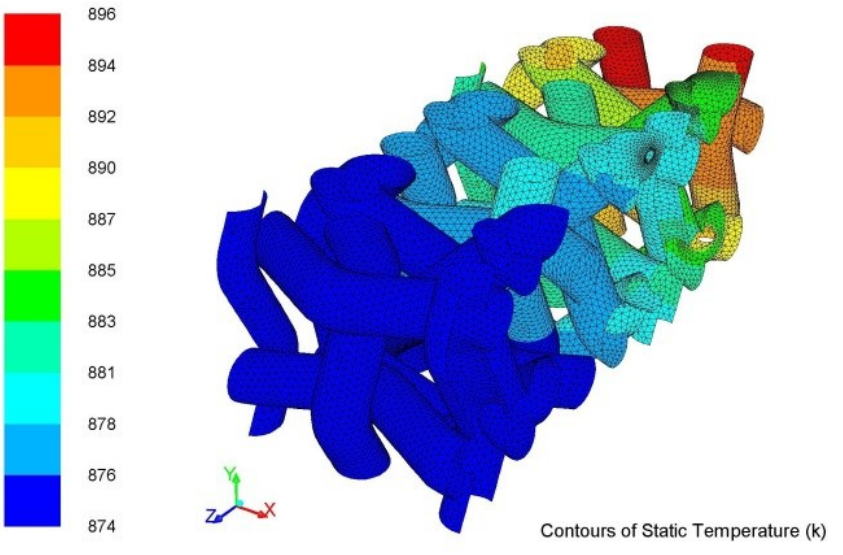

(c)

Figure 5. 9: Temperature contours through Stacked woven wire matrix S110-60%-X for Re ≈ 50 (0.9m/s) at 0.02s

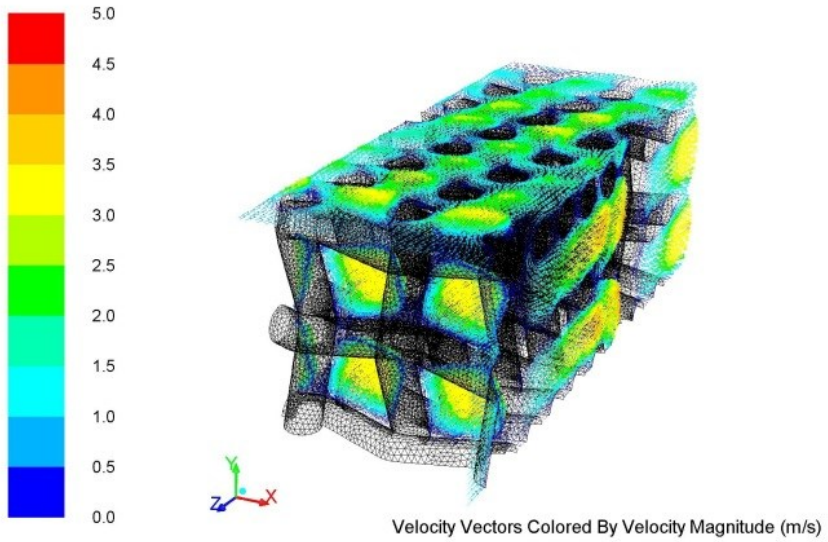

(a)

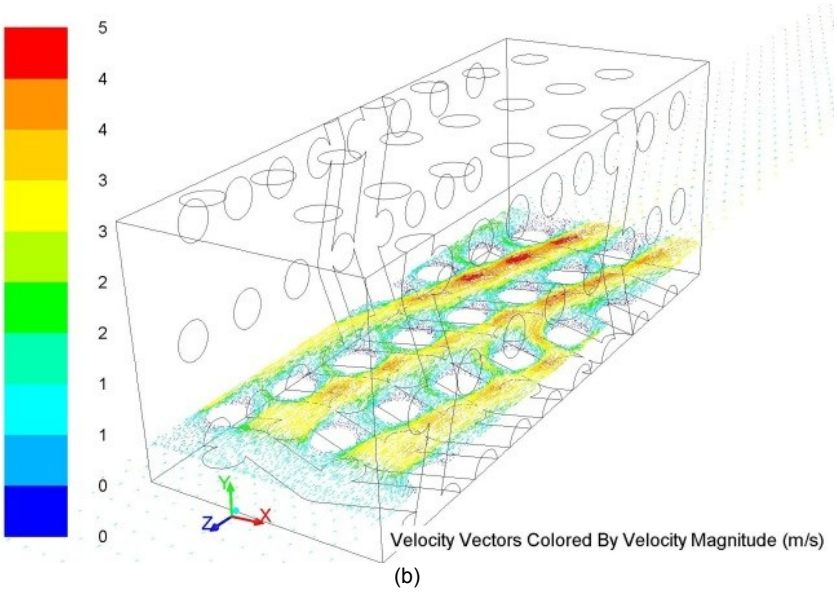

(b)

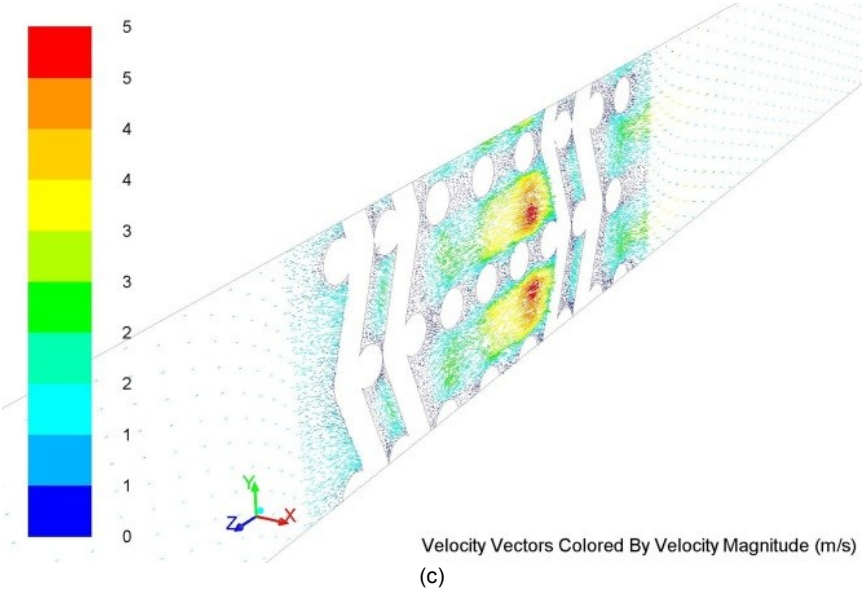

(c)

Figure 5. 10: Velocity vector through Stacked woven wire matrix S80-68% for Re ≈ 50 (1m/s) at 0.02s

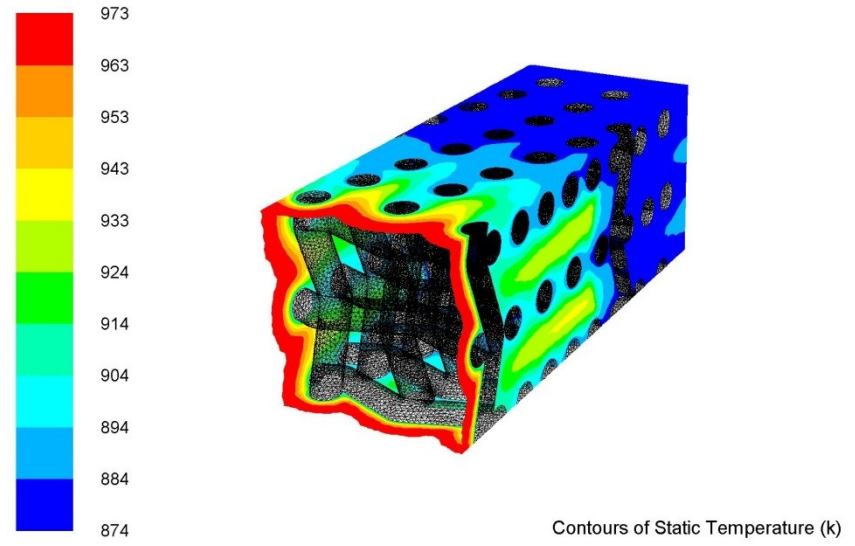

(a)

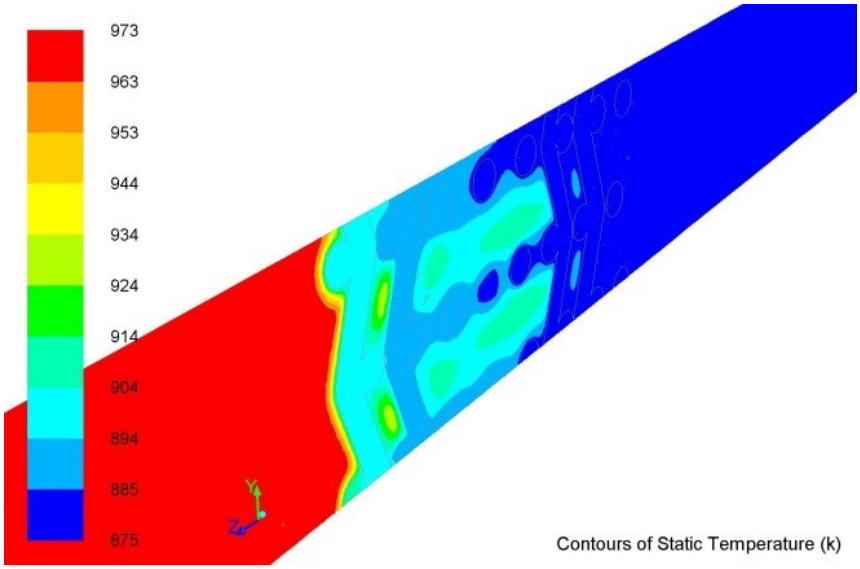

(b)

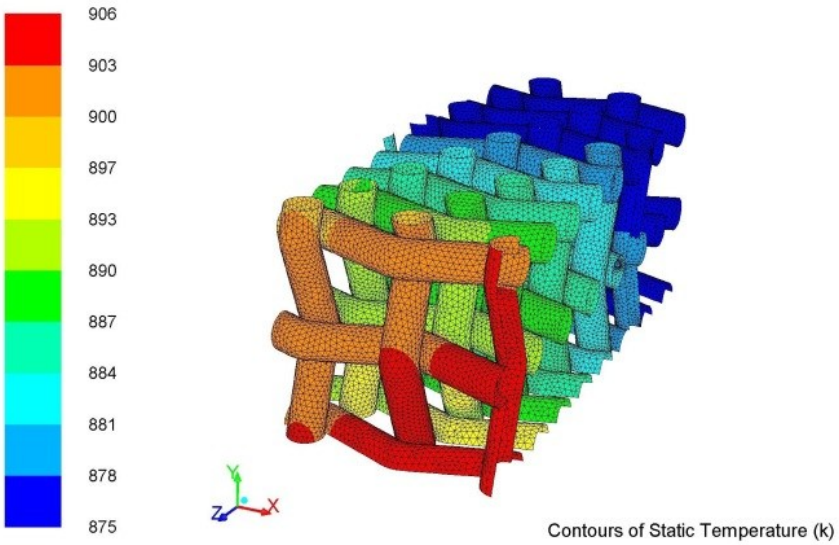

(c)

Figure 5. 11: Temperature contours through Stacked woven wire matrix S80-68% for Re ≈ 50 (1m/s) at 0.02s

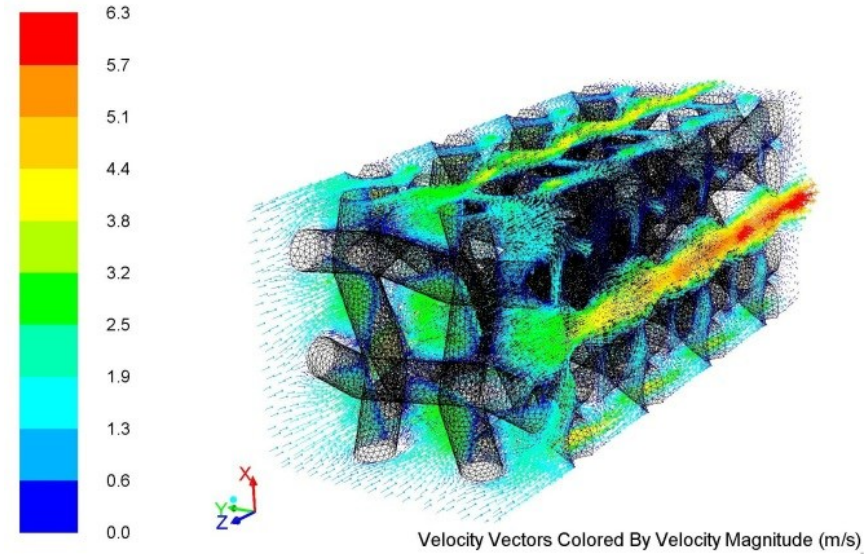

(a)

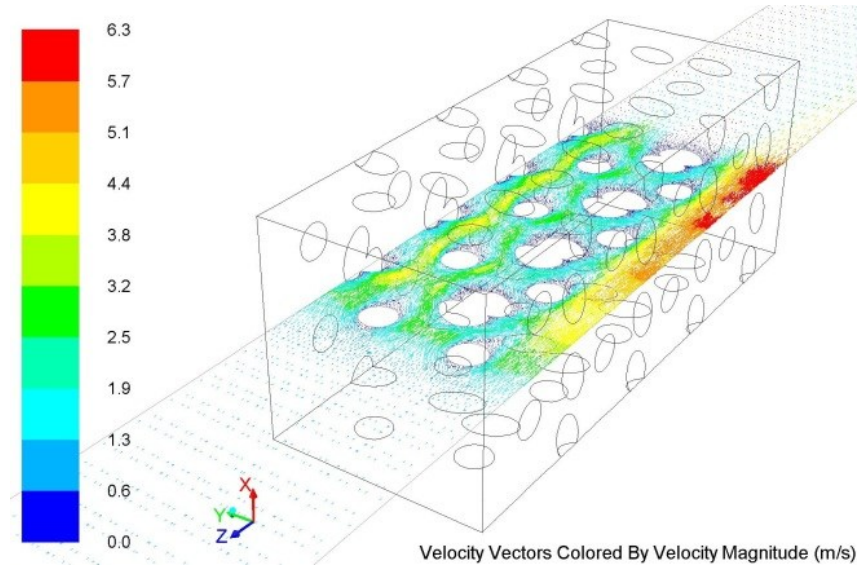

(b)

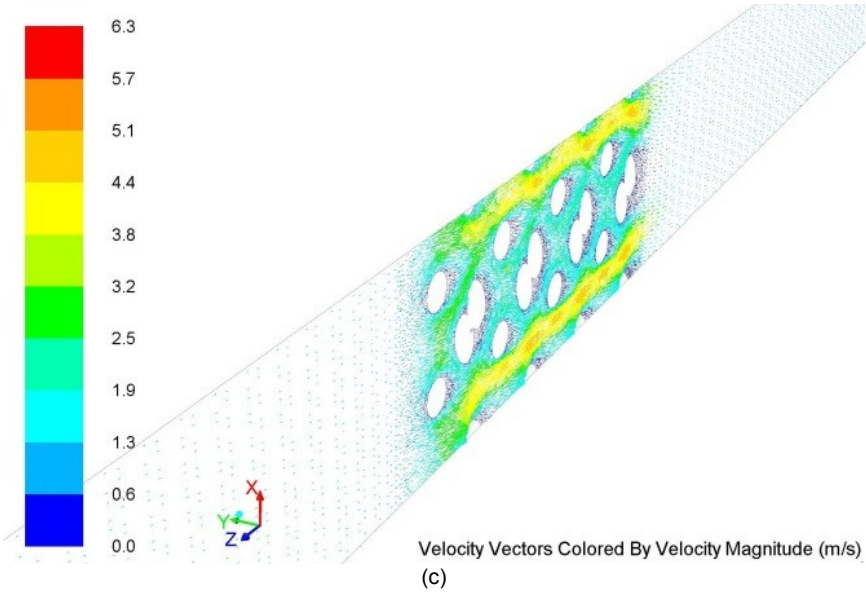

(c)

Figure 5. 12: Velocity vector through Stacked woven wire matrix S80-68%-X for Re ≈ 50 (1m/s) at 0.02s

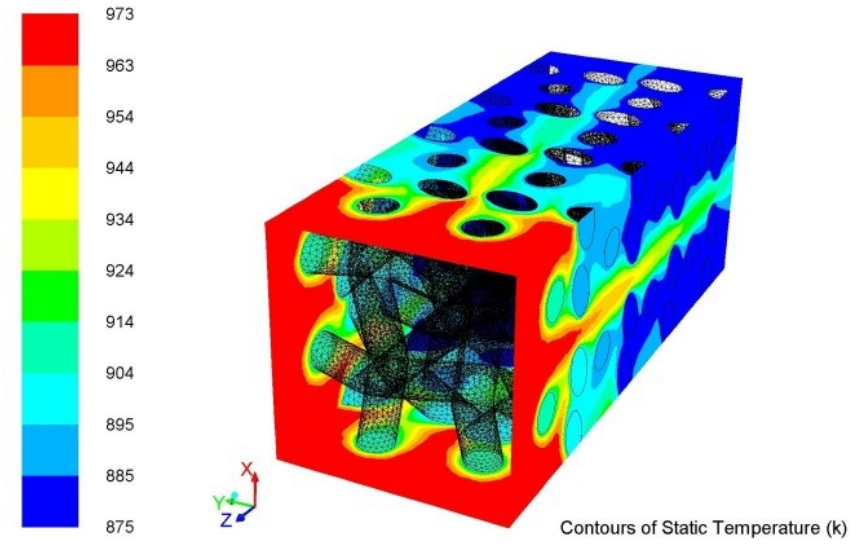

(a)

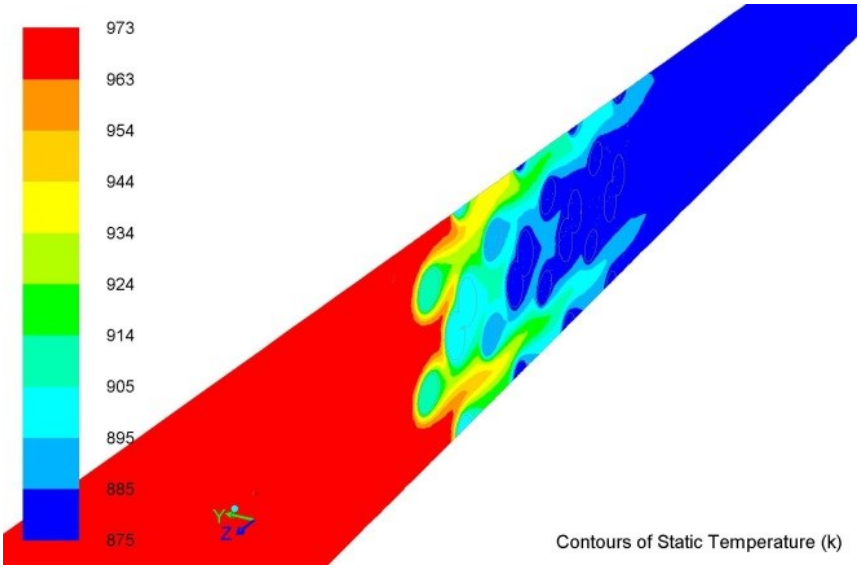

(b)

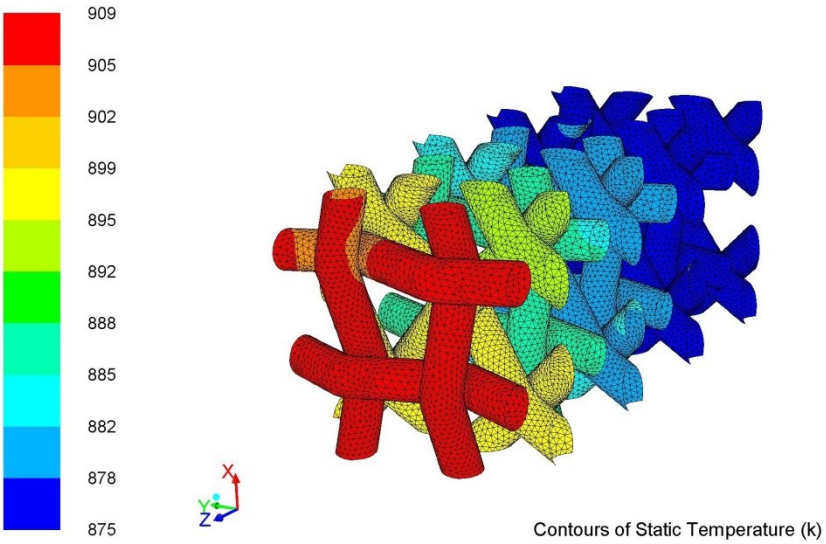

(c)

Figure 5. 13: Temperature contours through Stacked woven wire matrix S80-68%-X for Re ≈ 50 (1m/s) at 0.02s

Figure 5. 14 shows the numerical results obtained for aligned and no-contact stacked woven wire matrices for both wire diameters (see Table 3.4). The solid line shown in Figure 5. 14 represents the heat transfer correlation proposed in Eq. [5.15]. The results also clearly signify the relative change in heat transfer performance for aligned, no-contact and random configurations.

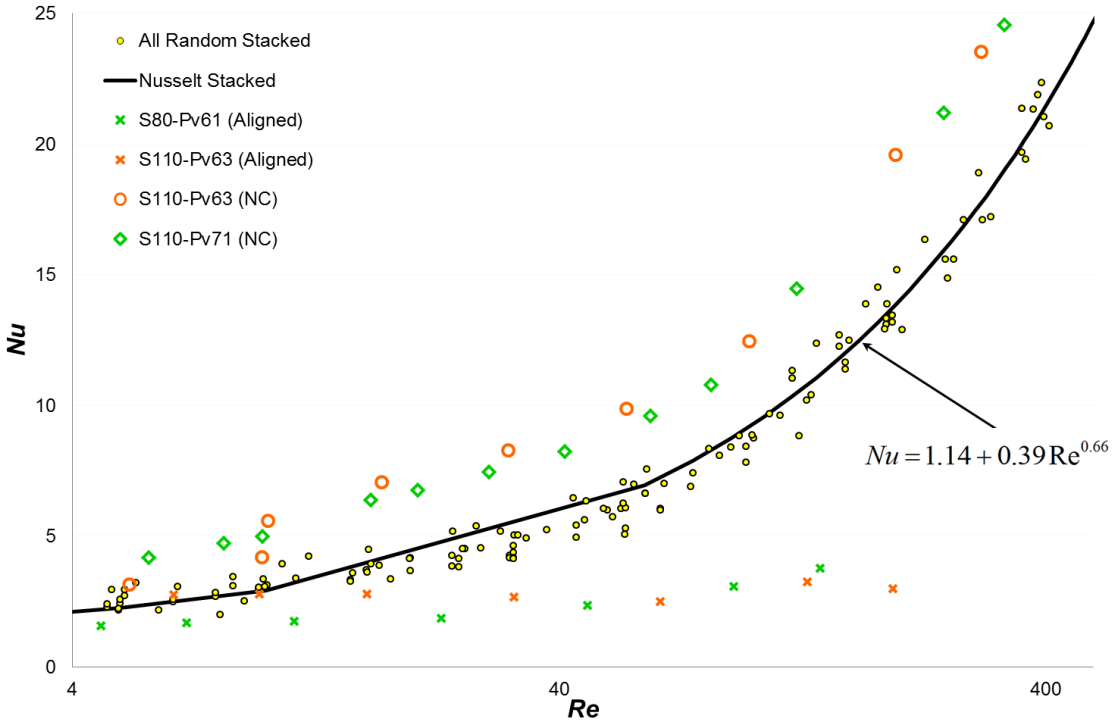

Figure 5. 14: Aligned and No-Contact Stacked woven wire matrices versus Reynolds number

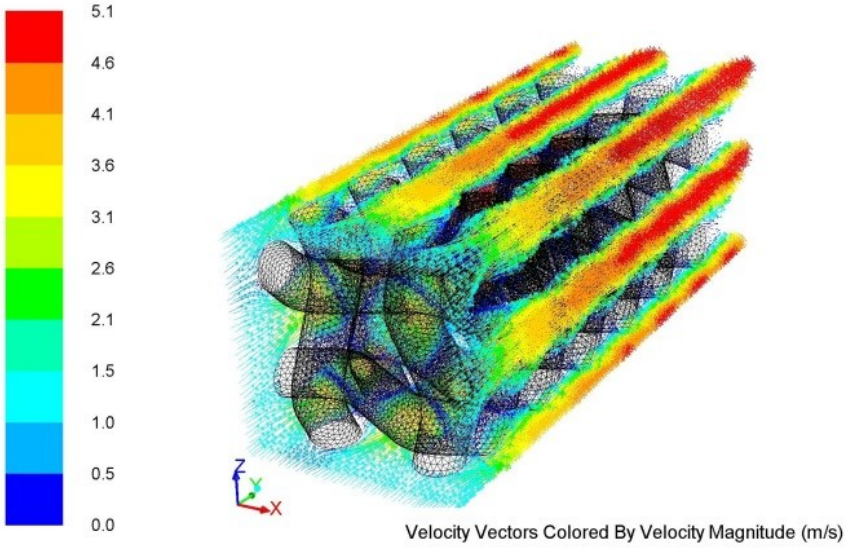

Figure 5. 15: Velocity vector through Stacked woven wire matrix S110-63%-A for Re ≈ 50 (1m/s) at 0.02s

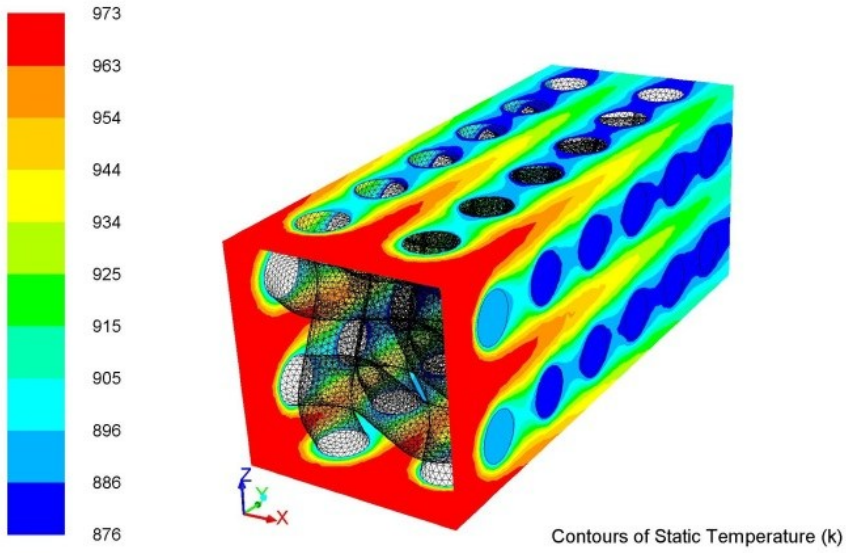

(a)

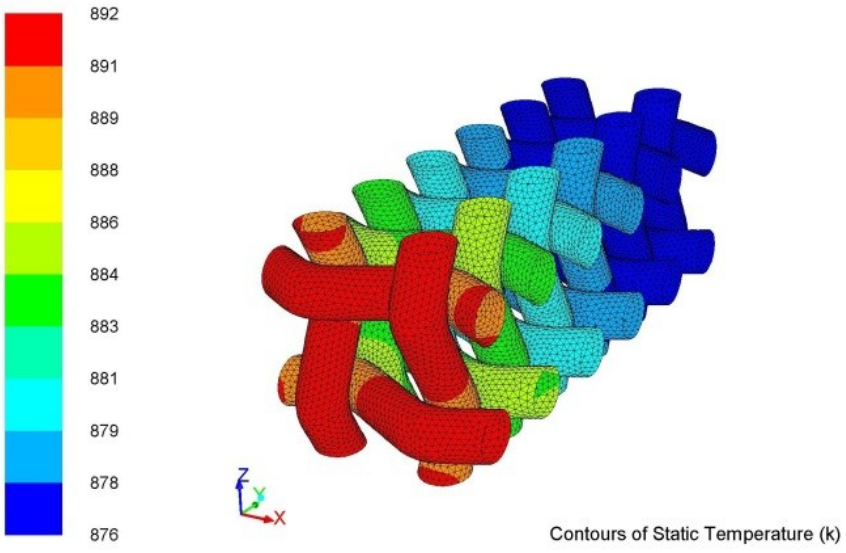

(b)

Figure 5. 16: Temperature contours through Stacked woven wire matrix S110-63%-A for Re ≈ 50 (1m/s) at 0.02s

In the case of aligned configurations, the computed Nusselt number is practically constant along the Reynolds number range investigated and is lower than the Nusselt numbers obtained for random configurations. The qualitative results obtained in terms of velocity and temperature fields for the aligned stacked woven matrices are illustrated in Figure 5. 15 and Figure 5. 16 at Reynolds number of 50 for 110 μm wire diameter. It can be observed that the flow path is clearly defined in detriment of the heat transfer phenomena.

In the case of no-contact configuration the heat transfer performance is improved independently from the matrix volumetric porosity compared to all other configurations. In this configuration, the losses due to conduction in the direction of the flow are eliminated; therefore, the heat transfer performance is improved in comparison to configurations with high heat conduction losses (wound configurations for example). Figure 5. 17 shows the velocity vectors and Figure 5. 18 the temperature contours for the no-contact configuration at Reynolds number of 80 for matrix volumetric porosity of 0.71.

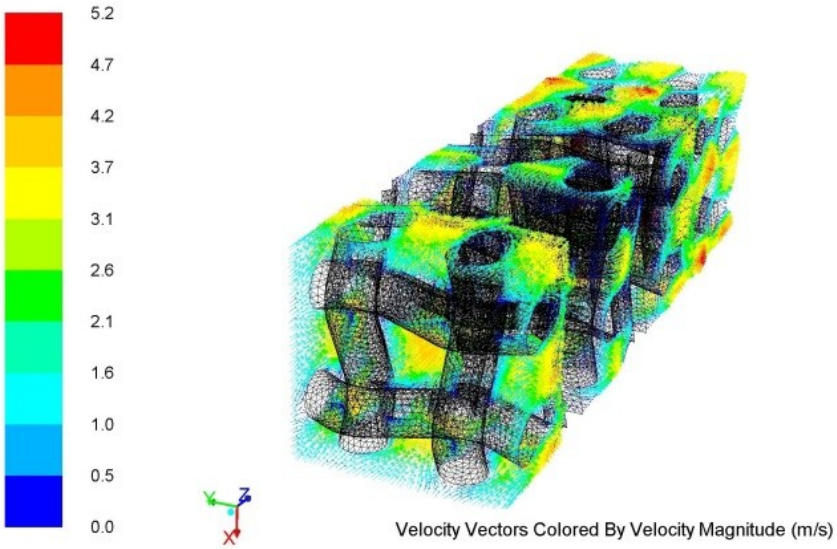

(a)

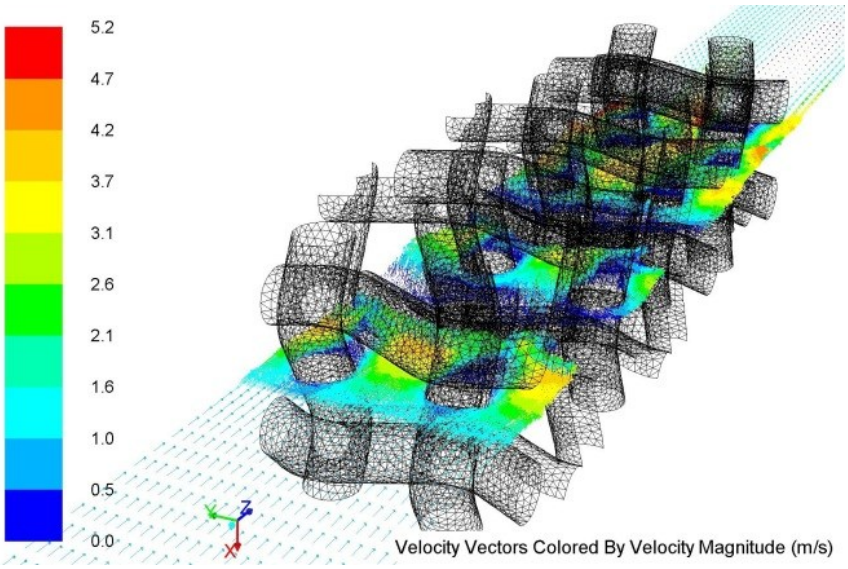

(b)

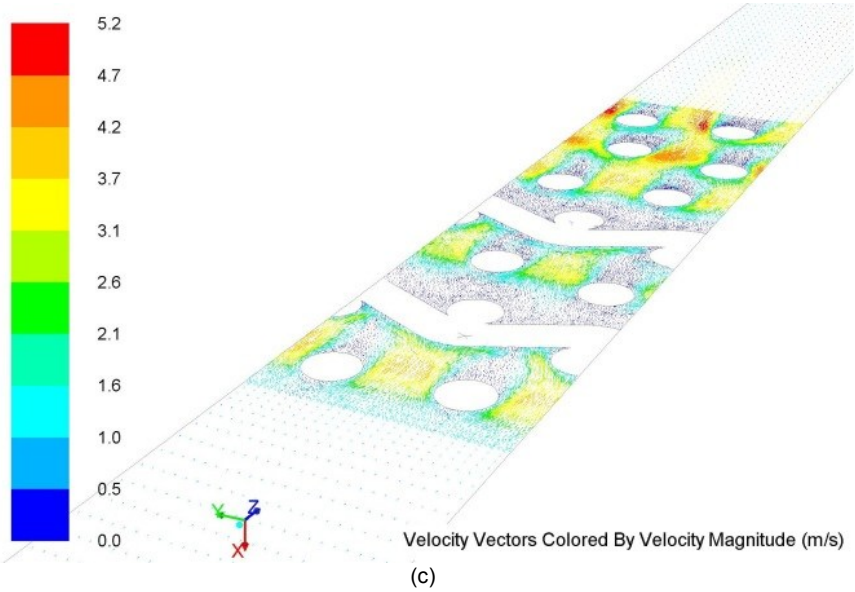

(c)

Figure 5. 17: Velocity vector through Stacked woven wire matrix S110-71%-NC for Re ≈ 80 (1.0m/s) at 0.02s

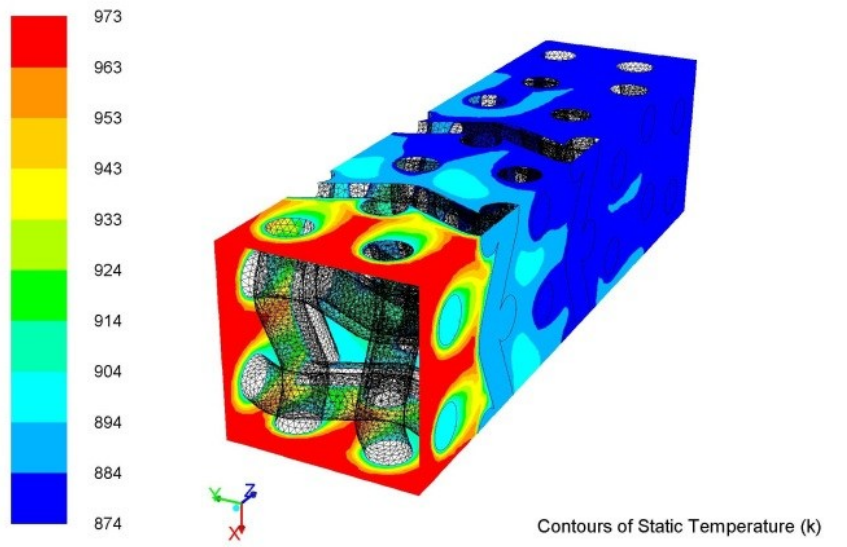

(a)

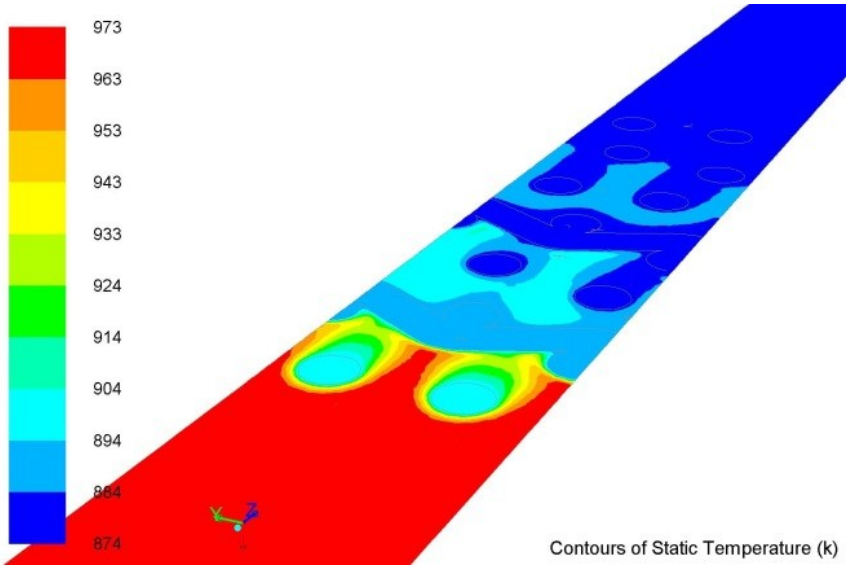

(b)

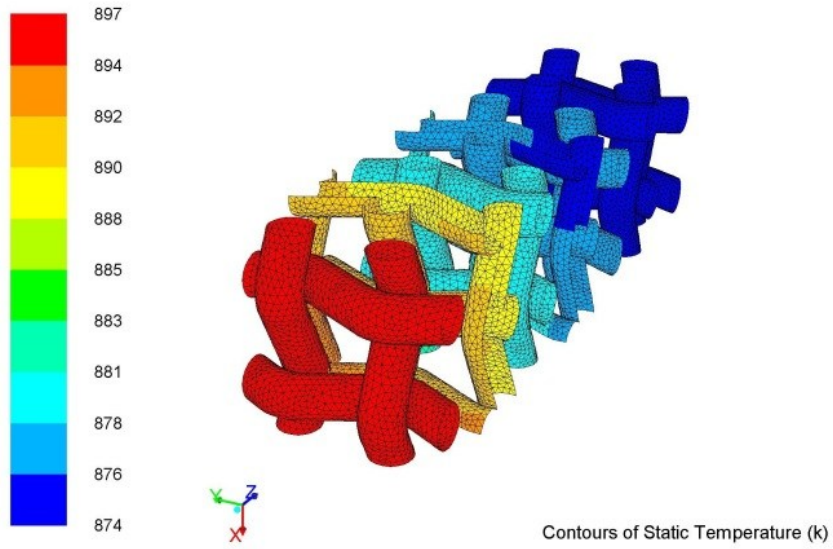

(c)

Figure 5. 18: Temperature contours through Stacked woven wire matrix S110-71%-NC for Re ≈ 80 (1.0m/s) at 0.02s

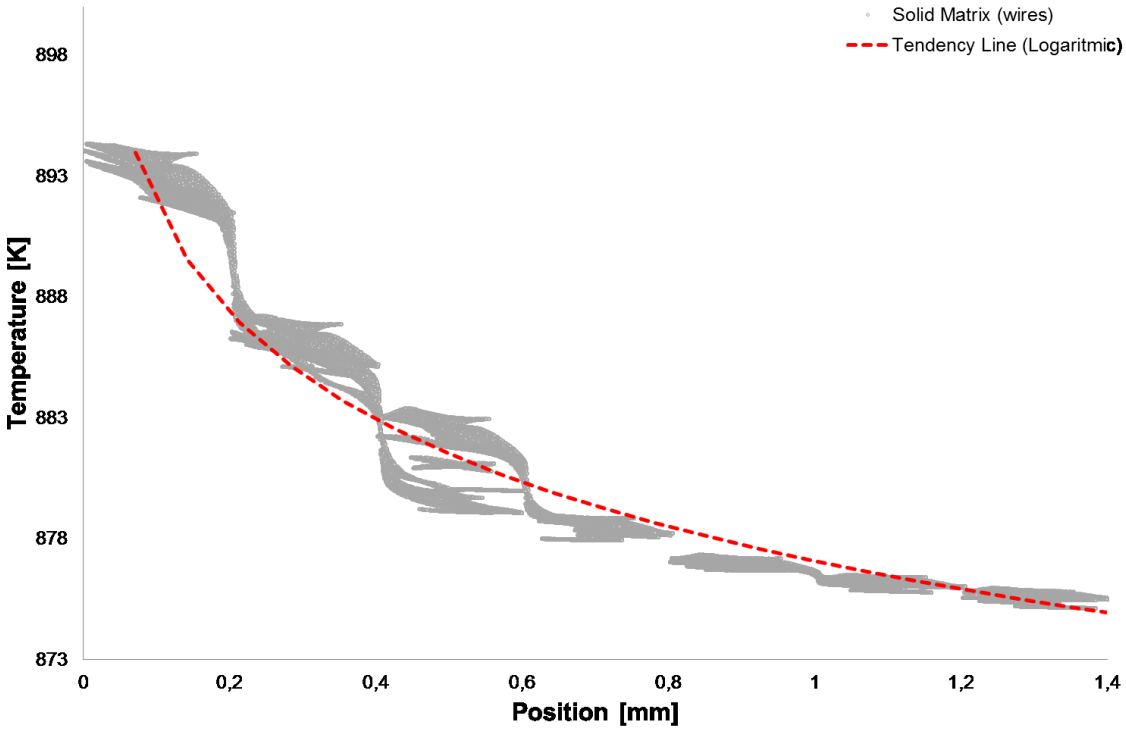

(a)

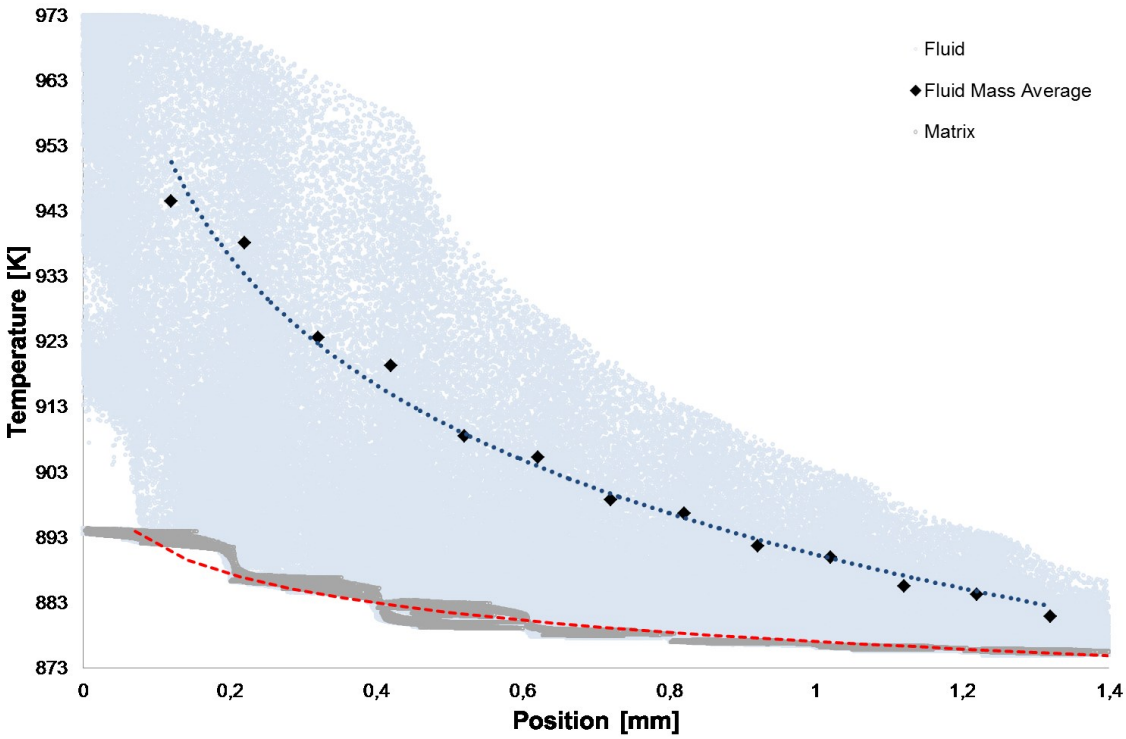

(b)

Figure 5. 19: Temperature vs Position through Stacked woven wire matrix S110-63% for Re ≈ 50 (1m/s) at 0.02s: (a) Solid matrix temperature and (b) Solid matrix temperature and working fluid temperature

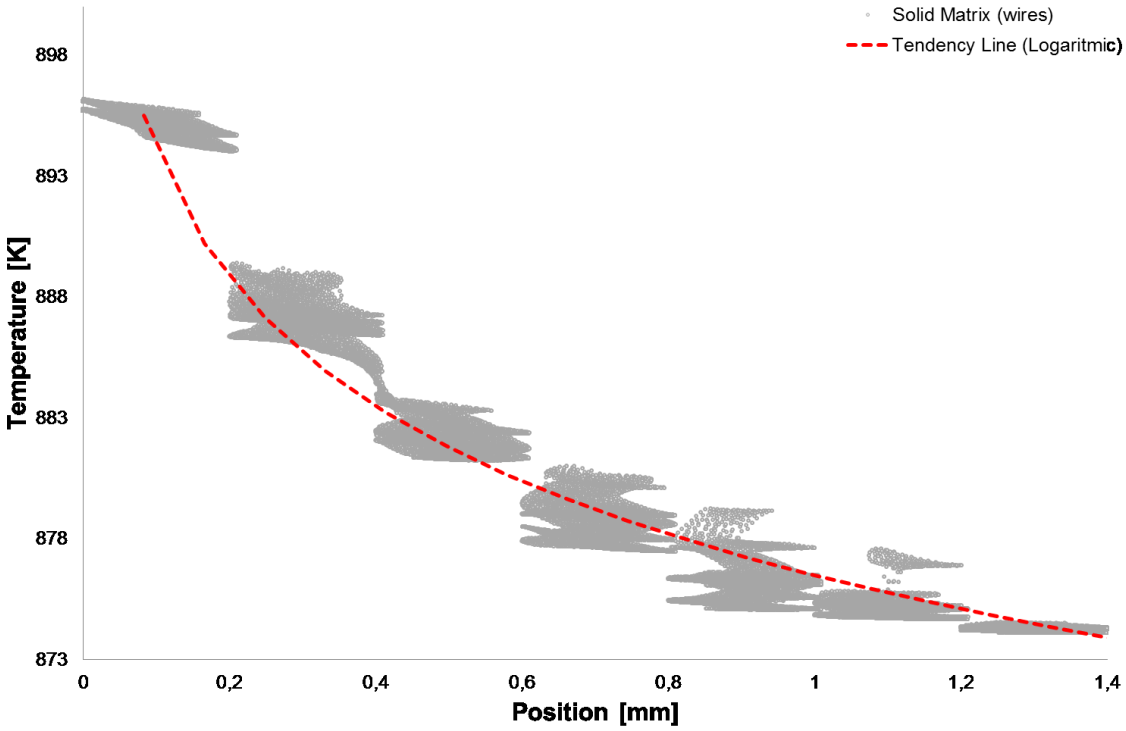

(a)

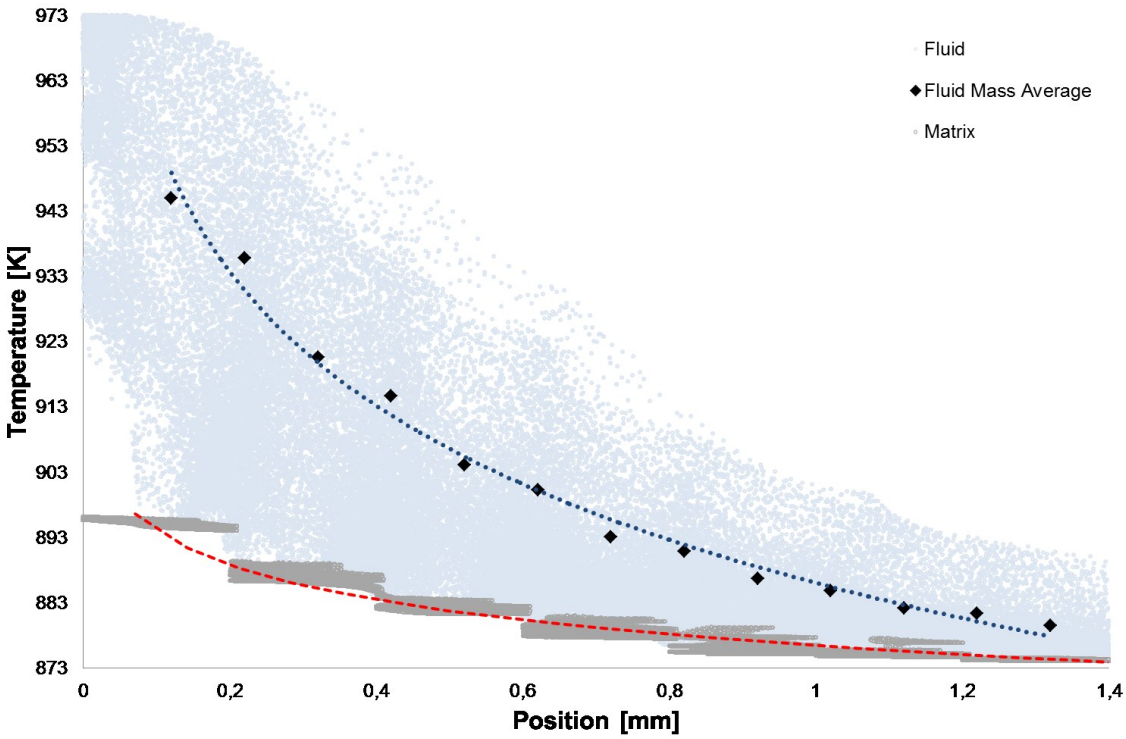

(b)

Figure 5. 20: Temperature vs Position through Stacked woven wire matrix S110-63%-X for Re ≈ 50 (1m/s) at 0.02s: (a) Solid matrix temperature and (b) Solid matrix temperature and working fluid temperature

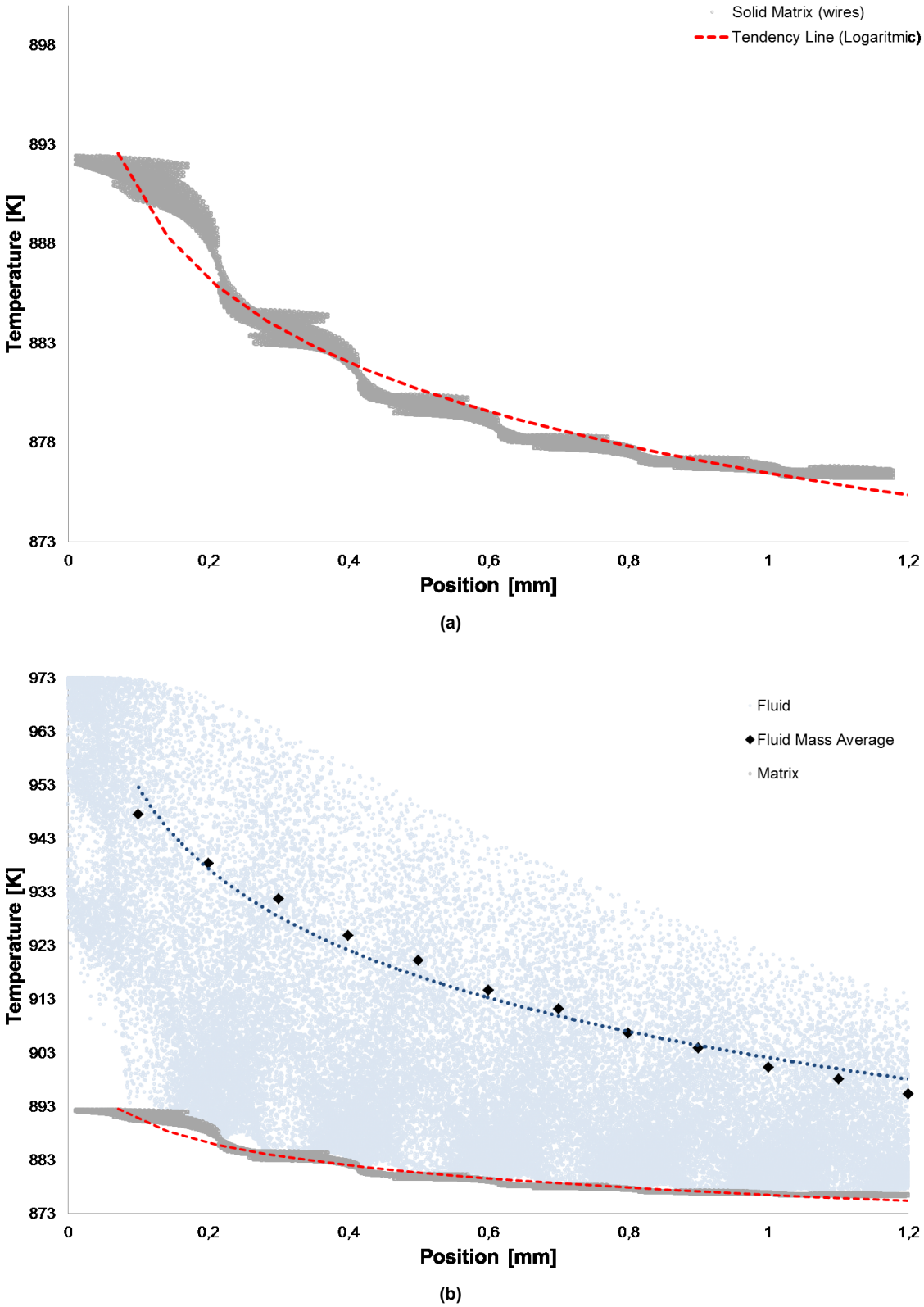

Figure 5. 21: Temperature vs Position through Stacked woven wire matrix S110-63%-A for Re ≈ 50 (1m/s) at 0.02s: (a) Solid matrix temperature and (b) Solid matrix temperature and working fluid temperature

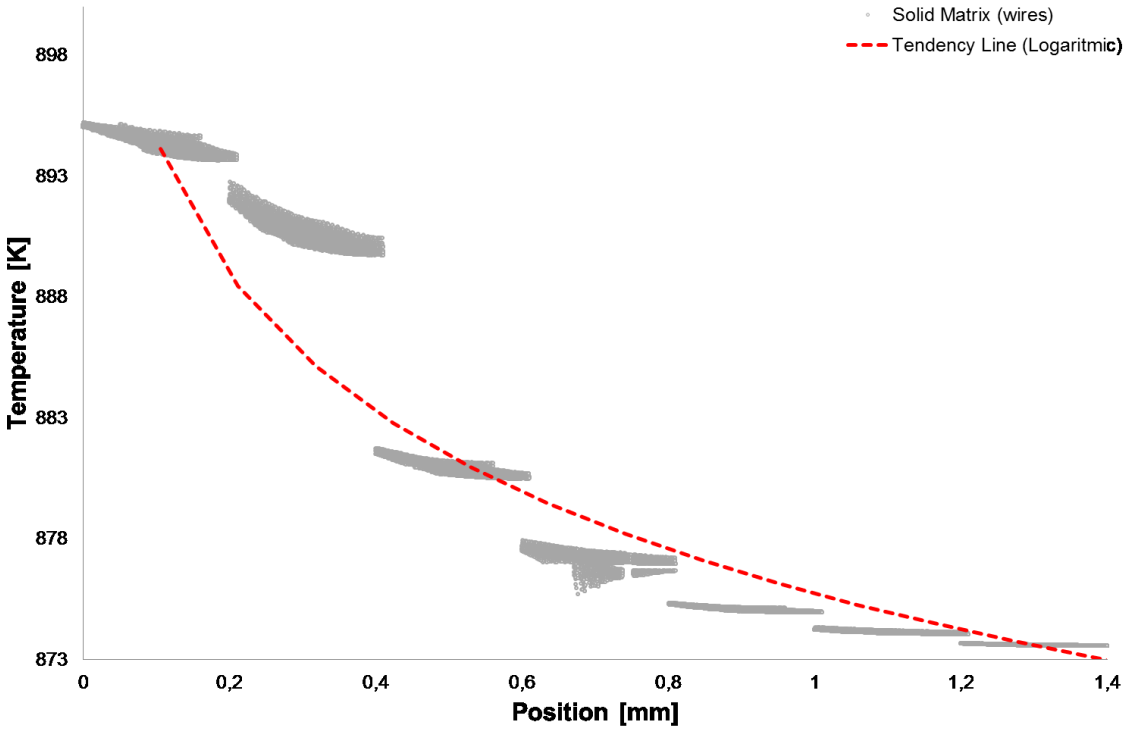

(a)

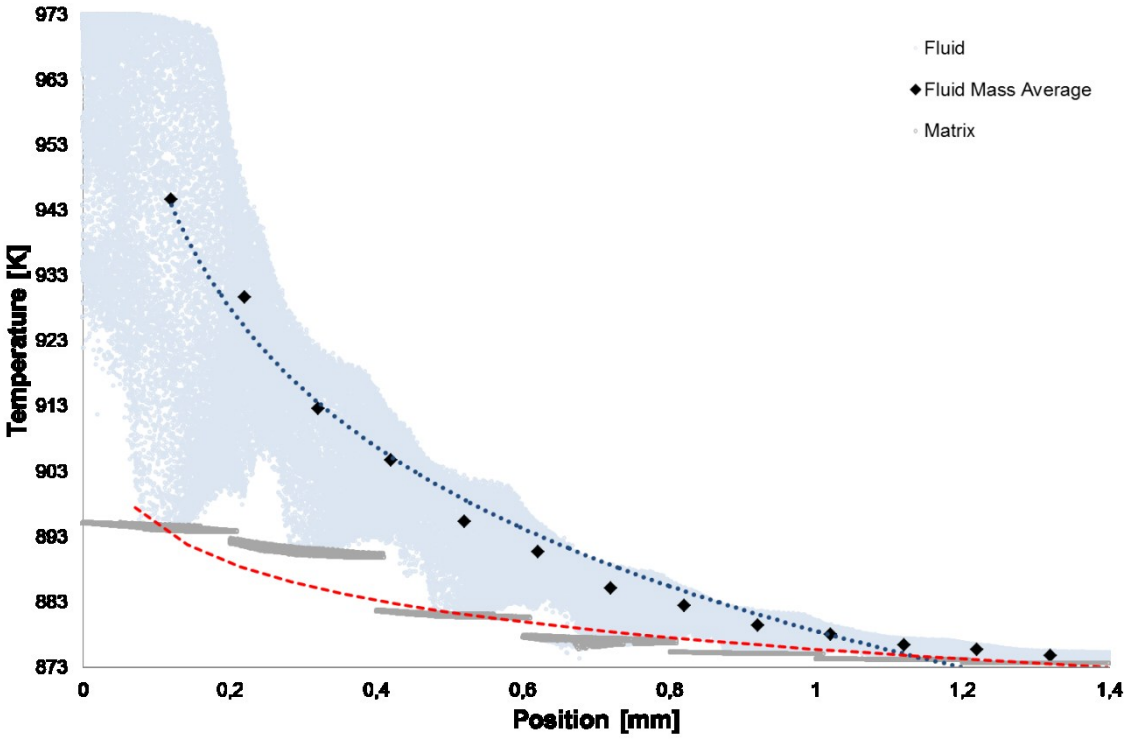

(b)

Figure 5. 22: Temperature vs Position through Stacked woven wire matrix S110-63%-NC for Re ≈ 50 (1m/s) at 0.02s: (a) Solid matrix temperature and (b) Solid matrix temperature and working fluid temperature

Figure 5. 22 shows the temperature distribution as a function of the length through the regenerator matrix for configuration with no contact between layers. It is observed a clear defined stepwise temperature gradient due to the absent of longitudinal conduction losses

through the contact between stacked layers. This result improves the heat transfer performance through the regenerator matrix as expected. On the other hand, the fluid local temperature gradient is smaller compared with all the other configurations studied.

V.3.2. Heat Transfer correlation for wound woven wire matrix

Having been validated for the stacked woven wire matrices, the present numerical approach is extended to investigate the heat transfer mechanism and the corresponding heat transfer coefficients for wound woven wire matrix configurations. The configurations are the same ones which are studied for parallel misaligned stacked woven wire matrices (see Table 3.4).

Figure 5. 23 shows the relationship between Nusselt number and Reynolds number for the wound woven wire matrix configuration. The dashed lines are the Nusselt number calculated for the stacked woven wire matrix using Eq.[5.15] and Eq.[5.13] for the matrix volumetric porosity studies. In Figure 5. 23 the solid line is Nusselt number correlation line which is derived from the present results. For the wound woven wire matrix configuration, the three coefficient correlation that better fits with the numerical results is shown in the Eq. [5.16], where the Reynolds number is calculated based on the hydraulic diameter:

$$Nu = 1.54 + 0.29\,\mathrm{Re}^{0.66} \qquad [5.16]$$

It is found that the average Nusselt number coefficients obtained for the wound woven wire matrix are significantly lower (20%) than those obtained from the stacked woven wire matrix in the Reynolds number range investigated.

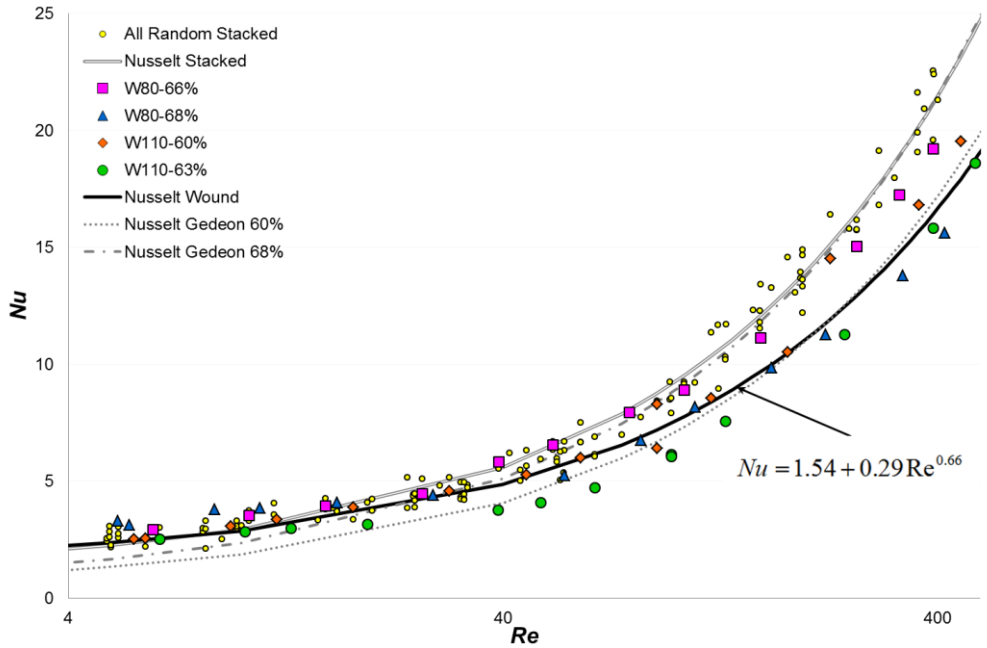

Figure 5. 23:Nusselt number correlation comparison for Wound woven wire matrices

Figure 5. 23 shows the Nusselt number results for different volumetric porosities, specific heat transfer areas and hydraulic diameters in a range of Reynolds number. As expected, the higher Nusselt numbers are obtained for the matrix configuration with higher specific heat transfer area (see Table 3.4). Regarding the influence of the hydraulic diameter, the results show an inverse proportionality with the Nusselt number, in other words, the Nusselt numbers increase when the hydraulic diameter decreases which indirectly means with volumetric porosity decreases. However, the Nusselt number results as function of the volumetric porosity are not evident mainly due to the relations between heat transfer area (Eq. [3.32]), hydraulic diameter (Eq. [3.28]), Reynolds number (Eq. [3.33]) with the volumetric porosity.

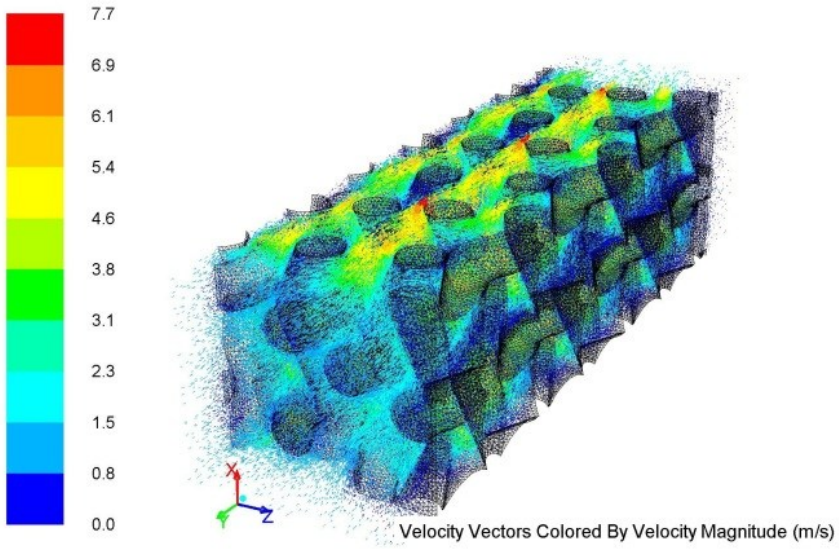

(a)

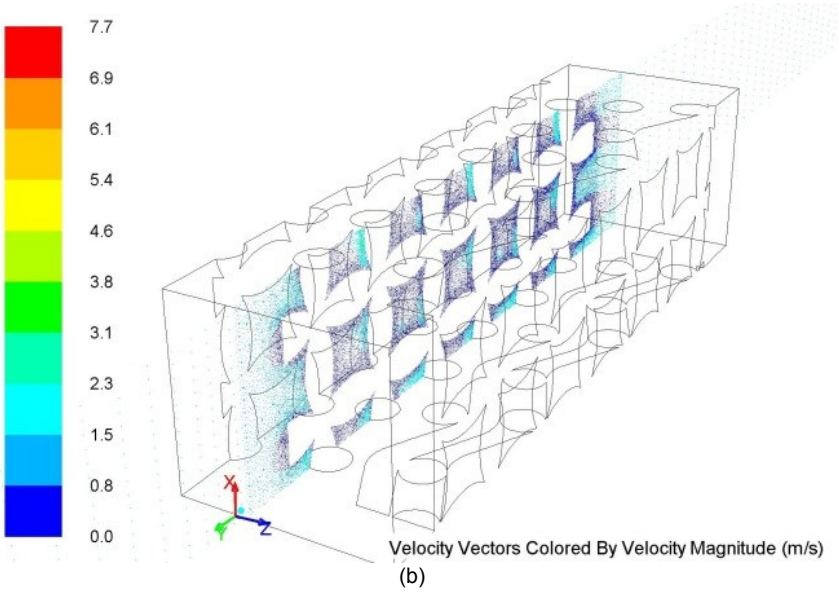

(b)

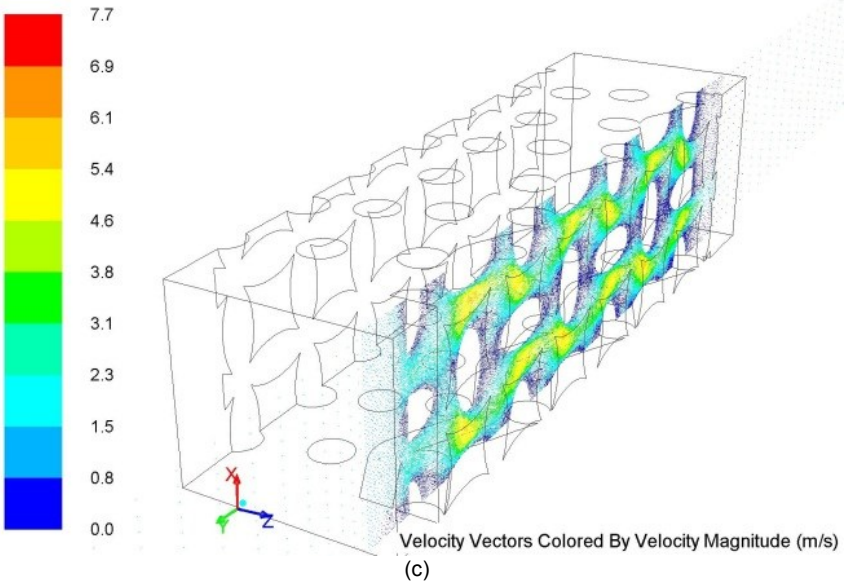

(c)

Figure 5. 24: Velocity vector through Wound woven wire matrix W110-Pv60 for Re ≈ 60 (1.0m/s) at 0.02s

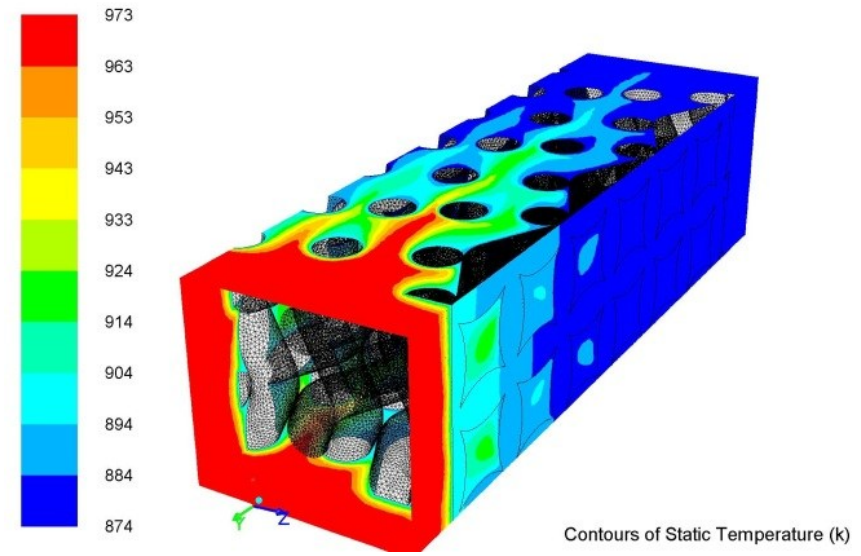

(a)

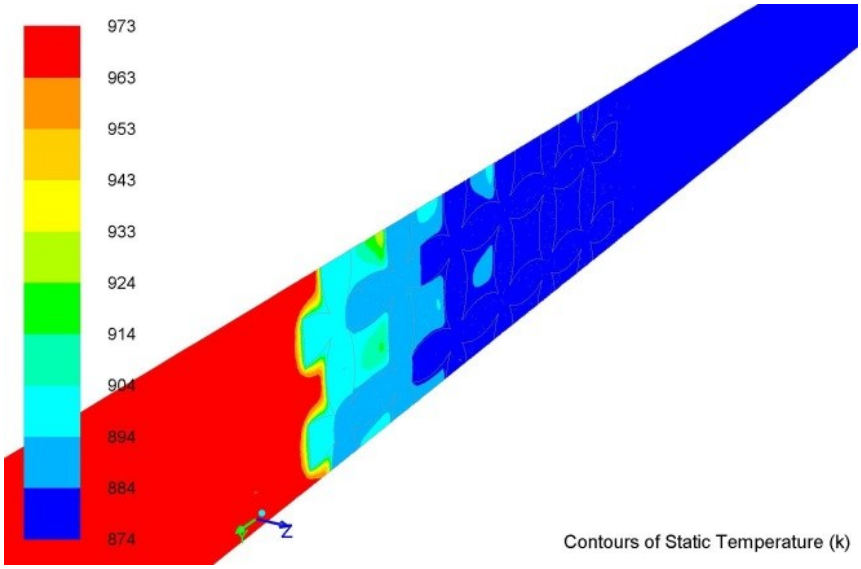

(b)

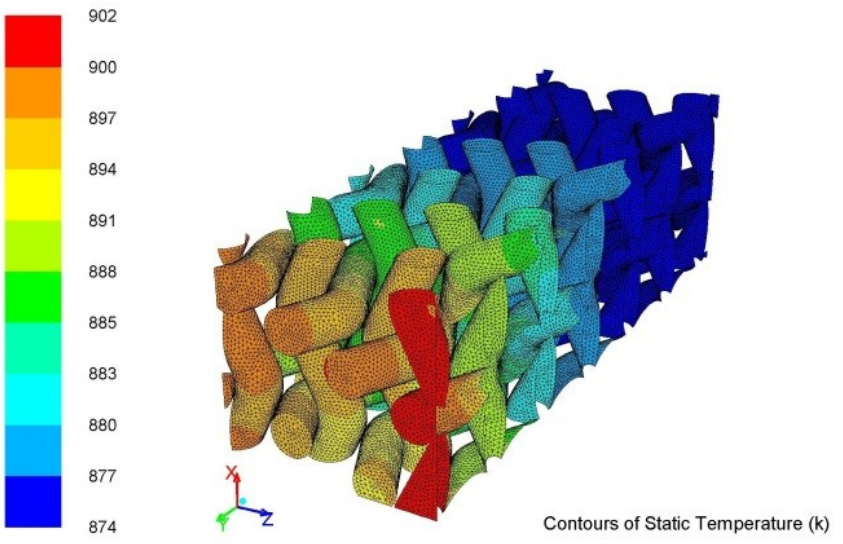

(c)

Figure 5. 25: Temperature contours through: Wound woven wire matrix W110-Pv60 for Re ≈ 60 (1.0m/s) at 0.02s

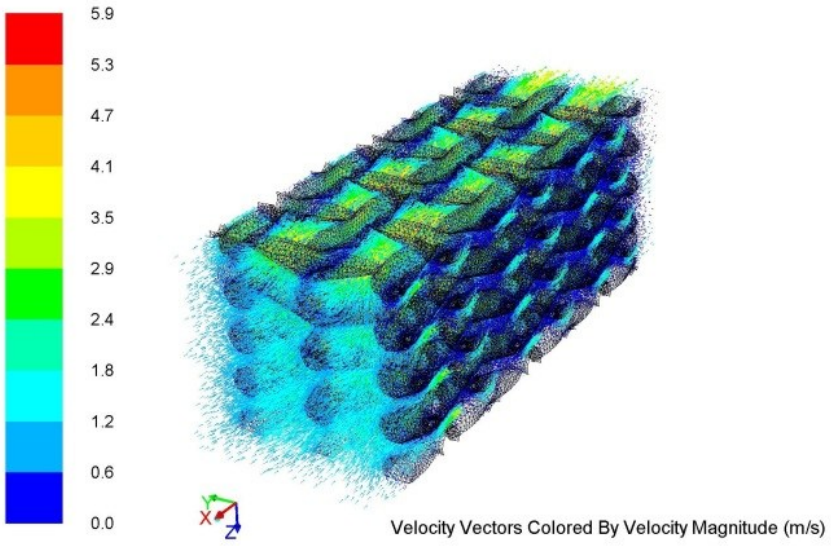

(a)

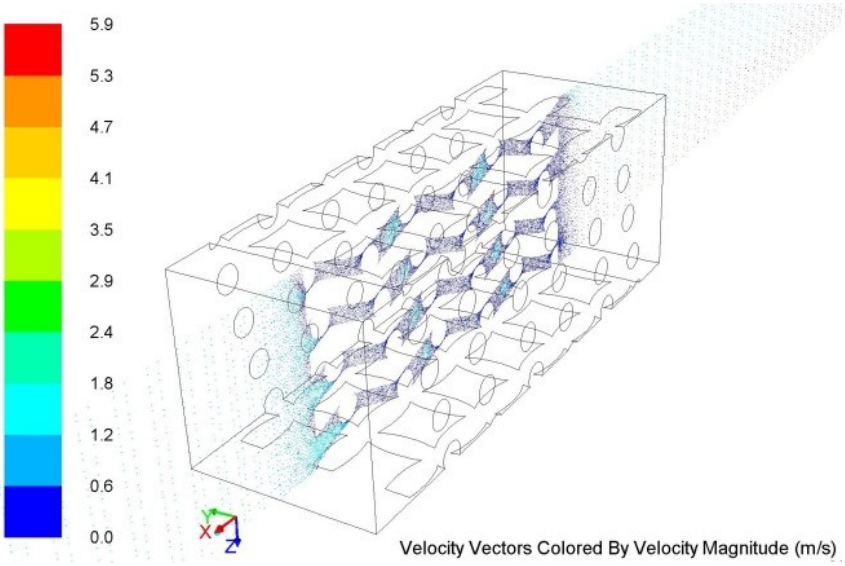

(b)

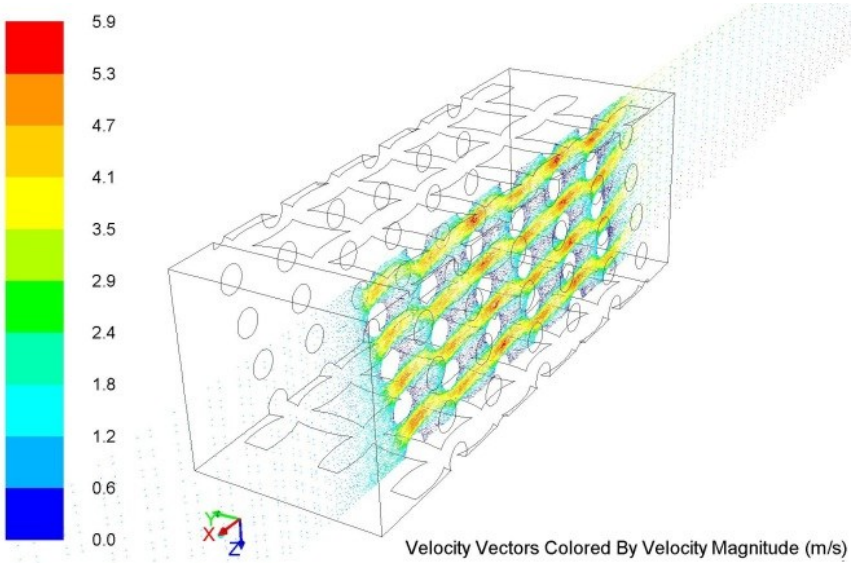

(c)

Figure 5. 26: Velocity vector through Wound woven wire matrix W80-Pv68 for Re ≈ 55 (1.0m/s) at 0.02s

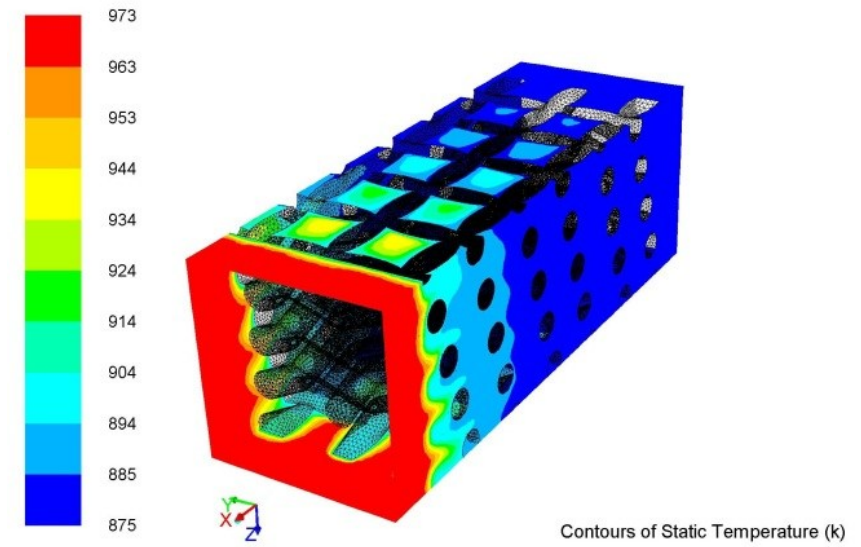

(a)

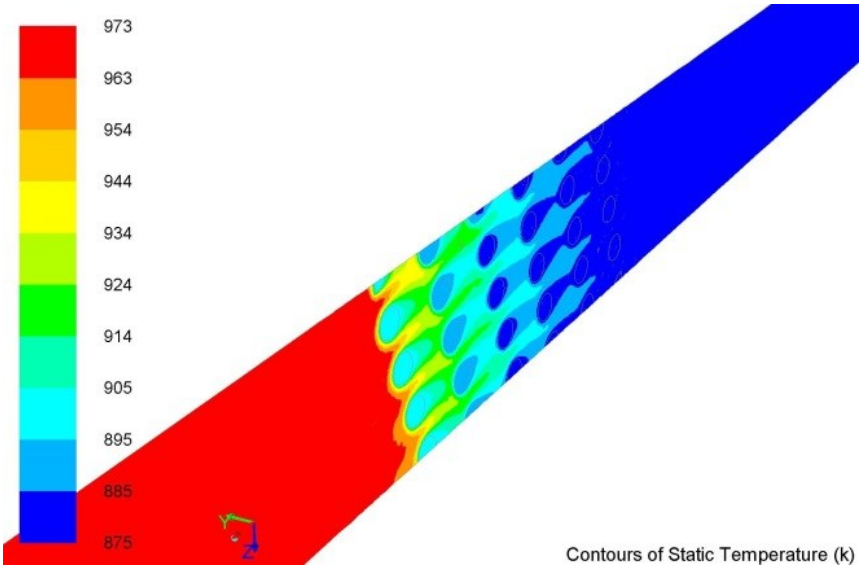

(b)

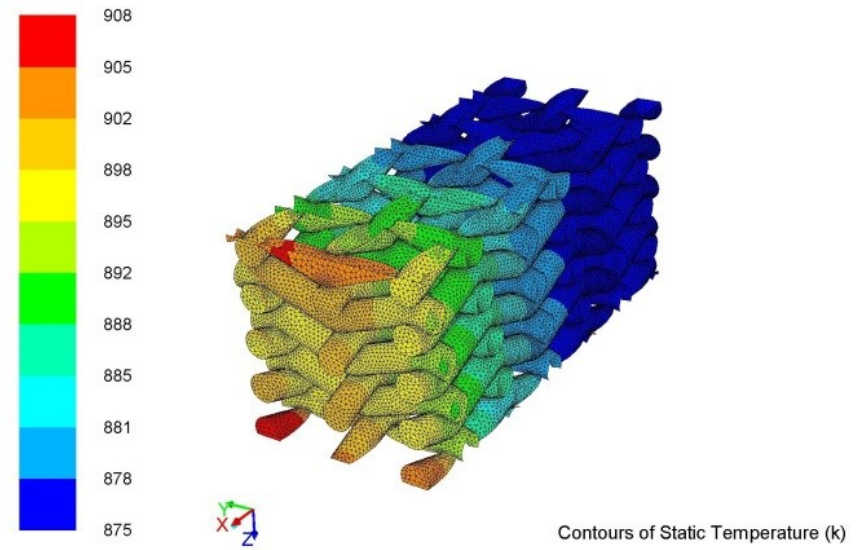

(c)

Figure 5. 27: Temperature contours through: Wound woven wire matrix W80-Pv68 for Re ≈ 55 (1.0m/s) at 0.02s

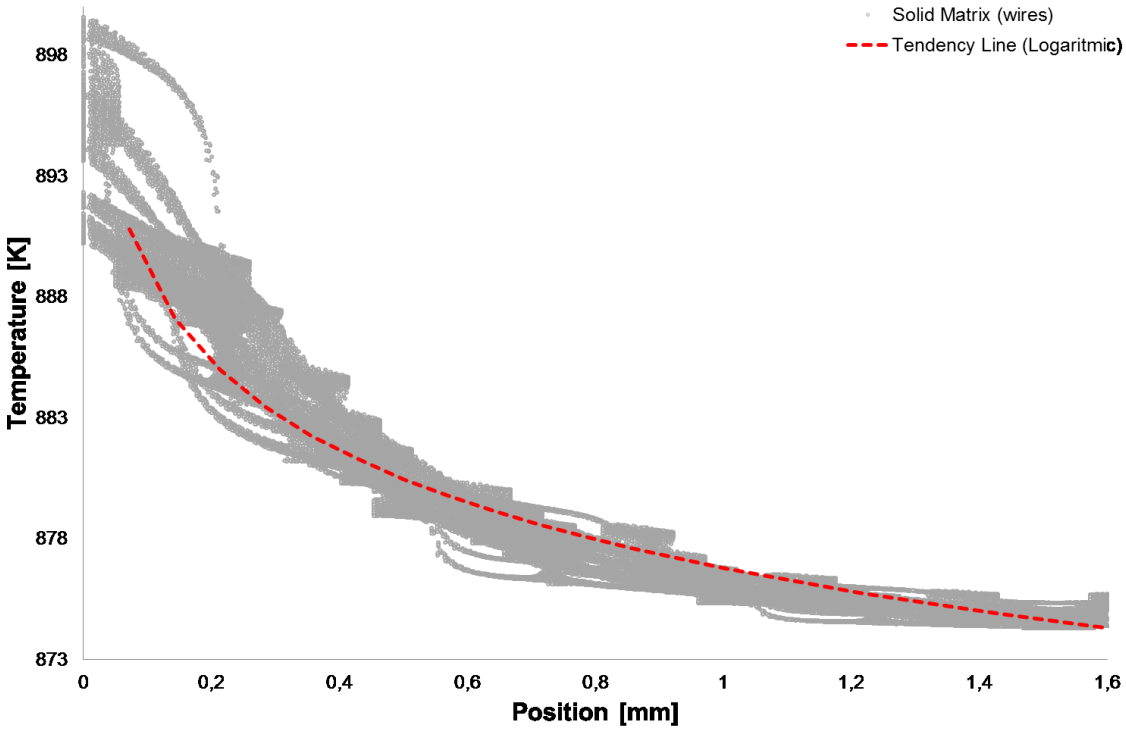

(a)

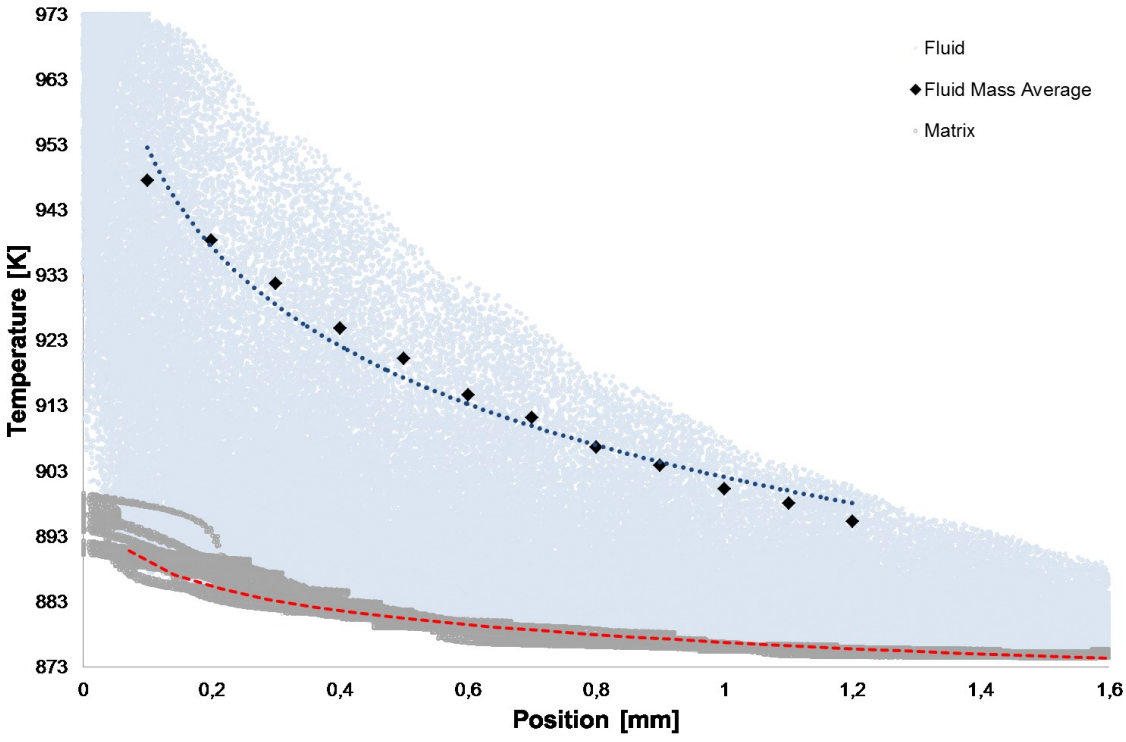

(b)

Figure 5. 28: Temperature vs Position through Wound woven wire matrix W110-63% for Re ≈ 50 (1m/s) at 0.02s: (a) Solid matrix temperature and (b) Solid matrix temperature and working fluid temperature

Next figures (from Figure 5. 24 to Figure 5. 27) show the local variation of velocity and temperature field values for the wound woven wire matrices at Reynolds number of 60 for two

wire diameters of 80 and 110 μm. Similar space-wise evolution of the temperature and velocity contours are also observed here except slightly higher maximum velocity values obtained from the wound woven wire matrix case.

Figure 5. 28 shows the temperature distribution as a function of the length through the regenerator matrix for the wound woven wire matrix. In the solid temperature distribution the trend observed is not stepwise. This is due to the high thermal conduction losses through the longitudinal wire in this kind of configurations.

The above numerically derived Nusselt correlation equation (Eq. [5.16]) could be considered to be a good general approximation to be applied to all configurations studied here for the wound woven wire mesh matrix. In addition it should be noted here that the dispersion at high Reynolds number (Maximum standard deviation of 4.4) for the wound woven wire mesh matrix is higher than that for the stacked woven wire mesh (Maximum standard deviation of 1.4). Therefore, it is suggested that the geometrical parameters should be studied carefully in this configuration.

The matrix geometrical parameters, hydraulic diameter (Eq. [3.28]) and specific heat transfer area (Eq. [3.32]), are function of wire diameter and volumetric porosity. Consequently, a decrease of the matrix volumetric porosity causes a decrease in the hydraulic diameter and an increase in the specific heat transfer area for the same wire mesh. Accordingly, the interaction between the matrix geometrical parameters, specific heat transfer area, hydraulic diameter and volumetric porosity require an in-depth study to isolate the influence of each one.

V.4. Conclusions

A general correlation equation for the Nusselt number (Eq. [5.16]) is numerically derived to characterize heat transfer for wound woven wire regenerator matrices following by an initial numerical validation against experimentally obtained correlation for stacked woven wire.

The validation results show that the derived correlation can be successfully applied in the Re number working range in Stirling engine regenerators $(4 < Re < 400)$, for diameter range from 80 to 110 μm and a volumetric porosity range from 0,60 to 0,68. The numerical study, which is extended to wound woven wire model case, also demonstrates an easy and effective use of the derived correlation for determining the Nusselt number for the wound woven wire model for a large Reynolds number range up to 400. The good correspondence of the stacked woven wire matrix configuration with the experimental data suggests that the derived correlations can be used with confidence to characterize and hence to optimize the wound woven wire matrix Stirling regenerator.

Regenerator Nusselt number and flow friction factor correlations are generally required to calculate the Stirling cycles, for this reason is fundamental the characterization of this key component. The results shown here demonstrate that the numerical tool can be used to study the influence of matrix geometric parameters (volumetric porosity, hydraulic diameter, specific heat transfer area, etc.) to improve the woven wire matrix heat transfer mechanism.

It is also observed that for the matrix configurations studied, the higher Nusselt numbers are obtained through the no-contact matrix and the lower Nusselt numbers through the aligned matrix configuration. Comparing the pressure drop results presented in previous chapter and the heat transfers results presented here for the matrix configuration studied, it is clear that both are conflicting requirements. In other words, the higher pressure drop and the higher Nusselt number are obtained for the same matrix configuration.

Regarding the fluid and matrix temperature difference, it is noteworthy here that no linear trend of the temperature gradient through the regeneration matrix is found.

CHAPTER VI:

Equivalent Porous Media Model

VI. EQUIVALENT POROUS MEDIA MODEL

This chapter is the final step in the approach following for the CFD numerical characterization of a woven wire Stirling regenerator matrix. First, it presents a CFD numerical methodology to obtain the inputs required (viscous/inertia resistance and heat transfer coefficient) for modelling the regenerator as a porous media based on pressure drop and heat transfer numerical results of previous chapters. The equivalent porous media is obtained for two matrix configurations with volumetric porosity of 63% for stacked and wound woven wire. Finally, the full size regenerator matrix is modelled as a porous media under oscillating regeneration cycles based on local instantaneous friction factor and Nusselt number correlations.

VI.1. Introduction

There are many methods of analysis for Stirling engines classified by Martini (Martini, 1983) as first-order, second-order and third order. However, the recent Stirling engines studies mainly focus on the multi-dimensional (multi-D) or also called fourth order analysis (Ibrahim, et al., 2001) (Wilson, et al., 2004) (Dyson, et al., 2005) (Tew, et al., 2006) (Dyson, et al., 2008) (Avdeychik, et al., 2009) (Kraitong, 2009), which is based on full Stirling engine modelling, and can reproduce useful Stirling engine performance results in a time-frame short enough to impact on design decisions (Dyson, et al., 2005). Moreover, the Stirling engine three-dimensional (3-D) simulations can provide a high level of geometry, flow physics and heat transfer detail which are necessary for final stages of design and optimization.

In the multi-D analysis, the regenerator is a difficult component to be modelled because any numerical inaccuracies in this component will influence the full scale Stirling simulation (Dyson, et al., 2005). In the Stirling engine´s multi-D analysis the regenerator is usually modelled as a macro-scale porous medium (large number of pores). The continuum approach of the porous media used in regenerator matrix necessitates the definition of the laws for conservation of mass, momentum and energy. Porous media numerical models request the input of the friction factor and the heat transfer coefficient which mostly are empirically obtained. Accordingly, a CFD numerical methodology to obtain the inputs required (viscous/inertia resistance and heat transfer coefficient) for modelling the regenerator as a porous media is presented.

VI.2. Stirling engine regenerator modelled as porous media

As it has been already explained, the main physical phenomena to be considered in the study of the Stirling regenerator are the pressure drop and the heat transfer. In Chapter III is shown that the flow through a porous media is modelled by adding an momentum source term to the standard flow equations (Eq. [3.21] and Eq. [3.22]) and the heat transfer in the interface to the standard energy equations for non-thermal equilibrium model (Eq. [3.26] and Eq.[3.27]).

VI.2.1. Numerical pressure drop characterization

The momentum source term (Eq. [3.21]) is composed of two parts: a viscous loss term (Darcy) and an inertial loss term. In the case of homogeneous or isotropic porous media, the source term is given by Eq. [3.22], where the permeability and the inertial factor are commonly obtained from experimental results.

Here, both coefficients are obtained based on previous numerical results through a small detailed 3-D woven wire matrix domain as a representative of the whole Stirling regenerator. The micro scale model includes individual wires trying to catch any non-uniformity of 3-D flow inside the matrix.

Considering one-dimension equations, the pressure drop given by Eq. [4.2] is transformed into Eq. [6.1] using the Ergun equation (Eq.[2.20]) and Reynolds number Eq.[3.33] where the coefficients of Eq.[3.22] can be easily obtained from two-parameters friction factor correlation equations.

$$\Delta p = \frac{\mu \cdot a_1}{2} \frac{L}{d_h^{\,2}} u_{\max} + \frac{a_2}{2} \frac{L}{d_h} \rho_f u_{\max}^2 \qquad [6.1]$$

where a_1 is a correlation constant related with the form drag, a_2 is a correlation constant related with the skin friction, u_{max} is the maximum flow velocity through the matrix defined by Eq. [3.31], d_h is the hydraulic diameter of the regenerator matrix defined by Eq. [3.28].

Next, the detailed numerical results for two specific matrix configurations with a volumetric porosity of 63% for 110μm wire diameter for both, stacked and woven configurations are presented (S110-63% and W110-63%). These results are used as input of the porous media model for the Stirling regenerator.

Figure 4.14 and Figure 4.20 shows the pressure drop results as a function of the length through the regenerator matrix, for stacked and wound configuration with a volumetric porosity of 63%. It is observed that the pressure drop behaviour is linear, stepwise and uniform through the regenerator matrix. The lowest pressure drop gradient is obtained through the stacked matrix configuration and the highest through the wound matrix configuration.

Figure 6. 1 presents the plot of the pressure drop as a function of the inlet velocity through a stacked and wound matrix configuration with a volumetric porosity of 63%. It is observed that the trend-line is approximated to a second order polynomial which corresponds to Forchheimer´s law (Eq. [2.19]). These numerical results can be extrapolated to determine the coefficients for the equivalent porous media. It should be noted here that all numerical results are obtained under constant working fluid properties of density and viscosity.

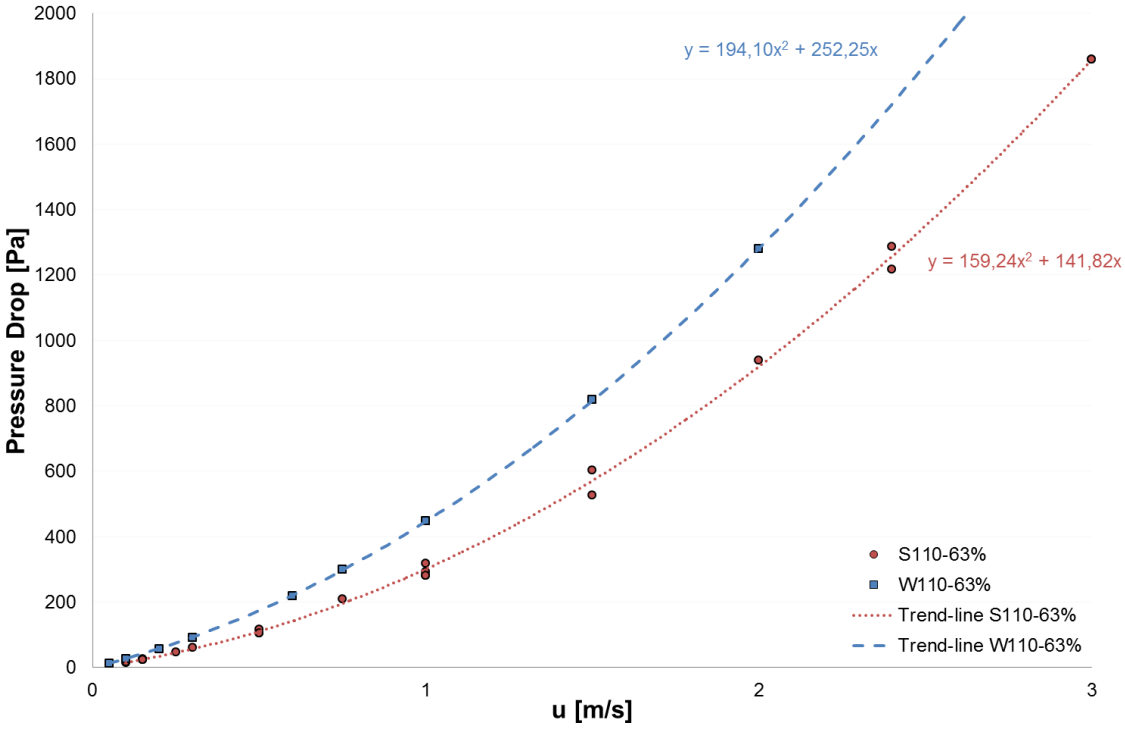

Figure 6. 1 Pressure drop [Pa] vs inlet velocity [m/s] trend-line for volumetric porosity of 63% at constant working fluid properties

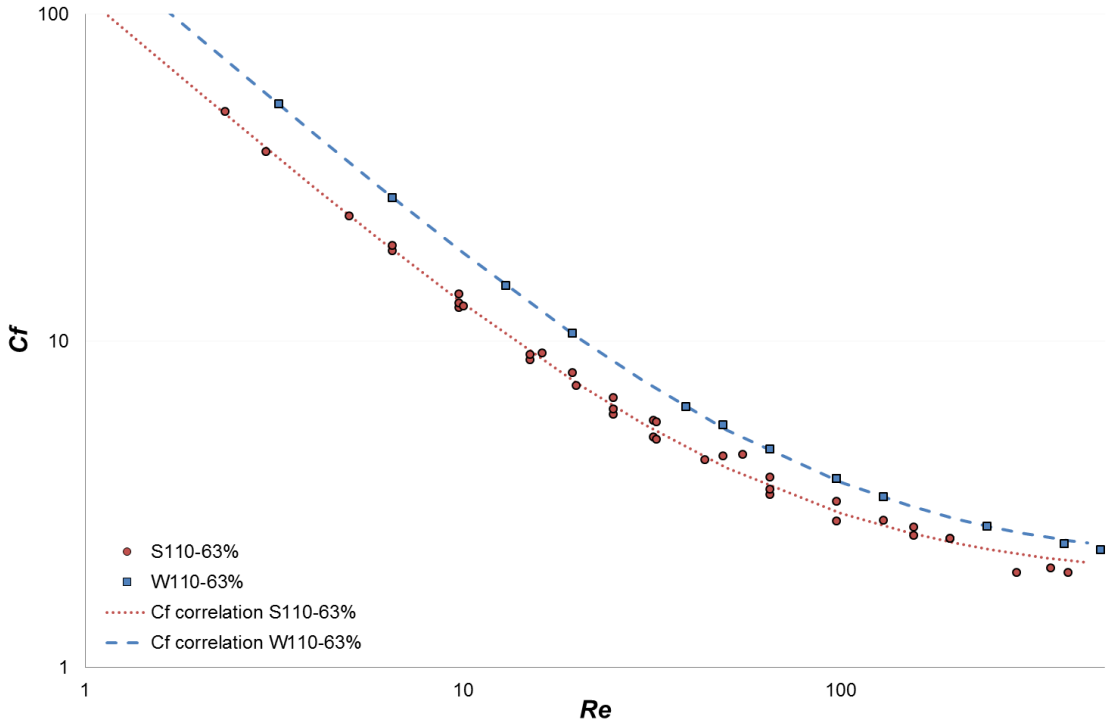

Figure 6. 2 Specific friction factor versus Reynolds number for stacked and wound woven wire matrices of 63% volumetric porosity:

Figure 6. 2 shows the relationship between friction factor and Reynolds number for the numerical results obtained for a stacked and wound woven wire matrix configuration with a volumetric porosity of 63%. Based on the numerical results, a specific friction factor correlation equation is obtained for each matrix configuration, stacked and wound for volumetric porosity of 63%. The specific correlation equation for S110-63% is given by Eq. [6.2]:

$$C_f = \frac{111.8}{\mathrm{Re}} + 1.85 \qquad [6.2]$$

And the specific friction factor correlation equation for W110-63% is given by Eq. [6.3]:

$$C_f = \frac{165.5}{\mathrm{Re}} + 2.04 \qquad [6.3]$$

Although the previously proposed three-parameters based general correlation equations Eq. [4.6] and Eq. [4.8] can be used for stacked and wound woven wire matrix configurations, the above derived specific correlation equations (Eq. [6.2] and Eq. [6.3]) can be directly used for each matrix configuration to model the porous media. In both configurations, the two-parameter Ergun form (Eq. [2.20]) fits very well with the numerical results and the use of the third parameter is not required as shown in Figure 6. 2.

Considering the above specific friction factor correlation equations (Eq. [6.2] and Eq.[6.3]), by rearranging Eq.[6.1] and making use of the relation between maximum velocity and inlet velocity, the viscous and the inertial resistance coefficients can also be also obtained. Table 6. 1 summarizes the resistance coefficients and the matrices characteristics for both configurations.

Table 6. 1: Geometry Parameters of Woven Wire Screen

Matrix	L [mm]	1/α	C_2
S110-63%	1.41	2.47E+09	2.49E+04
W110-63%	1.63	3.72E+09	2.69E+04

VI.2.2. Numerical heat transfer characterization

As it has been explained in Chapter III, in the heat transfer model through a porous media, there are two possible thermodynamic scenarios: local thermal equilibrium and local thermal non-equilibrium. In Chapter V it is observed that for the unidirectional flow through the regenerator matrix the scenario is the local thermal non-equilibrium, and the heat transfer coefficient is required to define the source term in both energy equations.

Here the detailed heat transfer numerical results for the two specific matrix configurations, S110-63% and W110-63% are presented. These results are used as the input of the porous media model for the Stirling regenerator.

Figure 5.19a and Figure 5.28a show the wire temperature distribution as a function of the length through the regenerator matrix for a stacked and wound woven wire matrix with a volumetric porosity of 63%. A clear stepwise temperature gradient is observed in the S110-63% matrix while a smooth temperature gradient mainly due to the longitudinal conduction through the wires is observed in the W110-63% matrix. However, in both cases the temperature across the regenerator matrix is not linear, and the trend-line is logarithmic. Figure 5.19b and Figure 5.28b plot the wire and working fluid temperature distribution as a function of the length through the regenerator matrix for the stacked and wound woven wire matrices with volumetric porosity of 63%. The figure also plots the trend-line for the wire temperature and the trend-line for the mass-average working fluid, it can be appreciated that the temperature difference is rather logarithmic than linear through the matrix under the flow condition studied.

Figure 6. 3 presents the plot of the heat transfer coefficient as a function of the inlet velocity through a stacked and wound matrix. All the numerical results are obtained at the same constant working fluid properties (density and viscosity). It is observed that the tendency is linear and the heat transfer coefficient is perceptibly higher through the S110-63% matrix. These heat transfer coefficients are used to define the equivalent porous media under a local thermal non-equilibrium scenario.

Figure 6. 4 shows the relationship between Nusselt number and Reynolds number for the numerical results obtained for a stacked and wound matrix configuration with a volumetric porosity of 63%. Based on the numerical results obtained for different solid and working fluid properties, a specific Nusselt correlation equation is obtained for each matrix configuration. The specific Nusselt correlation equation for S110-63% is given by Eq. [6.4]:

$$Nu = 1.91 + 0.17\,\mathrm{Re}^{0.80} \qquad [6.4]$$

And the specific Nusselt number correlation equation for W110-63% is given by Eq. [6.5]:

$$Nu = 2.15 + 0.07\,\mathrm{Re}^{0.88} \qquad [6.5]$$

The Nusselt number correlation equations are used to define the heat transfer coefficient through a local thermal non-equilibrium porous media model for the full Stirling regenerator. The heat transfer coefficient is defined by Eq. [6.6].

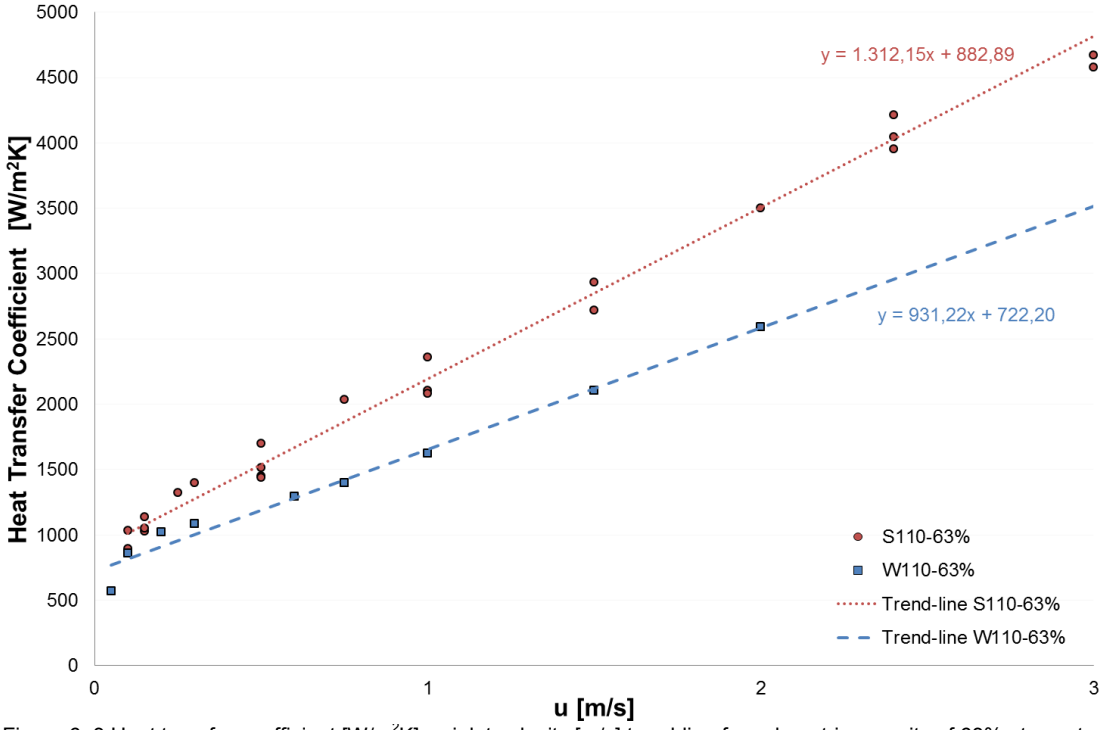

Figure 6. 3 Heat transfer coefficient [W/m^{2}K] vs inlet velocity [m/s] trend-line for volumetric porosity of 63% at constant working fluid properties

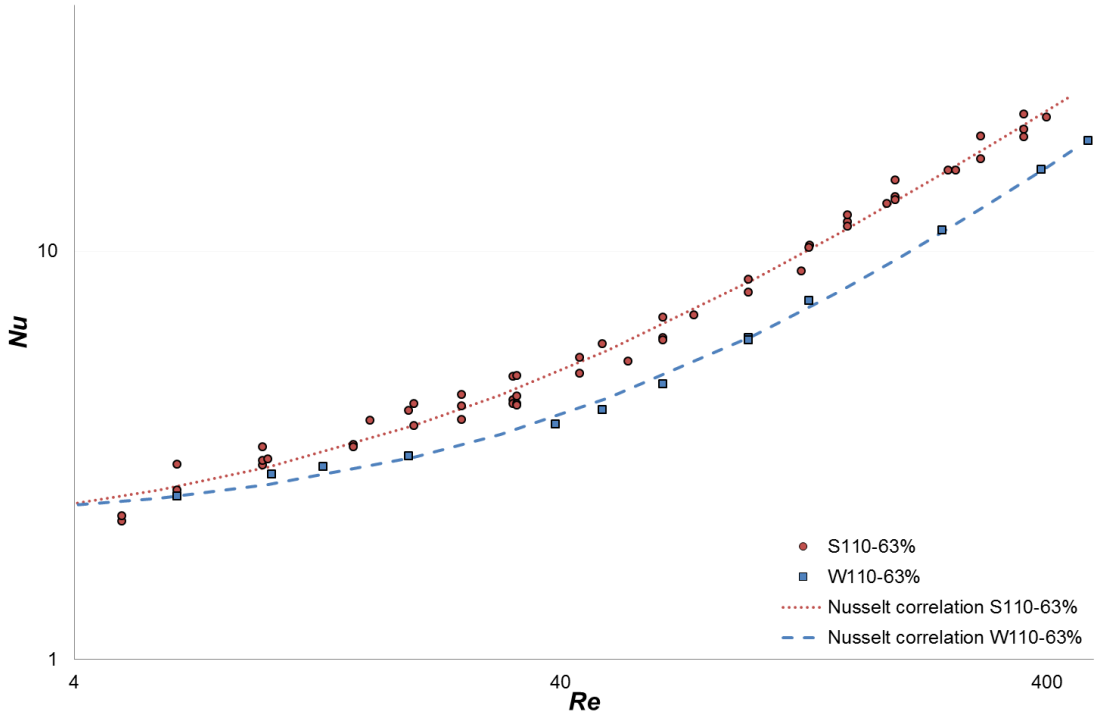

Figure 6. 4: Specific Nusselt number versus Reynolds number for stacked and wound woven wire matrices of 63% volumetric porosity

$$h = \frac{Nu \cdot k_g}{d_h} \qquad [6.6]$$

where d_h is the hydraulic diameter (Eq. [3.28], k_g is the thermal conductivity of the working fluid, and Nu is the Nusselt number.

VI.3. Computational Principles

The porous media governing equations for momentum and energy (thermal non-equilibrium) are described in Chapter III.

VI.3.1 Numerical Methodology

In the porous media model the fluid is considered to be viscous, incompressible, Newtonian and two-dimensional (2-D) through the equivalent porous media zone based on physical velocity and with assumption of laminar flow. The three-dimensional (3-D) detailed geometry is relevant for the modelling of a woven wire regenerator matrix because the flow characteristic is intrinsically three-dimensional. However, modelling an equivalent isotropic porous media a simplified 2-D domain fully represents the detailed 3-D model. On the other hand, the 2-D domain is the optimal model for minimizing computational memory and time which is especially important under oscillating flow conditions. The convergence criterion for all the velocity components and for the continuity is set to 10^{-6}, whereas for energy it is set to 10^{-8} for all simulations.

VI.3.1.1. Numerical methodology for equivalent porous media

The equivalent porous media models (micro-scale) consider that the flow is unidirectional, unsteady and due to the small range of temperature used in each case (micro-scale model) all fluid properties (including density, viscosity, specific heat, and conductivity) are assumed constant.

VI.3.1.2. Numerical methodology for full size regenerator as a porous media

Through the full size porous media models the flow is considered to be oscillating, unsteady, and the properties of the working fluid and the solid metal wire depends on the temperature. The working fluid is nitrogen and the metal wire matrix is made of stainless steel.

VI.3.2 Computational domain and boundary conditions

VI.3.2.1. Computational domain and boundary conditions for equivalent porous media

Figure 6. 5 illustrates the 2-D domain of the flow of interest (geometry set-up) which includes a porous zone. The porous zone size is equivalent to the detailed woven wire matrix characterized in previous chapters. The rest of the domain remains the same and the boundary conditions and simulation options are not modified with respect to previous heat transfer studies for woven wire matrix.

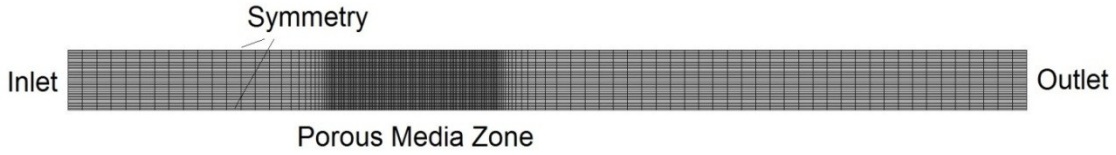

Figure 6. 5: Computational domain for equivalent porous media model

The effect of the mesh resolution and time step size on the present flow is assessed through a grid independence study for three different mesh systems containing non-uniformly hexahedral grid cells and for three non-dimensional time step at a Reynolds number of 200. In the temperature distribution values obtained from different mesh configurations and a non-

dimensional time step, there is no major difference among the computed values through a porous zone.

The porous media model simulations are carried out by considering the following boundary conditions:

1. Inflow boundary: Constant velocity inlet boundary conditions at constant temperature are used to define the fluid uniform velocity profile.

2. Outflow boundary: Pressure outlet boundary conditions are assigned to define the static (gauge) pressure by eliminating the reverse flow problem.

3. Side boundary: Free-slip symmetry flow boundary conditions at the two side boundaries of the computational domain are imposed. The normal velocity components and the normal gradients of all velocity components are assumed to have a zero value.

4. Porous media zone: the settings and inputs for the porous media are the following: physical velocity formulation, viscous and the inertial resistance coefficients summarized in Table 6. 1, isotropic porosity of 63%, .interfacial area density (see Table 3.4) and constant heat transfer coefficient (numerical data shown in and Figure 6. 3).

VI.3.2.2. Computational domain and boundary conditions for full regenerator as a porous media

The purpose of these simulations is to model a full size regenerator porous media under oscillating regeneration cycles. The full size regenerator matrix consists of the total length of a Stirling regenerator used in a micro-CHP reference engine (30mm), and the full flow area in the regenerator is not modelled. The computational domain is constructed of hexahedral meshes and 200 time steps per cycle at 25Hz is chosen.

The porous media model simulations are carried out by considering the following boundary conditions:

1. Inflow boundary: Oscillating inlet velocity boundary conditions at constant temperature (corresponding with the engine hot end) are used to define the fluid sinusoidal velocity profile defined with a user-defined-function (UDF) as follows:

$$u = u_0 \sin\left(2\pi f_e t\right) \qquad [6.7]$$

Where u_0 is the amplitude of the oscillating inlet velocity (1.5m/s) and f_e is the engine frequency (25Hz).

2. Outflow boundary: Pressure outlet boundary conditions at constant temperature (423K, corresponding with the engine cold end). The working pressure is constant at 26bar.

3. Side boundary: Free-slip symmetry flow boundary conditions at the two side boundaries of the computational domain are imposed. The normal velocity components and the normal gradients of all velocity components are assumed to have a zero value.

4. Porous media zone: the settings and inputs for the porous media are the following: physical velocity formulation, viscous and the inertial resistance coefficients summarized in Table 6. 1, isotropic porosity of 63%, constant interfacial area density (see Table 3.4) and variable heat transfer coefficient. The variable heat transfer

coefficient of the porous medium is defined through a UDF using Eq.[6.6], Eq.[6.4], and Eq.[6.5].

VI.4. Results and Discussion

VI.4.1 Numerical validation for equivalent porous media

The numerical simulations for the equivalent 2-D porous media of the stacked woven wire matrix S110-63% and of the wound woven wire matrix W110-63% are performed based on the numerical results obtained for the detailed matrix.

Figure 6. 6 shows the pressure drop results as a function of the inlet velocity for S110-63% and W110-63% equivalent porous media (indicated as PM). The figure also shows the numerical results obtained from the detailed regenerator matrix simulation solutions for both configurations. Excellent agreement between the results of 3-D regenerator matrix and the equivalent 2-D porous media are obtained using the viscous and inertia resistance coefficients derived from the detailed 3-D regenerator matrix summarized in Table 6. 1.

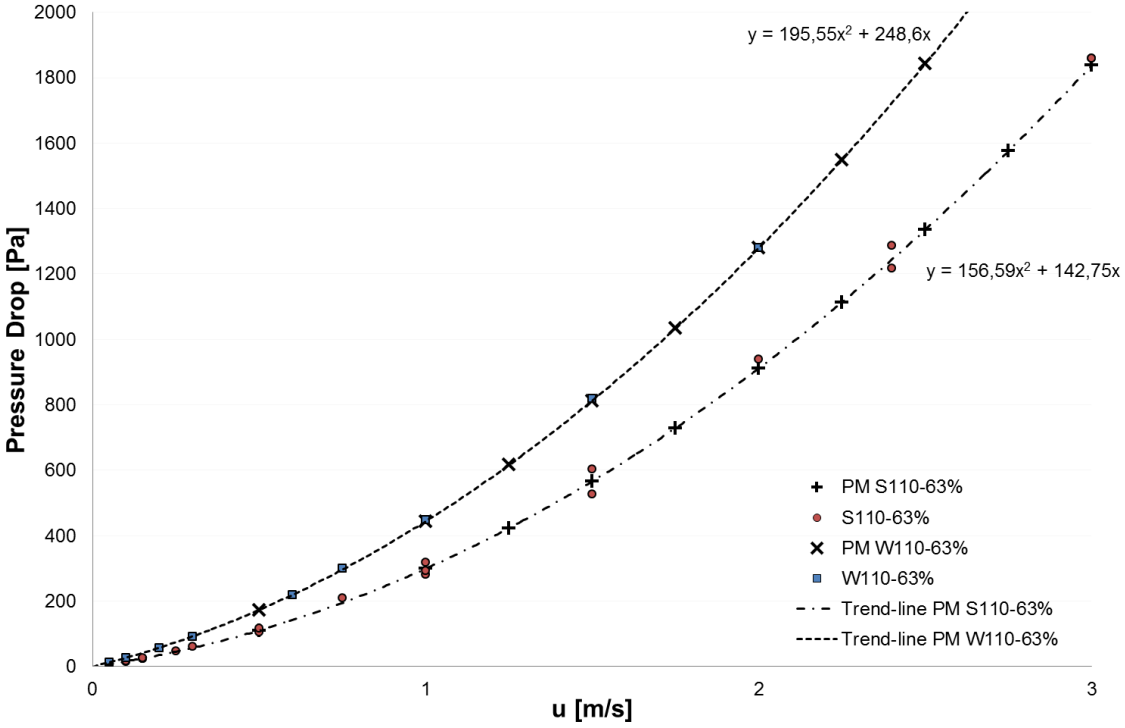

Figure 6. 6: Equivalent porous media pressure drop [Pa] vs inlet velocity [m/s] trend-line for volumetric porosity of 63% at constant working fluid properties

Next figures show the numerical results for fluid and solid temperature distribution as a function of the length through the equivalent porous media. Figure 6. 7 compares the results for the detailed stacked woven wire matrix against its equivalent fluid and solid porous media, and Figure 6. 8 is the comparison for the wound woven wire matrix. The fluid temperature distribution for the detailed matrix corresponds to the mass-average temperature.

In the results shown, it is observed that there is a good agreement between the detailed matrix temperatures and the equivalent porous media. It is noteworthy here that the temperature distribution through the isotropic porous media is smooth and the present model cannot reproduce the stepped behaviour in the solid wire matrix.

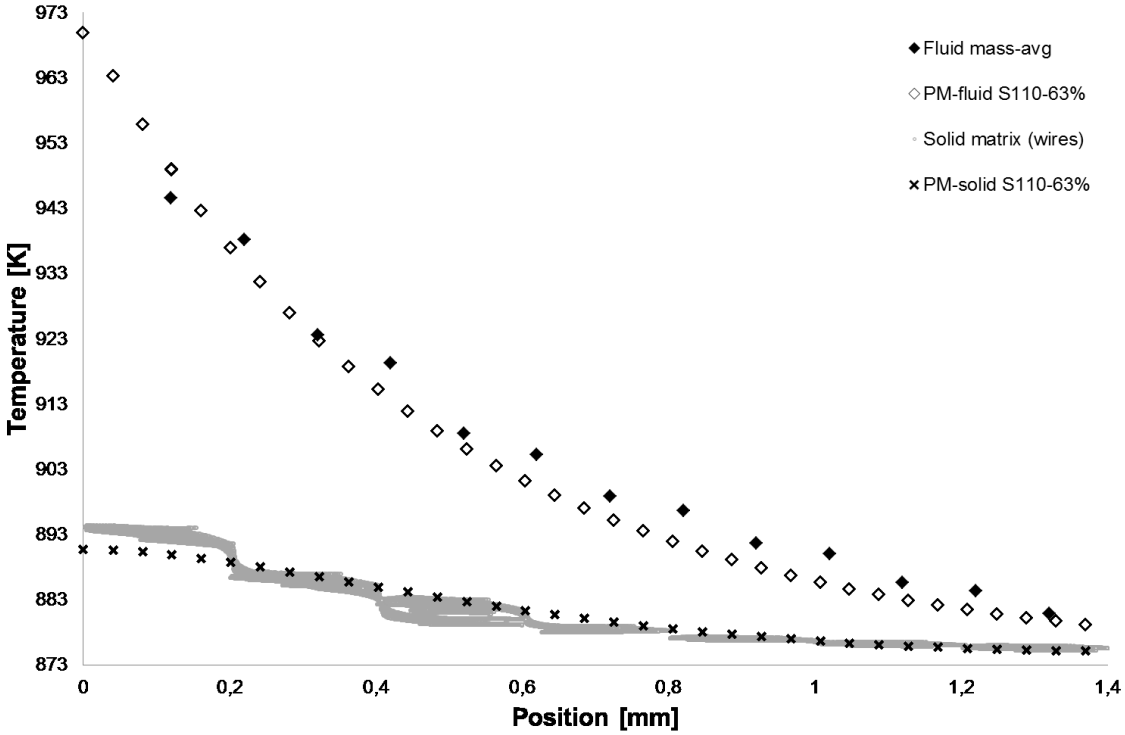

Figure 6. 7: Stacked equivalent porous media temperature [K] vs position [mm] through woven wire matrix of 63% volumetric porosity for Re ≈ 65 (1m/s) at 0.02s

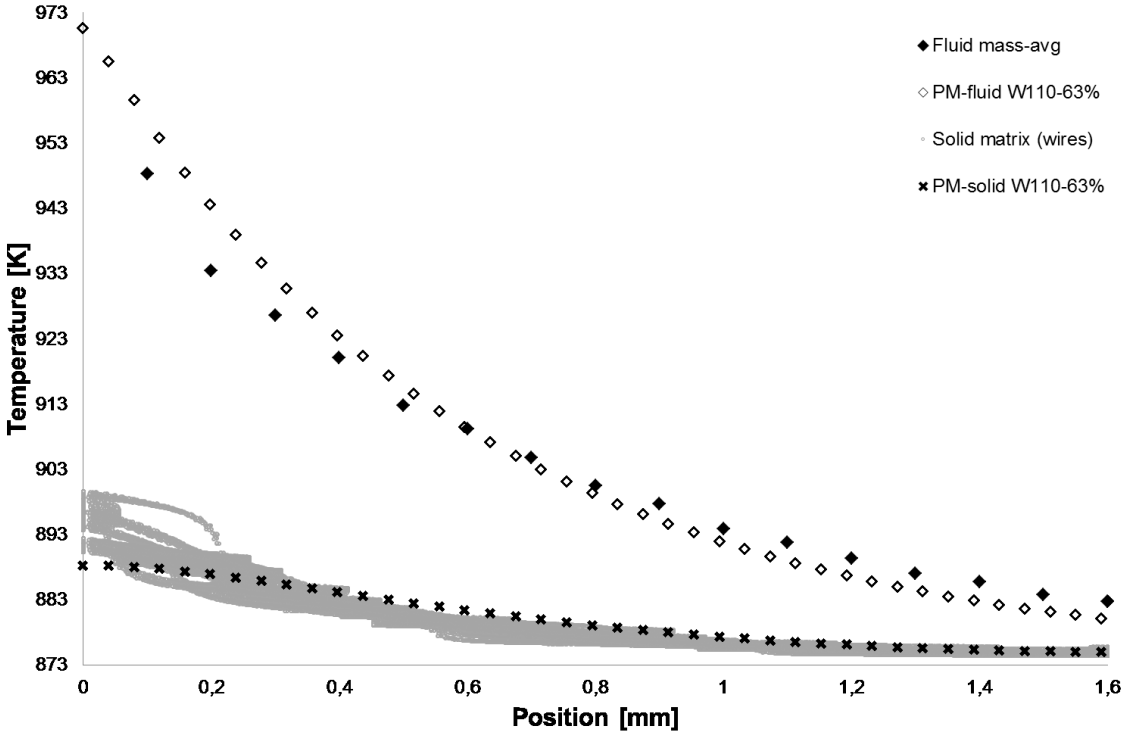

Figure 6. 8: Wound equivalent porous media temperature [K] vs position [mm] through woven wire matrix of 63% volumetric porosity for Re ≈ 65 (1m/s) at 0.02s

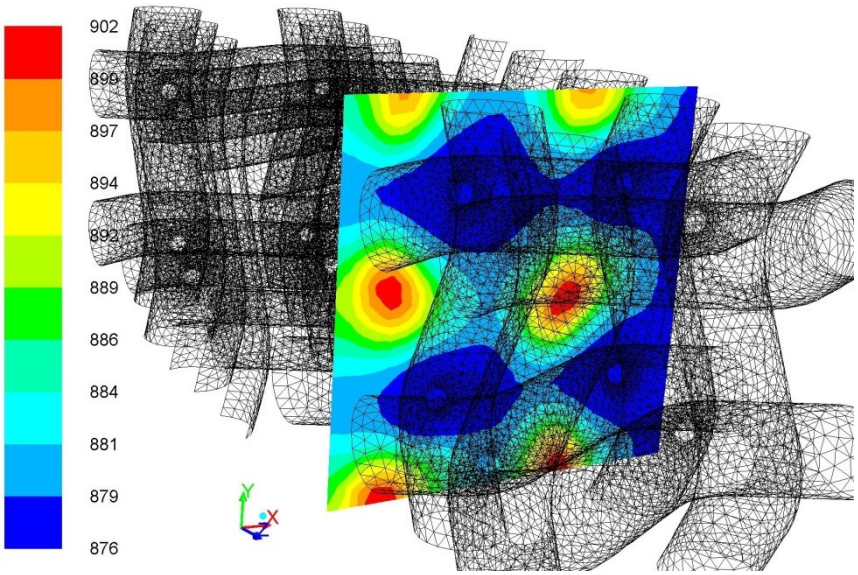

(a)

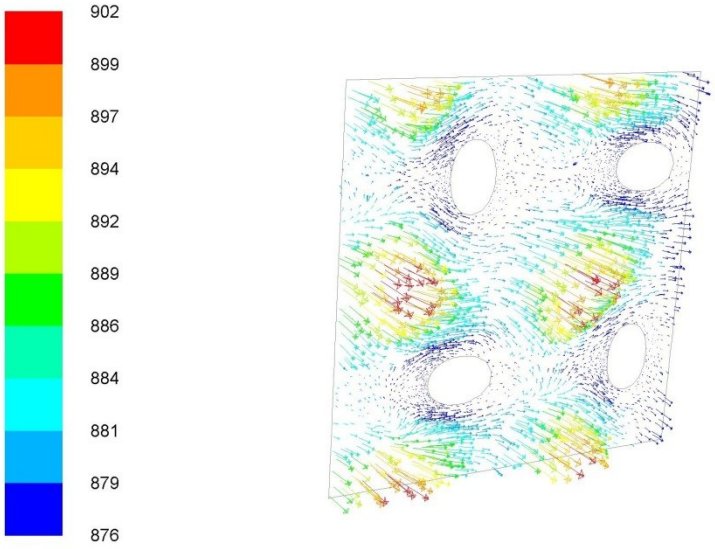

(b)

Figure 6. 9: Stacked woven wire matrix of 63% volumetric porosity for Re ≈ 65 (1m/s) at 0.02s: (a) Temperature contours [K] and (b) Velocity vectors coloured by temperature [K] in section plane at 1mm

Figure 6. 9 and Figure 6. 10 present the temperatures contours and velocity vectors in a cutting plane through both detailed 3-D regenerator matrices, it can be appreciated that the temperature gradient in the fluid is significant for both configurations, and it depends of the sections chosen due to the geometry of the woven wire matrix where the low flow velocity can be observed around some wires. Through an isotropic porous media in a transversal cutting plane, the temperature of the fluid and solid are constant. For this reason the differences observed in the results of the equivalent porous media and the 3-D model are acceptable considering the temperature gradient behaviour shown in the Figure 6. 9 and Figure 6. 10. Therefore, it is believed that the results verify the suitability of the local thermal non-equilibrium porous media model as an equivalent of the detailed 3-D regenerator matrices for pressure drop and heat transfer phenomena.

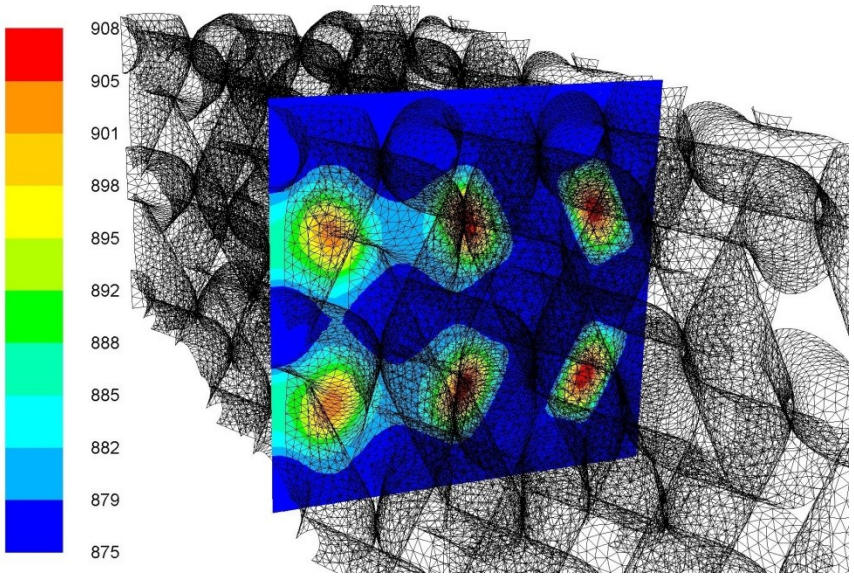

(a)

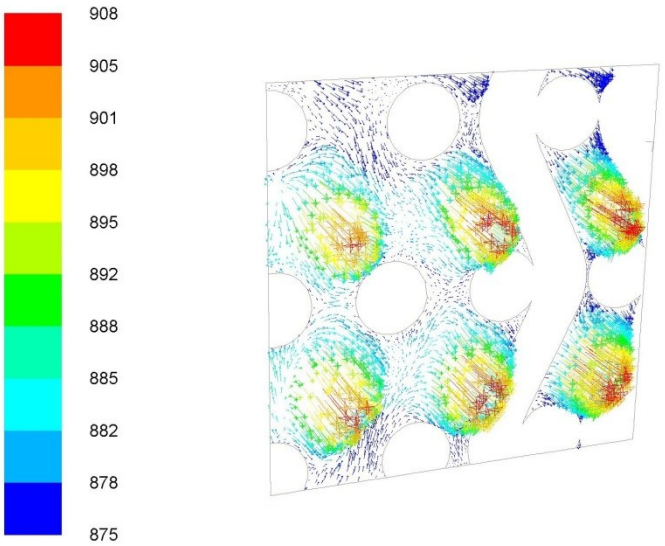

(b)

Figure 6. 10: Wound woven wire matrix of 63% volumetric porosity for Re ≈ 65 (1m/s) at 0.02s: (a) Temperature contours [K] and (b) Velocity vectors coloured by temperature [K] in section plane at 1mm

VI.4.2 Numerical validation for full regenerator as a porous media

In this section, the numerical simulations for the full length 2-D equivalent porous media of the stacked and of the wound woven wire matrix are performed under oscillating flow conditions. In these models under oscillating regeneration cycles the desired solution is the quasi-steady solution, when the results for two consecutive cycles are identical. The results present and discussed here are obtained in a quasi-steady state for the working pressure of 26 bar and the flow oscillating frequency of 25Hz.

Figure 6. 11 shows the variations of the computed pressure drop through the porous media matrix for both configurations during a complete quasi-steady cycle. It is noted that for the frequency studied, the pressure drop varies sinusoidal and a small phase lag during the first half of the cycle (hot-blow) with respect to the inlet fluid velocity is observed. The cycle-averaged pressure drop for the S110-63% equivalent regenerator porous media is 4700Pa and for the W110-63% equivalent regenerator porous media is 5780Pa.

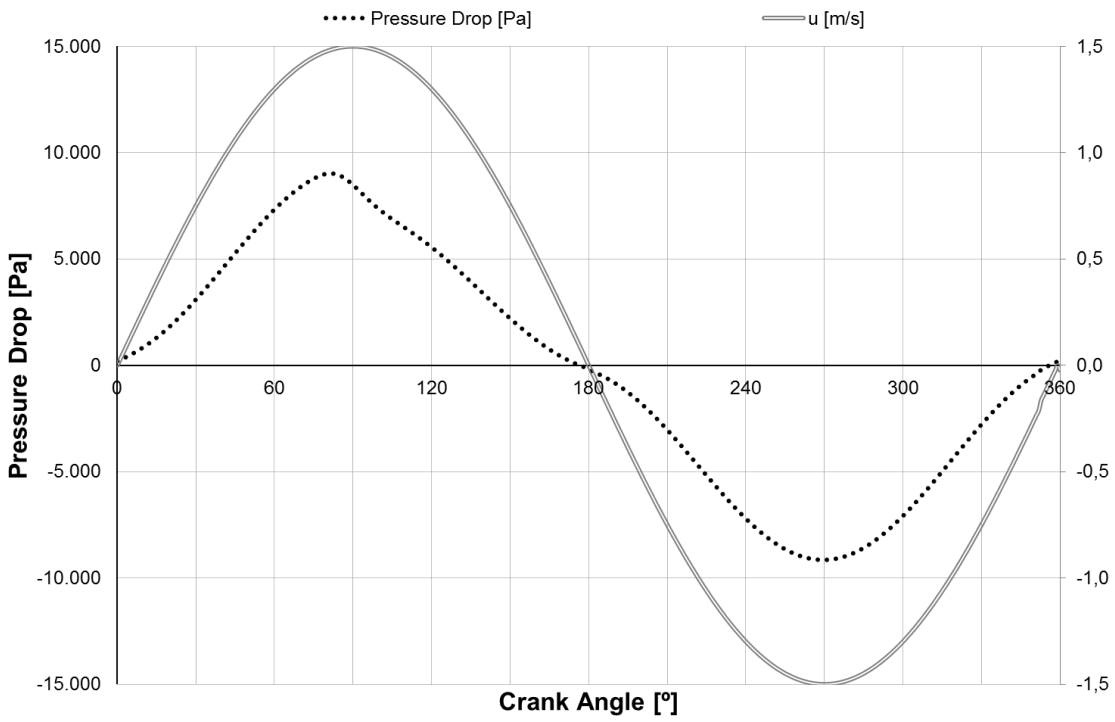

(a)

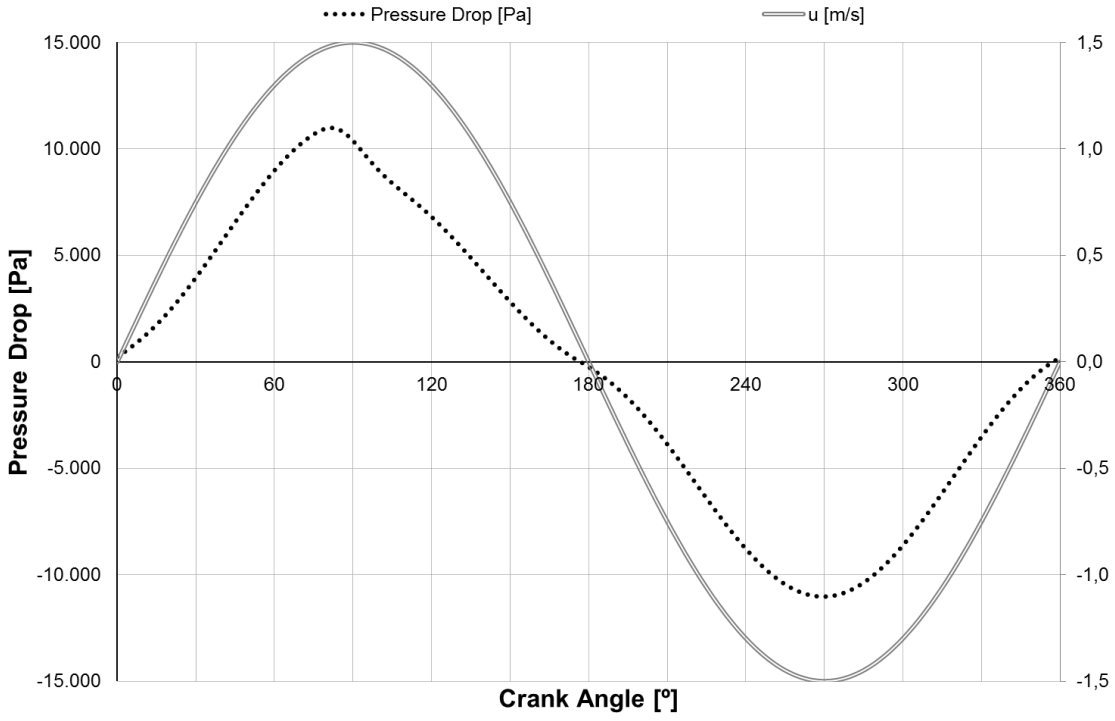

(b)

Figure 6. 11: Pressure drop [Pa] vs. crank angle [º] through woven wire matrix of 63% volumetric porosity: (a) Stacked and (b) Wound matrices

The temperature profiles through the regenerator porous matrix for the fluid and solid are presented in Figure 6. 12. Logarithmic and linear trend-lines are both included in to the figure as reference lines. It can be found that the temperature profile through the regenerator can be better fitted to a logarithmic curve (regression coefficient of about 1) rather than linear line. Therefore, the logarithmic mean temperature difference between fluid and solid is used for the present heat transfer calculations.

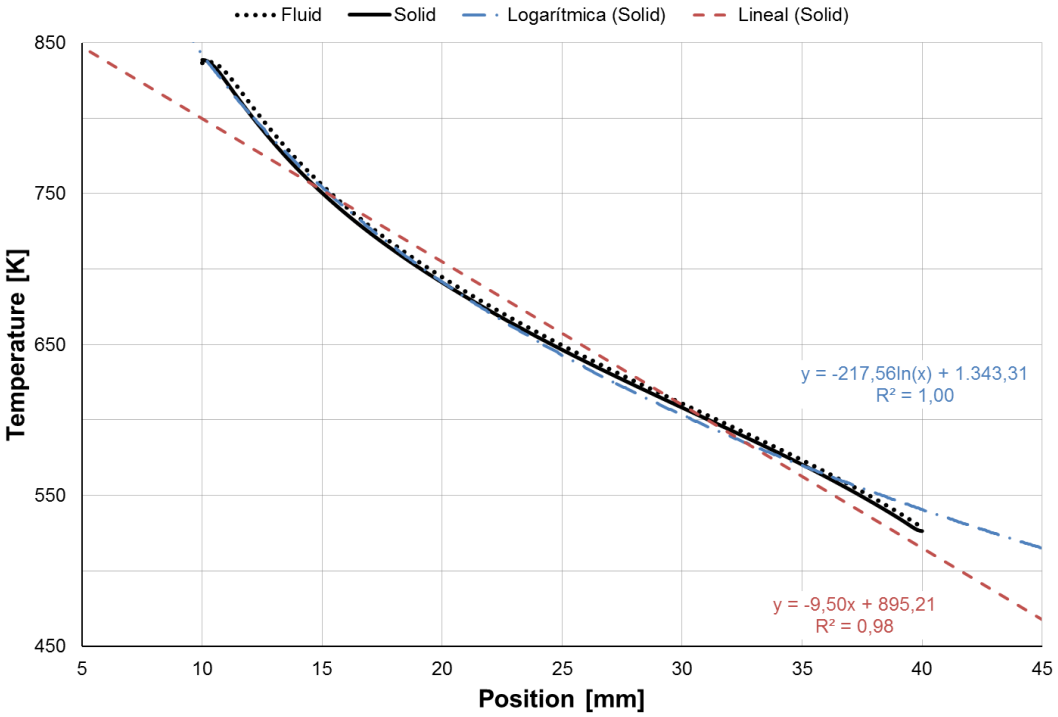

(a)

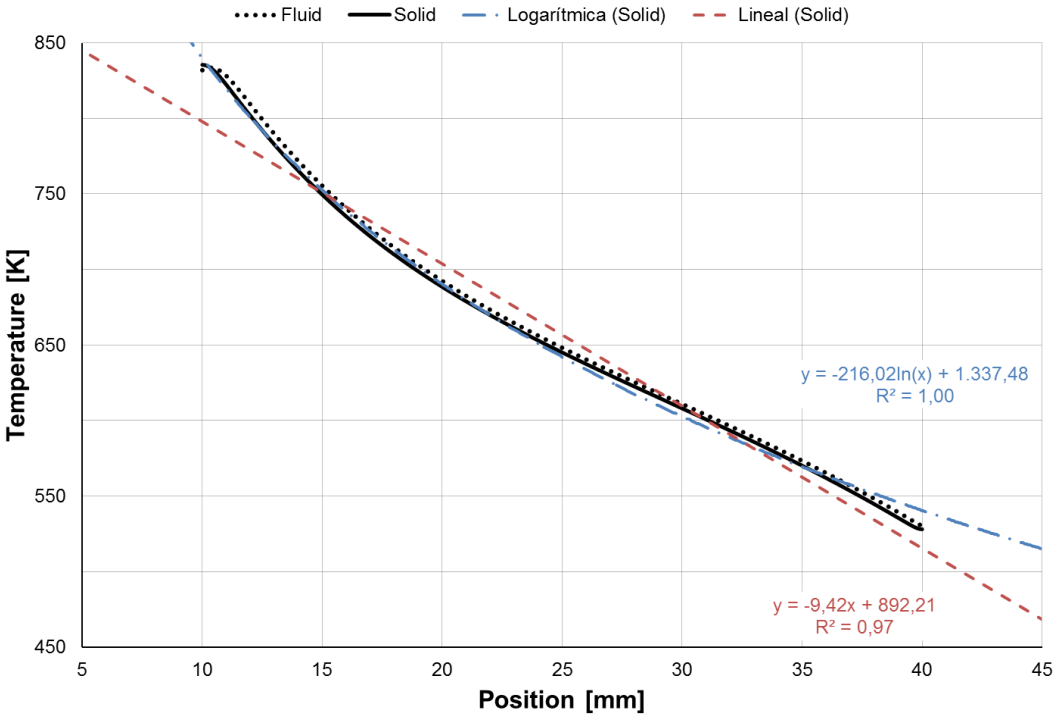

(b)

Figure 6. 12: Temperature profile [K] vs Position [mm] through porous matrix of 63% volumetric porosity: (a) Stacked and (b) Wound matrices

Figure 6. 13 illustrates the temperature fluctuations in three sections of the regenerator porous media matrix (mid-plane, hot-end (1mm) and cold-end (1mm)) during three complete quasi-steady cycles. It is observed that in different axial sections the solid matrix temperature corresponds to the mean fluid matrix temperature. On the other hand, both fluid and solid temperatures change periodically with the oscillating flow and the variations of the fluid temperature is larger than the solid temperature (almost constant or independent of time).

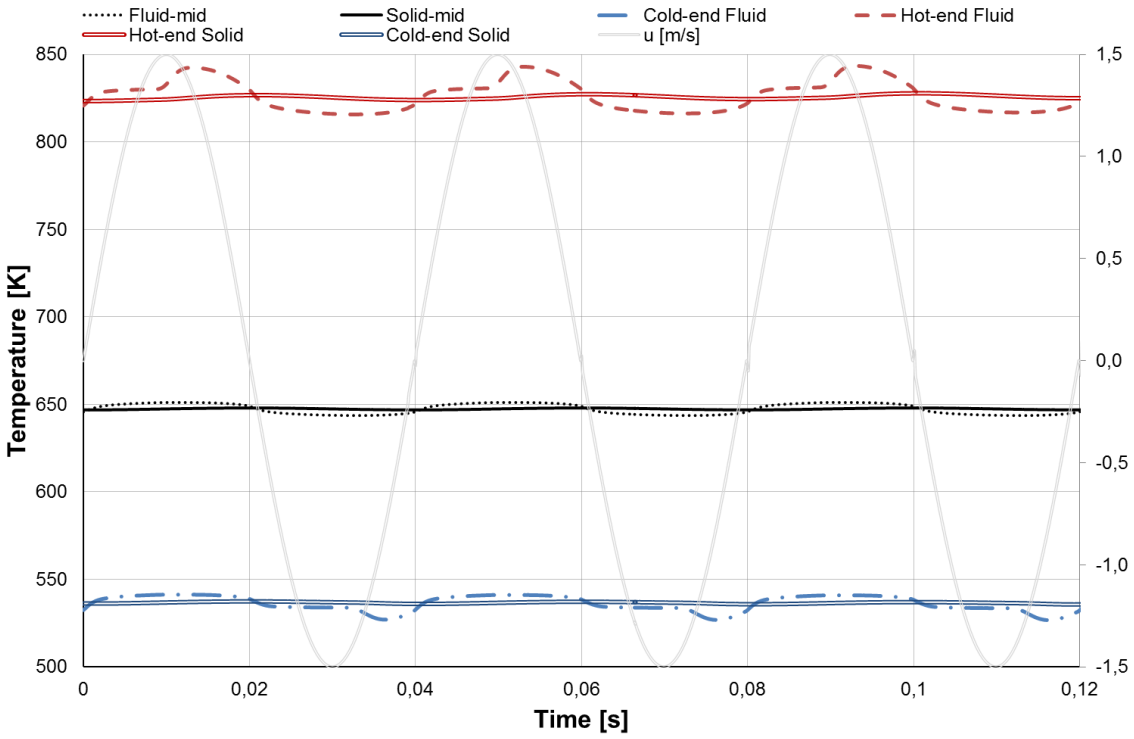

(a)

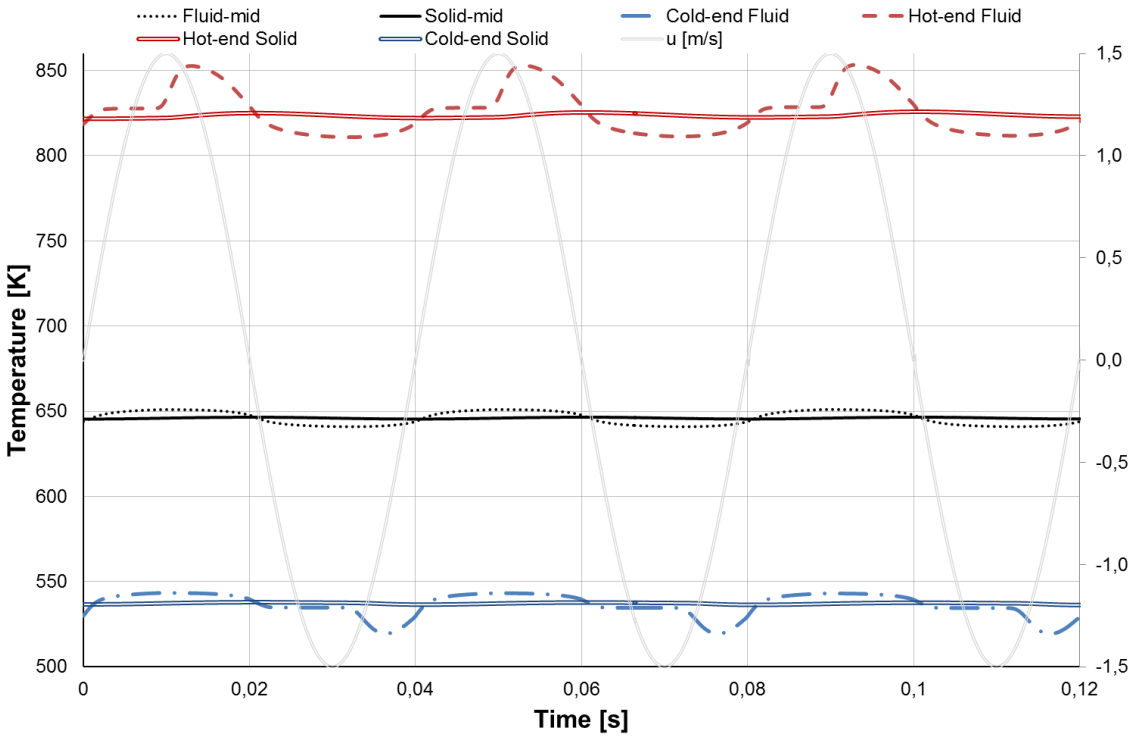

(b)

Figure 6. 13: Temperature fluctuations [K] in three porous matrix regenerator sections vs. time [s] for: (a) Stacked and (b) Wound

The temperature fluctuations in the mid-section for stacked and wound matrix configurations are also illustrated in Figure 6. 14. A phase lag is clearly identified for the matrix temperature due to the heat transfer process. Basically, the fluid temperature is higher during the first half of the oscillating cycle, while at the second half, the solid temperature is higher.

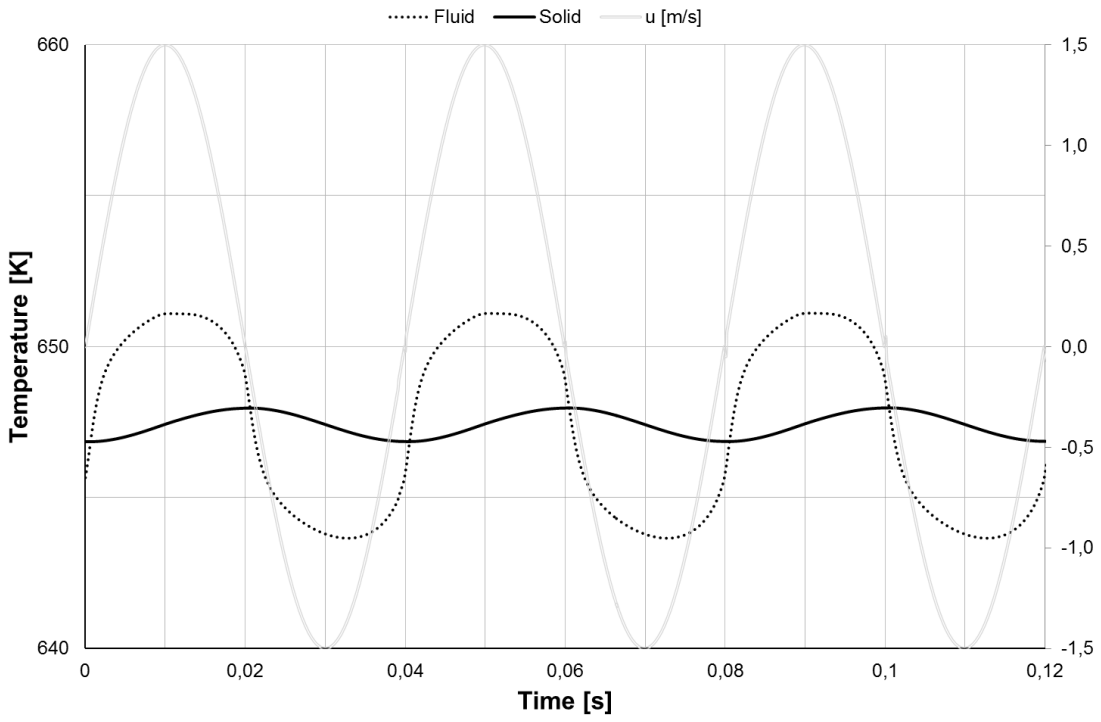

(a)

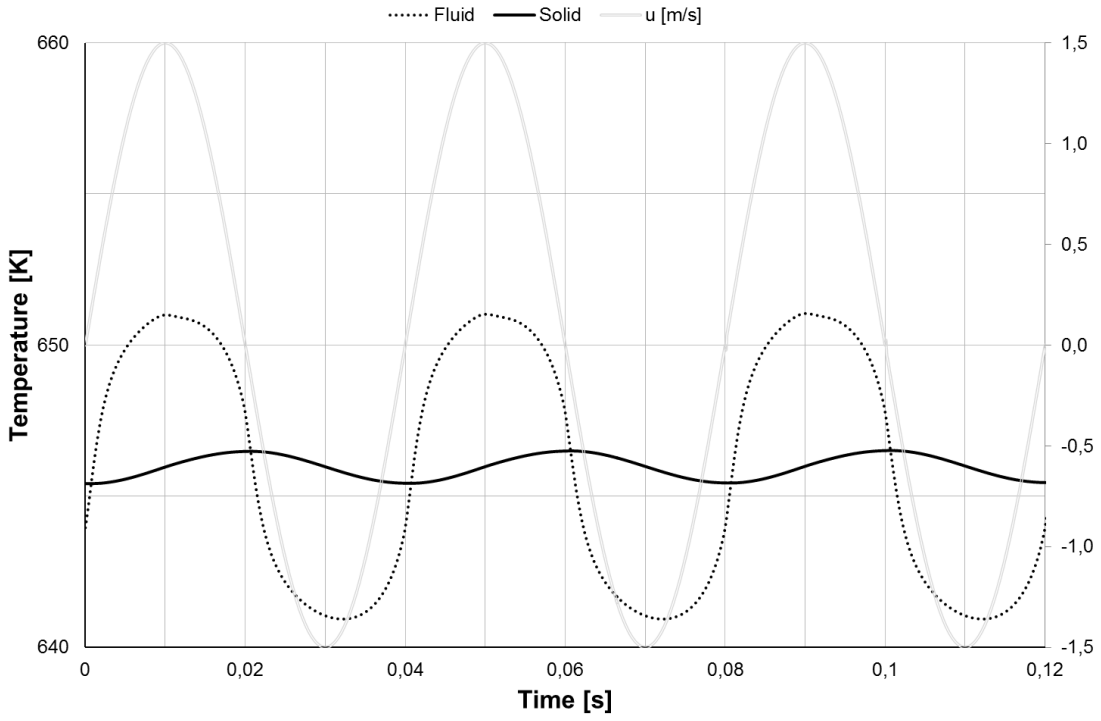

(b)

Figure 6. 14: Temperature fluctuations [K] in the mid-section vs. time [s] for: (a) Stacked and (b) Wound

Figure 6. 15 represents a comparison between the friction factor numerically obtained from the 3-D detailed matrix (Eq.[6.2] and Eq. [6.3]) at local instantaneous Re number with the friction factor obtained through a whole porous media under oscillating flow conditions at average Re number. The figure clearly shows that the profile of the computed local instantaneous friction factor corresponds well with that of average friction factor.

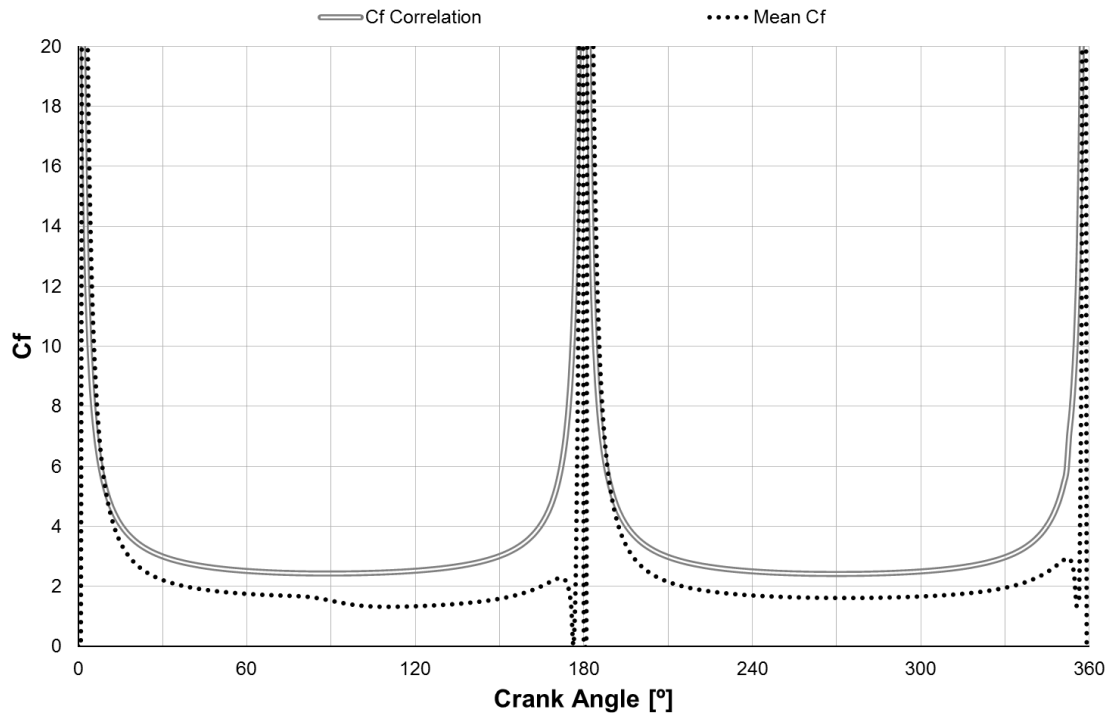

(a)

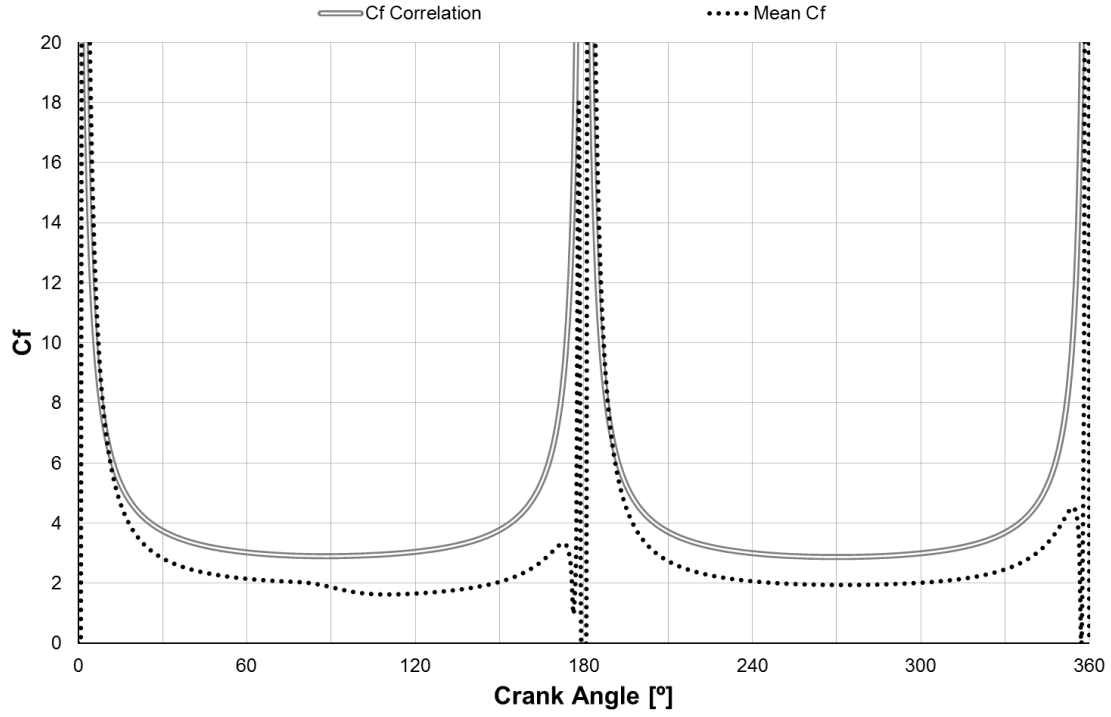

(b)

Figure 6. 15: Porous matrix friction factor and Specific friction factor correlation equation vs. crank angle [º] for: (a) Stacked and (b) Wound

Figure 6. 16 illustrates the Nusselt number variation with respect to the crank angle for the specific numerically obtained correlation from the 3-D detailed matrix (Eq.[6.4] and Eq. [6.5]) with the average Nusselt number obtained in the present study through a porous media under oscillating flow conditions. The Nusselt number peaks observed in the figures above are due to the very small temperatures difference between the fluid and the solid matrix during direction change under oscillating flow. The mean Nusselt number obtained through the porous media

under oscillating flow conditions characterize the heat transfer performance of the 3-D detailed regenerator matrix.

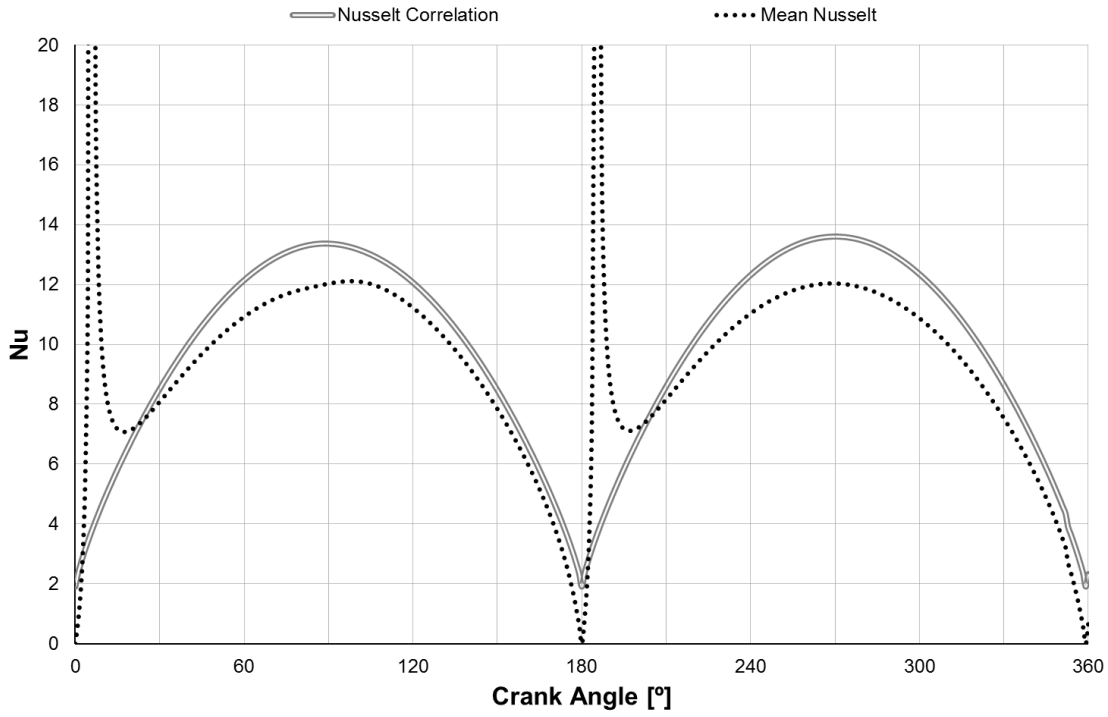

(a)

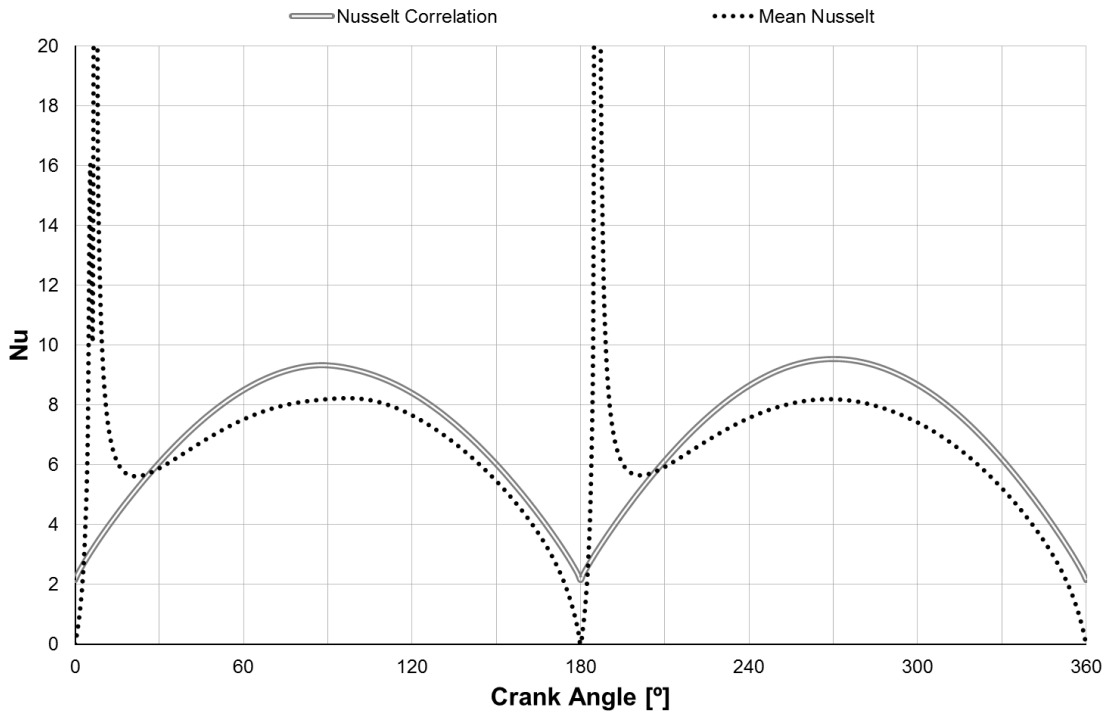

(b)

Figure 6. 16: Porous matrix Nusselt number and Specific Nusselt number correlation vs. crank angle [º] for: (a) Stacked and (b) Wound

Table 6. 2 presents the working gas temperatures at both ends of the porous media matrices. The nomenclature used in this table corresponds to the one used in Figure 2.13. The table clearly suggests that there is no significant variation in the computed mean temperature values

for both stacked and wound configurations. However, there is a variation in the maximum and minimum temperatures in both ends, suggesting higher temperature fluctuations for the wound configurations as previously depicted in Figure 6. 13 and Figure 6. 14. On the other hand, the solid matrix temperature is practically the same as the mean working gas temperature along the regenerator matrix.

Table 6. 2: Working gas temperatures [K] through regenerator porous matrix

Matrix	$T_{g-Lr_{\max}}$	$T_{g-Lr_{\min}}$	T_{r-Lr}	$T_{g-0_{\max}}$	$T_{g-0_{\min}}$	T_{r-0}
S110-63%	843	816	826	541	527	537
W110-63%	853	811	824	543	519	537

The thermal regenerator efficiency is evaluated in terms of the gas working temperatures and matrix temperature as it is defined by Eq. [2.7] for heating process and by Eq. [2.8] for cooling process. Table 6. 3 shows the heating and cooling thermal efficiencies calculated for both regenerator matrix configurations at the pressure of 26 bar.

Table 6. 3: Regenerator thermal efficiency

Matrix	ε^+	ε^-
S110-63%	96.7%	98.7%
W110-63%	95.7%	98.1%

It is observed in Table 6. 3 that the efficiency is higher for stacked matrix configuration than for wound matrix configuration. Furthermore, it is observed that the thermal efficiency is higher during the cooling process than during the heating process in both configurations. These results are consistent with the smaller amplitude of temperature fluctuations observed in Figure 6. 13 at the regenerator cold end. This is probably due to the fact that the efficiency is defined in terms of temperature differences here. On the other hand, the mean Nusselt numbers obtained during the cooling process are slightly higher than during the heating process as it is shown in Figure 6. 16.

Figure 6. 17 shows the ratio NPH/NTU given by the Eq. [2.6] for stacked and wound woven wire matrices. In each figure are plotted two ratios, the first is calculated using the specific correlation equations for friction factor (Eq. [6.2] and Eq. [6.3]) and Nusselt number (Eq. [6.4] and Eq. [6.5]); and the second is calculated for the mean Reynolds number during the oscillating cycles.

Table 6. 4 summarizes the ratios of NPH/NTU. It is observed in the table that in both matrices, the ratio NPH/NTU based on correlations equations are higher than the ratio based on the cycle results. On the other hand, the results obtained for the stacked configuration are lower indicating a generally better performance of the regenerator. The results presented are in the range obtained by Rühlich and Quack (see Figure 2.12).

Table 6. 4: Regenerator Ratio NPH/NTU

Matrix	NPH/NTU Correlations	NPH/NTU Cycle
S110-63%	6.2	4.9
W110-63%	10.7	8.2

In summary, the comparison of the thermal efficiency for S110-63% and W110-63% shows no differences between both matrices while, the ratio NPH/NTU shows a difference between both configurations. However, the ratio NPH/NTU obtained for wound woven wire matrix W110-63% is in the range of stacked screen presented by other authors (Rühlich, et al., 1999).

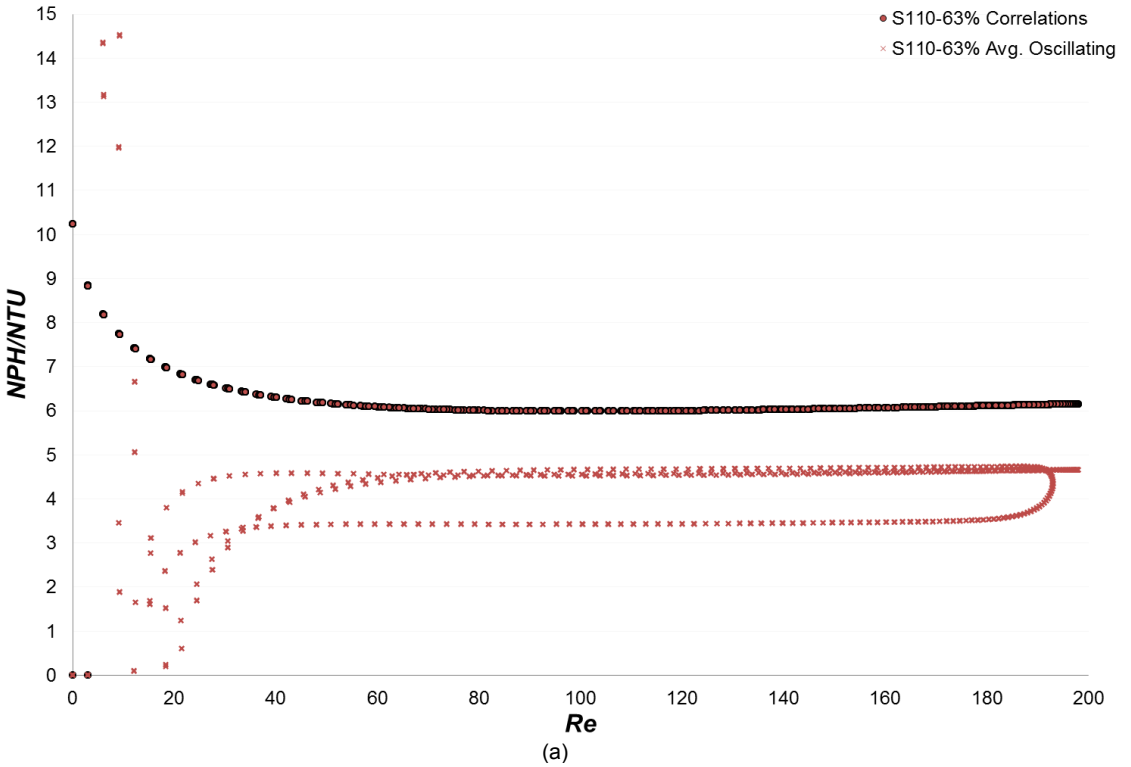

(a)

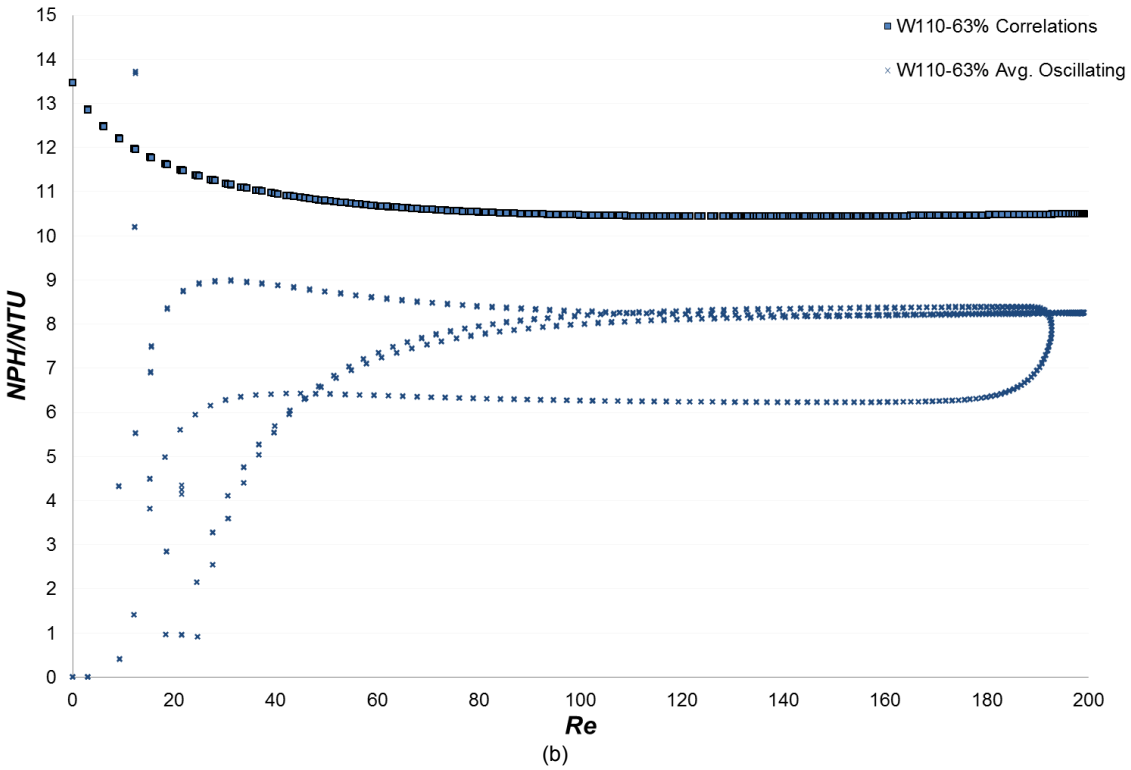

(b)

Figure 6. 17: NPH/NTU vs. Re for Pr=0.7 for matrix of 63% volumetric porosity: (a) Stacked and (b) Wound.

VI.5. Conclusions

A stepwise numerical modelling procedure for the derivation of the viscous and inertial resistance coefficients as well as thermal non-equilibrium coefficient for porous media under unidirectional flow conditions is proposed. The accuracy of the equivalent porous media model is verified against the validated numerical results obtained for the detailed woven wire matrices. The methodology is described for the flow and heat transfer characterization of two different woven wire matrix configurations, stacked and wound with 63% of volumetric porosity.

It is remarkable that for specific matrix configuration the friction factor correlation equation form that better fit the numerical results is a two-parameter Ergun form (Eq. [6.2] and Eq. [6.3]). In the case of a general correlation equation a third parameter could be necessary to better fit the curve at high Reynolds numbers (Eq. [4.1]).

The heat transfer results demonstrate that the trend-line obtained for the temperature profiles through the regenerator modelled as a porous media can be better fitted to a logarithmic curve rather than linear under oscillating flow conditions, for both zone, fluid and solid.

Based on the obtained results, the pressure drop and heat transfer performance of the different configuration matrices can be evaluated and compared as well as the thermal efficiency and the Figure of Merit. In the characterization of the stacked and the wound woven wire matrices is observed a lower ratio of NPH/NTU for the stacked configuration, which means that the ratio between pressure drop and heat transfer is lower than for the wound woven wire configuration.

It can be concluded that the numerical characterization methodology described here is advantageous for the design and optimization of the regenerator matrix under diverse working conditions (oscillating frequency, working pressure, working gas, matrix material, etc.) and useful for the multi-D Stirling engine models.

CHAPTER VII:

Conclusions

VII. CONCLUSIONS AND RECOMMENDATIONS

This chapter provides the conclusions of the developed work as well as the recommendations for future work.

VII.1. Conclusions

In this PhD study, a numerical modelling methodology to characterize the fluid flow and heat transfer through a detailed 3-D woven wire regenerator matrix is proposed and validated. The obtained results can be summarized as follows:

1. A general friction factor and a Nusselt number correlation equations are numerically derived for stacked woven wire regenerator matrices in a representative small detailed 3-D domain. The numerical results are validated with the use of well-known correlation equations obtained under oscillating flow testing conditions. The good agreement with the experimental data confirms that the proposed approach is able to characterize the flow and heat transfer behaviour in a woven wire regenerator matrix.

2. It is found that the pressure drop results are not affected by the non-isothermal flow conditions. However, it is observed the geometric configuration of the matrix significant influence over the friction factor, independently of the volumetric porosity. For the studied stacked woven wire matrix configurations, the highest Nusselt numbers are obtained for the no-contact matrix and the lowest for the aligned matrix configuration. The numerically obtained pressure drop and the heat transfers results for the different matrix configurations clearly show that the minimization of the pressure drop and the maximization of the heat transfer are conflicting requirements in the regenerator.

3. A general three-parameter correlation equation is numerically derived to characterize pressure drop through wound woven wire regenerator matrices under isothermal flow conditions. The validation results show that the derived correlation equation can be successfully applied in the Reynolds number working range of Stirling regenerators for the studied configurations. The quantified comparative analysis between both woven wire matrix configurations, stacked and wound, shows that even the pressure drop for the wound woven matrices is higher than that of the stacked case, the numerical methodology can be used to optimize wound woven wire matrix configuration by reducing the pressure losses and the cost of this component in the engine. It is remarkable that for the specific matrix configuration, the friction factor correlation equation form that better fit the numerical results is a two-parameter Ergun form. In the case of general correlation equations a third parameter could be necessary to better fit the curve at high Reynolds numbers.

4. A general correlation equation for the Nusselt number is numerically derived to characterize heat transfer through wound woven wire regenerator matrices. It is noteworthy that no linear tendency of the temperature gradient through the regeneration matrix is found for the fluid and the solid matrix.

5. Regenerator Nusselt number and flow friction factor correlation equations are generally required to calculate the Stirling cycles. For this reason, the characterization of both phenomena through this component is crucial. The results demonstrate that the numerical modelling methodology can be used to: derive friction factor and heat transfer correlation for complex regenerator matrix geometries; study the influence of matrix geometric parameters (volumetric porosity, hydraulic diameter, specific heat transfer area, etc.); reduce and support testing; improve the woven wire matrix general performance, etc. Based on the agreement of the correlation equations obtained for the stacked configuration, it is considered that the correlation equations can be used with confidence as a cost effective tool to optimize pressure drop and heat transfer through woven wire regenerator matrix to reduce the experimental cost.

6. A stepwise numerical procedure for the derivation of the resistance coefficients and heat transfer coefficient for thermal non-equilibrium porous media under unidirectional flow conditions is described. The equivalent porous media results accuracy is verified against the validated numerical results for the 3-D detailed woven wire matrices. The 3-D detailed geometry is relevant for the modelling of a woven wire regenerator matrix because the flow characteristic is intrinsically 3-D. However, it is demonstrated that a simplified 2-D domain of an equivalent isotropic porous media fully represent the detailed 3-D model, minimizing computational memory and time which is especially important under oscillating flow conditions.

7. The heat transfer results under oscillating flow conditions demonstrate that the trend-line obtained for the temperature profiles through the regenerator porous matrix, fluid and solid, can be better fitted to a logarithmic curve rather than linear under oscillating flow conditions.

8. Based on the numerical results for the pressure drop and heat transfer performance of the different configuration matrices, the thermal efficiency and the Figure of Merit can be evaluated in order to obtain a general performance of the regenerator. In the characterization of a stacked and a wound woven wire matrices is observed a better overall performance in terms of pressure drop and heat transfer for the stacked configuration.

9. It is believed that the numerical characterization methodology presented is advantageous for the design and optimization of the regenerator matrix under diverse working conditions (oscillating frequency, working pressure, working gas, matrix material, etc.) and useful for the multi-D Stirling engine models.

VII.2. Recommendations for future work

The numerical methodology proposed in this study can be effectively used for the optimization and improvement of the Stirling regenerator matrices. Accordingly, the general correlation equations derived in this work can be used with confidence to evaluate the pressure drop and heat transfer through the regenerator matrix. However, the correlation equations can be adjusted to provide a better accuracy in specific matrix configurations. Recommendations for future work on the characterization of Stirling regenerator can be as follows:

1. Analysis of the effect of different geometric parameters of the regenerator matrix, especially volumetric porosity and wire diameter, on the pressure drop and heat transfer performance would be useful to clarify the confronted opinion obtained based on experimental data.

2. Obtaining friction factor and Nusselt number correlations under oscillating flow conditions for a detailed 3-D woven wire regenerator matrices would be valuable to dissipate the confronted opinions about the effect of the oscillating flow on regenerator performance, and the correct implementation of the steady-flow correlations that are typically used to predict the performance of Stirling regenerators.

3. Study of the regenerator performance under variables engine working conditions would be beneficial to understand the effects and importance of these parameters.

4. Extension of the proposed numerical modelling methodology to model other regenerator types could be advantageous for the study of new regenerator types and support of the regenerator testing.

CHAPTER VIII:

Bibliography

VII. BIBLIOGRAPHY

Andersen, O.; Kostmann, C.; Stephani, G. and Korb, G. Advanced porous structures made from intermetallic and superalloy fibers. Proceedings of the 1st International Conference on Materials Processing for Properties and Performance. Singapore, 2002.

ANSYS ANSYS FLUENT Theory Guide. 2009.

Avdeychik V., Evstigneev N. and Shmelev, A. Application of the 3-dimensional CFD model to a geometric parameters optimization and an analyse of dimensional aspects of the Stirling engine. ISEC International Stirling Engine Conference, 2009.

Bangert K. Production of Optimised Metal Foams for Stirling Engine Regenerators. The Royal Society, Sheffield, 2010.

Bartolini C. and Naso V. Parametric thermal analysis of the Stirling engines metallic regenerators. Proceedings of the 19th Inter-Society Energy Conversion Engineering Conference. San Francisco, USA 1984. pp. 2067-2072.

Bommisetty R., Dhanvantrii, J. and Vighneswara, R.K. Flow Loss in Screens: A Fresh Look at Old Correlation. Asian International Conference on Fluid Machinery. Chennai, India, 2011.

Cha, J.S., Ghiaasiaan, S.M., Harvey, J.P. and Desai, P.V. Hydrodynamic Parameters of Pulse Tube or Stirling Cryocooler Regenerators for Periodic Flow. International Cryocoolers Conference. 2007. Vol. 14.

Cha, J.S., Ghiaasiaan, S.M. and Kirkconnell C.S. Oscillatory flow in microporous media applied in pulse – tube and Stirling – cycle cryocooler regenerators. Experimental Thermal and Fluid Science, 2008. Vol. 32. pp. 1264–1278.

Cheadle M.J., Nellis G.F. and Klein, S.A. Microscale CFD Modeling of Oscillating flow in a Regenerator. Advances in Cryogenic Engineering: Transaction of the Cryogenic Engineering Conference. 2010. Vol. 55. pp. 157-164.

Cheadle M.J., Nellis G.F. and Klein, S.A. Regenerator Friction Factor and Nusselt Number Information Derived from CFD Analysis. International Cryocooler Conference. 2011. Vol. 16. pp. 397-404.

Chen, N.C. J. and Griffin, F.P. Effect of Pressure-Drop Correlations on Stirling-Engine Predicted Performance. DOE EERE Research Reports, Thermally Activated Heat Pumps, Engine Driven Heat Pumps. Oak Ridge, Tennessee, 1983. Vols. CONF-830812-52.

Chen, P.H., Chang, Z.C. and Huang, B.J. Effect of overzise in wire-screen matrix to the matrix-holding tube on regenerator thermal performance. Cryogenics, 1996. Vol. 36. pp. 365-372.

Collins, R. D., Daws L.F. and Taylor J.V. Heat Transfer in Regenerators. BISRA Report SM/A/169/55, 1955.

Conrad, T.J., Landrum, E.C., Ghiaasiaan, S.M., Kirkconnell, C.S., Crittenden, T. and Yorish, S. Anisotropic Hydrodynamic Parameters of Regenerator Materials Suitable for Miniature Cryocoolers. International Cryocooler Conference. 2009.

Costa, S.C., Barrutia, H., Esnaola, J.A. and Tutar, M. Numerical study of the pressure drop phenomena in wound woven wire matrix of a Stirling regenerator. Energy Conversion and Management, 2012. Vol. 67. pp.57-65.

Dybbs, A. and Edwards, R.V. A new look at porous media fluid mechanics – Darcy to Turbulence. Fundamentals of Transport Phenomena in Porous Media, 1984. Vol. 82. pp. 199-256.

Dyson, R.W., Wilson, S.D., Tew, R.C. and Demko, R. Fast Whole-Engine Stirling Analysis. Ohio, USA: NASA/TM-2005-213960, 2005.

Dyson, R.W., Wilson, S.D., Tew, R.C. and Demko, R. On the Need for Multidimensional Stirling Simulations. Ohio, USA: NASA/TM-2005-213975, 2005.

Dyson R.W., Geng S.M. Tew R.C. and Adelino, M. Towards fully three-dimensional virtual Stirling convertors for multi-physics analysis and optimization. Engineering Applications of Computational Fluid Mechanics, 2008. Vol. 2. pp. 95-118.

Ecotec. 2009. [Online] 2009. Web. 11 Mar. 2011. http://www.ecotec2000.de/espanol/stir2.htm.

Edwards J.V., Evans R. and Probert S.D. Computation of Transient Temperatures in Regenerators. International Journal Heat and Mass Transfer, 1971. Vol. 14. pp. 1175-1202.

Energy Transition. Energiewende Germany. [Online]. Web. 10 Dec. 2013. http://energytransition.de/2012/10/240/).

EHE Efficient Home Energy. 2011. [Online]. Web. 10 Dec. 2013. http://www.ehe.eu/.

ExxonMobil. The outlook for Energy: A view to 2040. [Online]. Texas, 2013. Web. 10 Dec. 2013.

Forooghi, P., Abkar M. and Saffar-Avval, M. Steady and Unsteady Heat Transfer in a Channel Partially Filled with Porous Media under Thermal Non-Equilibrium Condition. Transp Porous Media, 2010.

Gedeon, D. and Wood J.G. Oscillating-Flow Regenerator Test Rig: Woven Screen and Metal Felt Results. Ohio, USA: NASA-CR-190689, 1992.

Gedeon, D. and Wood J.G. Oscillating-Flow regenerator Test Rig: Hardware and Theory With derived Correlations for Screens and Felts. Ohio, USA: NASA Contractor report 198442, 1996.

GKD Gebr. Kufferath AG GKD World Wide Weave [Online]. - 2010-2014. Web. 10 Dec. 2013. http://www.gkd.de/en.html.

Green, G.F. and Superczynski, W.F. Ribbon Regenerator Performance in a Single-Stage GM Cryocooler. International Cryocooler Conference. 2007. Vol. 14. pp. 373-379.

Hamaguchi, K., Takahashi, S. and Miyabe, H. Flow Losses of Regenerator matrix (Case of Packed Wire Gauzes). Washington, USA: NASA Technical Memorandum, NASA TM-77448, 1984.

Hargreaves, C.M. The Philips Stirling Engine. Eindhoven, The Netherlands: ELSEVIER, 1991.

Harvey, Jeremy Paul. Oscillatory Compressible Flow and Heat Transfer in Porous Media – application to Cryocooler Regenerator. Doctoral Dissertation. Georgia Institute of Technology, 2003.

Hieke, Michael. Theoretical and Experimental Study for the Development of efficient and economic Stirling Regenerator. Final Technical Report: ENK5-CT-2001-00527. Dresden, 2005.

Ibrahim, M.B., Simon, T., Gedeon, D. and Tew, R. Improving Performance of the Stirling Converter: Redesign of the Regenerator with Experiments, Computation and Modern Fabrication Techniques. Ohio, USA: DE-FC36-00G010627, 2001.

Ibrahim, M.B., Tew, R., Zhang, Z., Gedeon, D. and Simon, T. CFD Modelling of Free Piston Striling Engine. Ohio, USA: NASA/TM—2001-211132, 2001.

Ibrahim, M.B., Wang M. and Gedeon D. Experimental Investigation of Oscillatory Flow Pressure and Pressure Drop through Complex Geometries. Proceedings of the 2th International Energy Conversion Engineering Conference. Providence, USA: 2004.

Ibrahim, M.B., Danila, D., Simon, T., Mantell, S., Sun, L., Gedeon, D., Qiu, S., Wood, G. Kelly, K. and McLean, J. A Microfabricated Segmented-Involute-Foil Regenerator for Enhancing Reliability and Performance of Stirling Engines. Phase II. Ohio, USA: NASA Contractor report NASA/CR-2007-215006, 2007.

Ibrahim, M.B., Danila, D., Simon, T., Gedeon, D. and Tew, R. Computational Modeling of a Segmented-Involute-Foil Regenerator for Stirling Engines. Journal of Thermophysics and Heat Transfer, 2009. Vol. 23. pp. 786-800.

Ibrahim, M.B. and Tew R.C. Stirling Convertor Regenerators. USA : CRC Press, 2012. ISBN: 978-1-4398-3006-2.

Ju Yonglin and Shen, Qingqing. Comparative study of oscillating flow characteristics of cryocooler regenerator at low temperatures. China: Energy Power Eng., 2009. Vol. 3(1). pp. 80-84.

Kagawa, N., Takeuchi T. and Matsuguchi A. Performance of a new matrix for high performance Stirling Engine Regenerator. International Stirling Engine Conference . Durham, UK: 2005. Vol. 12th.

Kays, W.M. and London, A.L. Compact Heat Exchangers. New York. Mc. Graw Hill, 1964.

Kim, Sung-Min. Numerical Investigation on Laminar Pulsating Flow through Porous Media Doctoral Dissertation. Georgia Institute of Technology, 2008.

Knefel, M. and Wegenke, E. Choice and Optimization of Technical Woven Wire Meshes in the Solid Liquid Separation. GKD & GeoDict, Duren, 2009.

Knight, I. and Ugursal, I. Residential Cogeneration Systems: A Review of the Current Technologies. Ottawa, Ontario, Canada: Inernational Energy Agency, 2005.

Knowles, Timothy. Composite-Matrix Regenerators for Stirling Engines. USA: NASA, Contrator Report 202322, 1997.

Kolodziej, A., Lojewska, J., Jaroszynski, M. and Gancarczyk, A. Heat transfer and flow resistance for stacked wire gauzes: Experiments and modelling. International Journal of Heat and Fluid Flow, 2012. Vol. 33. pp. 101-108.

Kraitong, K. and Mahkamov, K. Thermodynamic and CFD modelling of Low-Temperature Difference Stirling Engines. ISEC International Stirling Engine Conference, 2009.

Landrum, E.C., Conrad, T.J., Ghiaasiaan, S.M. and Kirkconnell, C.S. Effect of Pressure on Hydrodynamic Parameters of Several PTR Regenerator Fillers in Axial Steady Flow. International Cryocooler Conference, 2009. Vol. 15.

Luo, Ercang. A New Angle of View for Understanding and Evaluating Flow Characteristics of Cyclic Regenerators. New York: Cryocoolers, 2004. Vol. 13. pp. 431-438.

Martini, William. Stirling Engine Design Manual. Hawaii, USA: University Press of the Pacific, 1983. ISBN: 1-4102-1604-7.

Matsuguchi, A., Kagawa N. and Koyama S. Improvement of a Compact 3 kW Stirling Engine with Mesh Sheet. ISEC International Stirling Engine Conference, 2009.

Mitchell, M., Gedeon, D., Wood, G. and Ibrahim, M. Results of Test of Etched Foil Regenerator Material. Cryocoolers 14. International Cryocooler Conference, 2007.

Miyabe, H., Takahashi S. and Hamaguchi K. An approach to the design of Stirling Engine Regenerator matrix using packs of wire gauzes. Los Angeles, USA: In: Proc. of the 17th Inter-Society Energy Convertion Engineering Conference, 1982. pp. 1839-1844.

Moran, M., Stelter S. and Stelter M. Micro-Scale Regenerative Heat Exchanger. Ohio, USA: NASA/TM-2004-213353, 2004.

Morgado, D. and Slowe J. Micro-CHP finally arrives in Europe - but future growth uncertain, 2010.

Mortazavy, H.R., Golneshan A.A. and Zarinchang J. The effect of angular velocity in Stirling engine on the thermal performance of heat regenerator. Osnabrück, Germany: International Stirling Forum, 2008.

Nair Anjan R. and Krishnakumar, K. Numerical modelling of single blow transient testing of a wire screen mesh heat exchanger. 10th National Conference on Technological Trends., 2009.

O´Hern T.J. and Torezynski, J.R. Reynolds number dependence of the drag coefficient for laminar flow through fine-scale photoetched screens. Experiments in Fluids, 1993. Vol. 15. pp. 75-81.

Omaña, D. Estudio Teórico del Regenerador para un Motor Stirling. - México: Instituto Politécnico Nacional, Escuela Superior de Ingeniería Mecánica y Eléctrica, 2007.

Onovwiona, H.I. and Ugursal, V.I. Residential cogeneration systems: review of the current technology. Renewable and Sustainable Energy Reviews, 2006. Vol. 10. pp. 389-431.

Organ, A. J. and Maeckel P. "Connectivity" and Regenerator Thermal Shorting. Osnabrück, Germany: In: Proc. of the 3th European Stirling Forum, 1996.

Organ, A. J. Solution of the classic thermal regenerator problem. Cambridge : Proc. Instn Mechanical Engineers, 1994. Vol. 208: pp. 187-197.

Organ, A.J. The Regenerator and the Stirling Engine. London: Mechanical Engineering Publications Limited, 1997. ISBN 1 86058 010 6.

Organ, A.J. Transient Thermal Performance of the Stirling Engine Wire Regenerator. London: Proceedings: Mathematical and Physical Sciences, 1994. Vol. 444. pp. 53-72.

Parente, A., Galletti, C., Riccardi, J. Schiavetti, M. and Tognotti, L. Experimental and numerical investigation of a micro-CHP flameless unit. Applied Energy, 2012. Vol. 89. pp. 203-214.

Park, J.W., Ruch, D. and Wirtz, R.A. Thermal/Fluid characteristics of isotropic plain-weave screen laminates as Heat Exchange Surfaces. American Institute of Aeronautics and Astronautics, 2002. Vol. AIAA 2002-0208.

Pathak, M.G. and Ghiaasiaan, S.M. Thermal Dispersion and Convection Heat Transfer during Laminar Transient FLow in Porous Media. Cryocoolers 16. International Cryocooler Conference, 2011.

Pathak, Mihir Gaurang. Periodic flow physics in porous media of regenerative cryocoolers. Doctoral Dissertation. Georgia Institute of Technology, 2013.

Prieto, J.I. and Díaz R. Relaciones Adimensionales para el estudio analitico y experimental del motor Stirling. Conferencia del Grupo de trabajo de Análisis Dimensional. Madrid, 1990. pp. 95-107.

Prieto, J.I. Dimensionamiento del mortor Stirling y revisión de sus aplicaciones marinas. Ingeniería Naval. Gijón (Asturias), 2003. pp. 365-372.

Radebaugh, R. and Louie, B. A first simple step to the optimization of regenerator geometry. Proc. of the 3rd Cryocooler Conference. Washington DC, 1985. pp.177.

Rühlich, I. and Quack, H. Investigations on Regenerative Heat Exhangers. Cryocooler. New York, 2002. Vol. 10. pp. 265-274.

Rühlich, I. and Quack H. New Regenerator Design for Cryocoolers. Dresden, Germany: Technische Universität Dresden, 1999.

Schalkwijk, W.K. A simplified regenerator theory. British Chemical Engineering, 1960. pp.33-34.

Schultz, B.H. Aproximative formulae in the theory of thermal regenerators. App. Sc. Res. Section A., 1951. Vol. 3. pp. 165-173.

Simon, T.W. and Seume, J.R. Oscillating Flow in Stirling Engine Heat Exchangers. San Diego, USA: In: 21st Inter-Society Energy Conversion Engineering Conference, 1986.

Sodré, J.R. and Parise, J.A.R. Friction Factor Determination for Flow Through Finite Wire-Mesh Woven-Screen Matrices. Journal of Fluids Engineering, 1997. Vol. 119. pp. 847-851.

Sun, Liyong. Fluid Mechanics and Heat Transfer Experiments in the Large Sclae Mock Up of the Microfabricated Stirling Engine Regenerator. Doctoral Dissertation. Department of Mechanical Engineering. The University of Minnesota (Twin Cities). 2007.

Tanaka, M., Yamashita I. and Chisaka F. Flow and Heat Transfer characteristics of the Stirling Engine Regenerator in an Oscillating Flow. Japan: JSME International Journal, Series II, 1990. Vol. 33. pp. 283-289.

Tao, Y.B., Y.W Liu and Chen X.Y. and He, Y.L. Numerical analysis on pressure drop and heat transfer performance of mesh regenerators used in cryocoolers. Cryogenics, 2009. Vol. 49. pp. 497-503.

Tew, R., Simon, T., Gedeon, D., Ibrahim, M. and Rong, W. An Initial Non-Equilibrium Porous-Media Model for CFD Simulation of Stirling Regenerators. Ohio, USA: NASA/TM-2006-214391, 2006.

Tew, R., Ibrahim, M.B., Danila, D., Simon, T., Mantell, S., Sun, L., Gedeon, D., Qiu, S., Wood, G. Kelly, K. and McLean, J. A Microfabricated Involute-Foil Regenerator for Stirling Engines. Ohio, USA: NASA/TM-2007-214973. AIAA-2007-4739, 2007.

Thomas, B. and Bolleber, F. Evaluation of 5 different Correlations for the Heat Transfer of Stirling Engine Regenerators. Osnabrück, Germany: Proc. Europ. Stirling Forum, 2000. pp. 111-119.

Thomas, B. and Pittman D. Update on the Evaluation of Different Correlations for the FLow Friction Factor and Heat Transfer of Stirling Engine Regenerators. Reutlingen, Germany: American Institute of Aeronautics and Astronautics, 2000. Vols. AIAA-2000-2812.

Thomas, Bernd. Evaluation of 6 different Correlations for the Flow Friction Factor of Stirling Engine Regenerators. Vancouver : Proc. 34th IECEC, 1999. Vols. 1999-01-2456.

Tian, J., Kim, T., Lu, T.J., Hodson, H.P., Queheillalt, D.T., Sypeck, D.J. and Wadley, H.N.G. The effects of topology upon fluid-flow and heat-transfer within cellular copper structures. Heat and Mass Transfer, 2004. Vol. 47. pp. 3171-3186.

Timoumi, Y., Tlili I. and Nasrallah S.B. Performance optimization of Stirling Engines. Monastir, Tunisie: Renewable Energy, 2008. Vol. 33. pp. 2134-2144.

Tong, L.S. and London, A.L. Heat-transfer and Flow-friction characteristics of woven-screen and crossed-rod matrices. New York: The American Society of Mechanical Engineers, 1957.

Urieli, Israel. A Computer Simulation of Stirling Cycle Machines. Johannesburg : University of the Witwatersrand, 1977.

Walker, G. Stirling-Cycle Machines. Claredon Press - Oxford, 1973.

Wilson, S.D., Dyson R.W., Tew R.C. and Ibrahim, M. Multi-D CFD Modeling of a Free-Piston Stirling Convertor at NASA Glenn. Ohio, USA: NASA/TM-2004-213351. AIAA-2004-5673, 2004.

White, Frank M. Fluid Mechanics. University of Rhode Island: McGraw-Hill Series in Mechanical Engineering, 2009. 7th. ISBN 978–0–07–352934–9.

Wu, W.T., Liu J.F. and Hsieh W.J. Li and W.H. Measurement and correlation of hydraulic resistance of flow through woven metal screens. Heat and Mass Transfe, 2005. Vol. 48. pp. 3008-3017.

Yakhot, V. and Orszag, S.A. Renormalization group analysis of turbulence. I. Basic theory. J Sci Comput, 1986.

Yarbrough, S.A., Flake B.A. and Razani, A. Computational Fluid Dynamic Modelling of Pressure Drop Through Wire Mesh Screen Regenerators. Advances in Cryogenic Engineering: Transactions of the Cryogenic Engineering Conference, 2004. Vol. 49. pp. 1138-1145.

Yaron, Ran. Low cost, High efficiency regenerator for cryocoolers. PL-TR-94-1037 / Phillips Laboratory. Palo Alto, CA 94306, 1994.

Zhao, T.S and Cheng, P. Oscillatory pressure drops through a woven-screen packed column subjected to a cyclic flow. Cryogenics, 1996. Vol. 36. pp. 333-341.

ANEXO I:

Publications

ANNEX I: PUBLICATIONS

S.C. Costa, I. Barreno, M. Tutar, J.A. Esnaola and H. Barrutia. The thermal non-equilibrium porous media modelling for CFD study of woven wire matrix of a Stirling regenerator. *Submitted in Energy Conversion and Management Journal in May 2014*

Sol-Carolina Costa, Mustafa Tutar, Igor Barreno, Jon-Ander Esnaola, Haritz Barrutia, David García, Miguel-Angel González and Jesús-Ignacio Prieto "Experimental and numerical flow investigation of Stirling engine regenerator". *Under third revision in [Journal] // Energy (ISSN: 0360-5442) in May 2014.*

S.C. Costa, I. Barreno, J.A Esnaola and M. Tutar. "Figure of Merit for Stirling Regenerator Matrix based on Engine Experimental Data". *To be presented in the 16th International Stirling Engine Conference (ISEC), Bilbao, Spain. September 2014.*

S.C. Costa, H. Barrutia, J.A Esnaola and M. Tutar. Numerical study of the heat transfer in wound woven wire matrix of a Stirling regenerator. Energy Conversion and Management, vol. 79 (2014), pp. 255-264.

S.C. Costa, H. Barrutia, J.A Esnaola and M. Tutar. Numerical study of the pressure drop phenomena in wound woven wire matrix of a Stirling regenerator". Energy Conversion and Management, vol. 67 (2013), p. 57–65

S.C. Costa, I.Barreno, J.I.Prieto, M.A.González and D.García. "Stirling Regenerator Test Bench Design for Pressure Drop and Thermal Efficiency measurements". 15th International Stirling Engine Conference (ISEC), Dubrovnik, Croatia, 2012

S.C. Costa, I.Barreno, M.Cordón, J.A.Esnaola and H.Barrutia. "Development of a CFD based tool to characterize the pressure drop through a Wound Woven Wire Mesh Stirling Regenerator". 15th International Stirling Engine Conference (ISEC), Dubrovnik, Croatia, 2012.